Finite element solution of two-regime flow towards wells. December 1973.

Author:
Huyakorn, P. S.

Publication details:
Report No. UNSW Water Research Laboratory Report No. 137
0858241455 (ISBN)

Publication Date:
1973

DOI:
https://doi.org/10.4225/53/579add1ed0732

THE UNIVERSITY OF NEW SOUTH WALES
water research laboratory
Manly Vale, N.S.W., Australia

Report No. 137

FINITE ELEMENT SOLUTION OF TWO-REGIME FLOW TOWARDS WELLS

by

P. S. Huyakorn

December, 1973

The University of New South Wales

Water Research Laboratory

FINITE ELEMENT SOLUTION OF TWO-REGIME FLOW TOWARDS WELLS

by

Pongsarl Huyakorn

Report No. 137

December, 1973.

---

https://doi.org/10.4225/53/579add1ed0732

BIBLIOGRAPHIC DATA SHEET	1. REPORT No. 137	2. I.S.B.N. 0/85824/145/5

3. TITLE AND SUBTITLE
Finite Element Solution of Two- regime Flow towards Wells.

4. REPORT DATE
September, 1974.

5. AUTHOR(S) Huyakorn, P.S.

6. SPONSORING ORGANIZATION
Water Research Laboratory

7. SUPPLEMENTARY NOTES Ph. D. thesis submitted to the University of New South Wales in October 1973.

8. ABSTRACT

This report describes an investigation of two-regime flow of groundwater towards pumped wells. The work included can be divided into two parts. The first part deals with the general theory, variational principles and finite element methods for confined and unconfined flow problems. Numerical solutions obtained for several transient and steady flow cases are presented in graphical form. The second part discusses verification of the finite element analysis by laboratory and field investigations. Type curve methods developed for determining aquifer hydraulic coefficients are presented. Typical pumping test results are compared with the numerical solutions.

9. DISTRIBUTION STATEMENT Enquiries re purchase of report should be directed to the Officer-in-Charge, Water Research Laboratory, University of New South Wales, King St., Manly Vale, N.S.W. 2093.

10. KEY WORDS Finite element analysis; groundwater; base flow; water wells.

11. CLASSIFICATION	12. NUMBER OF PAGES 191	13. PRICE $10.00

Summary

This thesis describes an investigation into two-regime flow of groundwater towards a pumped well constructed in unconsolidated material. Emphasis is laid on the effect of a non-linear regime on the drawdown distribution near the well and the well discharge-drawdown relationship.

The basic principles of well hydraulics based on Darcy's law are reviewed and extended to two-regime flow. Generalised field equations and a variational principle applicable to transient three-dimensional flow are developed. An energy approach to well flow problems is also presented and directly related to the variational principle.

The finite element method is briefly described and formulated to solve a variety of problems, ranging from the simplest problem of steady one-dimensional radial flow through a confined aquifer to the most complex problem of transient free surface flow. Techniques developed to handle various types of boundary conditions and non-linearity of the field equations are described. Solutions for both wholly Darcy flow and two-regime flow situations are presented in graphical form for each flow problem. Several new type curves characterising two-regime flow behaviour are included.

Verification of the Darcy flow solutions by comparison with known analytical solutions and of the two-regime flow solutions by laboratory experiments and field investigations is described.

New type curve methods for determining from pumping test results the hydraulic coefficients required in the analysis of two-regime flow are presented.

The theory, numerical techniques and type curve methods developed in this work may be applied to specific cases of well flow encountered in practice. Alternatively, they may be used to produce solutions to a wider range of problems than that covered in this thesis. These solutions could then be used as an aid in interpreting pumping test results.

Table of Contents

Table of Contents (cont'd.)

Table of Contents (cont'd.)

Table of Contents (cont'd.)

Acknowledgements

The author would like to gratefully acknowledge Mr. C.R. Dudgeon, Senior Lecturer in Civil Engineering, University of New South Wales, for supervision and guidance in carrying out this work. Thanks are also given to Mr. D.N. Foster, Senior Lecturer in Civil Engineering and Officer-in-Charge of the Water Research Laboratory, for acting as supervisor during Mr. Dudgeon's absence overseas on study leave.

The author would also like to acknowledge with thanks the financial support provided by the Australian Water Resources Council through its funding of Project 68/8, "Extraction of Water from Unconsolidated Sediments".

Thanks are also given to my colleagues, Mr. W.H.C. Swan and Mr. R. Cox for their participation in the laboratory and field investigations and to the New South Wales Water Conservation and Irrigation Commission and the Queensland Irrigation and Water Supply Commission for their co-operation in carrying out the field investigations.

Finally, particular thanks are due to Mrs. P.U. Decent and Mrs. P.M. Auld, for their painstaking effort in typing the manuscript and careful drafting of the figures, and to Mr. W.T. Spurge for printing the figures.

The assistance of other staff members of the Water Research Laboratory, particularly Mrs. J.A. Massey, the Librarian of the Water Reference Library, is also gratefully acknowledged.

1. Introduction

1.1 General

Problems involving flow of groundwater towards pumped wells have traditionally been solved on the assumption that a linear velocity-hydraulic gradient relationship, known as Darcy's law, is valid over the entire flow region. This assumption leads to a linear field equation which has been solved analytically for several cases where the aquifer is uniform and the boundary conditions are relatively simple. A number of analytical solutions (Theis, 1935), (Hantush, 1960, 1961), (Boulton, 1963) and methods for evaluating aquifer properties via these solutions have been widely applied to the results of pumping tests. Recently, the rapid development of numerical methods and high speed digital computers has encouraged many workers to solve more complex cases such as those involving multi-layered aquifers, free surfaces and unsaturated flow. Among these workers are Javandel and Witherspoon (1965), Neuman and Witherspoon (1969, 1970, 1971), Taylor and Luthin (1969), Cooley (1971).

It has long been recognised that the linear velocity - hydraulic gradient relationship may be invalidated in the immediate vicinity of a well boundary if velocities exceed a certain limiting value (Muskat, 1937), (Kristianovich, 1940), (Wentworth, 1946). When deviation from Darcy's law occurs, both linear and non-linear regimes must be

considered in analysing the flow over the entire region. Thus the term "two-regime flow" may be used in this context.

Despite the increased amount of research effort which has been put into flow towards wells, there is still a lack of a sound theoretical basis and methods for handling the situation of two-regime flow. The need for a clearer understanding of non-Darcy flow behaviour near a well and for means of predicting its effect on the well discharge-drawdown relationship has become increasingly important as a result of more intensive use of groundwater and the consequent demand for improved design of extraction facilities.

The objectives of this thesis are:-

(i) to extend the basic theory and principles of well hydraulics based on Darcy's law to allow two-regime flow to be handled;

(ii) to develop a finite element method for solving the field equations;

(iii) to verify the finite element analysis by laboratory and field investigations.

1.2 Literature Review

1.2.1 Empirical Approach to Two-Regime Well Flow

A number of workers recognised that although non-Darcy flow is often restricted to a comparatively narrow zone around the well, such a narrow zone can affect the discharge quite considerably. On the basis of their field experience, these workers proposed empirical equations relating the drawdown in a well pumping from a confined aquifer to the discharge.

Jacob (1947) used the following equation:-

$$s_w = BQ + CQ^2 \qquad (1.1)$$

where s_w is the drawdown in the well, Q is the well discharge, B and C are empirical constants of the equation. In adopting equation (1.1) he assumed that flow in the aquifer formation obeys Darcy's law up to a certain radius, termed the effective radius of the well, and that inside this radius the flow is fully turbulent. The effective well radius was defined by Jacob as that distance, measured radially from the axis of the well, at which the theoretical drawdown based on the logarithmic distribution equals the actual drawdown just outside the screen. The term CQ^2 in equation (1.1) was referred to as "well loss" and represents the head loss resulting from turbulent flow inside the effective radius and the flow through the screen and inside the casing.

Rorabaugh (1953) proposed an equation slightly different from equation (1.1). His equation is given by

$$s_w = BQ + CQ^n \qquad (1.2)$$

where n is an unknown exponent. On the basis of field data from several pumping tests, he demonstrated that equation (1.2) predicted the total drawdown in the well more closely than Jacob's equation.

Whilst the two empirical equations proposed by Jacob and Rorabaugh have been found to fit many field data, doubt usually exists regarding their general applicability. As pointed out by Rorabaugh himself, equation (1.2) and the constants B, C and n determined from analysis of data from the step-drawdown pumping test should not be applied if computations must be made for discharges greatly in excess of those used in the test.

1.2.2 Theoretical Analyses and Model Studies

Due to the complexity arising from the nature of two-regime flow and the non-linear equation for flow in the non-linear regime, only a limited number of theoretical analyses have been made.

The earliest attempt to obtain an analytical solution to the non-linear field equation of steady state non-Darcy flow was made by Khristianovich (1940). He considered a general velocity-hydraulic gradient gradient relation of the form

$$i = \emptyset(V) \qquad (1.3)$$

and described an approximate method of solution by conformal transformation.

Engelund (1953) carried out a more general theoretical investigation into steady, two-regime well flow. He employed the following equation to describe both Darcy and non-Darcy flow in the aquifer.

$$\vec{\nabla}h = - F(|V|)\,\vec{V} \qquad (1.4)$$

where $\vec{\nabla}h$ is the hydraulic gradient vector, $\vec{V}$ is the velocity vector and $F(|V|)$ is a scalar function of the absolute velocity $|V|$ and the aquifer properties.

The function $F(|V|)$ is given by

$$F(|V|) = \frac{1}{K} \qquad \text{for } |V| \leqslant V_{cr}$$

$$F(|V|) = a + b|V| \quad \text{for } V > V_{cr}$$

where K is the coefficient of hydraulic conductivity, a and b are termed linear and non-linear coefficients of hydraulic resistance of the aquifer respectively, and V_{cr} is the critical velocity at which transition from

linear to non-linear regime occurs.

By combining equation (1.3) with the continuity equation, Engelund obtained a general field equation which is valid for both Darcy and non-Darcy flow. He transformed this equation into a linearised form by introducing new variables and employing the technique of conformal transformation. However, the transformed equation still remains virtually intractable to direct analytical solution for complex boundary conditions encountered in practice. Engelund was able to obtain solutions for only simple cases of steady one-dimensional two-regime flow towards a well in a confined aquifer and two-dimensional turbulent flow at high Reynolds number.

Recognising the difficulties encountered in the theoretical analysis of two-regime well flow, a number of workers resorted to experimental studies using either an electrical or hydraulic model of the flow system.

Grcic (1961) used a sand box model to study steady flow towards a well in an unconfined aquifer. He investigated the effect of non-Darcy flow on base pressure heads and free surface heights in the immediate vicinity of the well.

Baturic-Rubcic (1966) used an electrical analog model to study steady two-regime flow towards a fully screened well in a confined aquifer. His model was a network consisting of discrete non-linear elements with electrical properties analogous to the hydraulic properties of the aquifer material. He compared the model results with the theoretical solution given earlier by Engelund (1953) and obtained good agreement.

1.2.3 Finite Element Solutions

The difficulties which render the two-regime flow problems intractable to analytical solution can now be overcome by applying a numerical technique known as "the finite element method". Recently, a number of workers have employed this technique to obtain numerical solutions to several complex problems of flow through porous media.

Zienkiewicz et al (1966) were the first workers to use the finite element method to solve problems of steady state Darcy flow through porous media. Their work was later extended by Finn (1967) and Taylor and Brown (1967) to treat more complex problems involving free surfaces.

Among the first workers who applied the method to problems of transient Darcy flow towards wells in confined aquifers were Parekh (1967), Javandel and Witherspoon (1968) and Neuman and Witherspoon (1969). The last two workers, Neuman and Witherspoon (1970), (1971), also developed the generalised variational principles for transient confined and unconfined flows and solved several cases of flow in multilayer confined systems and flow in an unconfined aquifer. The usefulness and validity of their finite element approach was demonstrated by comparing the computer results with known analytical solutions.

In all the work mentioned so far, the finite element analysis was based on the assumption that flow in the entire region of the system obeyed Darcy's law. Problems involving non-Darcy flow received little attention until very recently when the non-linear field equations

suitable for numerical solutions were derived by a number of workers. These workers include Fenton (1968), Volker (1969), McCorquodale (1969), (1970) and Parkin (1971).

Trollope et al (1970) were the first to analyse the steady cases of non-Darcy well flow using the field equations and the finite element technique outlined by Volker (1969). Their analysis was based on the assumption that the Forchheimer non-linear velocity-hydraulic gradient relationship (Forchheimer, 1901) may be used to describe flow in the entire aquifer region. No attempt was made to investigate the practical problems of two-regime well flow where the non-Darcy flow behaviour prevails only in the immediate vicinity of the well boundary.

In the present work, the finite element method was used to obtain numerical solutions to the general problems of transient and steady state two-regime flow. To bring into focus the localised nature of non-Darcy flow, the Forchheimer relation was applied only in the near-well zone when computed velocities exceeded a certain critical value. For a given aquifer material the critical value may be determined by permeability tests. Alternatively the value may be based on a critical Reynolds number in the range of 1 to 10 as it has been shown by many investigators that the transition from Darcy to non-Darcy flow generally occurs within this range (Todd 1959).

1.3 Outline of Present Work

The work described in this thesis can be divided into two major parts as follows:-

(i) The first part is concerned with the general theory and finite element analysis of transient, two-regime well flow. Chapter 2 presents the development of the basic principles and field equations which are applicable to the general situation of three-dimensional flow. Chapte 3 and 4 deal with the development of the variational principle and finite element method for analysing axisymmetric flow problems. A number of techniques developed to handle various types of boundary conditions and non-linearity of the field equations are presented. These techniques can readily be extended to other types of linear and non-linear porous media flow.

(ii) The second part of the work deals with verification of the finite element analysis. The finite element method was used to solve a variety of problems, ranging from the simplest problem of one-dimensional radial flow through a confined aquifer to the most complex problem of transient free surface flow through an unconfined aquifer. Solutions to typical Darcy and two-regime flow cases are presented in Chapter 5. The Darcy flow solutions were checked against known analytical solutions which are listed in Appendix 3. As analytical solutions for the two-regime flow situations could not be obtained, the two-regime flow solutions were verified by comparison with pumping test results obtained from laboratory and field investigations which are described in chapters 6 and 7. In making such a comparison, it was necessary to know the hydraulic coefficients to be fed into the finite element model. New type curve methods which enable all coefficients

in the linear and non-linear velocity-hydraulic gradient relationships to be determined are also presented.

2. Basic Principles and Field Equations of Two-regime Well Flow

2.1 General

The flow towards a pumped well constructed in an unconsolidated aquifer may involve two flow regimes. The first, referred to as the Darcy regime, lies in the main portion of the aquifer where the flow obeys Darcy's law. The second regime occurs in the immediate vicinity of the well if high flow velocities result in the violation of the Darcy linear velocity-hydraulic gradient relationship.

The basic principles of well hydraulics which have been outlined in the literature are based on the assumption that the flow remains laminar and obeys Darcy's law right to the face of the well boundary. In order to analyse the more general problem of two-regime well flow, it is necessary to extend these principles and develop generalised field equations describing both Darcy and non-Darcy flow.

The principles and field equations developed herein are applicable to the general case of three-dimensional, two-regime well flow. In the development, it is assumed that the two flow regimes are distinct and that the Forchheimer non-linear velocity-hydraulic gradient relationship may be used to describe non-Darcy flow. The concept of Reynolds number is introduced and a critical velocity corresponding to the critical Reynolds number is used to distinguish between the two regimes. Tensor subscript notation is employed in the derivation of the field equations to enable flow through anisotropic aquifer material to be conveniently described.

2.2 Darcy's Law

2.2.1 Differential Form

According to Darcy's law, the macroscopic flow velocity is proportional to the hydraulic gradient measured in the flow direction. The constant of proportionality is termed "coefficient of hydraulic conductivity" and is observed to be dependent on the properties of the groundwater as well as the characteristics of the aquifer. Among the various factors influencing this coefficient are grain size distribution, packing and shape of granular particles and temperature and chemical composition of the groundwater.

The following generalisations are now introduced in order that Darcy's law may be written in its differential form :-

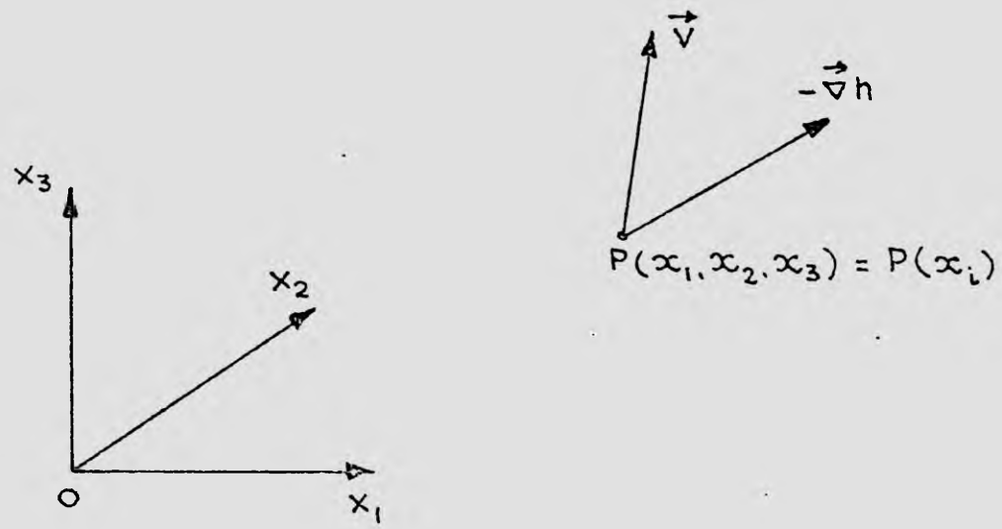

Fig. 2.1: Velocity and hydraulic gradient at a point.

A right hand system of Cartesian coordinate axes (x_1, x_2, x_3) with axis x_3 pointing vertically upwards and plane x_1 - x_2 corresponding to the datum plane is adopted as shown in Fig. 2.1.

The hydraulic head $h(x_i, t)$ at point $P(x_1, x_2, x_3)$ is defined as the sum of the pressure and elevation heads above plane x_1-x_2. Thus $h(x_i, t)$ may be expressed as

$$h(x_i, t) = p/\gamma + x_3 \qquad (2.1)$$

where p is the hydrostatic pressure at the point, γ is the specific weight of water and x_3 is the elevation of the point above the datum plane.

Let v_1, v_2, v_3 be the three components of the velocity vector, $\frac{\partial h}{\partial x_1}$, $\frac{\partial h}{\partial x_2}$, $\frac{\partial h}{\partial x_3}$ be the three components of the hydraulic gradient vector and $\vec{e}_1$, $\vec{e}_2$, $\vec{e}_3$ be the three unit vectors along x_1, x_2 and x_3 axes respectively.

The velocity vector $\vec{V}$ and the hydraulic gradient vector $\vec{\nabla} h$ may now be expressed as

$$\vec{V} = v_i \vec{e}_i \qquad (2.2)$$

$$\vec{\nabla} h = \frac{\partial h}{\partial x_i} \vec{e}_i \qquad (2.3)$$

where the repeated subscripts denote summation over the full range, from 1 to 3.

Thus for three-dimensional flow through anisotropic aquifers, the general vector differential form of Darcy's law is given by

$$\vec{V} = - \vec{\vec{K}} \vec{\nabla} h \qquad (2.4)$$

where $\vec{\vec{K}}$ denotes the hydraulic conductivity tensor; a second order symmetric tensor which may be expressed as

$$\vec{\vec{K}} = K_{ij} \vec{e}_i \vec{e}_j \qquad (2.5)$$

in which K_{ij} refers to the components of $\vec{\vec{K}}$.

Equation (2.4) may also be written in the following tensor subscript form:-

$$v_i = - K_{ij} \frac{\partial h}{\partial x_i} \qquad (2.6)$$

If the aquifer is isotropic, then $\vec{\vec{K}}$ has only one independent component which is the coefficient of hydraulic conductivity. It follows that

$$K_{ij} = K\delta_{ij} \qquad (2.7)$$

where δ_{ij} denotes the Kronecker delta.

On substituting equation (2.7) into equation (2.6), the following equation for Darcy flow through isotropic material is obtained

$$v_i = - K \delta_{ij} \frac{\partial h}{\partial x_j} \qquad (2.8a)$$

Contracting subscript j gives

$$v_i = - K \frac{\partial h}{\partial x_i} \qquad (2.8b)$$

In general K_{ij} and K are functions of coordinates, unless the aquifer is homogeneous.

2.2.2 Range of Validity

The linear velocity-hydraulic gradient relationship known as Darcy's law has been derived theoretically by applying the Navier-Stokes differential equations of motion to the microscopic flow through porous media. ((Hubbert (1956), Irmay (1958)). In the derivation the microscopic flow velocity is assumed to be sufficiently small for the inertial terms in the Navier-Stokes equations to be negligible when compared with the viscous terms. Experimental investigations have confirmed that the linear relationship ceases to be valid as the

inertial effects become more important and that turbulent flow develops when Reynolds numbers become sufficiently high (Wright, (1968)).

By analogy to flow through pipes, several investigators have employed the Reynolds number as an index to classify the flow into linear and non-linear flow regimes. This approach has been justified by the application of dimensional analysis ((Rose (1945), Rose and Rizk (1949)). When adapted to flow through porous media, the Reynolds number is given by

$$\mathbb{R} = \frac{V\bar{d}\rho}{\mu} \qquad (2.9)$$

where ρ is the fluid density, V is the macroscopic velocity, $\bar{d}$ is a length characteristing the grains or pore size and μ is the dynamic viscosity of the fluid. The characteristic length suggested by Hazen (1893) is the grain diameter chosen such that 10 per cent by weight of the sample is of smaller size.

The Reynolds number defined in this manner is not a completely satisfactory criterion for determining the departure from Darcy's law or the onset of turbulence (Todd 1959, p.48), mainly because it does not take into account the general shape of separate grains and packing of these grains. Additional research is still needed to develop a better understanding of the flow transition. At present it is not possible to make reliable predictions of the validity limit of the linear relationship for a given porous medium. Permeability tests on natural sands and

artificial porous media have shown that the non-linear behaviour usually starts when $\mathbb{R}$ reaches a range between 1 and 10, depending on the range of grain size and shape and packing of the grains ((Lindquist (1933), Todd (1959)).

In view of the absence of a more satisfactory criterion, a critical value of the Reynolds number has been employed in the present study to distinguish Darcy from non-Darcy flow. The critical Reynolds number is defined as the limiting value above which the velocity-hydraulic gradient relationship is non-linear. The flow velocity corresponding to this Reynolds number is termed the "critical velocity"

In the theoretical and numerical analysis of two-regime well flow to be presented, it is more convenient to use the critical velocity than the critical Reynolds number. For a given sample of aquifer material, an approximate value of the critical velocity may be determined from the plot of its velocity-hydraulic gradient relationship.

2.3 Equations for Non-Darcy Flow in the Vicinity of Wells

Non-Darcy flow near a pumped well is described by the Forchheimer non-linear velocity-hydraulic gradient relation which, for one-dimensional parallel flow, may be written as

$$i = aV + bV^2 \qquad (2.10)$$

where i is the absolute hydraulic gradient, V is the absolute macroscopic flow velocity, a and b are termed the linear and non-linear coefficients of hydraulic resistance respectively.

The application of equation (2.10) to non-Darcy flow is justified as the equation has been derived theoretically using a microscopic

approach for both inertial laminar and turbulent flow (Irmay (1956), Sunada (1965), Stark and Volker (1967)). The non-linear term bV^2 has been shown to be caused by the increasing influence of inertial forces in the case of laminar flow and by inertial and turbulent effects if turbulence develops.

Permeability tests on natural and artifical porous media have confirmed that the equation may be used to describe the flow over a wide range of Reynolds number with the two coefficients a and b remaining approximately constant (Stark and Volker (1967)).

In order to describe three-dimensional non-Darcy flow through anisotropic media, equation (2.10) is transformed into the following vector differential form

$$\vec{\nabla} h = - (\vec{\vec{a}} + \vec{\vec{b}} |V|) \vec{V} \qquad (2.11)$$

where $\vec{\vec{a}}$ and $\vec{\vec{b}}$ denote the two hydraulic resistance tensors, the components of which are a_{ij} and b_{ij} respectively.

Equation (2.11) may also be written in the following tensor subscript form

$$\frac{\partial h}{\partial x_i} = - (a_{ij} + b_{ij} |V|) v_j \qquad (2.12)$$

where $|V|$ is the magnitude of the velocity vector

$$|V| = (v_i v_i)^{\frac{1}{2}} \qquad (2.13)$$

The components of the effective hydraulic conductivity tensor, E_{ij}, are now defined in accordance with

$$E_{ij} = (a_{ij} + b_{ij} |V|)^{-1} \qquad (2.14)$$

where E_{ij} are functions of $|V|$.

For isotropic aquifers, equation (2.12) reduces to

$$\frac{\partial h}{\partial x_i} = -(a + b|V|)v_i \qquad (2.15)$$

and equation (2.14) becomes

$$E_{ij} = (a+b|V|)^{-1}\,\delta_{ij} \qquad (2.16a)$$

or

$$E_{ij} = E\,\delta_{ij} \qquad (2.16b)$$

where E may be termed "the coefficient of effective hydraulic conductivity".

2.4 Derivation of Generalised Field Equations

2.4.1 The Continuity Equation

The continuity equation of flow in a slightly compressible porous medium may be developed by applying the law of conservation of matter to the flow of fluid. According to this law the net rate of mass of fluid entering the closed boundary of an arbitrary volume situated in the flow field is balanced by the rate of accumulation of fluid mass within the volume.

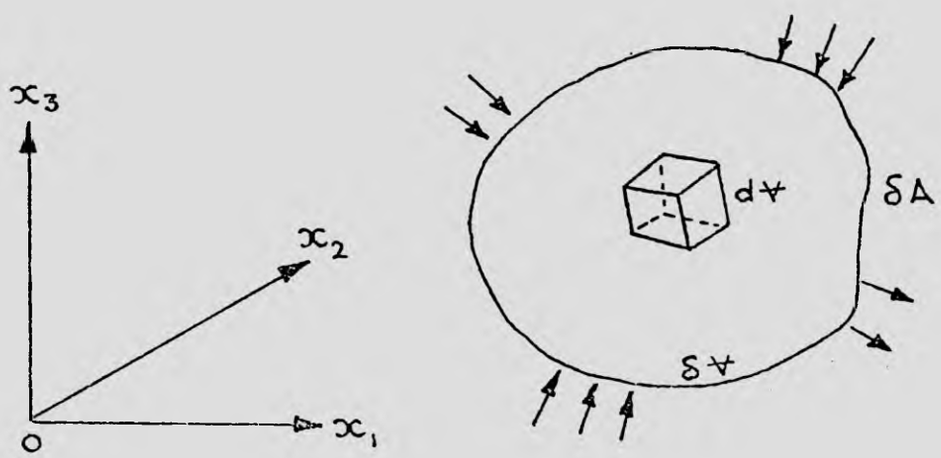

Fig. 2.2: An arbitrary closed region in the flow field.

Consider an elemental volume $\delta\forall$ of the aquifer situated in the flow field as shown in Fig. 2.2. Let δA be the surface area of the closed boundary of $\delta\forall$

The net rate of mass of water entering δA is given by

$$-\int_{\delta A} n_i \rho v_i \, dA$$

Where n_i are the components of the unit outward normal vector of the differential area dA, ρ is the density of water and v_i are the components of the velocity vector.

The rate of mass of water accumulated within $\delta\forall$ is

$$\int_{\delta\forall} \frac{\partial M}{\partial t} \frac{d\forall}{\delta\forall}$$

Since mass is conserved, it follows that

$$-\int_{\delta A} n_i \rho v_i \, dA = \int_{\delta\forall} \frac{\partial M}{\partial t} \frac{d\forall}{\delta\forall} \qquad (2.17)$$

The divergence theorem may now be applied to transform the surface integral into the volume integral. On replacing the left-hand term of equation (2.17) by its equivalent volume integral and re-arranging the terms, the following equation results.

$$\int_{\delta\forall} \left[\rho \frac{\partial v_i}{\partial x_i} + \frac{\partial M/\partial t}{\delta\forall} \right] d\forall = 0 \qquad (2.18)$$

Since the choice of $\delta\forall$ has been made arbitrarily, the integrand in equation (2.18) must vanish. It follows that

$$-\frac{\partial v_i}{\partial x_i} = \frac{\partial M/\partial t}{\rho \delta\forall} \qquad (2.19)$$

For a slightly compressible aquifer medium, it may be shown (Walton (1970), pp.122-123)) that the rate of mass of water accumulated and the rate of change of hydraulic head are related by

$$\frac{\partial M / \partial t}{\rho g \forall} = S_s \frac{\partial h}{\partial t} \qquad (2.20)$$

where S_s is termed the coefficient of specific storage of the aquifer.

Equation (2.20) may be substituted into equation (2.19) to give the required continuity equation as follows:

$$-\frac{\partial v_i}{\partial x_i} = S_s \frac{\partial h}{\partial t} \qquad (2.21)$$

2.4.2 The Differential Equations of Motion

The Darcy and the Forchheimer differential equations of motion have been set out in Sections 2.2 and 2.3. To describe two-regime well flow, the entire region of the aquifer is subdivided into two sub-regions namely R^D, where Darcy's law is valid, and R^N, where non-Darcy flow exists. Thus the Darcy differential equations are applicable in R^D whilst the Forchheimer equations are applicable in R^N. To determine whether a point in the flow field belongs to R^D or R^N, the critical velocity V_{cr} is employed. A point in the flow field belongs to R^N if and only if its absolute flow velocity is greater than V_{cr}.

The equations describing two-regime well flow may now be written as

$$v_i = - K_{ij} \frac{\partial h}{\partial x_j} \quad \text{for } |V| \leq V_{cr} \qquad (2.22a)$$

and

$$\frac{\partial h}{\partial x_i} = -(a_{ij} + b_{ij}|V|)\, v_j \qquad (2.22b)$$

for $|V| > V_{cr}$

2.4.3 The Generalised Field Equations

(i) Darcy Flow

The Darcy differential equations and the continuity equation can be combined to give the second order linear field equation which is generally applicable to transient three-dimensional Darcy flow in anisotropic and non-homogeneous aquifer media.

From equations (2.21) and (2.22a), it follows that

$$\frac{\partial}{\partial x_i}\left(K_{ij}\frac{\partial h}{\partial x_j}\right) = S_s \frac{\partial h}{\partial t} \qquad (2.23)$$

For isotropic and homogeneous aquifers, equation (2.23) reduces to

$$\frac{\partial}{\partial x_i}\left(K\frac{\partial h}{\partial x_i}\right) = S_s \frac{\partial h}{\partial t} \qquad (2.24)$$

where the coefficient K is a constant.

Equation (2.24) may be rearranged to give

$$\frac{\partial^2 h}{\partial x_i \partial x_i} = \frac{S_s}{K}\frac{\partial h}{\partial t} \qquad (2.25)$$

If the coefficient of diffusivity of the aquifer is defined as

$$\nu = \frac{K}{S_s}$$

then equation (2.25) becomes

$$\frac{\partial^2 h}{\partial x_i \partial x_i} = \frac{1}{\nu}\frac{\partial h}{\partial t} \qquad (2.26)$$

Equation (2.26) has been solved analytically for several cases of axi-symmetric Darcy flow involving relatively simple boundary conditions. A number of analytical solutions and methods for

evaluating the aquifer properties have been documented by Hantush (1964) and Walton (1971). In the present work, the available analytical solutions have been used to verify the finite element analysis to be described later.

(ii) Non-Darcy Flow

The non-linear field equation for non-Darcy flow through anisotropic aquifers may be obtained by combining the Forchheimer differential equations of motion with the continuity equation.

From equation (2.22b), it follows that

$$v_j = - (a_{ij} + b_{ij} |V|)^{-1} \frac{\partial h}{\partial x_i} \qquad (2.27)$$

Equation (2.27) may be substituted into equation (2.21) to result in

$$\frac{\partial}{\partial x_j} \left[(a_{ij} + b_{ij} |V|)^{-1} \frac{\partial h}{\partial x_i} \right] = S_s \frac{\partial h}{\partial t} \qquad (2.28)$$

Solution of the non-linear anisotropic equation (2.28) is beyond the scope of the present study. The present analysis assumed that the aquifer is isotropic in the non-Darcy zone. Such an assumption leads to a simplified non-linear field equation involving only h as a dependent variable.

For isotropic aquifers, equation (2.27) reduces to

$$\frac{\partial h}{\partial x_i} = - (a+b |V|) v_i \qquad (2.29)$$

Contracting subscript i gives

$$\frac{\partial h}{\partial x_i} \frac{\partial h}{\partial x_i} = (a + b |V|)^2 v_i v_i \qquad (2.30)$$

The absolute hydraulic gradient is now defined as

$$\left|\frac{\partial h}{\partial l}\right| = \left(\frac{\partial h}{\partial x_i}\ \frac{\partial h}{\partial x_i}\right)^{\frac{1}{2}} \qquad (2.31a)$$

Rearranging equation (2.31a) gives

$$\frac{\partial h}{\partial x_i}\ \frac{\partial h}{\partial x_i} = \left|\frac{\partial h}{\partial l}\right|^2 \qquad (2.31b)$$

Now

$$v_i\, v_i = |V|^2 \qquad (2.32)$$

Substituting equations (2.31b) and (2.32) into equation (2.30) gives

$$\left|\frac{\partial h}{\partial l}\right|^2 = (a + b\,|V|)^2\,|V|^2 \qquad (2.33)$$

Solving for $|V|$ results in

$$|V| = \frac{-a}{2b} + \sqrt{\left(\frac{a}{2b}\right)^2 + \frac{|\partial h/\partial l|}{b}} \qquad (2.34)$$

From equation (2.33), it follows that

$$\frac{|V|}{\left|\frac{\partial h}{\partial l}\right|} = \frac{1}{a+b\,|V|} \qquad (2.35)$$

Combining equations (2.29), (2.34) and (2.35) leads to

$$v_i = \left(\frac{-\frac{\partial h}{\partial x_i}}{\left|\frac{\partial h}{\partial l}\right|}\right)\left[-\frac{a}{2b} + \sqrt{\left(\frac{a}{2b}\right)^2 + \frac{|\partial h/\partial l|}{b}}\right] \qquad (2.36)$$

Equation (2.36) may now be substituted into the continuity equation to give the required field equation.

Hence

$$\frac{\partial}{\partial x_i}\left[\left(-\frac{a}{2b} + \sqrt{\left(\frac{a}{2b}\right)^2 + \frac{|\partial h/\partial l|}{b}}\right)\frac{(\partial h/\partial x_i)}{|\partial h/\partial l|}\right] = S_s\frac{\partial h}{\partial t} \qquad (2.37)$$

Equation (2.37) can also be written in a more compact form as follows:

$$\frac{\partial}{\partial x_i}\left[E\left(\frac{\partial h}{\partial x_i}\right)\right] = S_s \frac{\partial h}{\partial t} \qquad (2.38a)$$

where $$E = \left[-\frac{a}{2b} + \sqrt{\frac{a}{2b}^2 + \frac{\left|\frac{\partial h}{\partial l}\right|}{b}}\right] \frac{1}{\left|\frac{\partial h}{\partial l}\right|}$$

E has been termed "the coefficient of effective hydraulic conductivity".

The expression for E involves the square root term which may be rationalised to result in

$$E = 1/\left[\frac{a}{2} + \sqrt{\frac{a^2}{4} + b\left|\frac{\partial h}{\partial l}\right|}\right] \qquad (2.38b)$$

It is noted that if the non-linear Forchheimer coefficient b is set equal to zero, E merely becomes

$$E = 1/a \qquad (2.38c)$$

This is to be expected as the Forchheimer velocity-hydraulic gradient relation becomes linear when b = 0.

2.5 Initial and Boundary Conditions

Having derived the field equations governing transient two-regime well flow, it may now be stated that the flow problem is reducible to the mathematical problem of finding the function h satisfying these equations and the corresponding initial and boundary conditions.

To analyse various practical flow problems, the following types of initial and boundary conditions are considered:-

(i) Initial Condition

In solving transient well flow problems, the initial distribution of hydraulic head throughout the aquifer region is assumed to be a prescribed function of coordinates. The function is also assumed to be the known height of the water table above the datum plane. Accordingly, the initial condition may be expressed as

$$h(x_i, 0) = h^o(x_i) \; ; (x_i) \in \bar{R} \qquad (2.39)$$

where $h^o(x_i)$ is the initial height of the water table and $\bar{R}$ denotes the closed region of the flow system.

(ii) Boundaries and Boundary Conditions

(a) Pervious Boundaries

Pervious boundaries of the flow system are defined as boundaries across which there can be flux interchange between the flow system and its surroundings. Two types of conditions prevailing on these boundaries are considered as follows:-

Type 1: Prescribed Flux or Flow Rate

If the flux distribution on the boundary is known at any instant of time the resulting boundary condition is referred to as "prescribed flux condition". If, on the other hand, only the total flow rate across the boundary is known as a function of time, the resulting boundary condition is referred to as "prescribed flow rate condition".

Both the prescribed flux and prescribed flow rate conditions are classified as "type 1 boundary condition". They are expressed mathematically in the following manner:

Let B_1 be the portion of a pervious boundary where the flux distribution or flow rate is prescribed. If $\bar{q}$ denotes the prescribed inflow flux per unit area, the prescribed flux condition may be expressed as

$$v_i n_i = \bar{q} \qquad \text{on } B_1 \tag{2.40}$$

where v_i and n_i are the components of the velocity vector $\vec{V}$ and the outward normal vector $\vec{n}$ of the boundary surface respectively.

Also, if $\bar{Q}(t)$ denotes the prescribed flow rate at time t, the prescribed flow rate condition is given by

$$Q(t) = \bar{Q}(t) \quad \text{across } B_1 \tag{2.41}$$

Two common examples of "type 1" boundary conditions are the prescribed flux condition on the leaky boundary of an aquifer and the prescribed flow rate condition across the boundary of a well operating at a known discharge.

Type 2: Prescribed Head Condition

If the distribution of hydraulic head on the pervious boundaries is known at any instant of time, the resulting boundary condition is referred to as "Type 2" prescribed head condition and is written mathematically as

$$h = \bar{h} \qquad \text{on } B_2 \tag{2.42}$$

where $\bar{h}$ denotes the prescribed head function and B_2 denotes the boundary portion on which the hydraulic head is prescribed.

(b) Impervious Boundaries

Across impervious boundaries of the flow system, the velocities normal to the boundary surfaces are zero. The prevailing boundary condition is given by

$$v_i n_i = 0 \quad \text{on } B^c \tag{2.43}$$

where B^c denotes the impervious boundary portion.

(c) Free Surfaces

In the present work, a free surface is defined as a stream surface along which the pressure is atmospheric. In solving the problems of flow towards water table wells, the effects of capillary fringes on flow in the saturated region are neglected. The water table is taken as the upper bounding free surface. As the position of the water table at any instant of time during pumping is unknown a priori, it is located by trial and error during the course of solution of the flow problem.

Two conditions are satisfied on the free surface, the first of which is given by

$$h(x_i, t) = z(x_1, x_2, t) \quad \text{on } B^F \tag{2.44}$$

where $z(x_1, x_2, t)$ is the height of the free surface at point (x_1, x_2, t) above the datum plane and B^F denotes the free surface boundary.

The second condition is the requirement of continuity of flow across the boundary.

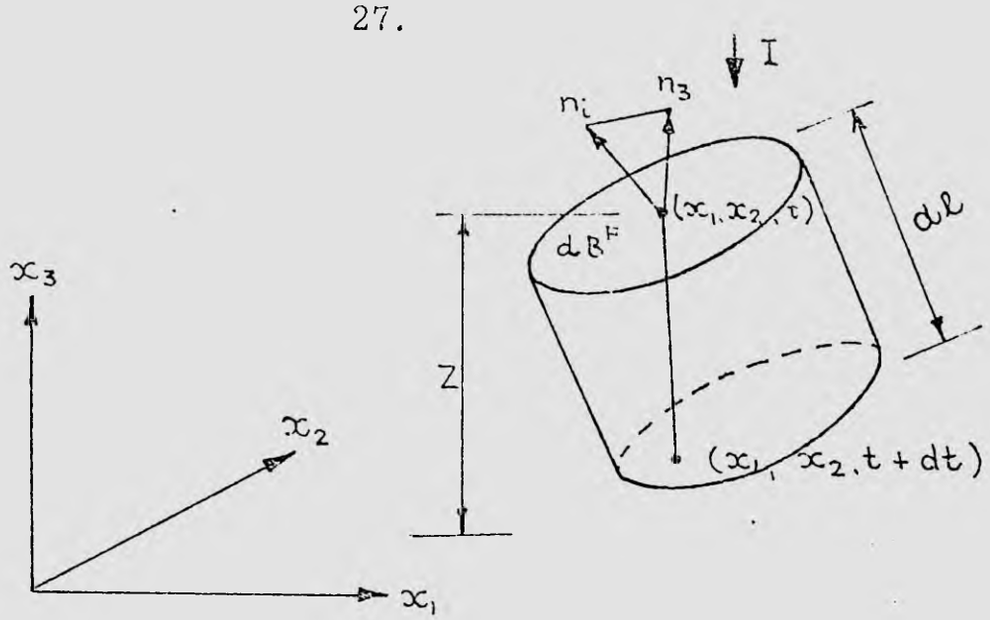

Fig. 2.3: Movement of a differential element of the free surface.

To derive this condition, consider a differential element of the free surface as shown in Fig. 2.3.

Let $z\,(x_1, x_2, t)$ denote the elevation at time t of a point (x_1, x_2) on dB^F. As pumping continues at a later time t+dt, the free surface position is lowered and point (x_1, x_2, t) now moves to $(x_1, x_2, t+dt)$.

If the net average of vertical infiltration is denoted by I, the volume of inflow into the free surface during an incremental time dt is given by

$$(v_i n_i + I n_3)\ dB^F\ dt$$

This inflow quantity must be balanced by the total volume of gravity drainage from storage within the elemental volume $d\forall = dB^F d\ell$.

To take into account the fact that the process of gravity drainage can take place slowly in finer aquifer materials, the expression for the total drainage volume is obtained by applying Boulton's concept and theory of delayed yield. ((Boulton (1955), (1963)). The theory is based on the assumption that the rate of delayed yield due to gravity drainage is an exponential function of time and proportional to the rate of lowering of the free surface.

Thus the total drainage volume taking place during an incremental time dt is given by

$$\left(\alpha \; S_y \int_o^t \frac{\partial z}{\partial \tau} \; e^{-\alpha (t-\tau)} \; d\tau \right) n_3 dB^F dt$$

where S_y is the ultimate volume of delayed yield per unit drawdown of the free surface per unit horizontal area, commonly referred to as the coefficient of specific yield, and α is an empirical constant termed the reciprocal of the delayed yield index.

The continuity equation may now be written as

$$(v_i n_i + In_3) \, dB^F dt = (\alpha S_y \int_o^t \frac{\partial z}{\partial \tau} e^{-\alpha(t-\tau)} d\tau) n_3 dB^F dt \qquad (2.45a)$$

Equation (2.45a) may be rearranged to result in the required boundary condition as follows:-

$$v_i n_i = - \left(I - \alpha S_y \int_o^t \frac{\partial z}{\partial \tau} \; e^{-\alpha(t-\tau)} d\tau \right) n_3 \qquad (2.45b)$$

For aquifer materials consisting of coarse sands or gravels in which the drainage process takes place quite rapidly, the delayed yield effect may be neglected and equation (2.45b) may be written in the following form:-

$$v_i n_i = - \left(I - S_y \frac{\partial z}{\partial t} \right) n_3 \qquad (2.45c)$$

where S_y becomes a constant taken to be approximately equal to the effective porosity of the aquifer material.

For the case of steady unconfined flow without vertical flux across the free surface, equations(2.45b) and (2.45c) reduce to

$$v_i n_i = 0 \qquad (2.46)$$

(d) Seepage Faces

In solving the unconfined flow problem, the presence of a vertical drainage or seepage face at the well is also considered. The seepage face is located directly below the water table and above the water level in the well. The prevailing boundary condition is written as

$$h\ (x_i, t) = x_3 \qquad \text{on } B^s \tag{2.47}$$

where B^s denotes the seepage face boundary.

3. Variational Principle for Two-regime Well Flow

3.1 General

In the previous chapter the fundamental approach to the general problem of transient two-regime well flow was presented, in which the flow was described by two field equations and the problem reduced to that of finding a function satisfying these equations as well as the initial and boundary conditions.

An alternative approach is possible via variational methods. In this approach an extremum principle valid over the entire flow region is postulated. The required solution is the one minimising a certain quantity Ω, termed "functional", subject to the same conditions of the flow system. The functional is defined by suitable integration of the unknown quantities over the region.

While the two approaches are mathematically equivalent in the sense that an exact solution of one is the solution of the other, the variational approach is particularly useful for the computation of an approximate solution by the finite element method to be described in the next chapter. Furthermore, the governing field equations may be obtained from the necessary conditions for minimisation of th. functional.

The variational principle for steady state Darcy flow through aquifers was first developed by Mau-ersberger (1965) and later extended by Neuman and Witherspoon ((1970), (1971)) to transient flow. The principle for non-Darcy flow has not been fully developed. Only the case of steady state two-dimensional flow was treated by Volker (1969) and McCorquodale (1969).

The purpose of this chapter is to present a generalised variational principle applicable to transient two-regime well flow through confined and unconfined aquifers. An energy theorem describing the flow is established and directly related to the variational principle. Via this theorem a physical meaning is assigned to the functional.

3.2 Development of Variational Principle

3.2.1 Variational Forms of the Field Equations

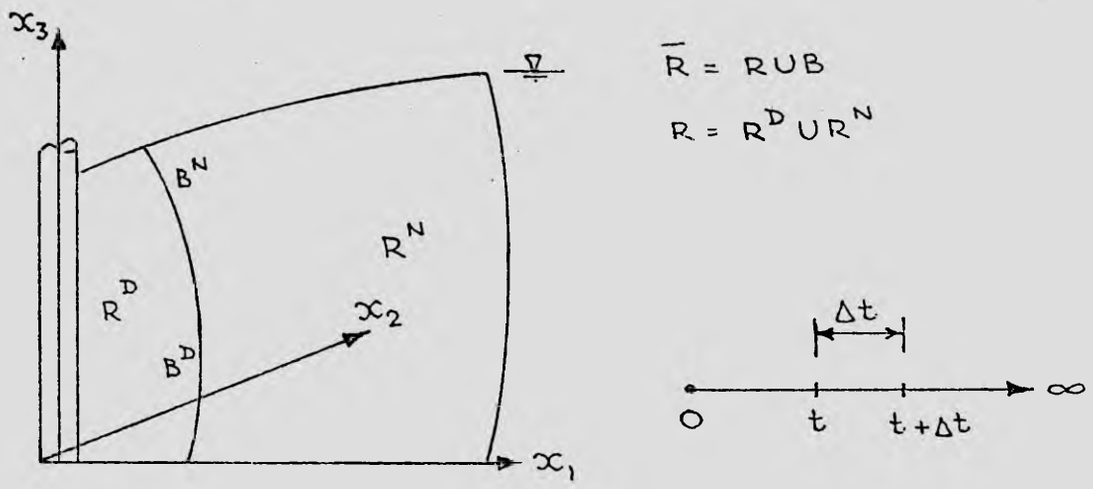

Fig. 3.1: A 3-dimensional space region and an open time domain.

Variational forms of the previously derived field equations may be obtained by considering an equivalent variational problem and employing the Euler-Lagrange equation from calculus of variations ((Wienstock (1952)).

Consider the general well-aquifer system shown in Fig. 3.1. As indicated above, (x_1, x_2, x_3) represents a right hand system of Cartesian coordinate axes, R^D and R^N are the Darcy and non-Darcy subregions of the flow system respectively.

Let $h(x_i, t)$ be an admissible function with the second order space and first order time derivatives

which are continuous everywhere in a given flow region R and let the time domain be subdivided into a number of finite time increments.

Assuming that h (x_i, t) is known at a particular time t, the general functional to be minimised over the space region R and the time increment Δt may be expressed as

$$\left[\Omega\,(h)\right]_R = \int_t^{t+\Delta t} \int_R G\left(h, \frac{\partial h}{\partial x_i}, \frac{\partial h}{\partial t}, x_i, t\right) dR\,dt \qquad (3.1)$$

The extremum problem is now reduced to seeking the function $h(x_i, t)$ which holds the above functional stationary. A necessary condition is the Euler-Lagrange equation which may be written as

$$\frac{\partial G}{\partial h} - \frac{\partial}{\partial x_i}\left(\frac{\partial G}{\partial\left(\frac{\partial h}{\partial x_i}\right)}\right) + \frac{\partial}{\partial t}\left(\frac{\partial G}{\partial\left(\frac{\partial h}{\partial t}\right)}\right) = 0 \qquad (3.2)$$

Equation (3.2) represents various classes of partial differential equation. The previously derived field equations can be shown to belong to one of these classes.

Thus on equating the field equations to equation (3.2), the expression for function G may be obtained.

(i) Non-Darcy Flow

The field equation describing non-Darcy flow through isotropic aquifers is now rewritten as

$$-\frac{\partial}{\partial x_i}\left[\left(\frac{-a}{2b} + \sqrt{\left(\frac{a}{2b}\right)^2 + \frac{\left|\frac{\partial h}{\partial l}\right|}{b}}\right) \frac{\left(\frac{\partial h}{\partial x_i}\right)}{\left|\frac{\partial h}{\partial l}\right|}\right] + S_s \frac{\partial h}{\partial t} = 0 \qquad (3.3)$$

Equation (3.3) is applicable everywhere in the non-Darcy flow subregion R^N. On equating it to equation (3.2), the following expressions result:

$$\frac{\partial G}{\partial h} = 0$$

$$\frac{\partial G}{\partial\left(\frac{\partial h}{\partial x_i}\right)} = \left(-\frac{a}{2b} + \sqrt{\left(\frac{a}{2b}\right)^2 + \frac{\left|\frac{\partial h}{\partial l}\right|}{b}}\right)\left(\frac{\frac{\partial h}{\partial x_i}}{\left|\frac{\partial h}{\partial l}\right|}\right)$$

$$\frac{\partial G}{\partial\left(\frac{\partial h}{\partial t}\right)} = h S_s$$

Integrating the above expressions leads to

$$G = -\frac{a}{2b}\left|\frac{\partial h}{\partial l}\right| + \frac{2}{3} b \left[\left(\frac{a}{2b}\right)^2 + \frac{\left|\frac{\partial h}{\partial l}\right|}{b}\right]^{3/2} + S_s h \frac{\partial h}{\partial t} \qquad (3.4)$$

Hence the required functional over the non-Darcy flow sub-region is given by

$$\left[\Omega(h)\right]_{R^N} = \int_t^{t+\Delta t} \int_{R^N} \left[-\frac{a}{2b}\left|\frac{\partial h}{\partial l}\right| + \frac{2}{3} b \left\{\left(\frac{a}{2b}\right)^2 + \frac{\left|\frac{\partial h}{\partial l}\right|}{b}\right\}^{3/2} + S_s h \frac{\partial h}{\partial t}\right] dR dt \qquad (3.5)$$

(ii) Darcy Flow

The field equation describing Darcy flow through anisotropic aquifers is rewritten as

$$-\frac{\partial}{\partial x_i}\left(K_{ij} \frac{\partial h}{\partial x_j}\right) + S_s \frac{\partial h}{\partial t} = 0 \qquad (3.6)$$

Equation (3.6) is applicable everywhere in R^D. On equating it to equation (3.2), the following equations are obtained :-

$$\frac{\partial G}{\partial h} = 0$$

$$\frac{\partial G}{\partial\left(\frac{\partial h}{\partial x_i}\right)} = K_{ij} \frac{\partial h}{\partial x_j}$$

$$\frac{\partial G}{\partial\left(\frac{\partial h}{\partial t}\right)} = h S_s$$

Integrating the above expressions leads to

$$G = \frac{1}{2} K_{ij} \frac{\partial h}{\partial x_j} \frac{\partial h}{\partial x_i} + S_s h \frac{\partial h}{\partial t} \qquad (3.7)$$

Hence the functional over subregion R^D is given by

$$[\Omega(h)]_{R^D} = \int_t^{t+\Delta t} \int_{R^D} \left[\frac{1}{2} K_{ij} \frac{\partial h}{\partial x_j} \frac{\partial h}{\partial x_i} + S_s h \frac{\partial h}{\partial t} \right] dR dt \qquad (3.8)$$

For isotropic aquifers, equation (3.8) reduces to

$$[\Omega(h)]_{R^D} = \int_t^{t+\Delta t} \int_{R^D} \left[\frac{1}{2} K \frac{\partial h}{\partial x_i} \frac{\partial h}{\partial x_i} + S_s h \frac{\partial h}{\partial t} \right] dR dt \qquad (3.9)$$

(iii) Statement of the Variational Problem

Let R be the union of R^N and R^D. The functional $[\Omega(h)]_R$ may be expressed as

$$[\Omega(h)]_R = [\Omega(h)]_{R^N} + [\Omega(h)]_{R^D} \qquad (3.10)$$

where $[\Omega(h)]_{R^N}$ and $[\Omega(h)]_{R^D}$ are the two portions contributed by R^N and R^D respectively. Their expressions are given by equations (3.5) and (3.8).

The variational problem reduces to finding an admissible function that minimises $[\Omega(h)]_R$ and also satisfies the existing initial and boundary conditions of the flow system. The classification of flow boundaries and boundary conditions according to their physical nature has been presented in Chapter 2.

3.2.2 Treatment of Initial and Boundary Conditions

(i) Initial Condition

At a particular time, taken as the initial time, the head distribution throughout the space region of the flow system is assumed to be known. If, in the minimisation of the functional, the time integration is carried out between time $t = 0$ and $t = \Delta t$, the admissible function will automatically satisfy the initial head condition represented by equation (2.39).

(ii) Boundary Conditions

In minimising the functional, the requirement of the conditions on the flow boundary must also be met. These requirements lead to extra terms that have to be added to the functional in Equation (3.10).

For the various types of boundary conditions described in the preceding chapter, the additional terms have been obtained by Neuman and Witherspoon ((1970), (1971)).

On boundary portion B_1 where the flux is prescribed, the additional term may be written as

$$\int_t^{t+\Delta t} \int_{B_1} h\,\bar{q}\, dB dt$$

On boundary portion B_2 where the function h is prescribed, it is given by

$$\int_t^{t+\Delta t} \int_{B_2} (h - \bar{h})\, v_i n_i\, dB dt$$

On the free surface B^F, there exist two additional terms which may be written as

$$\int_t^{t+\Delta t} \int_{B^F} (h-z)\, v_i n_i \, dB dt$$

and

$$-\int_t^{t+\Delta t} \int_{B^F} z\left(I - \alpha S_y \int_0^t \frac{\partial z}{\partial \tau} e^{-\alpha(t-\tau)} d\tau\right) n_3 \, dB dt$$

for the first and second free surface conditions respectively.

Finally on the seepage face B^S, the additional term is given by

$$\int_t^{t+\Delta t} \int_{B^S} (h - x_3)\, v_i n_i \, dB dt$$

where the expressions for v_i in terms of the hydraulic gradients are given by equations (2.22a) and (2.36) for Darcy and non-Darcy flow respectively.

3.3 Energy Approach to Well Flow Problems

3.3.1 General

Energy theorems provide an extremely powerful tool for the theoretical analysis of many physical problems. Via the energy approach, generalised field equations describing the physical phenomenon may be developed.

The energy concept for steady state groundwater flow complying with Darcy's law was first introduced by Muskat (1937). He postulated

that the actual distribution of hydraulic heads and flow velocities in a porous medium carrying a fluid under viscous flow conditions are such as to render the total loss of macroscopic energy of the fluid a minimum, subject to the existing boundary conditions of the flow system.

Engelund (1953) later extended the concept to two-dimensional steady non-Darcy flow. He showed that the integral expression of the rate of dissipation of hydraulic energy in the aquifer region is proportional to the functional of the non-linear field equation which he developed for non-Darcy flow through homogeneous and isotropic media.

In the development presented herein, the author attempts to establish in a rigorous manner the energy theorem for the general problem of three-dimensional, transient, two-regime flow through aquifers. It will be shown that the field equations governing the flow may be obtained by applying this theorem.

3.3.2 Dissipation of Energy in the Flow Region

The movement of groundwater occurs through the interconnected portion of the existing pore space within the aquifer medium. While flowing, the water particle loses some of its energy due to friction. The loss of hydraulic energy per unit distance travelled is usually expressed in terms of the hydraulic gradient.

When the macroscopic velocity lies within the range of the Darcy flow regime, it is observed to be linearly related to the hydraulic gradient. Departure from the linear relationship has been assumed to start at some critical velocity. Although experimental evidence shows

that the departure from linearity may not be abrupt, the assumption is sufficiently accurate for well flow analysis. The non-linear relationship has been represented by the Forchheimer equation.

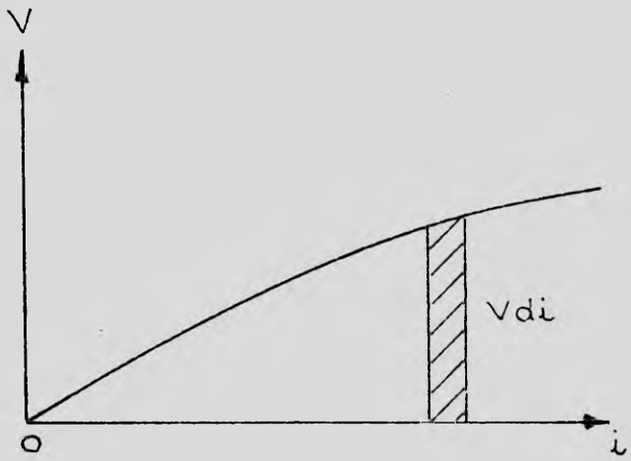

Fig. 3.2: Velocity-hydraulic gradient relationship for a hypothetical aquifer material.

A typical velocity-hydraulic gradient relationship for isotropic aquifers is shown in Fig. 3.2. The rate of dissipation of hydraulic energy within the aquifer volume may be evaluated as follows:-

Consider an arbitrary volume R of the aquifer situated in the flow field. Let a function $\dot{\phi}$, termed the "dissipation function", be defined in accordance with

$$\dot{\phi} = \int V di \tag{3.11}$$

$\dot{\phi}$ represents the rate of dissipation of hydraulic energy per unit weight of water. The rate of dissipation of energy within the volume R of the aquifer medium is given by

$$\dot{\chi}_1 = \gamma \int_R \dot{\phi}\, dR = \gamma \int_R \left(\int V di\right) dR \tag{3.12}$$

where γ is the specific weight of water.

The integral term in brackets may be evaluated, provided that an expression relating V and i is given.

3.3.3 Dissipation Function for Three-dimensional Flow

The general expression of the dissipation function for three-dimensional flow takes the following form

$$\dot{\phi} = - \int v_i \, d\left(\frac{\partial h}{\partial x_i}\right) \qquad (3.13)$$

where the repeated subscripts represent summation over the full range from one to three.

(i) Darcy Flow

For Darcy flow through anisotropic aquifers, the dissipation function becomes

$$\dot{\phi} = \int K_{ij} \frac{\partial h}{\partial x_j} \, d\left(\frac{\partial h}{\partial x_i}\right)$$

On integrating, the following expression is obtained

$$\dot{\phi} = \frac{1}{2} K_{ij} \frac{\partial h}{\partial x_j} \frac{\partial h}{\partial x_i} \qquad (3.14)$$

(ii) Non-Darcy Flow

The dissipation function for non-Darcy flow obeying the Forchheimer velocity-hydraulic gradient relation is given by

$$\dot{\phi} = \int (a_{ij} + b_{ij} |V|)^{-1} \frac{\partial h}{\partial x_j} \, d\left(\frac{\partial h}{\partial x_i}\right) \qquad (3.15a)$$

where the integration may not be readily carried out as $|V|$ is a function of the hydraulic gradient.

However, if the aquifer is isotropic, the integrated expression for $\dot{\phi}$ can be obtained in the following manner. For isotropic aquifer media equation (3.15a) reduces to

$$\dot{\phi} = \int (a + b|V|)^{-1} \frac{\partial h}{\partial x_i} \, d\left(\frac{\partial h}{\partial x_i}\right) \qquad (3.15b)$$

Now from equations (2.34) and (2.35), it follows that

$$(a + b|V|)^{-1} = \frac{-\frac{a}{2b} + \sqrt{\left(\frac{a}{2b}\right)^2 + \frac{\left|\frac{\partial h}{\partial l}\right|}{b}}}{\left|\frac{\partial h}{\partial l}\right|} \qquad (3.16)$$

Also

$$\left|\frac{\partial h}{\partial l}\right|^2 = \frac{\partial h}{\partial x_i} \frac{\partial h}{\partial x_i}$$

Differentiating gives

$$\left|\frac{\partial h}{\partial l}\right| d\left|\frac{\partial h}{\partial l}\right| = \frac{\partial h}{\partial x_i} d\left(\frac{\partial h}{\partial x_i}\right) \qquad (3.17)$$

Substituting equations (3.16) and (3.17) into equation (3.15b) gives

$$\dot{\phi} = \int \left(-\frac{a}{2b} + \sqrt{\left(\frac{a}{2b}\right)^2 + \frac{\left|\frac{\partial h}{\partial l}\right|}{b}}\right) d\left(\left|\frac{\partial h}{\partial l}\right|\right)$$

On integrating, the following expression for $\dot{\phi}$ is obtained

$$\dot{\phi} = -\frac{a}{2b}\left|\frac{\partial h}{\partial l}\right| + \frac{2}{3} b \left\{\left(\frac{a}{2b}\right)^2 + \frac{\left|\frac{\partial h}{\partial l}\right|}{b}\right\}^{3/2} \qquad (3.18)$$

3.3.4 Proposed Energy Theorem

(i) Development

Theorem 1: The movement of groundwater through saturated porous aquifer media takes place in such a manner that the total rate of energy change in the flow region is rendered a minimum, subject to the existing initial and boundary conditions of the flow system.

Proof:

Consider an arbitrary closed region $\bar{R}$ in the aquifer medium. Let R be the interior of $\bar{R}$ and dR be a differential volume of $\bar{R}$.

The total rate of energy change in the flow region consists of two portions, the first of which is given by

$$\dot{\chi}_1 = \gamma \int_R \dot{\phi} \, dR \tag{3.19}$$

where $\dot{\chi}_1$ denotes the rate of dissipation of hydraulic energy.

The second portion is due to volume compressibility of the elastic aquifer medium. It may be interpreted as the rate of change of elastic energy and may be expressed as

$$\dot{\chi}_2 = \gamma \int_R S_s h \frac{\partial h}{\partial t} \, dR \tag{3.20}$$

where S_s is the specific storage of the aquifer medium.

Let the region R be subdivided into subregions R^N and R^D, which are the non-Darcy and Darcy flow subregions respectively. It follows that

$$\dot{\chi} = \gamma \left[\int_{R^N} \dot{\phi} \, dR + \int_{R^N} S_s \frac{\partial h}{\partial t} h \, dR + \int_{R^D} \dot{\phi} \, dR + \int_{R^D} S_s \frac{\partial h}{\partial t} h \, dR \right] \tag{3.21}$$

where the expressions for $\dot{\phi}$ are given by equations (3.14) and (3.18) respectively.

Substituting equations (3.14) and (3.18) into equation (3.21) gives

$$\dot{\chi}/\gamma = \int_{R^N} \left[-\frac{a}{2b} \left|\frac{\partial h}{\partial l}\right| + \frac{2b}{3}\left\{\left(\frac{a}{2b}\right)^2 + \frac{\left|\frac{\partial h}{\partial l}\right|}{b}\right\}^{3/2} + S_s\, h \frac{\partial h}{\partial t}\right] dR + \int_{R^D} \left[\frac{1}{2} K_{ij} \frac{\partial h}{\partial x_i} \frac{\partial h}{\partial x_j} + S_s\, h \frac{\partial h}{\partial t}\right] dR \qquad (3.22)$$

The functional $\dot{\Omega}$ is now defined in accordance with

$$\dot{\Omega} = \dot{\chi}/\gamma \qquad (3.23)$$

The stationary condition of $\dot{\Omega}$ may be established by showing that the vanishing of its first variation leads to the admissible function satisfying the previously derived field equations. The condition of minimisation is assured by showing that the second variation is a positive definite quantity.

In order to find the first variation, let $h(x_j, t)$ be an admissible function which, together with its second order space and first order time derivatives, are continuous everywhere in region R. The function $h(x_i, t)$ must satisfy the initial and prescribed boundary conditions in order to be admissible.

The one-parameter family of "comparison functions" is now defined as

$$H(x_i, t) = h(x_i, t) + \lambda \delta h\ (x_i) \qquad (3.24)$$

where $\delta h(x_i)$ is an arbitrary function of coordinates, chosen to vanish on the flow boundary B, and λ is the real parameter of the family.

The first variation of $\dot{\Omega}$ is given by

$$\delta \dot{\Omega} = \frac{d}{d\lambda} \left[\dot{\Omega}(h + \lambda \delta h)\right]_{\lambda = 0} \qquad (3.25)$$

Since the function $\delta h(x_i)$ is chosen such that $\frac{\partial}{\partial t}(\delta h)$ vanishes, it follows that $\delta\dot{\Omega}$ may be written as

$$\delta\dot{\Omega} = \int_{R^N} \left[-\frac{a}{2b} \frac{\partial h}{\partial x_i} \frac{\partial(\delta h)}{\partial x_i} \Big/ \left|\frac{\partial h}{\partial l}\right| + \sqrt{\left(\frac{a}{2b}\right)^2 + \frac{\left|\frac{\partial h}{\partial l}\right|}{b}} \right.$$

$$\left. \frac{\partial h}{\partial x_i} \frac{\partial}{\partial x_i}(\delta h) \Big/ \left|\frac{\partial h}{\partial l}\right| + S_s \frac{\partial h}{\partial t} \delta h \right] dR$$

$$+ \int_{R^D} \left[K_{ij} \frac{\partial h}{\partial x_i} \frac{\partial}{\partial x_j}(\delta h) + S_s \frac{\partial h}{\partial t} \delta h \right] dR \qquad (3.26)$$

The theorem of integration by parts is now employed to obtain the following equation:

$$\int_{R^D} \left[K_{ij} \frac{\partial h}{\partial x_i} \frac{\partial}{\partial x_j}(\delta h) \right] dR = -\int_{R^D} \left[\frac{\partial}{\partial x_i}\left(K_{ij} \frac{\partial h}{\partial x_j}\right) \delta h \right] dR$$

$$+ \int_{B^D} \left[K_{ij} \frac{\partial h}{\partial x_i} n_j \delta h \right] dB \qquad (3.27)$$

where B^D is the boundary of subregion R^D.

Equation (3.27) may also be written in the form

$$\int_{R^D} \left[K_{ij} \frac{\partial h}{\partial x_i} \frac{\partial}{\partial x_j}(\delta h) \right] dR = -\int_{R^D} \left[\frac{\partial}{\partial x_i}\left(K_{ij} \frac{\partial h}{\partial x_j}\right) \delta h \right] dR$$

$$- \int_{B^D} \left[v_j n_j \delta h \right] dB \qquad (3.28)$$

In a similar manner, it may be shown that

$$\int_{R^N} \left[- \frac{a}{2b} \frac{\partial h}{\partial x_i} \frac{\partial}{\partial x_i} (\delta h) + \sqrt{\left(\frac{a}{2b}\right)^2 + \frac{\left|\frac{\partial h}{\partial l}\right|}{b}} \frac{\frac{\partial h}{\partial x_i}}{\left|\frac{\partial h}{\partial l}\right|} \frac{\partial}{\partial x_i} (\delta h) \right] dR$$

$$= - \int_{R^N} \left[\frac{\partial}{\partial x_i} \left\{ \left(- \frac{a}{2b} + \sqrt{\left(\frac{a}{2b}\right)^2 + \frac{\left|\frac{\partial h}{\partial l}\right|}{b}} \right) \frac{\frac{\partial h}{\partial x_i}}{\left|\frac{\partial h}{\partial l}\right|} \right\} (\delta h) \right] dR$$

$$- \int_{B^N} \left[v_j n_j \delta h \right] dB \qquad (3.29)$$

where B^N is the boundary of subregion R^N, which is in common with B^D as shown in Fig. 3.1.

Substituting equations (3.28) and (3.29) into equation (3.26) results in

$$\delta \dot{\Omega} = \int_{R^D} \left[- \frac{\partial}{\partial x_j} \left(K_{ij} \frac{\partial h}{\partial x_i} \right) + S_s \frac{\partial h}{\partial t} \right] \delta h \, dR + \int_{R^N} \left[\frac{\partial}{\partial x_i} \left\{ \left(- \frac{a}{2b} + \sqrt{\left(\frac{a}{2b}\right)^2 + \frac{\left|\frac{\partial h}{\partial l}\right|}{b}} \right) \frac{\frac{\partial h}{\partial x_j}}{\left|\frac{\partial h}{\partial l}\right|} \right\} + S_s \frac{\partial h}{\partial t} \right] \delta h \, dR - \int_{B^N} \left[v_j \, n_j \delta h \right] dB$$

$$- \int_{B^D} \left[v_j \, n_j \, \delta h \right] dB \qquad (3.30a)$$

where

$$\int_{B^N} \left[v_j \, n_j \, \delta h \right] dB + \int_{B^D} \left[v_j \, n_j \, \delta h \right] dB = 0$$

Equation (3.30a) reduces to

$$\delta\dot{\Omega} = \int_{R^D} \left[-\frac{\partial}{\partial x_i} \left(K_{ij} \frac{\partial h}{\partial x_j} \right) + S_s \frac{\partial h}{\partial t} \right] \delta h \, dR$$

$$+ \int_{R^N} \left[-\frac{\partial}{\partial x_i} \left\{ \left(-\frac{a}{2b} + \sqrt{\left(\frac{a}{2b}\right)^2 + \frac{\left|\frac{\partial h}{\partial l}\right|}{b}} \right) \frac{\left(\frac{\partial h}{\partial x_i}\right)}{\left|\frac{\partial h}{\partial l}\right|} \right\} + S_s \frac{\partial h}{\partial t} \right]$$

$$\delta h \, dR \qquad (3.30b)$$

The two integrals in equation (3.30b) can be shown to vanish independently when $\delta\dot{\Omega}$ is set to zero.

Thus it follows that

$$\int_{R^D} \left[-\frac{\partial}{\partial x_i} \left(K_{ij} \frac{\partial h}{\partial x_j} \right) + S_s \frac{\partial h}{\partial t} \right] \delta h \, dR = 0$$

and

$$\int_{R^N} \left[-\frac{\partial}{\partial x_i} \left\{ \left(-\frac{a}{2b} + \sqrt{\left(\frac{a}{2b}\right)^2 + \frac{\left|\frac{\partial h}{\partial l}\right|}{b}} \right) \frac{\left(\frac{\partial h}{\partial x_i}\right)}{\left|\frac{\partial h}{\partial l}\right|} \right\} + S_s \frac{\partial h}{\partial t} \right] \delta h \, dR = 0$$

Since the choice of δh may be made arbitrarily, the integrands of the above two integrals must vanish

Hence

$$-\frac{\partial}{\partial x_i} \left(K_{ij} \frac{\partial h}{\partial x_j} \right) + S_s \frac{\partial h}{\partial t} = 0 \qquad (3.31)$$

$$\text{for } (x_i) \in R^D$$

and

$$-\frac{\partial}{\partial x_i} \left[\left(-\frac{a}{2b} + \sqrt{\left(\frac{a}{2b}\right)^2 + \frac{\left|\frac{\partial h}{\partial l}\right|}{b}} \right) \frac{\left(\frac{\partial h}{\partial x_i}\right)}{\left|\frac{\partial h}{\partial l}\right|} \right] + S_s \frac{\partial h}{\partial t} = 0 \qquad (3.32)$$

$$\text{for } (x_i) \in R^N$$

Equations (3.31) and (3.32) are identical to the two field equations (2.23) and (2.37), previously derived for Darcy and non-Darcy flow respectively.

Thus it is now established that the flow of groundwater through porous aquifer media takes place in such a way that the total rate of energy change in the flow region is rendered stationary or extremised.

To ensure that the extremised functional corresponds to a minimum, it is sufficient to show that its second variation is a positive quantity. The remaining part of the proof is not presented. However, it is pointed out that the functional $\dot{\Omega}(h)$ is a positive definite quantity as in equation (3.22) the function h and its derivatives appear as squares and products.

(ii) Application

Before the introduction of the energy concept and theorem, the functional $[\Omega(h)]_R$ was constructed by applying the Euler-Lagrange equation to the field equations for Darcy and non-Darcy flow. It has just been established that via the energy approach the new functional $\dot{\Omega}(h)$ may be constructed without having to resort to these equations and that the minimisation of $\dot{\Omega}(h)$ leads to the same field equations. Also, if the function $h(x_i, t)$ is assumed to be known at an earlier time t and its time derivative is assumed to remain invariant between t and $t + \Delta t$, the two functionals are related by

$$[\Omega(h)]_R = \int_t^{t+\Delta t} \dot{\Omega}(h)\, dt \qquad (3.33)$$

Thus a physical meaning can be assigned to $[\Omega_{\cdot}(h)]_R$. It may be interpreted as the total energy change that takes place in the interior of the flow region between time t and $t + \Delta t$. Furthermore, the terms that have to be added to $[\Omega(h)]_R$ to account for additional boundary conditions of the flow system may be interpreted as energy exchanges between the system and its surroundings, which take place across the flow boundary over the time increment Δt.

It is finally pointed out that the energy theorem just proved remains invariant with respect to the choice of coordinate systems as energy is a scalar quantity which remains unchanged with change of coordinate systems.

4. Finite Element Analysis of Confined and Unconfined Flow Problems

4.1 General

In the previous chapter, variational forms of the field equations were derived and an equivalent variational problem was stated. The problem consists of finding an admissible function that minimises a certain functional subject to the existing initial and boundary conditions of the flow system.

An approximate solution of the above variational problem can be obtained by a numerical technique known as "the finite element method". In this technique, the continuous region of the flow system is subdivided into a finite number of closed subregions termed "finite elements". The finite elements are assumed to be interconnected at a discrete number of nodal points situated on their boundaries. Associated with each element is a chosen function that defines uniquely the hydraulic head distribution within the element in terms of its nodal parameters. The functional over the entire region of flow is assumed to be contributed by each element and the process of minimisation is accomplished by evaluating the elemental contributions, adding all such contributions, differentiating the resulting functional with respect to the nodal parameters and equating the differentials to zero. This process gives rise to a system of simultaneous algebraic equations which may be readily solved by either direct elimination or iterative methods.

The finite element analysis of axi-symmetric flow towards a pumped well is developed in this chapter. The analysis considers two flow regimes, namely the non-Darcy regime in the near well zone and the Darcy regime in the remaining portion of the flow region. Anisotropy of the aquifer material is taken into account only in the Darcy zone. The analysis of non-Darcy flow behaviour in anisotropic aquifers involves complex non-linear velocity-hydraulic gradient relations, the theoretical basis and experimental verification of which have not been established. Additional field and laboratory research is still required in order to develop a better understanding of the anisotropic character of the two coefficients of hydraulic resistance in the Forchheimer constitutive relation, namely coefficients a and b.

4.2 Subscript Notation

For convenience in presenting the finite element formulation for the general three-dimensional flow problem, the following subscript notation is adopted:-

Both capital letter and small letter subscripts are employed. The capital letter subscript refers to a particular node belonging to either an element or the entire flow region. The range of the subscript is from one to the number of nodes on the element boundary, if reference is made to the element, or from one to the total number of nodes, if reference is made to the entire flow region. The small letter subscript, as previously indicated, refers to a particular component along the coordinate axis. Its range is from one to three for three-dimensional space region.

Unless it is indicated, repeated subscripts are interpreted as summation over the full range and the same subscript does not appear more than twice in the same term of the expression.

4.3 Analysis of Flow through Confined Aquifers

4.3.1 Formulation of Element Matrices

(i) General

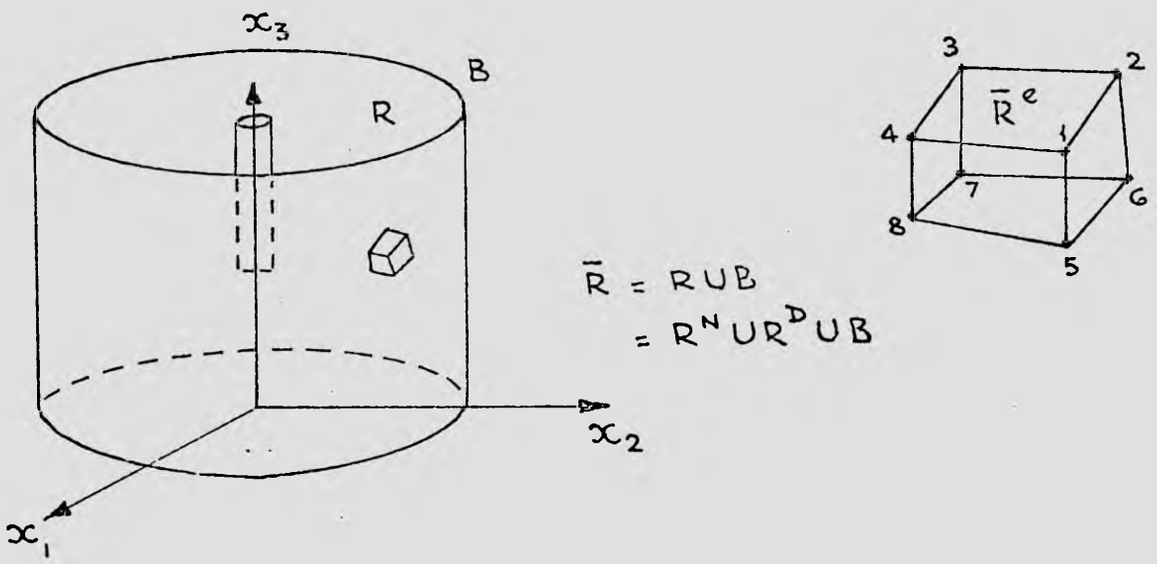

Fig. 4.1: Typical flow region of a confined aquifer and a finite element.

Consider the general problem of three-dimensional transient flow towards a pumped well penetrating a confined aquifer. A typical flow region $\bar{R}$ is shown in Fig. 4.1. As indicated, $\bar{R}$ is the union of R^N, R^D and B which are the non-Darcy flow subregion, the Darcy subregion and the flow boundary respectively.

The functional over $\bar{R}$ may be expressed as the sum of the functionals over R^N, R^D and B. Thus it follows that

$$\left[\Omega\,(h)\right]_{\bar{R}} = \left[\Omega\,(h)\right]_{R^N} + \left[\Omega\,(h)\right]_{R^D} + \left[\Omega\,(h)\right]_{B} \qquad (4.1)$$

The expressions for $[\Omega(h)]_{R^N}$ and $[\Omega(h)]_{R^D}$ have been derived in Chapter 3. They may be rewritten as

$$[\Omega(h)]_{R^N} = \int_t^{t+\Delta t} \int_{R^N} \left[-\frac{a}{2b}\left|\frac{\partial h}{\partial l}\right| + \frac{2}{3} b \left\{ \left(\frac{a}{2b}\right)^2 + \frac{\left|\frac{\partial h}{\partial l}\right|}{b} \right\}^{3/2} + S_s h \frac{\partial h}{\partial t} \right] dR dt \qquad (4.2)$$

and

$$[\Omega(h)]_{R^D} = \int_t^{t+\Delta t} \int_{R^D} \left[\frac{1}{2} K_{ij} \frac{\partial h}{\partial x_i} \frac{\partial h}{\partial x_j} + S_s h \frac{\partial h}{\partial t} \right] dR dt \qquad (4.3)$$

Let the closed boundary B of the confined flow region be subdivided into B_1 and B_2 which are the prescribed flow and the prescribed head portions respectively. The functional over the closed boundary $[\Omega(h)]_B$ is expressible as the sum of the functionals over B_1 and B_2. It follows that

$$[\Omega(h)]_B = \int_t^{t+\Delta t} \int_{B_1} h\bar{q}\, dB dt + \int_t^{t+\Delta t} \int_{B_2} (h - \bar{h})\, v_i\, n_i\, dB dt \qquad (4.4)$$

In solving the flow problem by the finite element method, the flow region $\bar{R}$ is discretised into a network consisting of m interconnected finite elements.

If the closed subregion of a typical element is denoted by $\bar{R}^e$ and if the number of nodes situated on the element boundary is n^e, the head distribution within the element may be approximated by

$$h(x_i, t) = N_I(x_i)\, h_I(t) \qquad (4.5)$$

where $N_I(x_i)$ are piecewisely defined functions of coordinates

(x_1, x_2, x_3) within the element, $h_I(t)$ are the nodal values at time t of the function h and the repeated subscript I denotes summation over the full range, from 1 to n^e.

The functional over the entire flow region, $[\Omega(h)]_{\bar{R}}$, may now be expressed as the sum of the functionals over the finite elements, $[\Omega(h)]_{\bar{R}^e}$, or more concisely $\Omega^e(h)$. Thus

$$[\Omega(h)]_{\bar{R}} = \sum_{e=1}^{m} \Omega^e(h) \qquad (4.6)$$

To obtain the final expression for $[\Omega(h)]_{\bar{R}}$, it is convenient to classify the finite elements in the entire network into "interior and exterior elements". The interior elements are defined as elements with their closed elemental boundaries contained within the interior of the flow region whilst the exterior elements are the remaining elements with portions of their closed boundaries as parts of the boundary of the flow region.

The evaluation of elemental contributions is thus accomplished by evaluating firstly the contributions from the interior elements and secondly the remaining contributions from the exterior elements. In the process of evaluation, it is assumed that the elements near the well are sufficiently small for $\bar{R}^e$ to be considered to belong to either R^N or R^D. The criterion for determining whether $\bar{R}^e$ belongs to R^N or R^D is as follows:-

If the absolute velocity at the centroid of the element is greater than the critical velocity, the element is considered to belong to R^N otherwise it belongs to R^D.

(ii) Interior Elements

(a) Elements belonging to R^N.

For the interior elements belonging to R^N, the functional over $\bar{R}^e$ is given by

$$\Omega^e(h) = \int_t^{t+\Delta t} \int_{R^e} \left[-\frac{a}{2b} \left|\frac{\partial h}{\partial l}\right| + \frac{2}{3} b \left\{ \left(\frac{a}{2b}\right)^2 + \frac{\left|\frac{\partial h}{\partial l}\right|}{b} \right\}^{3/2} + S_s h \frac{\partial h}{\partial t} \right] dR dt \qquad (4.7)$$

Differentiating equation (4.7) with respect to h_I gives

$$\frac{\partial \Omega^e(h)}{\partial h_I} = \int_t^{t+\Delta t} \int_{R^e} \left[-\frac{a}{2b} \frac{\partial}{\partial h_I} \left(\left|\frac{\partial h}{\partial l}\right|\right) + \left\{ \left(\frac{a}{2b}\right)^2 + \frac{\left|\frac{\partial h}{\partial l}\right|}{b} \right\}^{\frac{1}{2}} \frac{\partial}{\partial h_I} \left(\left|\frac{\partial h}{\partial l}\right|\right) + S_s h \frac{\partial}{\partial h_I} \left(\frac{\partial h}{\partial t}\right) + S_s \frac{\partial h}{\partial t} \frac{\partial h}{\partial h_I} \right] dR dt \qquad (4.8)$$

Where it should be noted that the small letter s is not regarded as a small letter subscript, S_s merely denotes the coefficient of specific storage of the aquifer.

From equation (4.5), it follows that

$$\frac{\partial h}{\partial x_i} = \frac{\partial N_I}{\partial x_i} h_I \qquad (4.9)$$

Contracting subscript i gives

$$\frac{\partial h}{\partial x_i} \frac{\partial h}{\partial x_i} = \frac{\partial N_I}{\partial x_i} h_I \frac{\partial N_J}{\partial x_i} h_J \qquad (4.10)$$

Now

$$\left|\frac{\partial h}{\partial l}\right|^2 = \frac{\partial h}{\partial x_i}\ \frac{\partial h}{\partial x_i} \tag{4.11}$$

Differentiating equation (4.11) with respect to h_I gives

$$\frac{\partial}{\partial h_I}\left(\left|\frac{\partial h}{\partial l}\right|\right) = \frac{\frac{\partial h}{\partial x_i}\ \frac{\partial}{\partial h_I}\left(\frac{\partial h}{\partial x_i}\right)}{\left|\frac{\partial h}{\partial l}\right|} \tag{4.12}$$

Also from equation (4.9) it follows that

$$\frac{\partial}{\partial h_I}\left(\frac{\partial h}{\partial x_i}\right) = \frac{\partial N_I}{\partial x_i} \tag{4.13}$$

Substituting equations (4.9) and (4.13) into equation (4.12) results in

$$\frac{\partial}{\partial h_I}\left(\left|\frac{\partial h}{\partial l}\right|\right) = \frac{\frac{\partial N_J}{\partial x_i}\ h_J\ \frac{\partial N_I}{\partial x_i}}{\left|\frac{\partial h}{\partial l}\right|} \tag{4.14}$$

Since N_I are functions which do not vary with time, it follows that

$$h\ \frac{\partial}{h_I}\left(\frac{\partial h}{\partial t}\right) = N_J h_J\ \frac{\partial N_I}{\partial t} = 0 \tag{4.15}$$

and

$$\frac{\partial h}{\partial t}\ \ \frac{\partial h}{\partial h_I} = \frac{\partial h_J}{\partial t} N_J N_I \tag{4.16}$$

Substituting equations (4.14) to (4.16) into equation (4.8) gives

$$\frac{\partial \Omega^e}{\partial h_I} = \int_t^{t+\Delta t}\int_{R^e}\left[-\frac{a}{2b} + \left\{\left(\frac{a}{2b}\right)^2 + \frac{\left|\frac{\partial h}{\partial l}\right|}{b}\right\}^{\frac{1}{2}}\right]\frac{1}{\left|\frac{\partial h}{\partial l}\right|}$$

$$\frac{\partial N_J}{\partial x_i}\ \ \frac{\partial N_I}{\partial x_i}\ h_J\ dRdt$$

$$+ \int_t^{t+\Delta t}\int_{R^e} S_s\ \frac{\partial h_J}{\partial t}\ N_J\ N_I\ dRdt \tag{4.17}$$

The following expressions are now introduced

$$E = \left[-\frac{a}{2b} + \left\{ \left(\frac{a}{2b} \right)^2 + \left\{ \frac{\left| \frac{\partial h_i}{\partial l} \right|}{b} \right\}^{\frac{1}{2}} \right] \frac{1}{\left| \frac{\partial h}{\partial l} \right|} \qquad (4.18a)$$

$$C^e_{JI} = \int_{R^e} E \frac{\partial N_J}{\partial x_i} \frac{\partial N_I}{\partial x_i} \, dR \qquad (4.18b)$$

$$D^e_{JI} = \int_{R^e} S_s \, N_J \, N_I \, dR \qquad (4.18c)$$

Substituting these expressions into equation (4.17) results in

$$\frac{\partial \Omega^e}{\partial h_I} = \int_t^{t+\Delta t} C^e_{JI} \, h_J \, dt + \int_t^{t+\Delta t} D^e_{JI} \frac{\partial h_J}{\partial t} \, dt \qquad (4.19)$$

where J and I range from 1 to the number of nodes on the element boundary, n^e.

(b) Elements belonging to R^D

For the interior elements belonging to R^D, the functional over R^e is given by

$$\Omega^e (h) = \int_t^{t+\Delta t} \int_{R^e} \left[\frac{1}{2} K_{ij} \frac{\partial h}{\partial x_j} \frac{\partial h}{\partial x_i} + S_s \, h \frac{\partial h}{\partial t} \right] dR dt \qquad (4.20)$$

Differentiating equation (4.20) with respect to h_I gives

$$\frac{\partial \Omega^e}{\partial h_I} = \int_t^{t+\Delta t} \int_{R^e} \left[K_{ij} \frac{\partial h}{\partial x_j} \frac{\partial}{\partial h_I} \left(\frac{\partial h}{\partial x_i} \right) + S_s \, h \frac{\partial}{\partial h_I} \left(\frac{\partial h}{\partial t} \right) + S_s \frac{\partial h}{\partial t} \frac{\partial h}{\partial h_I} \right] dR dt \qquad (4.21)$$

Substituting equations (4.13), (4.15) and (4.16) into equation (4.21) gives

$$\frac{\partial \Omega^e}{\partial h_I} = \int_t^{t+\Delta t} \int_{R^e} \left[K_{ij} \frac{\partial N_I}{\partial x_j} h_J \frac{\partial N_J}{\partial x_i} + S_s \frac{\partial h_I}{\partial t} N_J N_I \right] dR dt \qquad (4.22)$$

Introducing

$$C'^e_{JI} = \int_{R^e} K_{ij} \frac{\partial N_J}{\partial x_j} \frac{\partial N_I}{\partial x_i} dR \qquad (4.23)$$

and substituting equations (4.18c) and (4.23) into equation (4.22) lead to

$$\frac{\partial \Omega^e}{\partial h_I} = \int_t^{t+\Delta t} C'^e_{JI} h_J \, dt + \int_t^{t+\Delta t} D^e_{JI} \frac{\partial h_J}{\partial t} \, dt \qquad (4.24)$$

(iii) Exterior Elements

In evaluating the functional contributed by an exterior element, allowance must be made for the additional boundary conditions on the element boundary. Accordingly, extra terms must be added to the functional already derived for the interior elements. These terms only exist on the exterior portion of the element boundary and vanish elsewhere.

The additional boundary conditions of confined flow problems are the prescribed flux and prescribed head conditions. They may be dealt with in the following manner:-

If B_1^e and B_2^e denote the exterior portions of the closed element boundary where the flux and the head functions are prescribed respectively, the additional terms are given by

$$\int_t^{t+\Delta t} \int_{B_1^e} h\bar{q}\ dBdt$$

and

$$\int_t^{t+\Delta t} \int_{B_2^e} (h-\bar{h})\ v_i n_i\ dBdt$$

Thus for the exterior elements belonging to R^N, the resulting functional over $\bar{R}^e$ takes the form

$$[\Omega(h)]_{\bar{R}^e} = \int_t^{t+\Delta t} \int_{R^e} \left[\frac{-a}{2b} \left|\frac{\partial h}{\partial l}\right| + \frac{2b}{3} \left\{ \left(\frac{a}{2b}\right)^2 + \left|\frac{\frac{\partial h}{\partial l}}{b}\right| \right\}^{3/2} + S_s\, h \frac{\partial h}{\partial t} \right] dRdt + \int_t^{t+\Delta t} \int_{B_1^e} h\,\bar{q}\ dBdt$$

$$+ \int_t^{t+\Delta t} \int_{B_2^e} (h - \bar{h})\ v_i\, n_i\ dBdt \qquad (4.25a)$$

Since the admissible function h is chosen to automatically satisfy the prescribed head condition on the entire flow boundary, the term contributed by B_2^e may be dropped from equation (4.25a).

Equation (4.25a) now becomes

$$[\Omega^e(h)]_{\bar{R}^e} = \int_t^{t+\Delta t} \int_{R^e} \left[-\frac{a}{2b} \left|\frac{\partial h}{\partial l}\right| + \frac{2b}{3} \left\{ \left(\frac{a}{2b}\right)^2 + \left|\frac{\frac{\partial h}{\partial l}}{b}\right| \right\}^{3/2} + S_s\, h \frac{\partial h}{\partial t} \right] dRdt + \int_t^{t+\Delta t} \int_{B_1^e} h\bar{q}\ dBdt \qquad (4.25b)$$

Differentiating equation (4.25b) with respect to h_I gives

$$\frac{\partial \Omega^e}{\partial h_I} = \int_t^{t+\Delta t} C_{JI}^e \, h_J dt + \int_t^{t+\Delta t} D_{JI}^e \frac{\partial h_J}{\partial t} \, dt + \int_t^{t+\Delta t} F_I^e \, dt \qquad (4.26)$$

where

$$F_I^e = \int_{B_1^e} \bar{q} \, N_I \, dB \qquad (4.27)$$

Similarly for the elements belonging to R^D, the expression for the functional may be written as

$$\left[\Omega(h)\right]_{\bar{R}^e} = \int_t^{t+\Delta t} \int_{R^e} \left[\frac{1}{2} K_{ij} \frac{\partial h}{\partial x_j} \frac{\partial h}{\partial x_i} + S_s h \frac{\partial h}{\partial t}\right] dR dt + \int_t^{t+\Delta t} \int_{B_1^e} h\bar{q} \, dB dt \qquad (4.28)$$

Differentiating equation (4.28) with respect to h_I gives

$$\frac{\partial \Omega^e}{\partial h_I} = \int_t^{t+\Delta t} \acute{C}_{JI}^e \, h_J \, dt + \int_t^{t+\Delta t} D_{JI}^e \frac{\partial h_J}{\partial t} \, dt + \int_t^{t+\Delta t} F_I^e dt \qquad (4.29)$$

(iv) Element Matrices

The above formulation leads to various element matrices which have been expressed in subscript form. The expressions are given by equations (4.16b), (4.18c), (4.23) and (4.27). They can also be written in compact matrix form as follows:-

Let $[C^e]$, $[\acute{C}^e]$, $[D^e]$ and $[F^e]$ denote the element matrices having C_{IJ}^e, $\acute{C}_{IJ}^e$, D_{IJ}^e and F_I^e as matrix elements respectivcly. By

employing the matrix notation, the following equations may be written

$$[C^e] = \int_{R^e} E\,[S]^T\,[S]\;dR \tag{4.30}$$

$$[\acute{C}^e] = \int_{R^e} [S]^T\,[K]\,[S]\;dR \tag{4.31}$$

$$[D^e] = \int_{R^e} S_s\,[N]^T\,[N]\;dR \tag{4.32}$$

$$[F^e] = \int_{B_1^e} \bar{q}\,[N]^T\;dB \tag{4.33}$$

where E is given by

$$E = \left[-\frac{a}{2b} + \left\{ \left(\frac{a}{2b}\right)^2 + \left|\frac{\partial h}{\partial l}\right| \right\}^{\frac{1}{2}} \right] \frac{1}{\left|\frac{\partial h}{\partial l}\right|}$$

or

$$E = 1/\left[\frac{a}{2} + \sqrt{\frac{a^2}{4} + b\left|\frac{\partial h}{\partial l}\right|} \right] \tag{4.34a}$$

$$\left|\frac{\partial h}{\partial l}\right| = \left(\frac{\partial N_I}{\partial x_i}\,\frac{\partial N_J}{\partial x_i}\,h_I\,h_J \right)^{\frac{1}{2}} \tag{4.34b}$$

$[S]^T$ is the transpose of matrix $[S]$ which is given by

$$[S]^T = \begin{bmatrix} \frac{\partial N_1}{\partial x_1} & \cdots & \frac{\partial N_n^e}{\partial x_1} \\ \frac{\partial N_1}{\partial x_2} & \cdots & \frac{\partial N_n^e}{\partial x_2} \\ \frac{\partial N_1}{\partial x_3} & \cdots & \frac{\partial N_n^e}{\partial x_3} \end{bmatrix}^T \tag{4.35}$$

[K] is the hydraulic conductivity matrix, which may be written as

$$[K] = \begin{bmatrix} K_{11} & K_{12} & K_{13} \\ K_{21} & K_{22} & K_{23} \\ K_{31} & K_{32} & K_{33} \end{bmatrix} \tag{4.36}$$

[N]is the shape function matrix, which is given by

$$[N] = [N_1 \cdot \cdot \cdot \cdot \cdot \cdot \cdot \cdot \cdot N_{ne}] \tag{4.37}$$

The equations relating the differentials of the functional Ω^e and the nodal values of the function h may also be written in matrix form. The matrix equation for the exterior elements in the non-Darcy flow subregion is obtained from eq. (4.26)It follows that

$$\left[\frac{\partial \Omega}{\partial h}\right]^e = \int_t^{t+\Delta t} [C^e]\,[h^e]dt + \int_t^{t+\Delta t} [D^e]\left[\frac{\partial h}{\partial t}\right]^e dt + \int_t^{t+\Delta t} [F^e]\,dt \tag{4.38}$$

where

$$\left[\frac{\partial \Omega^e}{\partial h}\right] = \begin{bmatrix} \frac{\partial \Omega^e}{\partial h_1} \\ \vdots \\ \frac{\partial \Omega^e}{\partial h_{ne}} \end{bmatrix} \qquad [h^e] = \begin{bmatrix} h_1 \\ \vdots \\ h_{ne} \end{bmatrix}$$

The matrix equation for the interior elements in the non-Darcy flow subregion is obtained from equation(4.38) by dropping the last integral term on the right hand side.

Hence

$$\left[\frac{\partial \Omega^e}{\partial h}\right] = \int_t^{t+\Delta t} [C^e][h^e]\, dt + \int_t^{t+\Delta t} [D^e]\left[\frac{\partial h}{\partial t}\right]^e dt \qquad (4.39)$$

Similarly, the matrix equations for the exterior and interior elements in the Darcy flow subregion may also be obtained from equations (4.38) and (4.39) respectively by merely replacing matrix $[C^e]$ in these equations by $[\acute{C}^e]$.

4.3.2 Element Matrices for Triangular Ring Elements

The formulation of the element matrix just presented is a general procedure applicable to three-dimensional well flow. Many problems of flow towards wells encountered in practice are axi-symmetric flow problems. For problems of this kind, the formulation of element matrices may be simplified by employing cylindrical coordinate system (r, z). The entire flow region may be subdivided into a finite number of ring elements concentric about the vertical axis of the well. These elements are readily generated by revolving plane sections about the z-axis. A typical triangular ring element is shown in Fig. 4.2.

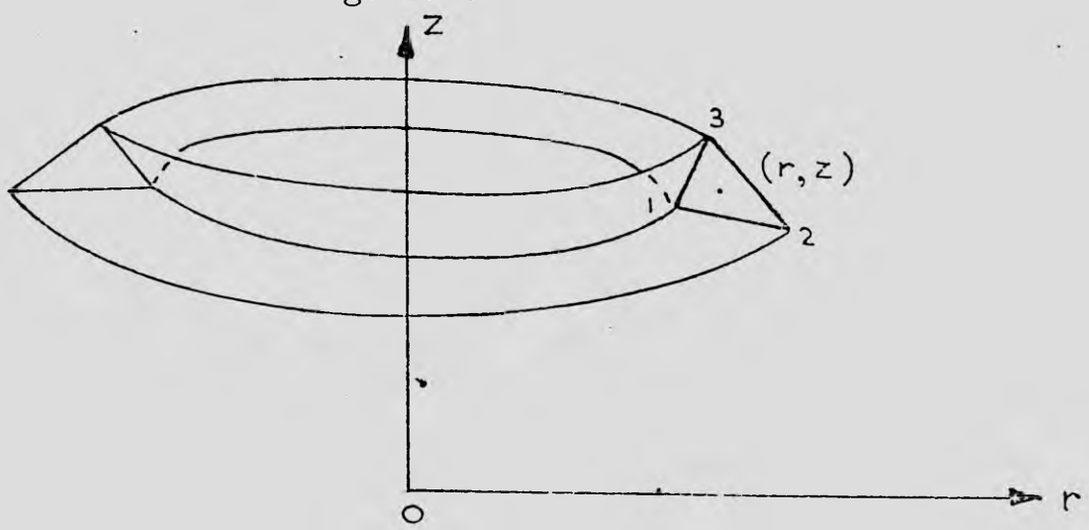

Fig. 4.2: A typical triangular ring element.

If the hydraulic head distribution at point (r, z) in the element is represented by a linear function of r and z in terms of the nodal values, then it can be shown ((Zienkiewicz and Cheung (1967)) that the shape functions may be expressed as

$$N_I = a_I + b_I r + c_I z \tag{4.40}$$

where a_1, b_1 and c_1 are given by

$$a_1 = (r_2 z_3 - r_3 z_2)/2\Delta \tag{4.41a}$$

$$b_1 = (z_2 - z_3)/2\Delta \tag{4.41b}$$

$$c_1 = (r_3 - r_2)/2\Delta \tag{4.41c}$$

and the remaining coefficients are obtained by cyclic permutation of subscripts and Δ is the area of triangle 1-2-3.

$$\Delta = \frac{1}{2} \begin{vmatrix} 1 & r_1 & z_1 \\ 1 & r_2 & z_2 \\ 1 & r_3 & z_3 \end{vmatrix} \tag{4.41d}$$

Now from equation (4.40) it follows that

$$\frac{\partial N_I}{\partial r} = b_I \tag{4.41e}$$

$$\frac{\partial N_I}{\partial z} = c_1 \tag{4.41f}$$

Hence the matrix $[S]^T$ may be written as

$$[S]^T = \begin{bmatrix} b_1 & b_2 & b_3 \\ c_1 & c_2 & c_3 \end{bmatrix}^T \tag{4.42a}$$

For cylindrical coordinate systems, the hydraulic conductivity matrix is given by

$$[K] = \begin{bmatrix} K_{rr} & K_{rz} \\ K_{rz} & K_{zz} \end{bmatrix} \tag{4.42b}$$

The shape function matrix for triangular elements is

$$[N] = [N_1, N_2, N_3] \tag{4.42c}$$

where the expressions for N_1, N_2 and N_3 are given by equation (4.40).

The expressions for element matrices $[C^e]$ and $[\acute{C}^e]$ can be obtained by direct integration, noting that dR has to be replaced by

$$dR = 2\pi r\,dr\,dz \tag{4.42d}$$

Thus

$$C^e_{IJ} = \int_{R^e} [E \frac{\partial N_I}{\partial x_i} \frac{\partial N_J}{\partial x_i}] 2\pi r\,dr\,dz \tag{4.43a}$$

Equation (4.43a) may be approximated by

$$C^e_{IJ} = 2\pi \bar{r} \Delta E(b_I b_J + c_I c_J) \tag{4.43b}$$

where $\bar{r}$ is the centroidal radius of the triangular plane section and the expression for E is given by equation (4.34a).

Similarly the array elements of matrix $[\acute{C}^e]$ are expressible as

$$\acute{C}^e_{IJ} = \int_{R^e} [K_{ij} \frac{\partial N_I}{\partial x_i} \frac{\partial N_J}{\partial x_j}] 2\pi r\,dr\,dz \tag{4.44a}$$

Substituting for the various terms on the right hand side leads to

$$\acute{C}^e_{IJ} = 2\pi \bar{r} \Delta (K_{rr} b_I b_J + K_{rz} b_I c_J + K_{zr} c_I b_J + K_{zz} c_I c_J) \tag{4.44b}$$

in which r and z are not regarded as small letter subscripts.

The integration for the matrix elements of $[D^e]$ and $[F^e]$ requires slightly more labour. The two matrices have been evaluated by

Parekh (1967). They may be written as

$$[D^e] = \frac{2\pi \bar{r}\, S_s\, \Delta}{3} \begin{bmatrix} \frac{1}{2} & \frac{1}{4} & \frac{1}{4} \\ \frac{1}{4} & \frac{1}{2} & \frac{1}{4} \\ \frac{1}{4} & \frac{1}{4} & \frac{1}{2} \end{bmatrix} \tag{4.45}$$

$$[F^e] = 2\pi \bar{r}\, \bar{q}\, L \begin{bmatrix} \frac{1}{2} \\ \frac{1}{2} \\ 0 \end{bmatrix} \tag{4.46}$$

where it is assumed in equation (4.46) that side 1-2 of triangle 1-2-3 corresponds to the exterior boundary portion on which the flux is prescribed and that $\bar{q}$ is constant on side 1-2 of the triangle; the length of this side is denoted by L.

4.3.3 Element Matrices for Isoparametric Ring Elements

(i) One-dimensional Elements

The problem of one-dimensional radial flow towards a pumped well fully screened through the entire thickness of an isotropic aquifer may be solved by using one-dimensional isoparametric elements.

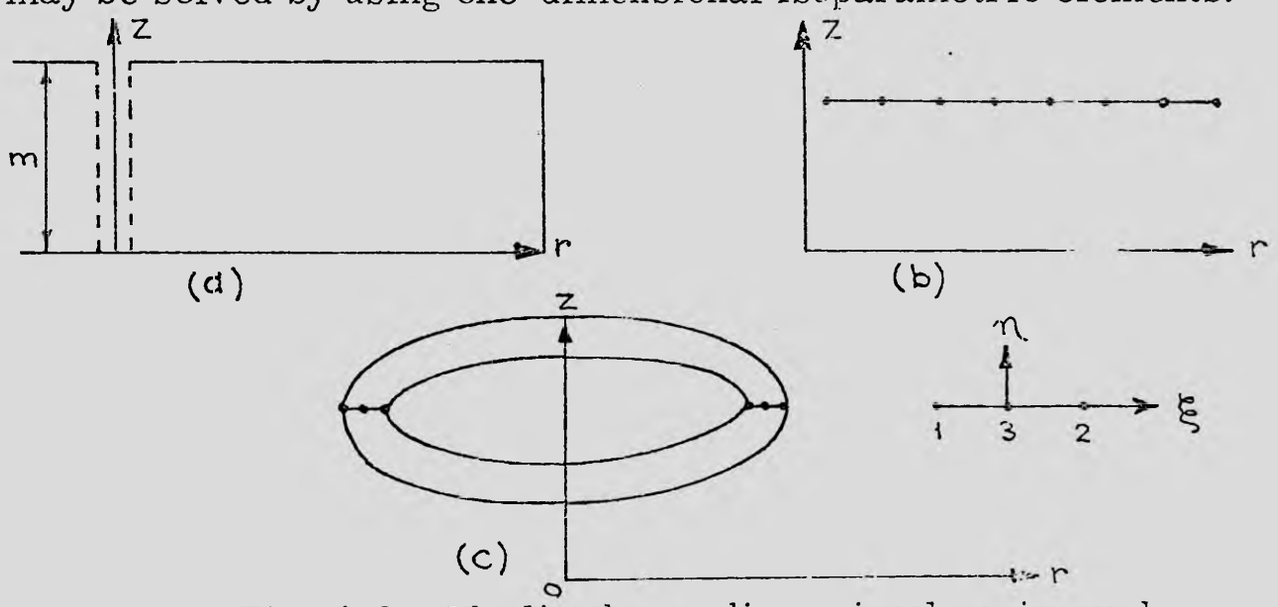

Fig. 4.3: Idealised one-dimensional region and one-dimensional isoparametric elements.

Consider a typical well-aquifer system shown in Fig. 4.3a. Since the velocity of flow is in the radial direction, it is sufficient to find the hydraulic head distribution along any radial line. Accordingly, the two-dimensional region in r-z plane shown in Fig. 4.3a may be reduced to a radial line shown in Fig. 4.3b. This line is discretised into a network of line elements. A typical 3-node element is shown in Fig. 4.3c. The planar ring section is readily generated by revolving the line element about the z-axis.

Let ξ be a local coordinate associated with each of the line elements. The coordinate is so determined as to give $\xi = 0$ at node 3, $\xi = 1$ at node 2 and $\xi = -1$ at node 1. The relationship between the radial coordinate and ξ-coordinate is given by

$$r = \alpha_1 + \alpha_2 \xi + \alpha_3 \xi^2 \qquad (4.47)$$

The general technique for deriving expressions for the shape functions of isoparametric elements has been described by Ergatoudis et al (1968). The following expression for the shape functions of the 3-node line element has been obtained by applying this technique.

$$[N_1, N_2, N_3] = [-0.5(\xi - \xi^2),\ 0.5(\xi + \xi^2),\ (1 - \xi^2)] \qquad (4.48)$$

Now the differentials dr and $d\xi$ are related by

$$dr = \frac{dr}{d\xi}\, d\xi \qquad (4.49)$$

from which it follows that

$$dr = \left(\frac{dN_I}{d\xi}\ r_I\right) d\xi \quad = \quad |J|\ d\xi \tag{4.50}$$

where subscript I ranges from 1 to 3, and $|J|$ is the determinant of Jacobian transformation matrix.

The expression for $|J|$ is given by

$$|J| = 0.5\ (-1 + 2\xi)\ r_1 + 0.5\ (1+2\xi) r_2 - 2\ \xi\ r_3 \tag{4.51}$$

Also

$$\frac{dN_I}{dr} = \frac{dN_I}{d\xi}\ \frac{d\xi}{dr} = \frac{1}{|J|}\ \frac{dN_I}{d\xi} \tag{4.52}$$

Hence the slope matrix [S] for the 3-node line element takes the form

$$[S] = \left[\frac{d\,N_1}{dr}\ ,\ \frac{d\,N_2}{dr}\ ,\ \frac{dN_3}{dr}\ \right] \tag{4.53}$$

$$[S] = \frac{1}{|J|}\ [0.5\ (-1+2\xi),\ 0.5(1+2\xi),\ -2\xi] \tag{4.54}$$

Now from equation (4.30) it follows that

$$[C^e] = \int_{R^e} E\ [S]^T [S]\, dR \tag{4.55}$$

where $$dR = 2\pi r dr \tag{4.56}$$

Substituting equations (4.56) and (4.50) into equation (4.55) results in

$$[C^e] = 2\pi \int_{-1}^{1} E\ [S]^T\ [S]\ N_I\ r_I\ |J|\ d\xi \tag{4.57}$$

The definite integral in equation (4.57) may be evaluated numerically by employing the Gaussian quadrature formula. The procedure for numerical integration has been described by Zienkeiwicz and Cheung (1967). On applying the 3-point quadrature formula to equation (4.57) and multiplying the matrices, the following expression results :-

$$[C^e] = 2\pi \sum_{i=1}^{3} \frac{E(\xi_i)}{J(\xi_i)} N_I(\xi_i)\, r_I\, W(\xi_i)$$

$$\times \begin{bmatrix} 0.25(-1+2\xi_i)^2 & 0.25(4\xi_i^2 - 1) & -0.5(1-2\xi_i)^2 \\ 0.25(4\xi_i^2 - 1) & 0.25(1+2\xi_i)^2 & 0.5(1-4\xi_i^2) \\ -0.5\,(1-2\xi_i)^2 & 0.50\,(1-4\xi_i)^2 & (1-2\xi_i)^2 \end{bmatrix} \qquad (4.58)$$

where $E(\xi_i)$, $N_I(\xi_i)$ and $J(\xi_i)$ are functions of the ξ-coordinate, to be evaluated at the Gaussian points (ξ_i), and $W(\xi_i)$ are the values of the weighting coefficient at the Gaussian points.

Similarly, expressions for matrices $[\acute{C}^e]$ and $[D^e]$ can be obtained from the following equations

$$[\acute{C}^e] = 2\pi \int_{-1}^{1} [S]^T [K] [S]\; N_I\; r_I\; |J|\, d\xi \qquad (4.59)$$

$$[D^e] = 2\pi \int_{-1}^{1} S_s\, [N]^T [N]\; N_I\; r_I\; |J|\, d\xi \qquad (4.60)$$

(ii) Quadrilateral Elements

In solving two-dimensional flow problems quadrilateral elements may be used to improve the accuracy of the numerical solution. This type of element provides higher forms of approximation to the hydraulic head function than the simple triangular element. Its use allows an appreciable reduction in the total number of nodes in the flow region for a given degree of accuracy. A typical 4-node element is shown in Fig. 4.4.

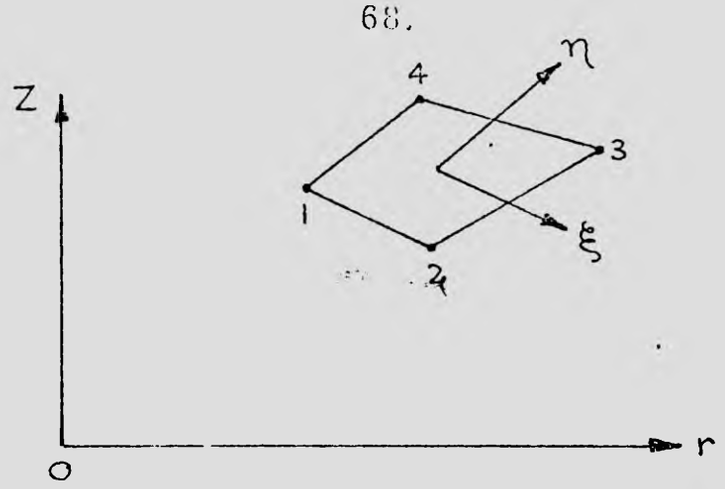

Fig. 4.4: A 4-node quadrilateral element

A quadrilateral ring can be generated by revolving the element about the z-axis.

To outline the derivation of the expressions for the element matrices, let a system of local coordinates (ξ, η) be associated with each element. These coordinates are so determined as to give $\eta = -1$ on side 1-2, $\eta = 1$ on side 4-3, $\xi = 1$ on side 2-3 and $\xi = -1$ on side 1-4. The relationships between the (r, z) coordinates and (ξ, η) coordinates are given by

$$r = N_I (\xi, \eta) \; r_I \qquad (4.61a)$$

$$z = N_I (\xi, \eta) \; z_I \qquad (4.61b)$$

where I ranges from 1 to 4.

The expressions for the shape functions N_I have been developed by Ergatoudis et al (1968). They may be written as

$$N_1 = \tfrac{1}{4}(1 - \xi)(1 - \eta) \; ; \; N_2 = \tfrac{1}{4}(1 + \xi)(1 - \eta)$$
$$N_3 = \tfrac{1}{4}(1 + \xi)(1 + \eta); \quad N_4 = \tfrac{1}{4}(1 - \xi)(1 + \eta) \qquad (4.62)$$

The differential operators with respect to r and z and those with respect to ξ and η are related by

$$\begin{bmatrix} \frac{\partial}{\partial r} \\ \frac{\partial}{\partial z} \end{bmatrix} = [J]^{-1} \begin{bmatrix} \frac{\partial}{\partial \xi} \\ \frac{\partial}{\partial \eta} \end{bmatrix} \tag{4.63}$$

where [J] is the Jacobian transformation matrix which is given by

$$[J] = \begin{bmatrix} \frac{\partial r}{\partial \xi} & \frac{\partial z}{\partial \xi} \\ \frac{\partial r}{\partial \eta} & \frac{\partial z}{\partial \eta} \end{bmatrix} \tag{4.64a}$$

$$[J] = \frac{1}{4} \begin{bmatrix} -(1-\eta), (1-\eta), (1+\eta), -(1+\eta) \\ -(1-\xi), -(1+\xi), (1+\xi), (1-\xi) \end{bmatrix} \begin{bmatrix} r_1 & z_1 \\ r_2 & z_2 \\ r_3 & z_3 \\ r_4 & z_4 \end{bmatrix} \tag{4.64b}$$

Also

$$dR = 2\pi r \, dr dz \tag{4.65a}$$

and

$$dr dz = |J| \, d\xi \, d\eta \tag{4.65b}$$

where $|J|$ is the determinant of the Jacobian matrix.

The slope matrix [S]may now be expressed as

$$[S] = [J]^{-1} \begin{bmatrix} \frac{\partial N_1}{\partial \xi}, & \frac{\partial N_2}{\partial \xi}, & \frac{\partial N_3}{\partial \xi}, & \frac{\partial N_4}{\partial \xi} \\ \frac{\partial N_1}{\partial \eta}, & \frac{\partial N_2}{\partial \eta}, & \frac{\partial N_3}{\partial \eta}, & \frac{\partial N_4}{\partial \eta} \end{bmatrix} \tag{4.66}$$

Hence the element matrices $[C^e]$, $[\acute{C}^e]$ and $[D^e]$ are now obtained as

$$[C^e] = 2\pi \int_{-1}^{1} \int_{-1}^{1} E \, [S]^T [S] \, N_I \, r_I \, |J| \, d\xi \, d\eta \tag{4.67a}$$

$$[\acute{C}^e] = 2\pi \int_{-1}^{1} \int_{-1}^{1} [S]^T [K][S] \, N_I \, r_I \, |J| \, d\xi \, d\eta \tag{4.67b}$$

$$[D^e] = 2\pi \int_{-1}^{1} \int_{-1}^{1} S_s [N]^T [N] N_I \; r_I \; |J| \; d\xi \; d\eta \qquad (4.67c)$$

where the numerical integration is accomplished by employing the Gaussian quadrature formula. A special case arises when the quadrilateral elements used become rectangular elements. In this case the element matrices $[C^e]$, $[\acute{C}^e]$ and $[D^e]$ are easily generated by employing the technique described in Appendix 1. This technique leads to considerable saving in computational time.

4.3.4 Assemblage of Elements

In the element assembling process, all elements are assembled through the specification of the reduced compatibility condition, which requires that the nodal values of the function be the same at coincident nodes of adjacent elements and also equal to prescribed value on the boundary portion where the function is prescribed.

Thus on assembling, the functional for the entire flow region becomes

$$[\Omega(h_I)]_{\bar{R}} = \sum_{e=1}^{m} \Omega^e (h_I) = \sum_{e} \Omega^e (h_I) \qquad (4.68)$$

for I = 1.....n

where the summation is taken over the elements adjacent to the I-th nodal point and subscript I ranges from one to the total number of nodes in the entire flow region.

The minimisation of $[\Omega(h_I)]_{\bar{R}}$ requires that

$$\frac{\partial}{\partial h_I}\left[\Omega(h_I)\right]_{\bar{R}} = \sum_e \frac{\partial \Omega^e}{\partial h_I} = 0 \qquad (4.69)$$

for I = 1.....n

The expressions for $\frac{\partial \Omega^e}{\partial h_I}$ have been obtained both for elements in the non-Darcy flow subregion and elements in the Darcy flow subregion. The general expression is now rewritten as

$$\frac{\partial \Omega^e}{\partial h_I} = \int_t^{t+\Delta t} C^e_{JI}\, h_J\, dt + \int_t^{t+\Delta t} D^e_{JI}\, \frac{\partial h_J}{\partial t}\, dt + \int_t^{t+\Delta t} F_I^e\, dt \qquad (4.70)$$

where for the elements in the Darcy flow subregion, C^e_{JI} is replaced by $\acute{C}^e_{JI}$

Substituting equation (4.70) into equation (4.69) gives

$$\sum_e \int_t^{t+\Delta t} C^e_{JI}\, h_J\, dt + \sum_e \int_t^{t+\Delta t} D^e_{JI}\, \frac{\partial h_J}{\partial t}\, dt + \sum_e \int_t^{t+\Delta t} F_I^e\, dt = 0 \qquad (4.71a)$$

The following gross matrices may now be introduced

$$C_{JI} = \sum_e C^e_{JI} \qquad (4.71b)$$

$$D_{JI} = \sum_e D^e_{JI} \qquad (4.71c)$$

$$F_I = \sum_e F_I^e \qquad (4.71d)$$

Substituting equations (4.71b) to (4.71d) into equation (4.71a) results in

$$\int_t^{t+\Delta t} C_{JI} h_J dt + \int_t^{t+\Delta t} D_{JI} \frac{\partial h_J}{\partial t} dt + \int_t^{t+\Delta t} F_I dt = 0 \qquad (4.72)$$

where subscripts J and I range from one to the total number of nodes in the entire region.

4.3.5 Integration with respect to Time

Equation (4.72) represents a system of n simultaneous equations involving the integral terms which must be integrated with respect to time. To carry out the integration, it is assumed that all the nodal values of h_I and F_I are known at earlier time t and that the nodal values vary linearly over the time increment Δt as shown in Fig. 4.5.

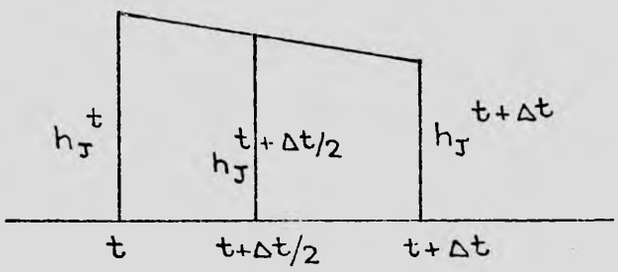

Fig. 4.5: Nodal values and their variation over Δt.

Thus on carrying out the integration, equation (4.72) becomes

$$\int_t^{t+\Delta t} C_{JI} h_J dt + D_{JI} (h_J^{t+\Delta t} - h_J^t) + (F_I^{t+\Delta t} + F_I^t) \frac{\Delta t}{2} = 0 \qquad (4.73)$$

where the superscripts denote the times at which the nodal values are evaluated.

The remaining integral term in equation (4.73) involves both C_{JI} and h_J as functions of time. This is because C_{JI} is associated with the effective hydraulic coefficient E which is given by equations (4.34a) and (4.34b) in terms of the nodal values of the hydraulic head function.

To avoid unnecessary complication in carrying out the integration, the following approximation is introduced:-

$$\int_t^{t+\Delta t} C_{JI}\, h_J\, dt \simeq \frac{(C_{JI} + C_{JI}^t)}{2} \frac{(h_J^{t+\Delta t} + h_J^t)}{2} \Delta t \qquad (4.74)$$

Substituting equation (4.74) into (4.73) gives

$$(C_{JI}^{t+\Delta t} + C_{JI}^t)(h_J^{t+\Delta t} + h_J^t)\frac{\Delta t}{4} + D_{JI}(h_J^{t+\Delta t} - h_J^t) + (F_I^{t+\Delta t} + F_I^t)\frac{\Delta t}{2} = 0 \qquad (4.75)$$

Rearranging equation (4.75) results in

$$\frac{1}{2}(h_J^t + h_J^{t+\Delta t})\left[\frac{\Delta t}{4}(C_{JI}^t + C_{JI}^{t+\Delta t}) + D_{JI}\right] = D_{JI} h_J^t - \frac{\Delta t}{4}(F_I^t + F_I^{t+\Delta t}) \qquad (4.76)$$

Now let $t + \frac{\Delta t}{2}$ denote the mid-time of t and $t+\Delta t$. It follows that

$$h_J^{t+\Delta t/2} = \frac{1}{2}(h_J^t + h_J^{t+\Delta t}) \qquad (4.77a)$$

$$F_I^{t+\Delta t/2} = \frac{1}{2}(F_I^t + F_I^{t+\Delta t}) \qquad (4.77b)$$

and $$C_{JI}^{t+\Delta t/2} = \frac{1}{2}(C_{JI}^t + C_{JI}^{t+\Delta t}) \qquad (4.77c)$$

On substituting these into equation (4.76), the following equation is obtained:-

$$\left(\frac{\Delta t}{2} C_{JI}^{t+\Delta t/2} + D_{JI}\right) h_J^{t+\Delta t/2} = D_{JI} h_J^t - \frac{\Delta t}{2} F_I^{t+\Delta t/} \qquad (4.78)$$

Also from equation (4.77a), it follows that

$$h_J^{t+\Delta t} = 2h_J^{t+\Delta t/2} - h_J^t \qquad (4.79)$$

The last two equations provide suitable recurrence relations for final solution of the initial value problem. The solution starts

at the initial time, $t = 0$, and proceeds in a step-wise manner. At the beginning of the first time step, the nodal head values h_J^o are specified by the initial conditions. These values may be substituted for h_J^t in equation (4.78) and used in solving for $h_J^{t+\Delta t/2}$ which may then be substituted into equation (4.79) to result in the head values at the end of the time step. The currently obtained head values, which become h_J^t at the beginning of the new time step, can be used in calculating the head values at the end of the second time step. The procedure can then be repeated until the nodal values at the end of the final time step have been determined.

For steady state flow cases, equation (4.78) becomes

$$C_{JI}h_J + F_I = 0 \qquad (4.80)$$

The steady flow problem reduces to that of finding the solution of equation (4.80), subject to the prevailing boundary conditions.

4.3.6 Iterative Solution of Non-linear Algebraic Equations

Equation (4.78) is a set of simultaneous algebraic equations involving the non-linear coefficients $C_{JI}^{t+\Delta t/2}$ which are contributed by the elements in the non-Darcy flow subregion. These coefficients have to be evaluated in terms of the unknown nodal values of the hydraulic head at time $t+\Delta t/2$ as they are associated with the coefficient E of the finite elements. However, provided that the values of h_J^t and $F_I^{t+\Delta t/2}$ at all the nodal points are known, it is possible to solve for $h_J^{t+\Delta t/2}$ iteratively.

The general procedure is first to calculate matrix $[C^{t+\Delta t/2}]$ in terms of the known nodal head values and solve for $h_J^{t+\Delta t/2}$, then use the values of $h_J^{t+\Delta t/2}$ just obtained to reform $[C^{t+\Delta t/2}]$ and re-solve for more accurate values of $h_J^{t+\Delta t/2}$. The process is repeated until the change in successive head values is negligible.

The iterative procedure employed in this study makes use of an over-relaxation factor to accelerate convergence of the solution. To describe this procedure, it is convenient to drop the superscript $t+\Delta t/2$ from the unknown terms in equation (4.78) and replace it by another superscript k which denotes an iteration number. Equation (4.78) now takes the form

$$\left(\frac{\Delta t}{2} C_{JI}^{k} + D_{JI} \right) h_J^{k+1} = D_{JI} h_J^{t} - \frac{\Delta t}{2} F^{t+\Delta t/2} \qquad (4.81)$$

For the first iteration, the array elements C_{JI}^{k} of matrix $[C]$ were calculated in terms of the known values of h_J^{t} and equation (4.81) was solved for h_J^{k+1} by direct Gaussian elimination method. To start the next iteration, the following over-relaxation formula was used to modify h_J^{k+1}

$$h_J^{k+1} = h_J^{k} + \omega(h_J^{k+1} - h_J^{k}) \qquad (4.82)$$

where ω is the over-relaxation factor, having a value between 1 and 2, and h_J^{k} denotes the old head values which are set equal to h_J^{t} when k=1.

The modified values h_J^{k+1} which become h_J^{k} for the current iteration, were used in calculating the absolute element velocities and

reforming the matrix $[C_J]$. Calculation of the element velocities was necessary to enable a check to be carried out to find if a particular finite element belonged to the Darcy or the non-Darcy flow sub-region. Equation (4.82) was then resolved for more accurate values of h_J^{k+1}.

The iterative process was repeated until convergence resulted when the following criterion was satisfied:-

$$\delta h = \max_J | h_J^{k+1} - h_J^k | \leq \epsilon \qquad (4.83)$$

where δh denotes the maximum absolute error in the nodal head values and ϵ is the prescribed head tolerance.

It was found that a value of ω between 1.5 to 1.9 gave fast convergence. Approximately 4 or 5 iterations were required to obtain satisfactory results. The optimum value of ω tends to increase with the total number of equations solved.

4.3.7 Treatment of Conditions on the Well Boundary

In solving the problem of transient flow towards a pumped well, special treatment must be given to the conditions prevailing at the well boundary. Two types of well boundary condition are possible, depending on the pumping operation. If the well is pumped at a constant discharge, the condition of constant prescribed flow rate will prevail. On the other hand, if it is pumped such that the water level in the well remains constant, the constant prescribed head condition will result. These two types of boundary condition were dealt with in the following manner:-

(i) Constant Prescribed Head Condition

Consider a typical pumped well shown in Fig. 4.6. As indicated in the figure, the first portion of the well boundary is screened and the remaining portion is cased. If the water level is maintained constant throughout the pumping period, the head values at the nodes situated on the well screen will be constant with time and equal to the known elevation of the water level above the datum plane.

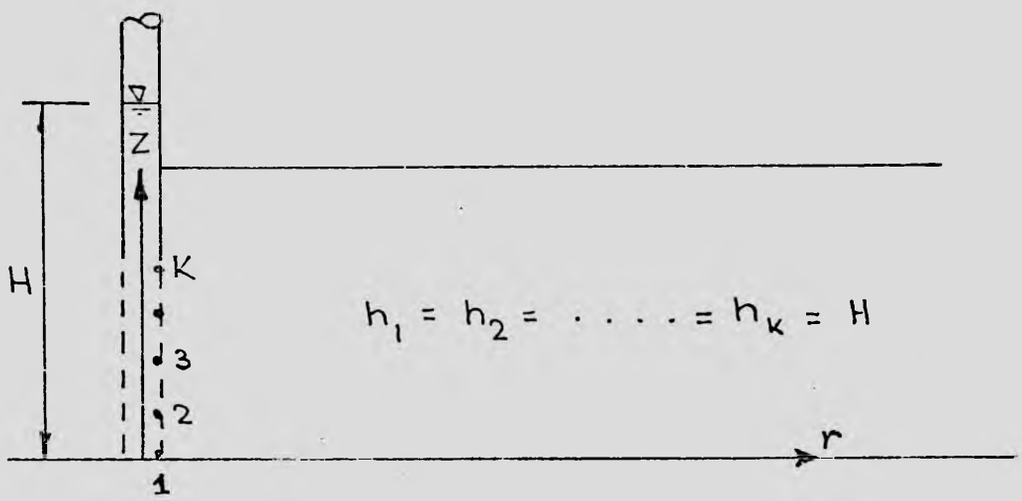

Fig. 4.6: The boundary of a typical pumped well.

In order to incorporate the resulting prescribed head condition into equation (4.78), the following scheme for partitioning the gross matrices in this equation was employed:-

Let α and j be additional subscripts referring to the nodes situated on the well screen and the remaining nodes in the flow region respectively. It follows that if α ranges from 1 to k, j ranges from k-1 to n and equation (4.78) may be expanded.

On introducing $x_J = h_J^{t+\Delta t/2}$ and expanding subscript J in equation (4.78) the following equation results :-

$$\left(\frac{\Delta t}{2} C_{\alpha I} + D_{\alpha I}\right)x_\alpha + \left(\frac{\Delta t}{2} C_{jI} + D_{jI}\right) x_j = D_{\alpha I} h_\alpha + D_{jI} h_j - \frac{\Delta t}{2} F_I \qquad (4.84)$$

where the superscripts have been dropped from matrices $[C^{t+\Delta t/2}]$, $[F^{t+\Delta t/2}]$ and $[h^t]$

Now the prescribed head condition requires that

$$x_\alpha = h_\alpha = H \qquad (4.85)$$

for $\alpha = 1.....k$

Substituting equation (4.85) into equation (4.84) and rearranging gives

$$\left(\frac{\Delta t}{2} C_{jI} + D_{jI}\right)x_j = -\frac{\Delta t}{2} C_{\alpha I} h_\alpha + D_{jI} h_j - \frac{\Delta t}{2} F_I \qquad (4.86)$$

By expanding subscript I, equation (4.86) can be expanded to give the following equations :-

$$\left(\frac{\Delta t}{2} C_{ji} + D_{ji}\right) x_j = -\frac{\Delta t}{2} C_{\alpha i} h_\alpha + D_{ji} h_j - \frac{\Delta t}{2} F_i \qquad (4.87)$$

and

$$\left(\frac{\Delta t}{2} C_{j\beta} + D_{j\beta}\right)x_j = -\frac{\Delta t}{2} C_{\alpha\beta} h_\alpha + D_{j\beta} h_j - \frac{\Delta t}{2} F_\beta \qquad (4.88)$$

where i is a subscript having the same range as j and β is a subscript having the same range as α.

Equation (4.87) represents a reduced set of n-k non-linear algebraic equations which may be readily solved by the iterative procedure described earlier. Also if required, the values of the flux at

the nodal points on the well screen can be calculated by substituting the last set of values of x_j into equation (4.88) and solving for F_β.

Thus it follows that

$$F_\beta = \frac{2}{\Delta t} D_{j\beta} h_j - C_{\alpha\beta} h_\alpha - (C_{j\beta} + \frac{2}{\Delta t} D_{j\beta}) x_j \qquad (4.89)$$

Knowing the nodal fluxes, the total discharge from the aquifer into the well may be computed from

$$Q = \sum_{\beta=1}^{K} F_\beta \qquad (4.90a)$$

(ii) Constant Prescribed Flow Rate Condition

In the extraction of groundwater by pumping, it is common practice to maintain constant total discharge from the well throughout the pumping period. Accordingly, since the total flow rate is fixed, the water level in the well and the prescribed hydraulic head along the screened portion of the well boundary must vary with time.

Once again consider the well shown in Fig. 4.6. If $\bar{Q}$ denotes the prescribed flow rate, the prescribed flow rate condition is given by

$$\bar{Q} = \sum_{\beta=1}^{K} F_\beta \qquad (4.90b)$$

where F_β are the unknown nodal flux values.

The requirement of prescribed head distribution along the well screen at time $t + \Delta t/2$ may be written as

$$h_1^{t+\Delta t/2} = h_2^{t+\Delta t/2} \quad . \quad . \quad . = H^{t+\Delta t/2} \qquad (4.91)$$

where $H^{t+\Delta t/2}$ is the unknown height of the water level at time $t+\Delta t/2$.

In the simple case of flow where the total discharge is uniformly distributed along the well screen, the constant flow rate condition may be treated by computing the values F_β from equation (4.90b) and incorporating these and equation (4.91) into equation (4.78). The detailed treatment has been presented by Javandel and Witherspoon (1968).

In the more general case where the flux distribution is non-uniform, the prescribed flow rate condition has to be satisfied by trial and error. Due to the non-linear field equation, the superposition technique used by Javandel and Witherspoon (1968) to correct the head to produce the prescribed discharge is not applicable. The following iteration solution technique was employed in this study:-

Let t_{n+1} and t_n denote the current and preceding times respectively, and let the mid-time $t_{n+\frac{1}{2}}$ be defined in accordance with $t_{n+\frac{1}{2}} = \frac{1}{2}(t_n + t_{n+1})$.

For the first iteration, k = 1, an initial estimate of the value of H at time $t_{n+\frac{1}{2}}$ was made from

$$H^1(t_{n+\frac{1}{2}}) = H(t_n) + \Delta H \qquad (4.92a)$$

for n = 0, 1

or from the following logarithmic extrapolation formula :-

$$H^1(t_{n+\frac{1}{2}}) = \frac{\log\left[t_{n+1/2}/t_{n-1}\right]}{\log\left[t_n/t_{n-1}\right]} \cdot \left\{H(t_n) - H(t_{n-1})\right\} + H(t_{n-1}) \qquad (4.92b)$$

for $n = 2, 3.....$

When equation (4.92a) was used, a guess had to be made as to the value of the head increment ΔH at the beginning of the first and second time steps, when $n = 0$ and 1 respectively.

The initial estimate of H was used in solving for the unknown nodal head and flux values in equations (4.87) and (4.89) respectively. Knowing the nodal flux F_β, the total discharge Q^k was calculated from equation (4.90a) and compared with the prescribed discharge $\bar{Q}$.

If

$$\left|\frac{Q^k - \bar{Q}}{\bar{Q}}\right| > \epsilon \qquad (4.93)$$

where ϵ is the prescribed tolerance of the discharge ratio, a new trial head was calculated from

$$H^2(t_{n+\frac{1}{2}}) = H(t_n) + \left[H^1(t_{n+\frac{1}{2}}) - H(t_n)\right] \frac{\bar{Q}}{Q^1} \qquad (4.94)$$

Solution for the unknown nodal head and flux values was then repeated and the total discharge from the aquifer was recalculated and re tested for convergence. If convergence was still not obtained, the following formula was applied :-

$$H^{k+1} = H^{k-1} + \frac{H^k - H^{k-1}}{Q^k - Q^{k-1}} (\bar{Q} - Q^{k-1}) \qquad (4.95)$$

where H^{k+1}, H^k and H^{k-1} refer to $H^{k+1}(t_{n+\frac{1}{2}})$, $H^k(t_{n+\frac{1}{2}})$ and $H^{k-1}(t_{n+\frac{1}{2}})$ respectively.

The solving procedure was then repeated and equation (4.95) was reapplied until convergence resulted.

It was found that the above iteration procedure gave quite satisfactory results. For earlier times of pumping, the convergence criterion was met after two or three iterations. For later times, convergence resulted after only one iteration.

4.3.8 Elimination Scheme for Solving a System of Linear Equations

The assemblage of element matrices led to a non-linear system of n simultaneous equations which, after imposing the conditions prevailing on the well boundary, reduced to a system of n-k equations as represented by equation (4.87). The reduced system was linearised by evaluating the non-linear coefficients C_{ji} in equation (4.87) in terms of the known nodal values of the hydraulic head.

A banded Gaussian elimination scheme was employed to solve for the n-k unknowns in the linearised system of equations. The scheme takes into account the banded character and symmetry of the gross matrices [C] and [D]. The two matrices were arranged in compact banded form by numbering the nodes in the entire flow region in consecutive order along the vertical lines extending from top to bottom of the aquifer. The process of elimination was accomplished by reducing the system of equations to an equivalent triangular form through a series of arithmetic operations on the coefficients of the equations.

Then starting from the last equation, the last unknown was solved and the remaining unknowns were obtained by back substitution into the preceding equations.

Due to symmetry of matrices [C] and [D], it is only necessary to operate on the elements in their upper triangles. The half band-width of each matrix is computed as the length between the diagonal element and the last non-zero element in each row. In the computer subroutine developed in the present work,the two matrices are converted into gross vectors by stringing together the half-bands of all successive rows. This conversion partly eliminates the problem of insufficient computer storage capacity, as only a small part of the two gross matrices needs to be stored. Furthermore, the smaller number of arithmetic operations required cuts down the solution time considerably.

4.4 Analysis of Flow through Unconfined Aquifers

4.4.1 General Approach to the Variational Problem

In the preceding section, the finite element formulation of the general axi-symmetric confined flow problem was presented. It is shown in this section that the previous formulation can readily be extended to treat the unconfined flow problem involving the presence of the moving boundary, namely the free surface.

Consider the general problem of transient, two-regime flow to a fu screened well constructed in an unconfined aquifer. A typical sketch of the radial cross-section of the three-dimensional flow region is shown in Fig. 4.7.

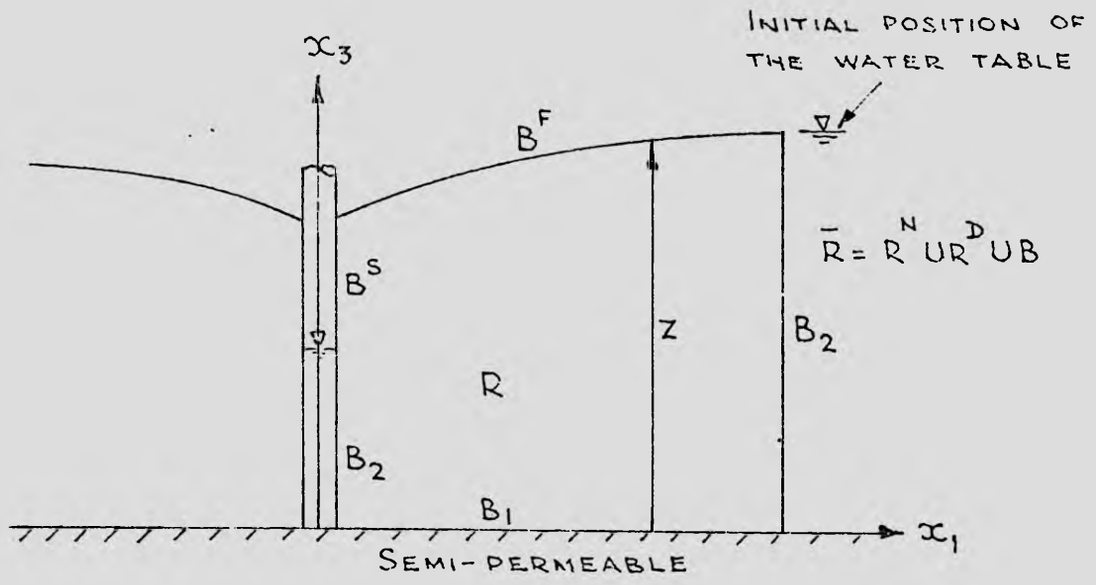

Fig. 4.7: Cross-section of 3-dimensional flow region in an unconfined aquifer.

Due to the presence of the free surface and seepage face, the expression of the functional obtained for the confined flow problem has to be modified to allow for the additional boundary conditions. The modified functional takes the following form:-

$$[\Omega(h,z)]_{\bar{R}} = [\Omega(h)]_{R^N} + [\Omega(h)]_{R^D} + \int_t^{t+\Delta t}\int_{B_1} h\,\bar{q}\,dBdt$$

$$+\int_t^{t+\Delta t}\int_{B_2} (h-\bar{h})\,v_i n_i\,dBdt + \int_t^{t+\Delta t}\int_{B^S} (h-x_3)\,v_i n_i\,dBdt$$

$$+\int_t^{t+\Delta t}\int_{B^F} (h-z)\,v_i n_i\,dBdt - \int_t^{t+\Delta t}\int_{B^F} z(I-\alpha S_y \int_0^t \frac{\partial z}{\partial \tau}$$

$$e^{-\alpha(t-\tau)}\,d\tau)\,n_3\,dBdt \qquad (4.96)$$

The general variational problem is to find the two unknown functions, h and z which minimise the functional in equation (4.96).

To solve the problem by the finite element method, it is necessary that the entire flow region be fixed so that the minimisation process

may be carried out. Thus the position of the free surface has to be initially assumed and then adjusted until all the prevailing boundary conditions are satisfied.

A general two-step iterative procedure employed by Neuman and Witherspoon (1970, 1971) was adopted as it generally leads to a rapidly converging solution. The procedure is described below.

For the first step of each iteration, the function h is prescribed on B^F and B^S. This leads to the following simplification of equation (4.96):-

$$[\Omega(h)]_{\bar{R}} = [\Omega(h)]_{R^N} + [\Omega(h)]_{R^D} + \int_t^{t+\Delta t} \int_{B_1} h\,\bar{q}\, dB dt \qquad (4.97)$$

After the functional in equation (4.97) has been minimised by the finite element method, the flux distribution on the seepage face may be determined.

For the second step of the iteration, the function h is no longer considered to be prescribed on B^F and B^S. Instead, the free surface and seepage face are treated as known flux boundaries. Equation (4.96) thus becomes

$$[\Omega(h)]_{\bar{R}} = [\Omega(h)]_{R^N} + [\Omega(h)]_{R^D} + \int_t^{t+\Delta t} \int_{B_1} h\,\bar{q}\, dB dt$$

$$+ \int_t^{t+\Delta t} \int_{B^S} q(x_3) h\, dB dt - \int_t^{t+\Delta t} \int_{B^F} (I - \alpha S_y \int_0^t e^{-\alpha(t-\tau)} \frac{\partial h}{\partial \tau}$$

$$d\tau)\, h n_3\, dB dt \qquad (4.98)$$

where $q(x_3)$ is the flux on the seepage face per unit area.

Next, the functional in equation (4.98) is minimised and a check made to ensure that

$$|h - z| \leq \epsilon_s \quad \text{on } B^F \tag{4.99}$$

where ϵ_s is the prescribed tolerance of the free surface height.

If condition (4.99) is not satisfied, the free surface position is adjusted in an appropriate manner along the vertical direction. The iterative procedure is repeated until $|h - z|$ is within the prescribed tolerance everywhere on B^F.

4.4.2 Modification of the Previous Finite Element Formulation

The functionals in equations (4.97) and (4.98) may be minimised by applying the technique described earlier in Section 4.3.

The minimisation of the functional in equation (4.97) leads to a system of algebraic equations identical to that represented by equation (4.78) as this functional is identical to the one obtained for the confined flow problem. Equation (4.78) is now rewritten as

$$\left(\frac{\Delta t}{2} C_{JI}^{t+\Delta t/2} + D_{JI}^{t+\Delta t/2}\right) h_J^{t+\Delta t/2} = D_{JI}^{t+\Delta t/2} h_J^{t} - \frac{\Delta t}{2} F_I^{t+\Delta t/2} \tag{4.100}$$

where the superscript $t+\Delta t/2$ is attached to D_{JI} to indicate that D_{JI} is time dependent as the elements in a certain part of the network must be allowed to deform to accommodate the movement of the free surface with time.

The minimisation of the functional in equation (4.98) leads to the following system of equation:-

$$\left(\frac{\Delta t}{2} C_{JI}^{t+\Delta t/2} + D_{JI}^{t+\Delta t/2}\right) h_J^{t+\Delta t/2} = D_{JI}^{t+\Delta t/2} h_J^{t} -$$

$$\frac{\Delta t}{2}\left(F_I^{t+\Delta t/2} + G_I^{t+\Delta t/2} - H_I^{t+\Delta t/2}\right) \qquad (4.101)$$

where $G_I^{t+\Delta t/2}$ and $H_I^{t+\Delta t/2}$ denote the extra flux terms for the nodes on the seepage face and the free surface respectively.

The expressions for $G_I^{t+\Delta t/2}$ and $H_I^{t+\Delta t/2}$ are given by

$$G_I^{t+\Delta t/2} = \sum_e \int_{(B^S)^e} q_J^{t+\Delta t/2}(x_3)\, N_J N_I \, dB \qquad (4.102)$$

$$H_I^{t+\Delta t/2} = \sum_e \int_{(B^F)^e} \left[IN_I\, n_3 - \left(\alpha S_y \int_o^{t+\Delta t/2} e^{-\alpha(t+\Delta t/2-\tau)} \frac{\partial h_J}{\partial \tau}\, d\tau \right) N_J N_I n_3 \right] dB \qquad (4.103)$$

To handle the Boulton exponential integral term in equation (4.103), the equation is rewritten in a more compact form as follows:-

$$H_I^{t+\Delta t/2} = \sum_e \int_{(B^F)^e} \left[IN_I n_3 - f_J^{t+\Delta t/2} N_J N_I n_3 \right] dB \qquad (4.104a)$$

where

$$f_J^{t+\Delta t/2} = \alpha S_y \int_o^{t+\Delta t/2} e^{-\alpha(t+\Delta t/2 - \tau)} \frac{\partial h_J}{\partial \tau}\, d\tau \qquad (4.104b)$$

Equation (4.104b) may be rearranged to give

$$f_J^{t+\Delta t/2} = \alpha S_y \left(\int_o^{t} e^{-\alpha(t-\tau)} e^{\alpha \Delta t/2} \frac{\partial h_J}{\partial \tau}\, d\tau \right.$$

$$\left. + \int_t^{t+\Delta t/2} \frac{\partial h_J}{\partial \tau} e^{-\alpha(t+\Delta t/2-\tau)}\, d\tau \right) \qquad (4.104c)$$

The second term on the right hand side of equation (4.104c) may be approximated by

$$\alpha S_y \int_t^{t+\Delta t/2} \frac{\partial h_J}{\partial \tau} e^{-\alpha(t+\Delta t/2 - \tau)} d\tau = \frac{2S_y}{\Delta t}(1 - e^{-\alpha \Delta t/2}) (h_J^{t+\Delta t/2} - h_J^t) \quad (4.104d)$$

Equation (4.104c) now takes the form

$$f_J^{t+\Delta t/2} = f_J^t + \frac{2}{\Delta t} S_e (h_J^{t+\Delta t/2} - h_J^t) \quad (4.105a)$$

where

$$f_J^t = \alpha S_y e^{-\alpha \Delta t/2} \int_o^t e^{-\alpha(t-\tau)} \frac{\partial h_J}{\partial \tau} d\tau \quad (4.105b)$$

$$S_e = S_y (1-e^{-\alpha \Delta t/2}) \quad (4.105c)$$

Substitution of equations (4.104a) and (4.105a) into equation (4.101) leads to the following system of algebraic equations:-

$$(\frac{\Delta t}{2} C_{JI}^{t+\Delta t/2} + D_{JI}^{t+\Delta t/2} + D'^{t+\Delta t/2}_{JI}) h_J^{t+\Delta t/2} = (D_{JI}^{t+\Delta t/2} + D'^{t+\Delta t/2}_{JI}) h_J^t - \frac{\Delta t}{2} (F_I^{t+\Delta t/2} + G_I^{t+\Delta t/2} - H'^{t+\Delta t/2}_I) \quad (4.106a)$$

where

$$D'^{t+\Delta t/2}_{JI} = S_e \sum_e \int_{(B^F)_e} N_J N_I n_3 dB \quad (4.106b)$$

$$H'^{t+\Delta t/2}_I = \sum_e \int_{(B^F)_e} [I N_I n_3 - f_J^t N_J N_I n_3] dB \quad (4.106c)$$

It is pointed out that f_J^t in equation (4.106c) may be calculated by applying Simpson's rule of numerical integration and the recurrence

relations represented by equations (4.105a) to (4.105c). Furthermore, the integral $\int_{(B^F)^e} N_J N_I n_3 \, dB$ is easily evaluated. For triangular and 4-node quadrilateral concentric ring elements, this integral is given by

$$\int_{(B^F)^e} N_J N_I n_3 dB = \frac{2\pi \bar{r}}{3} \Delta r \quad ; \quad \text{when} \quad I = J$$

$$\int_{(B^F)^e} N_J N_I n_3 dB = \frac{2\pi \bar{r}}{6} \Delta r \quad ; \quad \text{when} \quad I \neq J$$

where

$$\bar{r} = \tfrac{1}{2} (r_I + r_J)$$

$$\Delta r = |r_I - r_J|$$

4.4.3 Solution Procedure

The finite element formulation leads to two systems of non-linear algebraic equations represented by equations (4.100) and (4.106a) respectively. The following procedure was employed to obtain the final solution to the transient unconfined flow problem:-

(i) For the first step of the two-step iterative procedure, the free surface was assumed at the beginning of each time increment. The coefficient matrices of equations (4.100) and (4.106a) were formed, and equation (4.100) was solved by the iterative solution method described in Section 4.3.6.

Since the nodal values of the head function were prescribed on the free surface and seepage face during the first step, it was only necessary to solve for the remaining unknowns in equation (4.100). The general matrix partitioning scheme for reducing a set of n equations

to a set of n-k equations, described in section 4.3.7, was employed.

The final solution of equation (4.100) was then used to calculate the nodal fluxes $G_I^{t+\Delta t/2}$ on the seepage face.

(ii) For the second step of the two-step procedure, the free surface and seepage face were treated as prescribed flux boundaries. Equation (4.106a) was solved iteratively for the new values of $h_J^{t+\Delta t/2}$. These values were then used to calculate the nodal fluxes at the well boundary and the total discharge from the aquifer into the well.

(iii) At the end of the second step, the free surface position was checked and adjustment of the free surface heights was made according to the following equation:-

$$z_J^{k+1} = z_J^k + \omega(h_J^k - z_J^k) \qquad (4.107)$$

where the superscript k denotes the k-th iteration for the correct free surface and ω is an over-relaxation factor, having a value greater than or equal to 1.

After the free surface had been shifted in the vertical direction, the new vertical coordinates of the nodes in the variable part of the finite element network were calculated. The coefficient matrices in equations (4.100) and (4.106a) were then reformed.

(iv) The two-step iterative procedure was repeated until the following convergence criterion was satisfied:-

$$\max_J | h_J^{k+1} - z_J^{k+1} | \leqslant \epsilon_s \qquad (4.108)$$

(v) For the well operating under a prescribed discharge, the iteration for the correct well drawdown corresponding to the required discharge was then performed by applying a procedure similar to that described in Section 4.3.7.

After the correct well drawdown at time $t+\Delta t/2$ had been determined, the nodal head values at the end of the time step were obtained from equation (4.79), which is rewritten as

$$h_J^{t+\Delta t} = 2\, h_J^{t+\Delta t/2} - h_J^{t} \qquad (4.109)$$

(vi) To accelerate convergence of the two-step iteration for the final free surface, the following extrapolation formula was used for predicting the trial free surface for the next time step

$$z_J^{n+\frac{1}{2}} = \frac{\log\left[t^{n+\frac{1}{2}}/t^{n-1}\right]}{\log\left[t^{n}/t^{n-1}\right]} \left(z_J^{n} - z_J^{n-1}\right) + z_J^{n-1} \qquad (4.110)$$

where the superscript n refers to the n-th time step.

It was found that the use of equation (4.110) led to convergence after only two or three iterations except for the first few time steps.

5. Solutions to Typical Flow Problems

5.1 General

A number of computer programs were developed by applying the theory and finite element formulation presented in the preceding chapters. The programs coded in FORTRAN IV language were used to solve a variety of flow problems ranging from the simplest problem of steady one-dimensional confined flow to the most complex problem of transient free surface flow through an unconfined aquifer. Solutions to typical Darcy and two-regime flow cases are presented in this chapter.

The Darcy flow solutions were verified by comparison with known analytical solutions summarised in Appendix 3 of this thesis. The two-regime flow solutions were verified by comparison with results from laboratory and field investigations which are described in the next two chapters.

5.2 Flow towards a Fully Screened Well in a Confined Aquifer

5.2.1 Darcy Flow Solutions

A diagrammatic sketch of a well which is fully screened through the entire thickness of a confined aquifer is shown in Fig. 5.1. An analytical solution to the problem of transient Darcy flow at constant discharge was obtained by Hantush (1959), (1964). The solution becomes the well known Theis solution (Theis, 1935) for time $t > 30\frac{r_w^2 S_s}{K}$. The finite element solution to the same flow problem was obtained by Javandel and Witherspoon (1968). They employed triangular elements

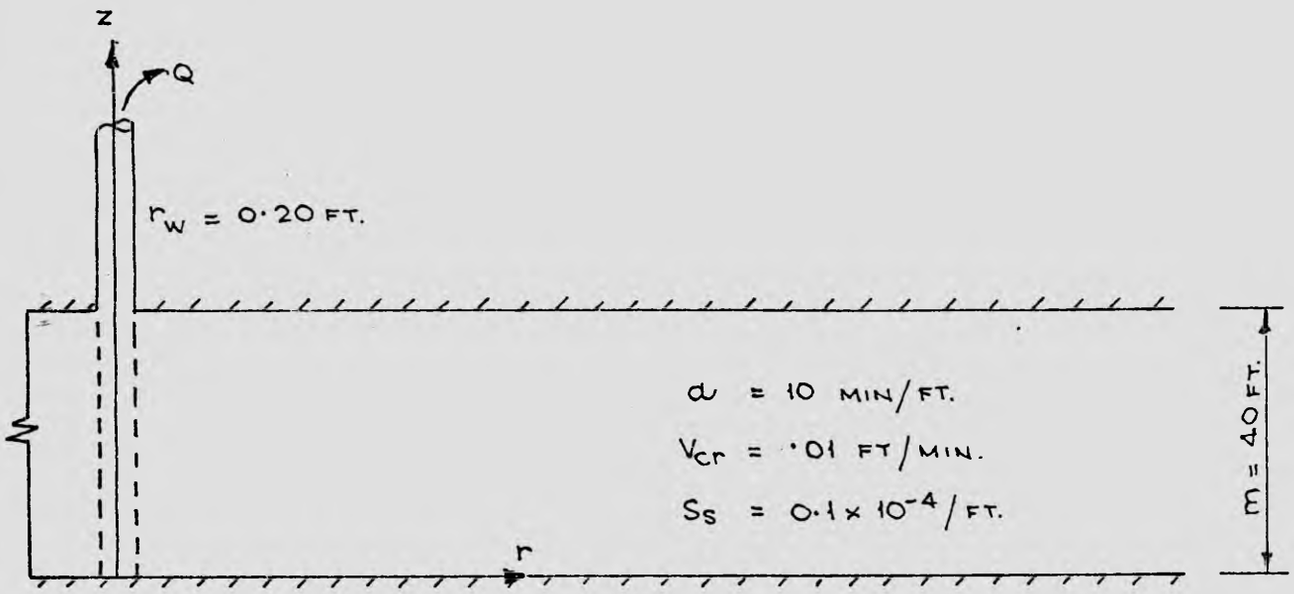

Flow CaseNo.	b(min^2/ft^2)	Q(ft^3/min)
0	0	100
1	20	25
2	20	50
3	20	75
4	20	100
5	20	125
6	20	400

Fig. 5.1: Data for the problem of transient flow towards a well in a confined aquifer.

and obtained good agreement with the analytical solution.

In the present work, one-dimensional elements were employed as the flow is strictly one-dimensional radial flow. The finite element network shown in Fig. 5.2 was set up to solve the problem defined in Fig. 5.1 (flow case No. 0). As shown in Fig. 5.2, the one-dimensional flow region is divided into a number of line segments, each of which is further subdivided into a number of 3-node quadratic elements. The length of the first line segment is 0.50 ft. The network, consisting of 18 elements and 37 nodes, is graded in such a manner that the length of each remaining line segment is twice that of the preceding line segment (i.e. $\Delta r_i = 2 \times \Delta r_{i-1}$) until an external radius r_o = 10,000 ft. is reached. An initial time step of 10^{-7} minutes was chosen. The time step size was then increased logarithmically such that any remaining time step was 1.4 times the previous time step (i.e. $\Delta t_i = 1.4 \times \Delta t_{i-1}$) until 30 time steps were computed. The numerical solution obtained was compared with Hantush's analytical solution. A logarithmic plot of the dimensionless type curves, W(u) versus 1/u, is shown in Fig. 5.3 for selected values of dimensionless radius r/r_w. The variables W(u) and 1/u were calculated from the following equations :-

$$W(u) = \frac{4\pi Ts}{Q} \qquad (5.1)$$

and

$$\frac{1}{u} = \frac{4Tt}{r^2 S} \qquad (5.2)$$

where s is the drawdown in the aquifer, T and S are the coefficients of transmissivity and storage of the aquifer respectively, Q is the

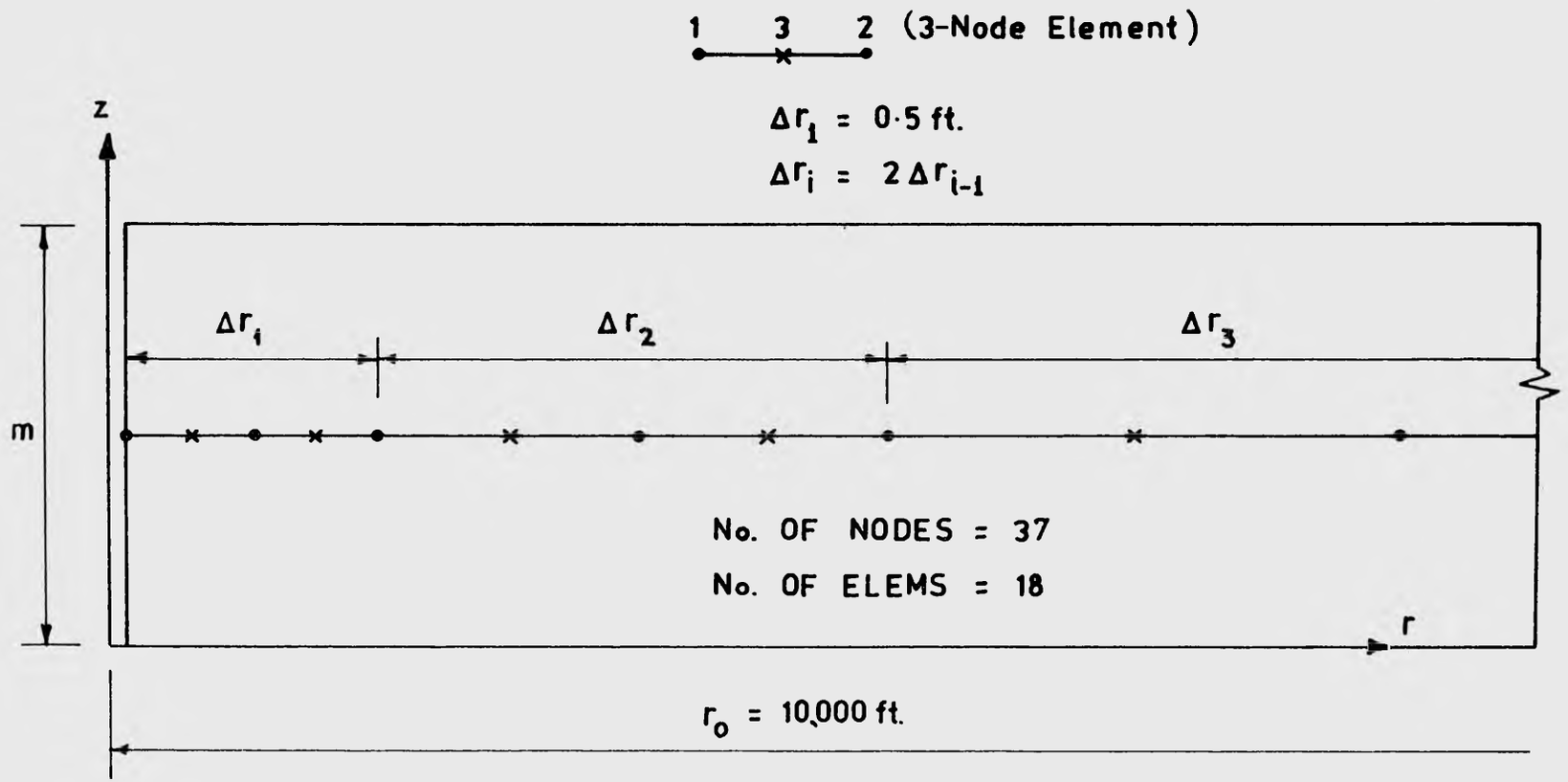

Fig. 5.2: One-dimensional finite element network for a confined aquifer with a fully screened well.

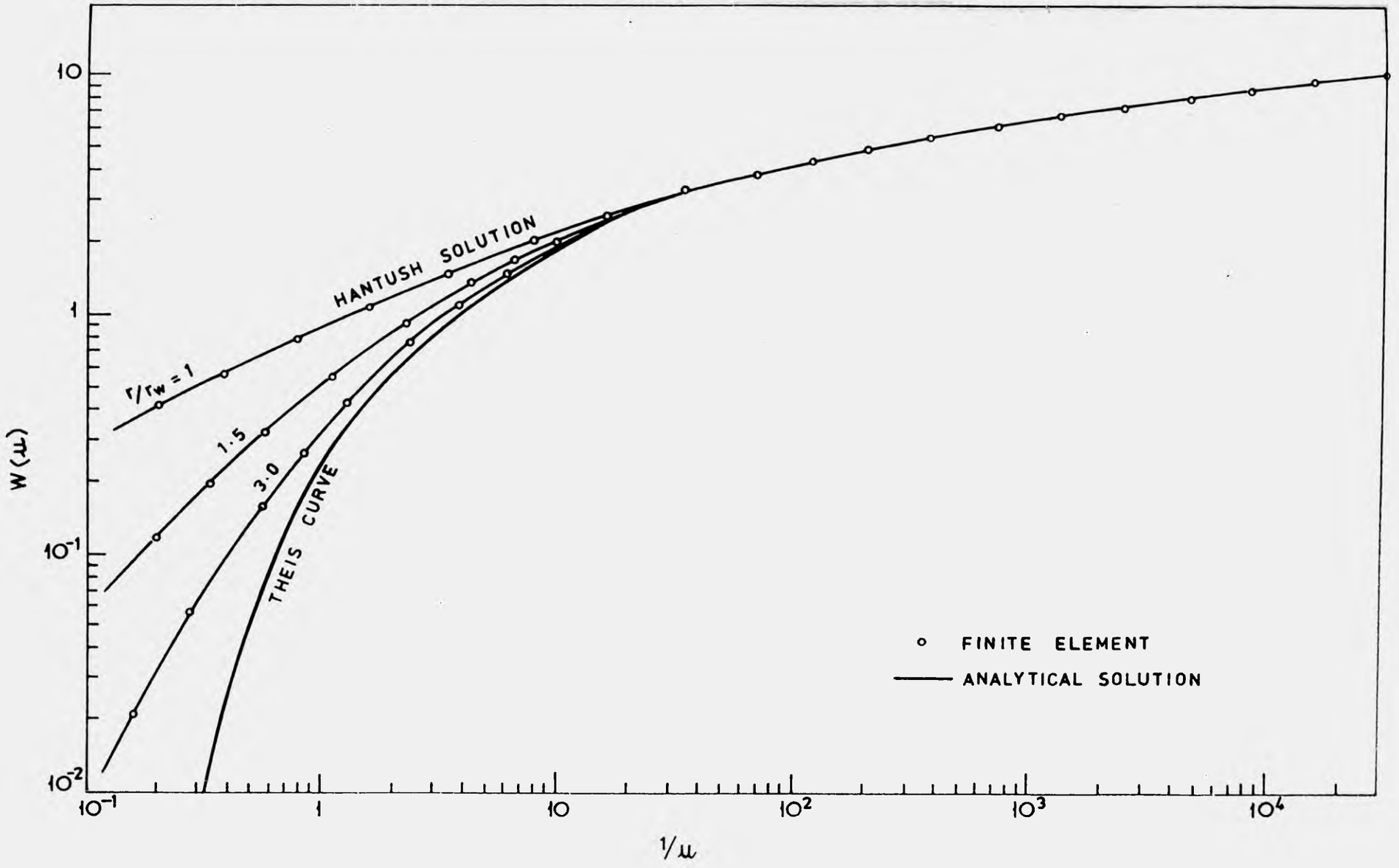

Fig. 5.3: Comparison of the finite element and Hantush's analytical solutions.

calculated well discharge, r is the radial distance from the well, and t is the elapsed time since the commencement of pumping. The drawdown s and the aquifer coefficients T and S were calculated from

$$s = h^{o} - h \tag{5.3}$$

$$S = S_s m \tag{5.4}$$

$$T = \frac{m}{a+bV_{cr}} \tag{5.5}$$

where m is the aquifer thickness, and h^{o} is the initial height of the water table above the datum plane. The remaining symbols have been defined previously.

It is seen in Fig. 5.3 that excellent agreement between the numerical and analytical solutions was achieved. The use of 3-node one-dimensional elements was found to result in a small number of equations to be solved and a considerable saving in computational time.

5.2.2 Two-regime Flow Solutions

(i) Transient Flow Cases

Analytical solutions of the problem of transient, one-dimensional, two-regime well flow are unavailable in the literature. In the present work, the finite element method was used to solve the flow problem shown in Fig. 5.1, and to investigate non-Darcy flow near the well. The effect of non-Darcy flow on drawdown distribution and the well discharge-drawdown relationship was examined.

Six flow cases of different discharge were solved. The numerical solutions were obtained by employing the computer program

which was used previously to solve the Darcy flow case. The network shown in Fig. 5.2 was again adopted. The initial time step was chosen to be .0018 minutes. Each remaining time step was generated by multiplying the preceding time step by 1.4 until the end of the pumping period at t=1000 minutes.

For flow case No. 6, Q = 400 cfm, the drawdown-time relationships at several points near the well were obtained in dimensionless form, W(u) vs 1/u, and are plotted in Fig. 5.4. The dimensionless parameters $\lambda = \frac{bQT}{2\pi m^2 r}$ and $\zeta = \frac{bV_{cr}}{a}$ were used to characterise the effect of non-Darcy flow on drawdowns. The justification for using these parameters is given in Appendix 2. It is noted that the dimensionless type curves for all points in the non-Darcy flow zone lie above the conventional Theis curve for the Darcy flow case, and that the deviation from the Theis curve becomes greater as the value of λ increases.

For flow cases Nos. 2 and 4, Q = 50 and Q = 100 cfm respectively, semi-logarithmic plots of the drawdown-radial distance relationships at times t = 0.46 and t = 118 minutes are shown in Figs. 5.5 and 5.6. It can be seen that the drawdown-distance curves are non-linear for radial distances less than a critical value. This value, indicated by the junction of the dotted and solid lines, represents the outer limit of the non-Darcy flow zone. The critical radius is observed to increase with increase in the well discharge. In both figures, the dotted curves represent the drawdown-distance relationships that would

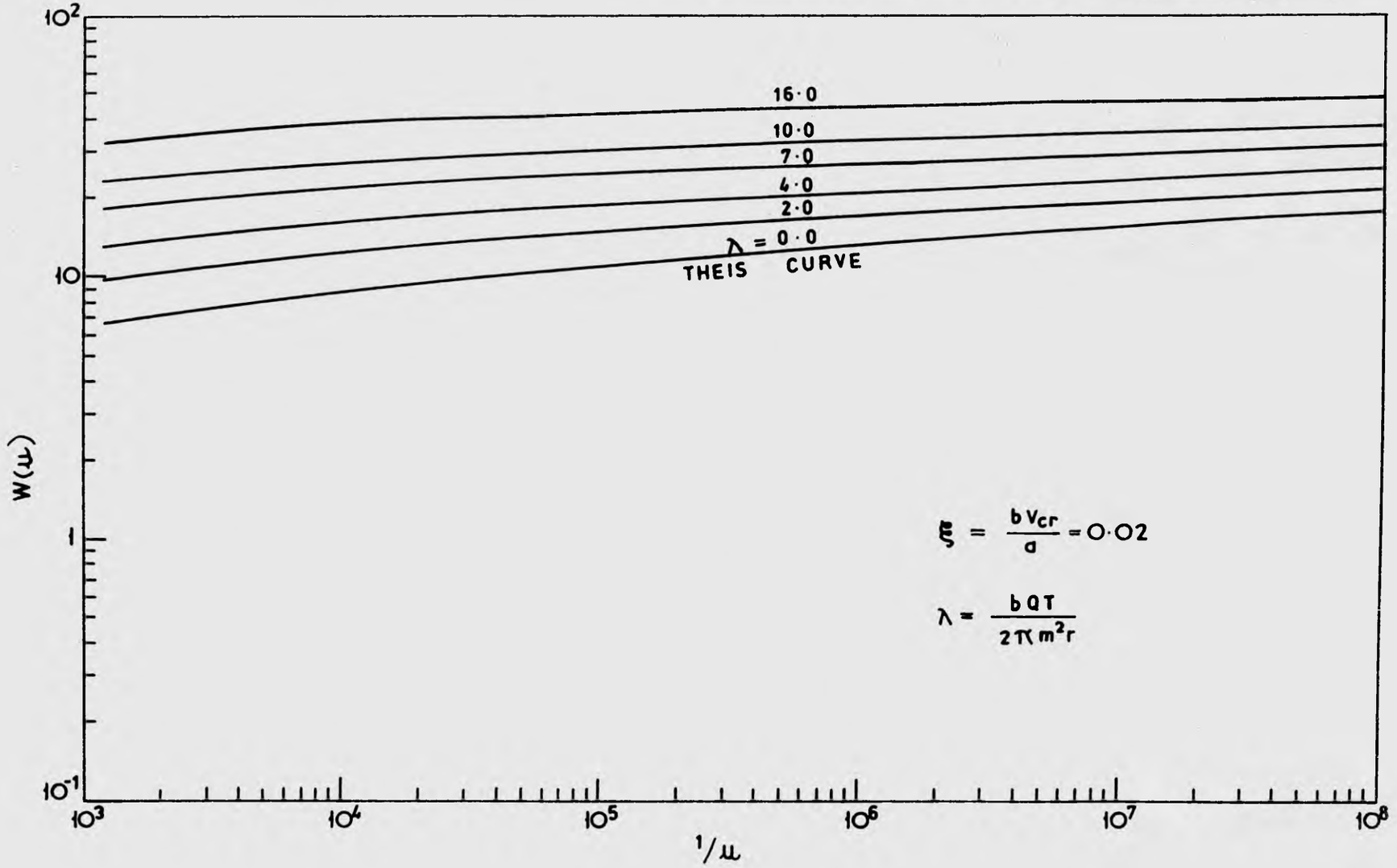

Fig. 5.4: Dimensionless drawdown-time relationships for points in the non-Darcy flow zone near the well. (Flow case No. 6, Q = 400 cfm).

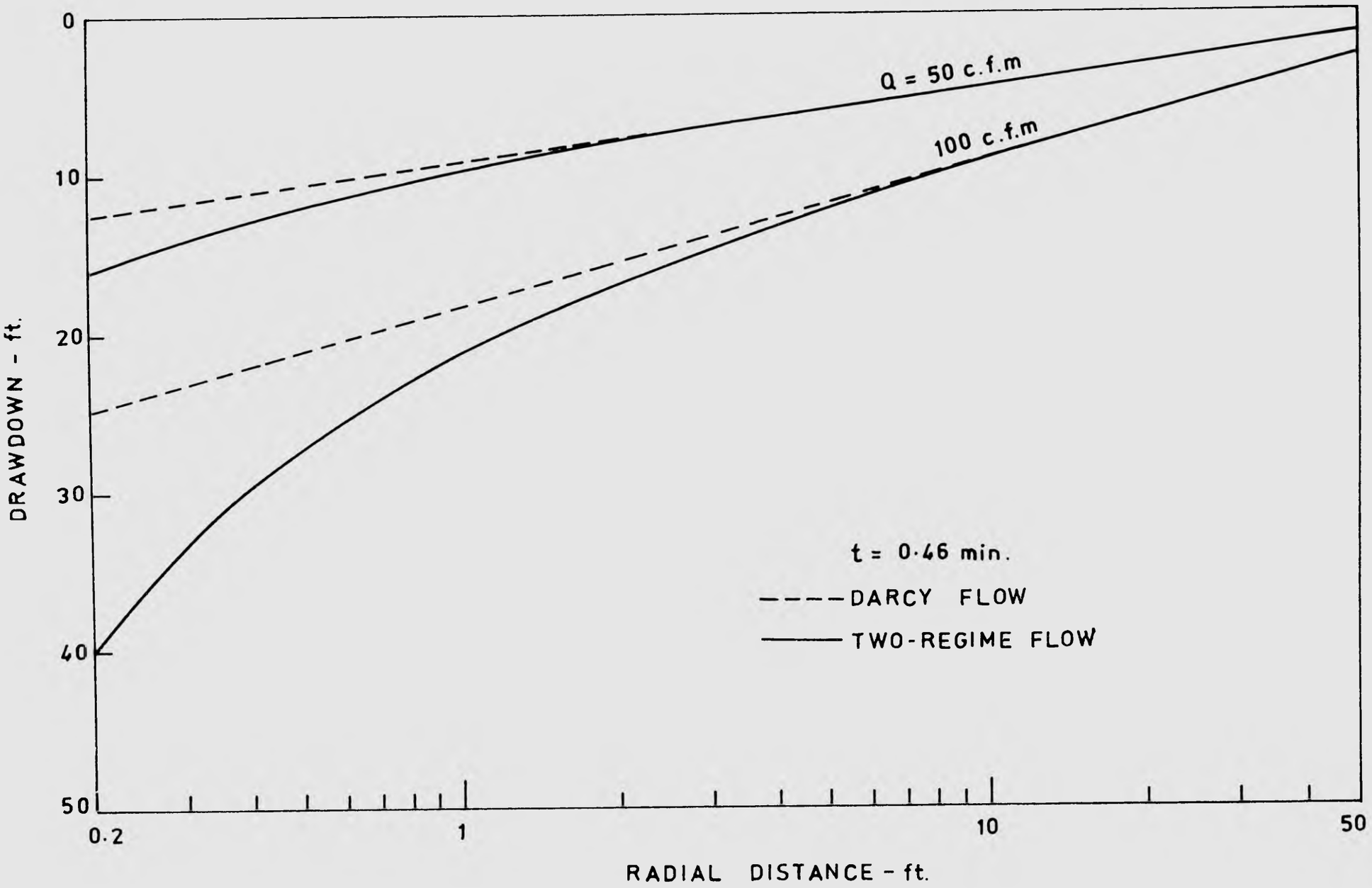

Fig. 5.5: Drawdown-radial distance curves at time t = 0.46 minutes.

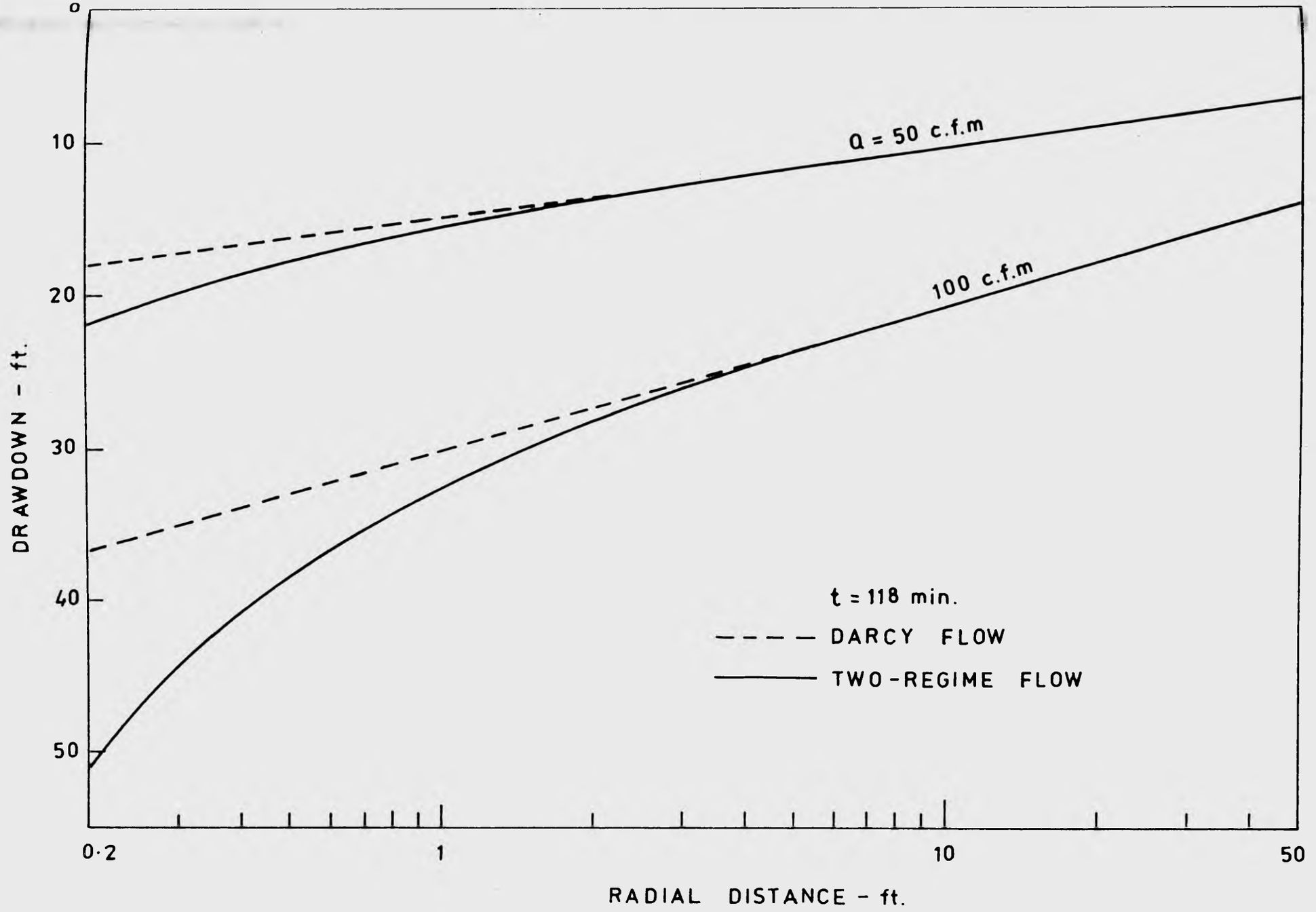

Fig. 5.6: Drawdown-radial distance curves at time t = 118 minutes.

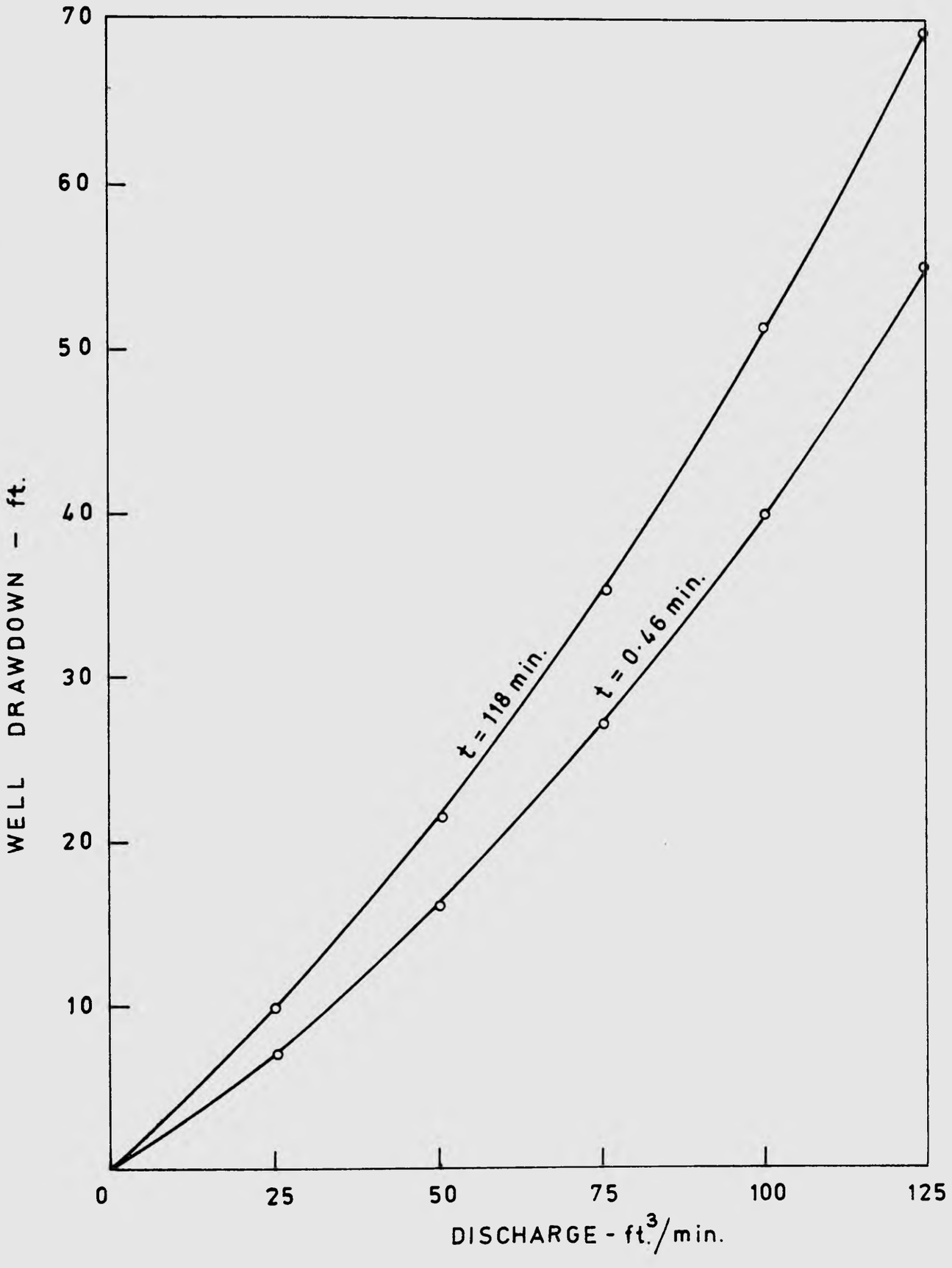

Fig. 5.7: Well discharge-drawdown relationships at times t = 0.46 and 118 minutes.

result if wholly Darcy flow were assumed. Comparison of Figs. 5.5 and 5.6 shows that the additional drawdowns due to non-Darcy flow remain the same for both times.

The effect of non-Darcy flow on the well discharge-drawdown relationship is illustrated in Fig. 5.7 for times t = 0.46 and t = 118 minutes. It is noted that as distinct from the wholly Darcy flow case, the relationships for two-regime flow are non-linear and may be described by the following equation:-

$$s_w = BQ + CQ^2 \qquad (5.6)$$

where s_w = drawdown at the well (s_w does not include the head loss resulting from flow through the well screen and inside the well)

Q = well discharge

B, C = empirical coefficients of the equation

CQ^2 = additional well drawdown due to non-Darcy flow

The values of B and C for the two curves in Fig. 5.7 were calculated and are listed in Table 5.1.

Table 5.1: Values of Coefficients B and C for the Well in Fig. 5.1

t(min.)	B(min./ft.^{2})	C(min^2/ft.^{5})
0.46	0.24	0.00155
118	0.36	0.00155

It is evident that for both times t = 0.46 and t = 118 minutes, the values of C are virtually the same. This evidence points to the fact that for transient flow at constant discharge, the additional non-Darcy losses remain constant with time after non-Darcy flow has been

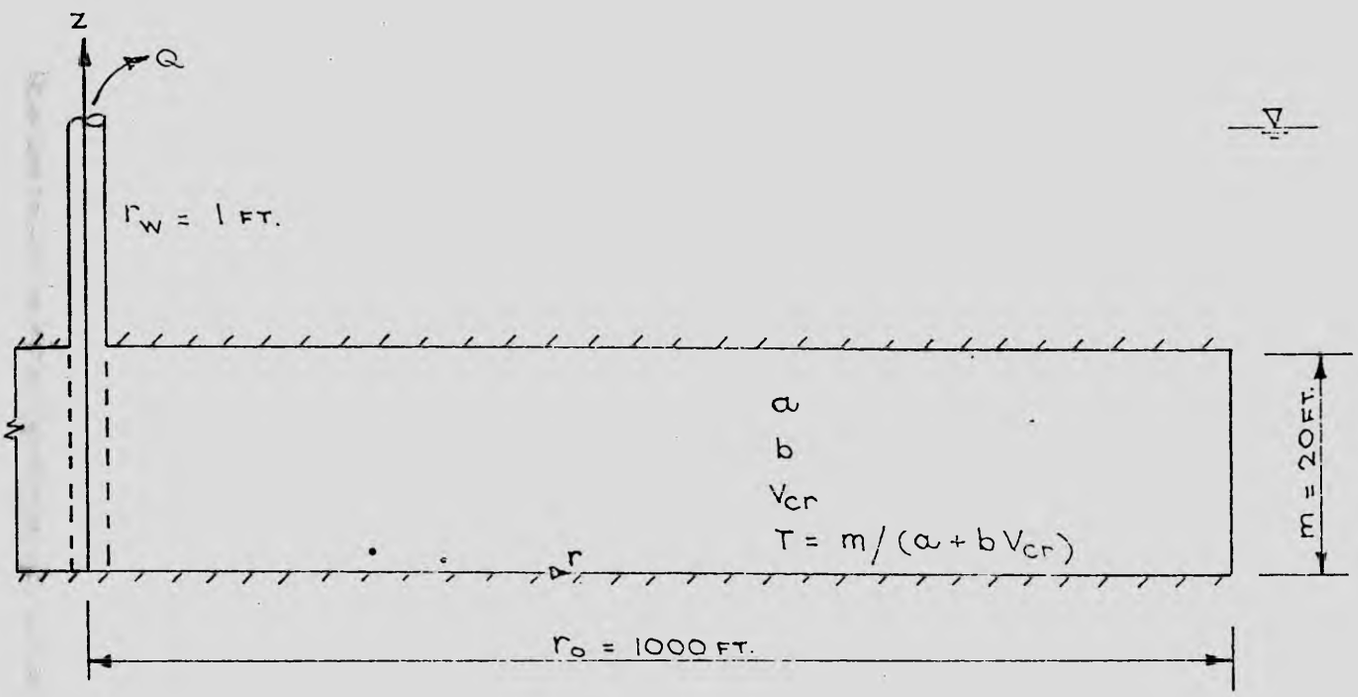

Flow Case No.	a min/ft.	b min^2/ft^2	V_{cr} ft/min	Q ft^3/min	$\lambda = \frac{bQT}{2\pi m^2 r_o}$
1	10	0	0	140	0
2	10	20	.060	140	.002
3	10	20	.060	280	.004
4	10	40	.030	280	.008
5	10	80	.016	280	.016

Fig. 5.8: Data for the problem of steady flow towards a fully screened well in a confined aquifer.

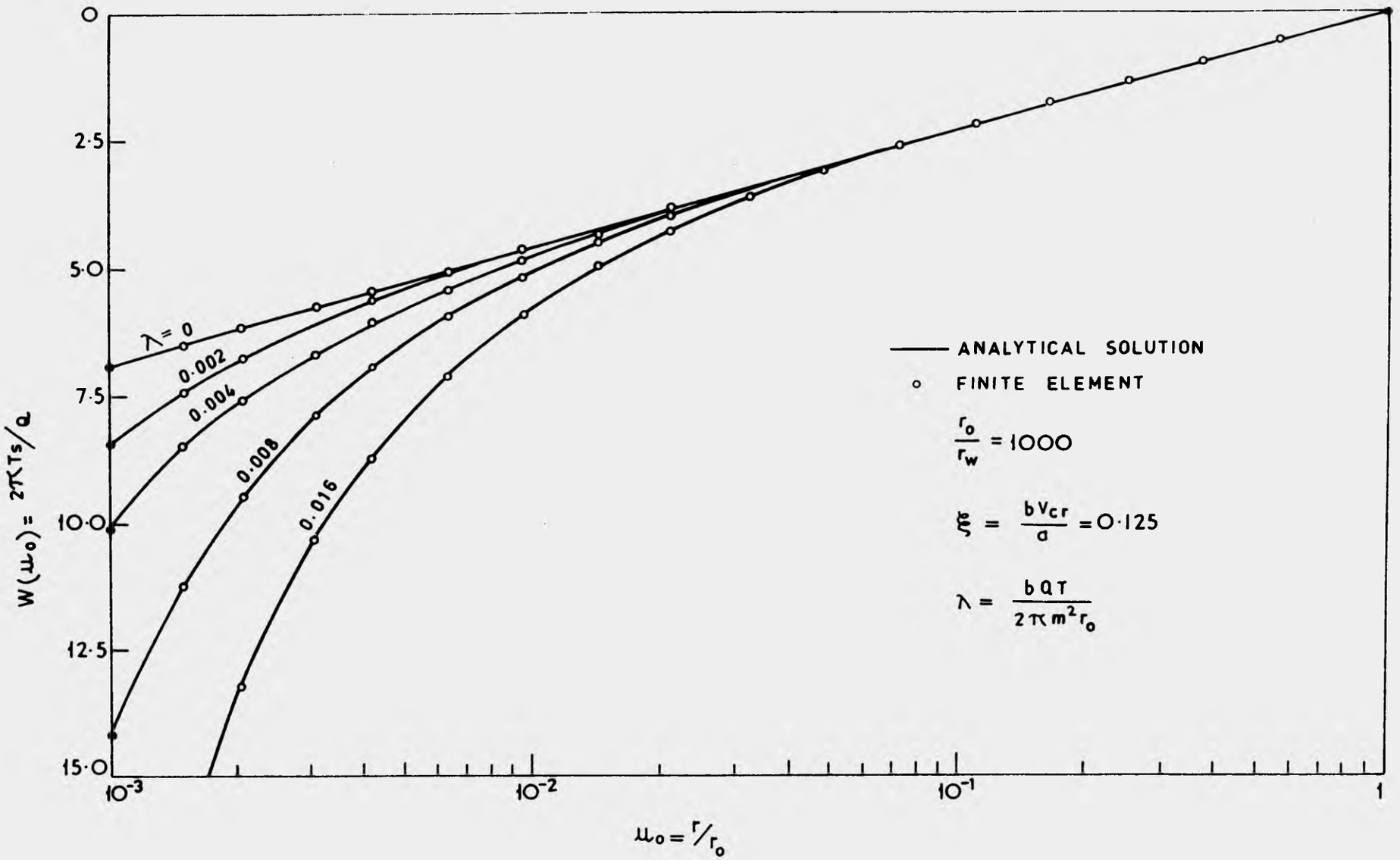

Fig. 5.9: Dimensionless drawdown-distance relationships for steady, one-dimensional, confined flow. λ and ξ characterise non-Darcy flow.

fully developed near the well.

(ii) Steady Flow Cases

A complete analytical solution of the problem of steady state, one-dimensional, two-regime well flow is presented in Appendix 2. The dimensionless parameters characterising non-Darcy flow near the well are shown to be $\lambda = \frac{bQT}{2\pi m^2 r_o}$ and $\xi = \frac{bV_{cr}}{a}$.

To verify the finite element analysis of the flow problem, five steady flow cases were generated. These flow cases, shown in Fig. 5.8, were chosen to have different values of λ but the same values of ξ and r_o/r_w. A network similar to that shown in Fig. 5.2 was adopted. This network consists of 9 elements and of 19 nodes. The external radius chosen is 1000 ft. For each flow case, the dimensionless drawdown-radial distance relationship was obtained and plotted on a semi-logarithmic scale. Fig. 5.9 shows the comparison of the finite element and the analytical solutions. It can be seen that excellent agreement between the two solutions was achieved.

5.3 Flow towards a Partially Screened Well in a Confined Aquifer

5.3.1 Darcy Flow Solutions

A diagrammatic sketch of a partially screened well in a confined aquifer is shown in Fig. 5.10. The well is screened from the base of the aquifer to a height equal to half of the aquifer thickness. A complete analytical solution to the problem of transient Darcy flow at constant discharge was presented by Hantush (1961). His simplified solution for drawdown distribution along the base of the aquifer is given in Appendix 3.

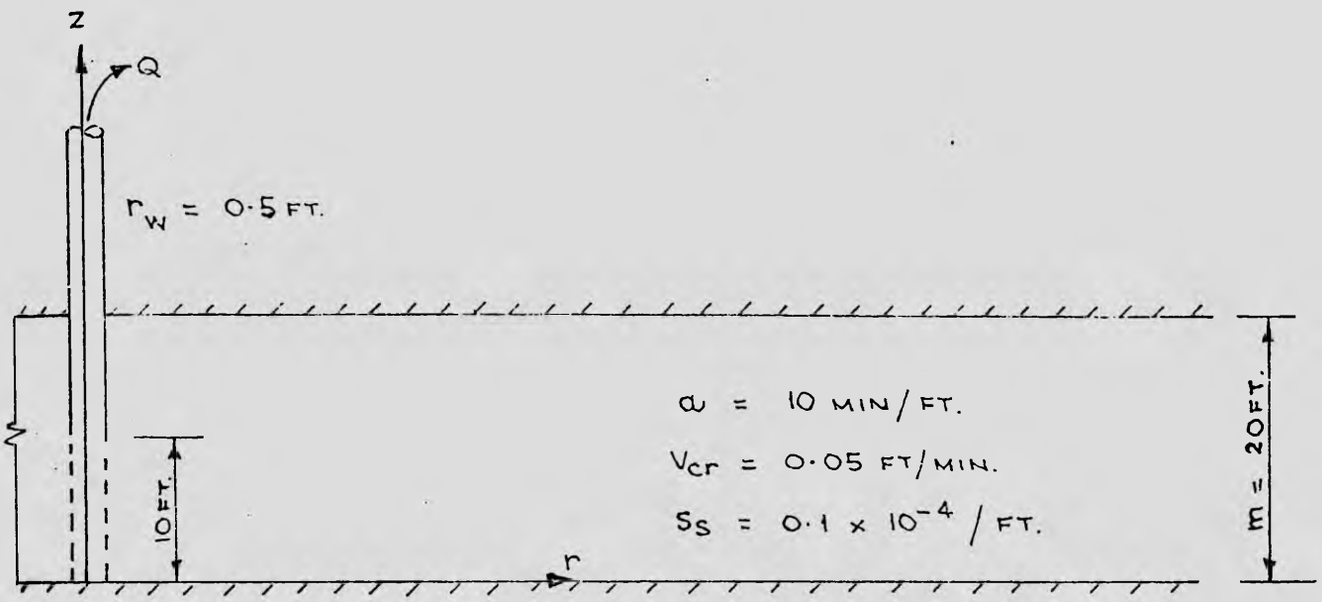

Flow Case No.	b(min^2/ft^2)	Q(ft^3/min)
0	0	100
1	20	25
2	20	50
3	20	75
4	20	100
5	20	125

Fig. 5.10: Data for the problem of transient flow towards a partially screened well in a confined aquifer.

To verify the finite element analysis, a hypothetical problem was formulated. The problem data are given in Fig. 5.10, flow case No.0. The network shown in Fig. 5.11 was adopted. The chosen external radius is 10,000 ft. As seen in the figure, the flow region is divided into a number of vertical blocks, each of which is further subdivided into a number of triangular ring elements. A total of 151 elements and 128 nodes was used. The elements increase in size along the radial distance from the pumped well. The width of the first vertical block is 0.20 ft., and the width of each remaining block is 1.4 times that of the preceding block (i.e. $\Delta r_i = 1.4 \times \Delta r_{i-1}$) until a maximum width $\Delta r_{max} = 400$ ft. is exceeded. The maximum width is prescribed to avoid ill-conditioned triangles.

An initial time step of 0.00054 minutes was chosen. Each remaining time step was generated by multiplying the previous time step by 1.4 until 30 time steps were completed. The numerical solution obtained was a drawdown distribution that varied with depth for radial distances less than approximately 1.5 times the aquifer thickness. The drawdowns along the base of the aquifer were used in the comparison with Hantush's analytical solution. For the nodes located at radial distances of 0.5 , 2.0 and 10.0 ft. from the pumped well, the drawdown-time relationships were obtained in dimensionless form of W(u) versus 1/u and are plotted in Fig. 5.12. Good agreement between the analytical and finite element solutions may be observed.

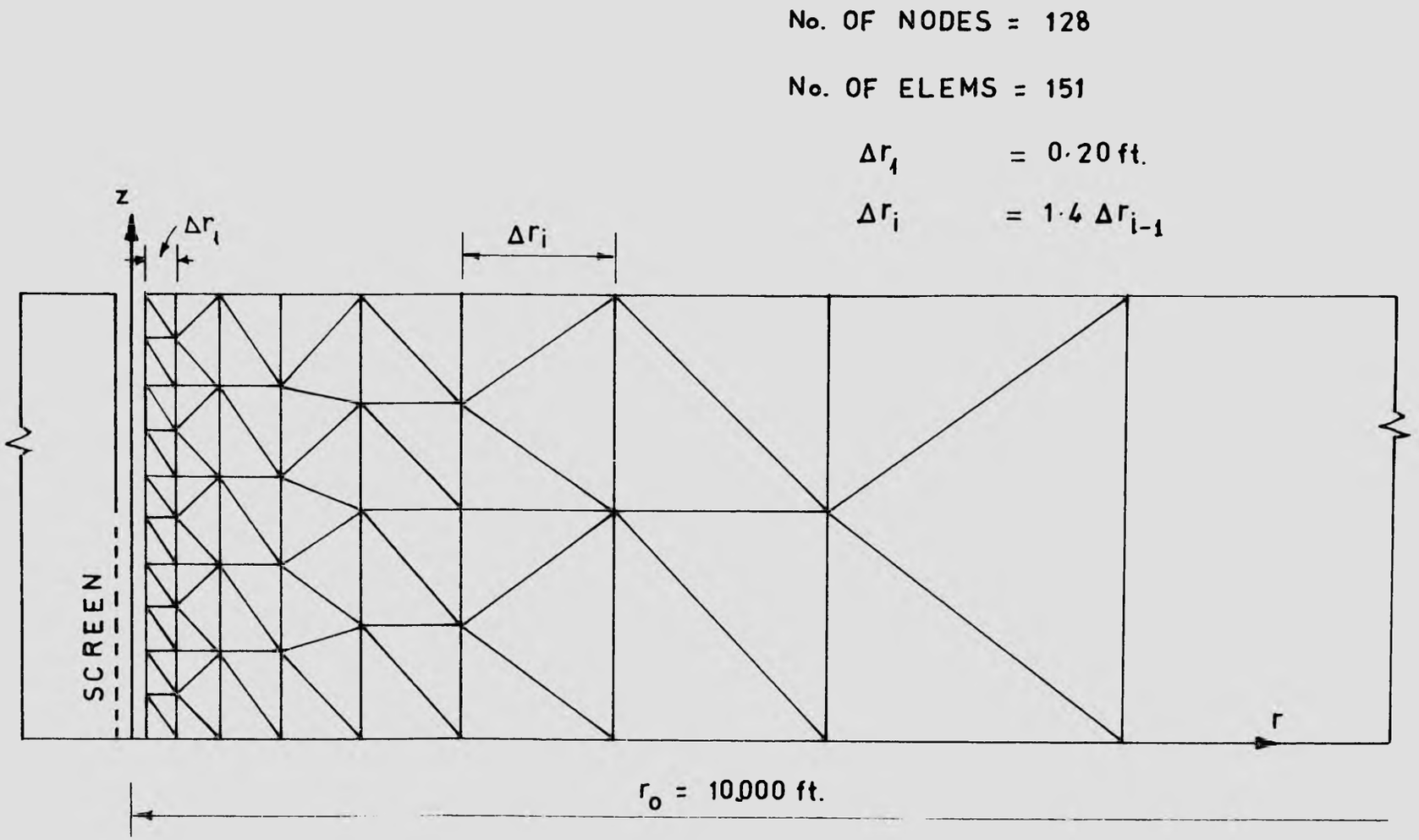

Fig. 5.11: Finite element network for a confined aquifer with a partially screened well.

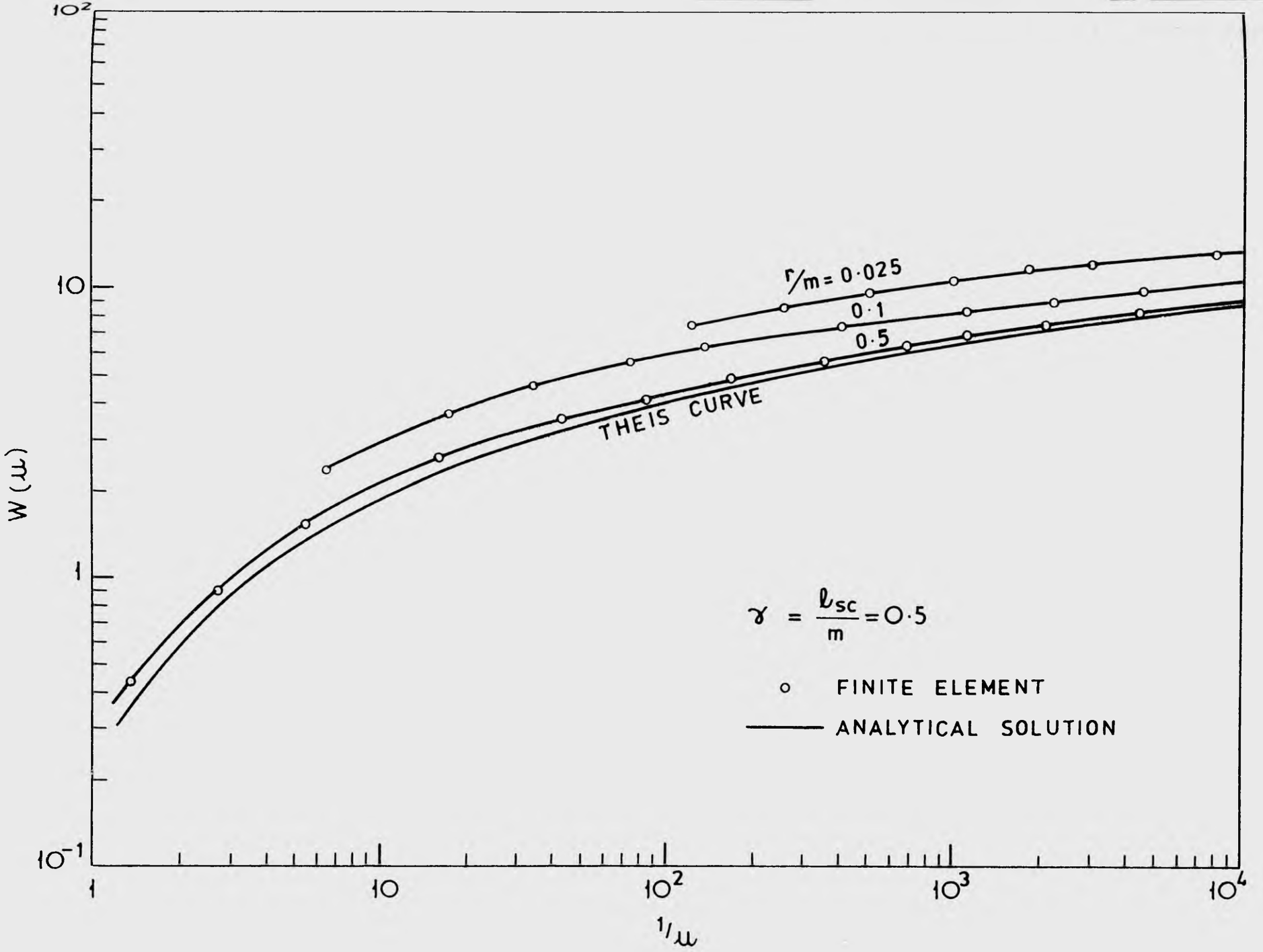

Fig. 5.12: Comparison of finite element and Hantush's analytical solutions.

5.3.2 Two-regime Flow Solutions

(i) Transient Flow Cases

To use the finite element method to investigate transient two-regime flow and study the effect of non-Darcy flow near the well, the problem defined in Fig. 5.10 was solved for five flow cases of different discharge. The numerical solutions were obtained by employing the computer program which was used previously to solve the Darcy flow case. The network shown in Fig. 5.11 was again adopted. An initial time step of 0.0042 minutes was chosen. The remaining time steps were generated in the manner described previously.

For flow cases Nos. 2, 3 and 5, the dimensionless drawdown-time relationships, W(u) versus 1/u, for a nodal point located at the base of the aquifer and at the well are plotted in Fig. 5.13. For flow cases Nos. 3 and 5, the plot of W(u) versus 1/u for a nodal point located at the base of the aquifer and at 2 ft. from the pumped well is shown in Fig. 5.14. In each figure λ and ξ are the two dimensionless parameters chosen to characterise non-Darcy flow near the well. The type curve for the wholly Darcy flow case, $\lambda = 0$, is also included. It can be seen that for all the two-regime flow cases solved, the type curves for the two points, r = 0.5 and 2.0 ft., in the non-Darcy flow zone lie above the Darcy flow type curve, and that the deviation from the Darcy flow curve becomes greater as the value of λ increases.

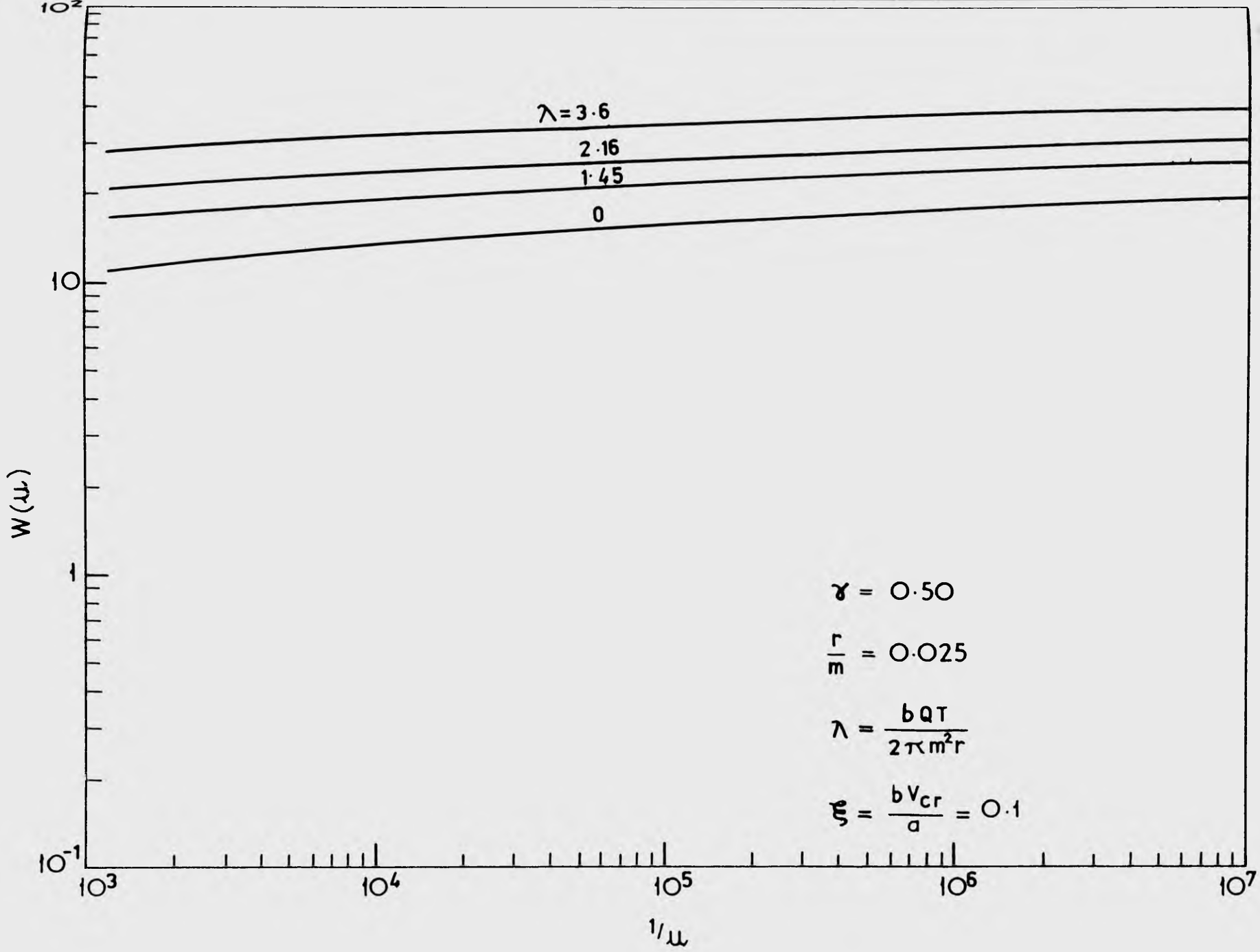

Fig. 5.13: Dimensionless drawdown-time relationships for a point located at the base of the aquifer and at the well. λ and ξ characterise non-Darcy flow.

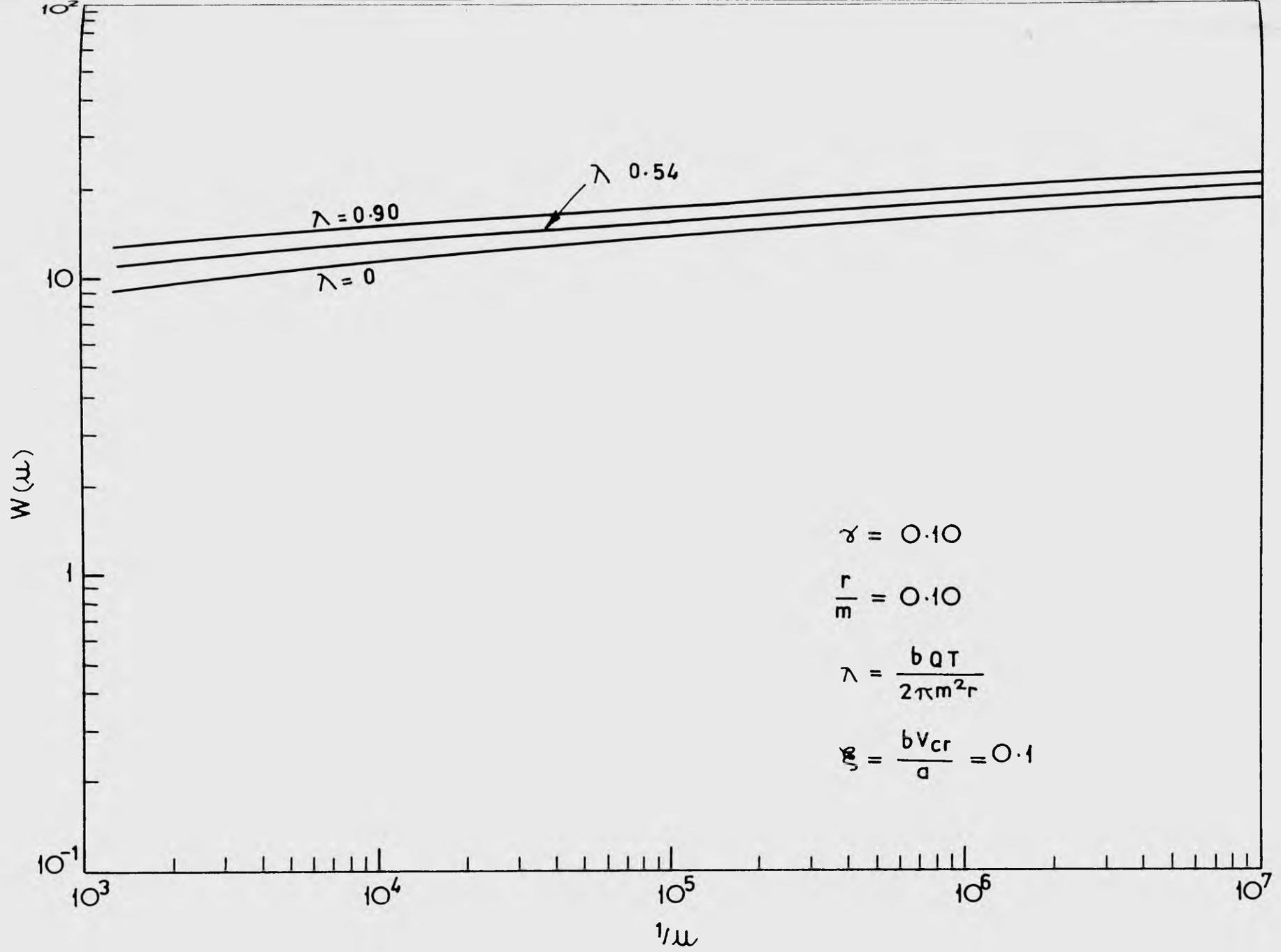

Fig. 5.14: Dimensionless drawdown-time relationships for a point located at the base of the aquifer and at 2 ft. from the well. λ and ξ characterise non-Darcy flow.

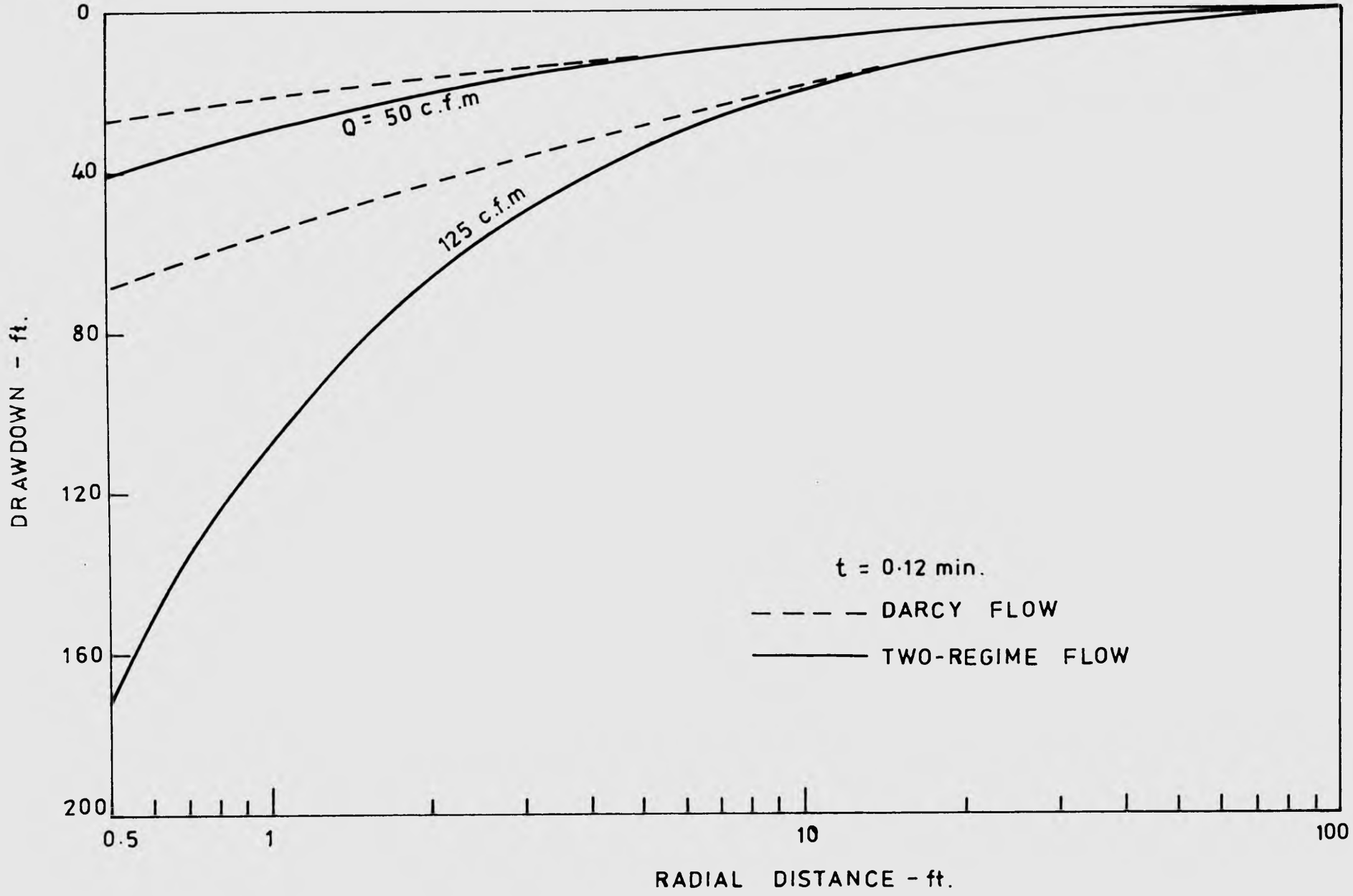

Fig. 5.15: Drawdown-radial distance curves along the base of the aquifer at time t = 0.12 minutes.

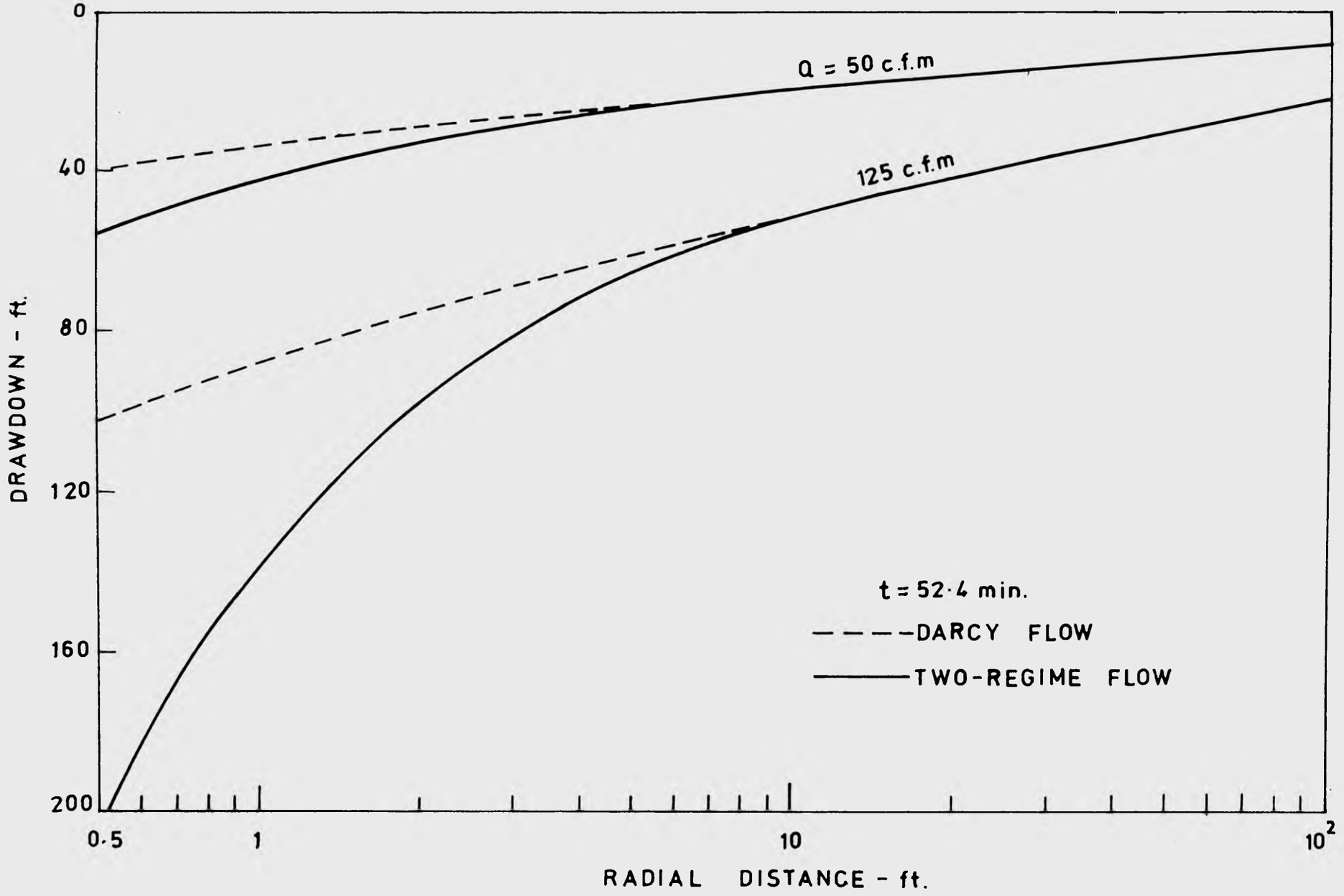

Fig. 5.16: Drawdown-radial distance curves along the base of the aquifer at time t = 52.4 minutes.

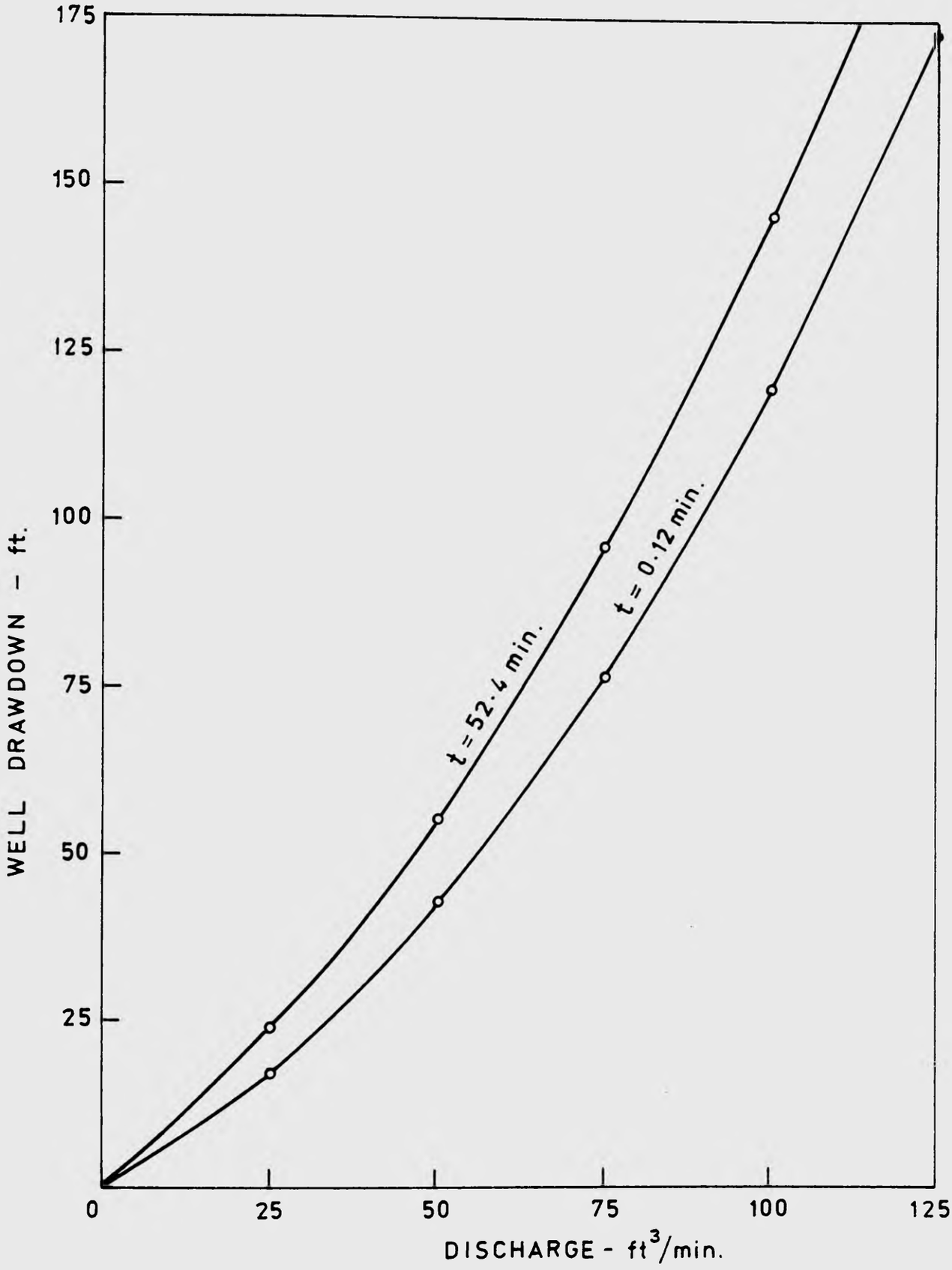

Fig. 5.17: Well discharge-drawdown relationships at times t = 0.12 and 52.4 minutes.

For flow cases Nos. 3 and 5, semi-logarithmic plots of drawdown versus radial distance at times t = 0.12 and 52.4 minutes are illustrated in Fig. 5.15 and 5.16 respectively. The drawdown-radial distance relationships for the corresponding Darcy flow cases are shown in dotted lines. It is noted that for each discharge the two-regime flow solution deviates from the Darcy flow solution in the immediate vicinity of the well where non-Darcy flow exists, and that the two solutions coincide at a certain critical radius which is observed to increase with increase in the discharge. On comparing Figs. 5.15 and 5.16, it can be seen once again that the additional drawdowns due to non-Darcy flow remain the same for both early and late times.

Finally, the effect of non-Darcy flow and partial screening on the well discharge-drawdown relationship is illustrated in Fig. 5.17. It is noted that for times t = 0.12 and 52.4 minutes, the well discharge-drawdown curves are non-linear and may be fitted by equation (5.6).

(ii) Steady Flow Cases

An analytical solution to the problem of steady state, two regime flow towards a partially screened well in a confined aquifer has not been developed. The finite element analysis of the flow problem was verified by comparison with experimental results to be presented in the next chapter. As in the one-dimensional flow cases, the same dimensionless parameters λ and ξ were employed to characterise non-Darcy flow in the vicinity of the well.

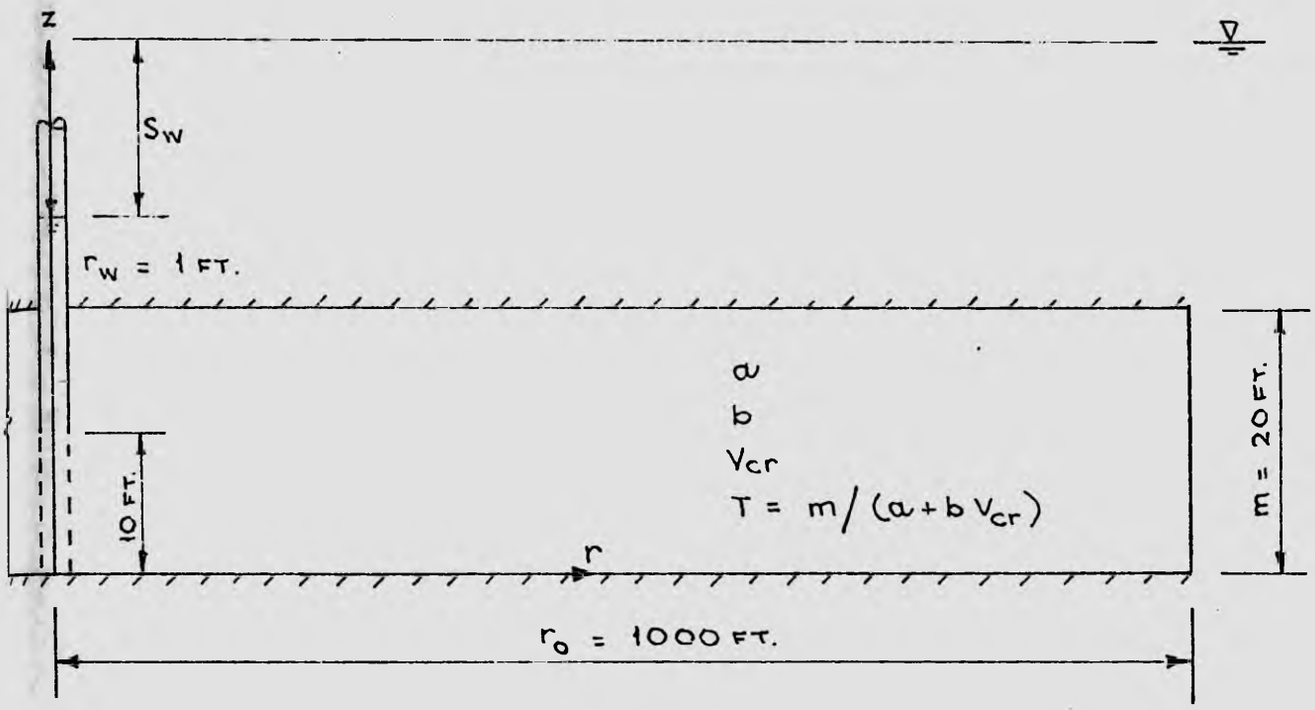

Flow Case No.	a min./ft.	b $min.^2/ft.^2$	V_{cr} ft./min.	S_w ft.
1	10	0	0	40
2	10	20	.062	40
3	10	20	.062	80
4	10	20	.062	160
5	10	40	.031	160
6	10	100	.0125	160

Fig. 5.18: Data for the problem of steady flow towards a partially screened well in a confined aquifer.

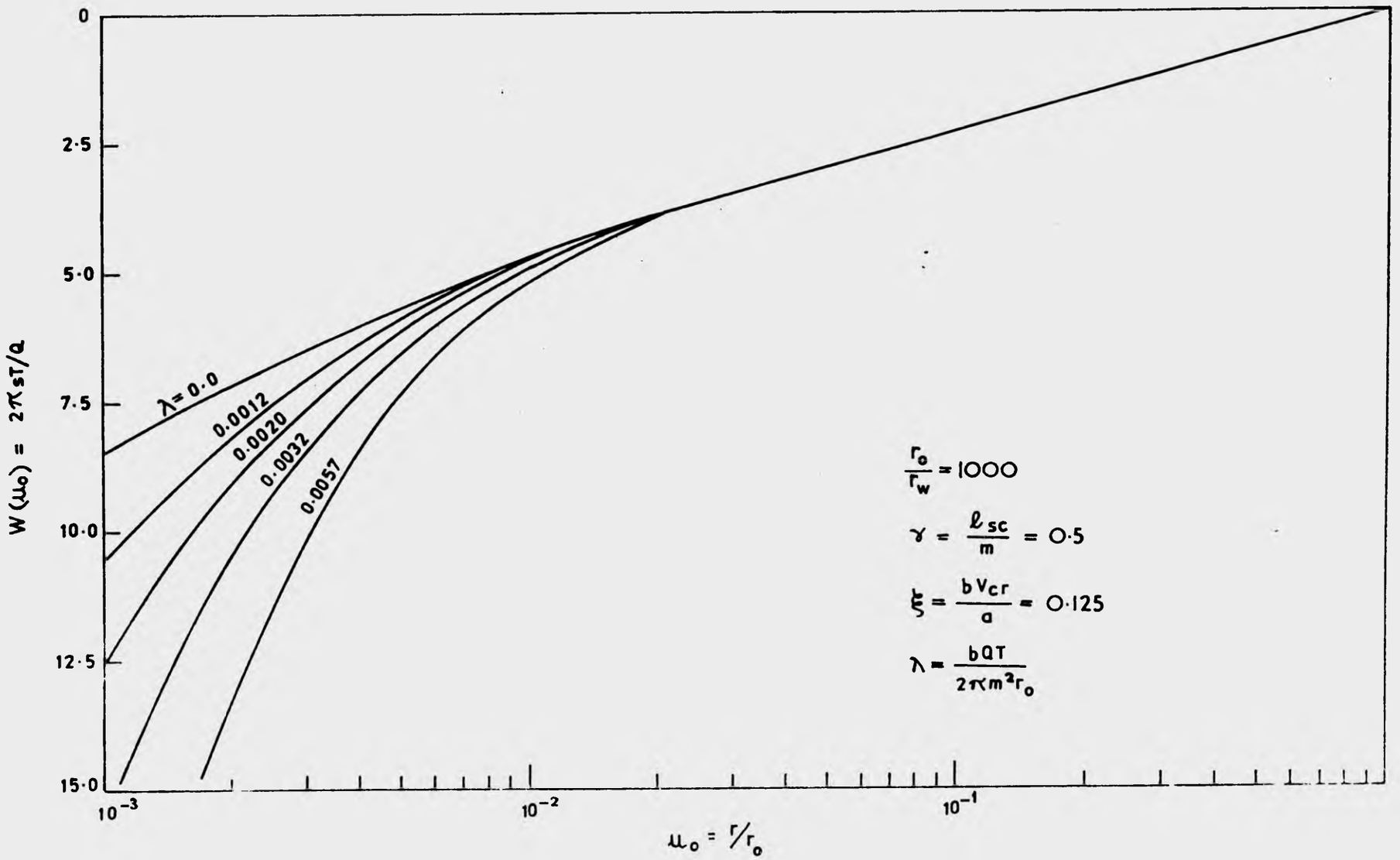

Fig. 5.19: Dimensionless base drawdown-distance curves for steady confined flow towards a partially screened well. λ and ξ characterise non-Darcy flow.

The problem shown in Fig. 5.18 was solved for 6 flow cases which were chosen to cover a range of values of λ and to have the same value of ξ, r_o/r_w and l_{sc}/m. A network similar to that shown in Fig. 5.11 was adopted. A total of 128 elements and 104 nodes was used. For each flow case, the dimensionless drawdown-radial distance relationship at the base of the aquifer is plotted on a semi-logarithmic scale as shown in Fig. 5.19. The effect of increasing the value of λ on the drawdown-radial distance curve may be observed. The curve for flow case No.1, which is the wholly Darcy flow case, corresponds to $\lambda = 0$.

5.4 Flow towards a Well in a Confined Aquifer-Aquitard System

5.4.1 Darcy Flow Solutions

A diagrammatic sketch of a well in a confined aquifer-aquitard system is shown in Fig. 5.20. The well is screened from the base to the top of the main aquifer and the entire system is confined by impermeable strata. An analytical approach to the problem of transient Darcy flow at constant discharge was first presented by Hantush (1960). He derived asymptotic solutions for drawdowns in the main aquifer but did not obtain solutions for drawdowns in the overlying aquitard.

Neuman and Witherspoon (1969) later extended Hantush's work to obtain a complete solution to a more complex problem of flow in a confined system consisting of two aquifers separated by an aquitard. They also developed asymptotic solutions for small values of time.

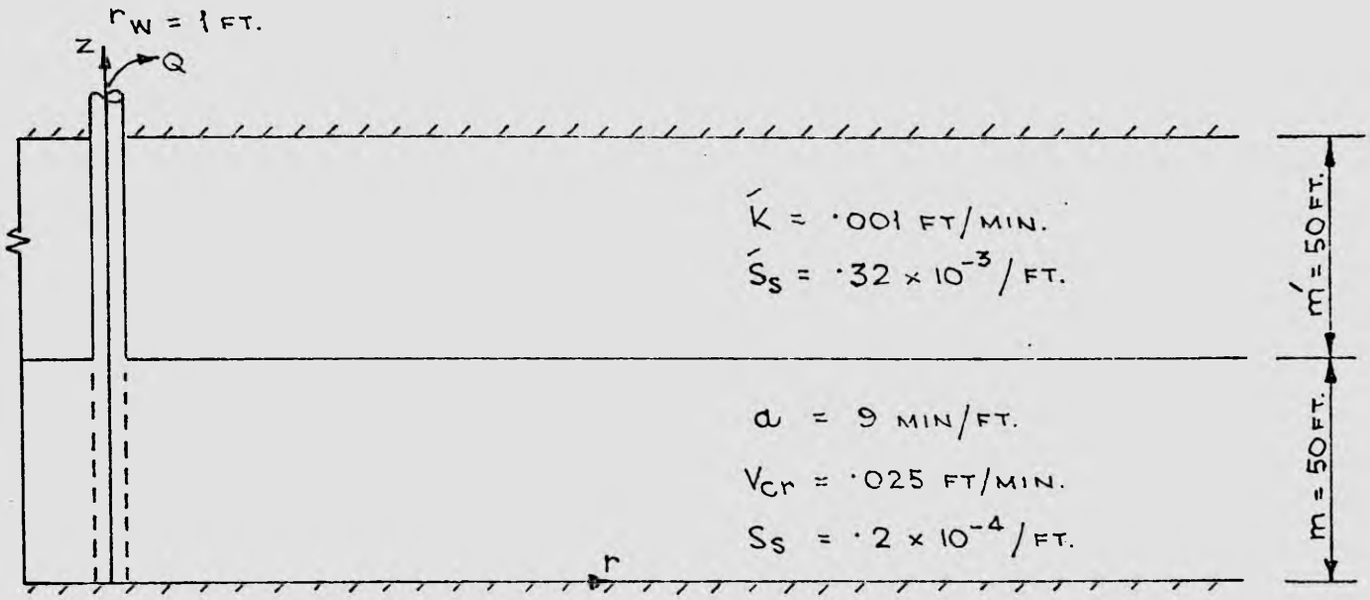

Flow Case No.	b min^2/ft^2	Q $ft^3/min.$
0	0	100
1	40	100
2	40	200
3	40	300
4	40	400
5	40	500
6	40	1000

Fig. 5.20: Data for the problem of transient flow towards a well in a confined aquifer-aquitard system.

These solutions have been adapted to the simpler problem of flow in the system shown in Fig. 5.20. All of the available analytical solutions are based on the assumption that the flow direction is horizontal in the aquifer and vertical in the aquitard. This assumption was shown by Neuman and Witherspoon (1969) to lead to errors of no more than 5 percent when the permeability of the aquifer is at least two orders of magnitude greater than that of the aquitard.

To verify the finite element analysis, a hypothetical problem was formulated. The problem data are given in Fig. 5.20, flow case No. 0. To ensure the validity of the analytical solutions, the permeability of the main aquifer was chosen to be more than 100 times greater than that of the overlying aquitard. The network shown in Fig. 5.21 was adopted. The external radius chosen for this network is 5000 ft. As seen in the figure, the flow region is divided into a number of vertical blocks, each of which is further subdivided into a number of rectangular ring elements. A finer subdivision of the vertical blocks is used in the aquitard where steep vertical hydraulic gradients occur at early pumping times. The width of the first block is 0.50 ft. and the width of each remaining block is 1.5 times that of the preceding block until a prescribed maximum width of 500 ft. is exceeded. The entire network consists of 184 nodes and 154 elements. An initial time step of 1.14 minutes was chosen. Each remaining time step was generated in the manner described previously. The numerical solution obtained was compared with the analytical solutions listed in Appendix 3.

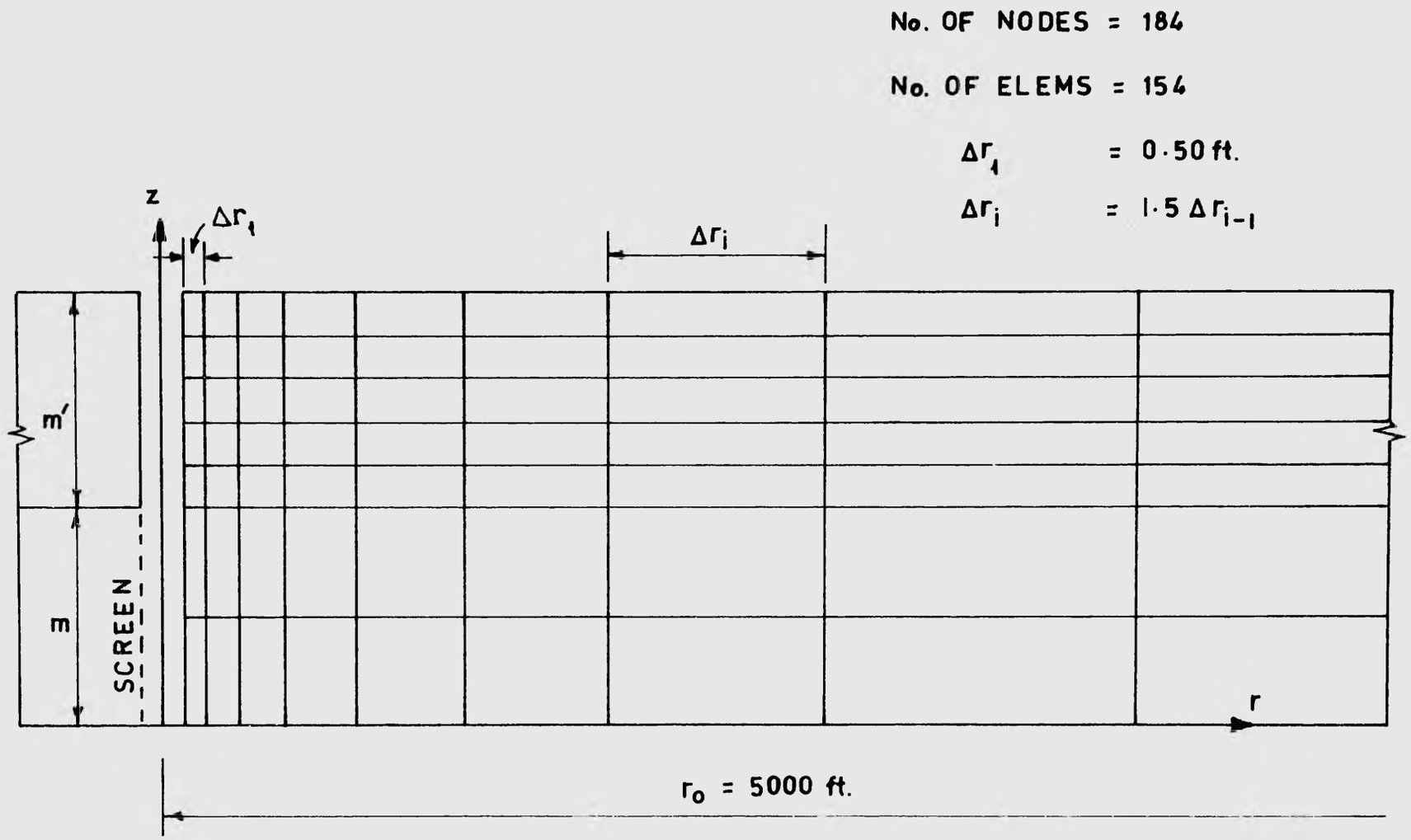

Fig. 5.21: Finite element network for a confined aquifer-aquitard system with a well which is screened through the thickness of the aquifer.

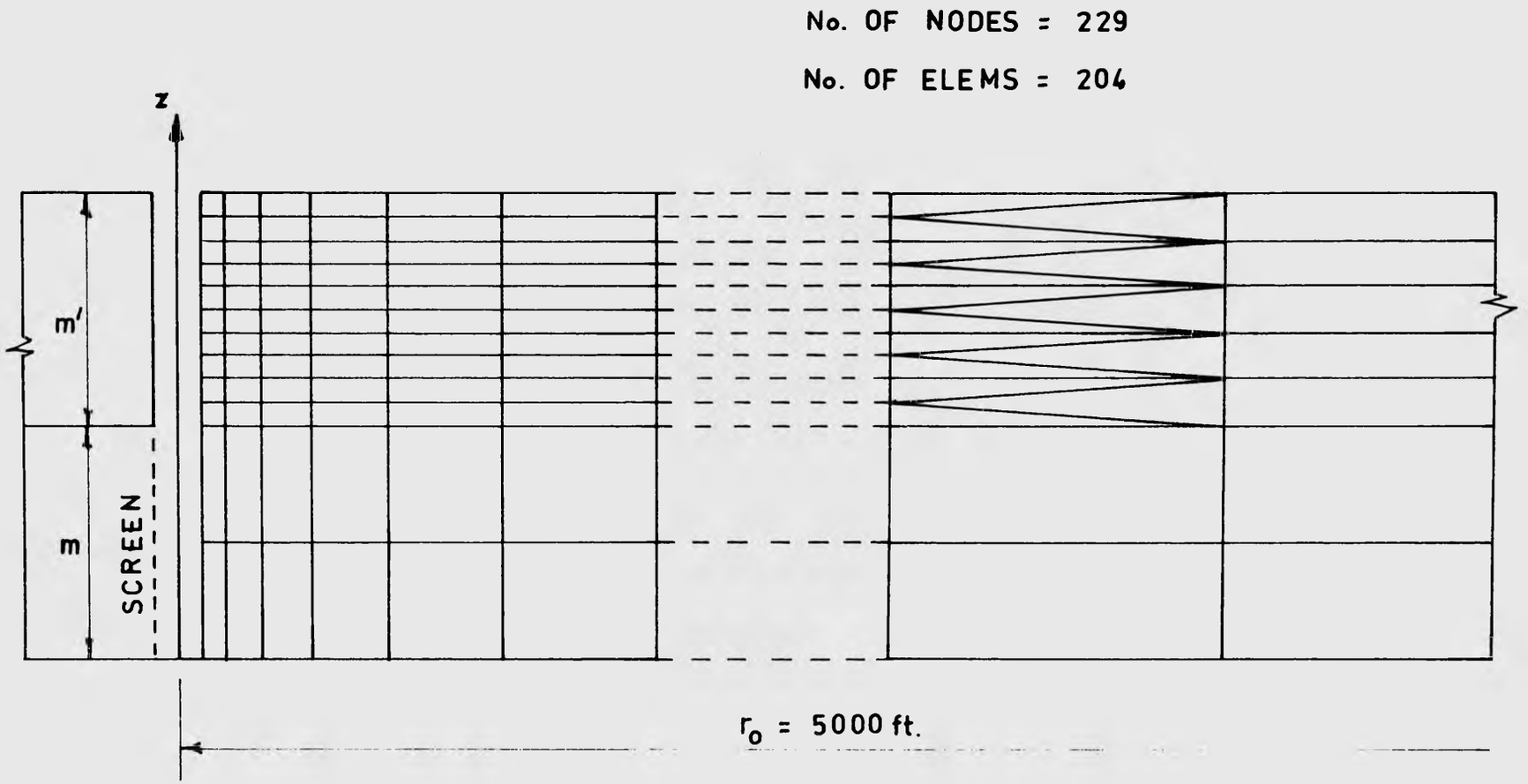

Fig. 5.22: Refined finite element network for a confined aquifer-aquitard system with a well which is screened through the thickness of the aquifer.

Fig. 5.23 illustrates a logarithmic plot of the dimensionless drawdown-time relationships for various nodal points in the aquifer and overlying aquitard. All of these points are located at a radial distance of 5 ft. from the pumped well. In the figure, the dimensionless parameters $\frac{r}{B}$, β, δ_1 and z'/m' were calculated from

$$\frac{r}{B} = r\sqrt{\frac{K'}{Kmm'}} \tag{5.7}$$

$$\beta = \frac{r}{4m}\sqrt{\frac{K'S_s'}{K S_s}} \tag{5.8}$$

$$\delta_1 = 1 + \frac{S_s'm'}{S_s m} \tag{5.9}$$

$$z'/m' = \frac{z - m}{m'} \tag{5.10}$$

where K', S_s', m' are the coefficient of permeability, specific storage and thickness of the aquitard respectively. The remaining symbols have been defined previously.

It can be seen that for large values of time ($t \geqslant \frac{2S_s' m'^2}{K'}$) the finite element solution agrees closely with the analytical solutions. Deviation occurs at small values of time ($t \leqslant \frac{S_s' m'^2}{10K'}$) along the steep portions of the type curves for the nodal points in the aquitard.

To determine whether the failure of the finite element method to yield satisfactory results for early times was due to the coarse mesh used, the network and time step sizes were refined. The new network shown in Fig. 5.22 was adopted. As seen in the figure, the number of vertical subdivisions in the aquitard zone near the well is double that

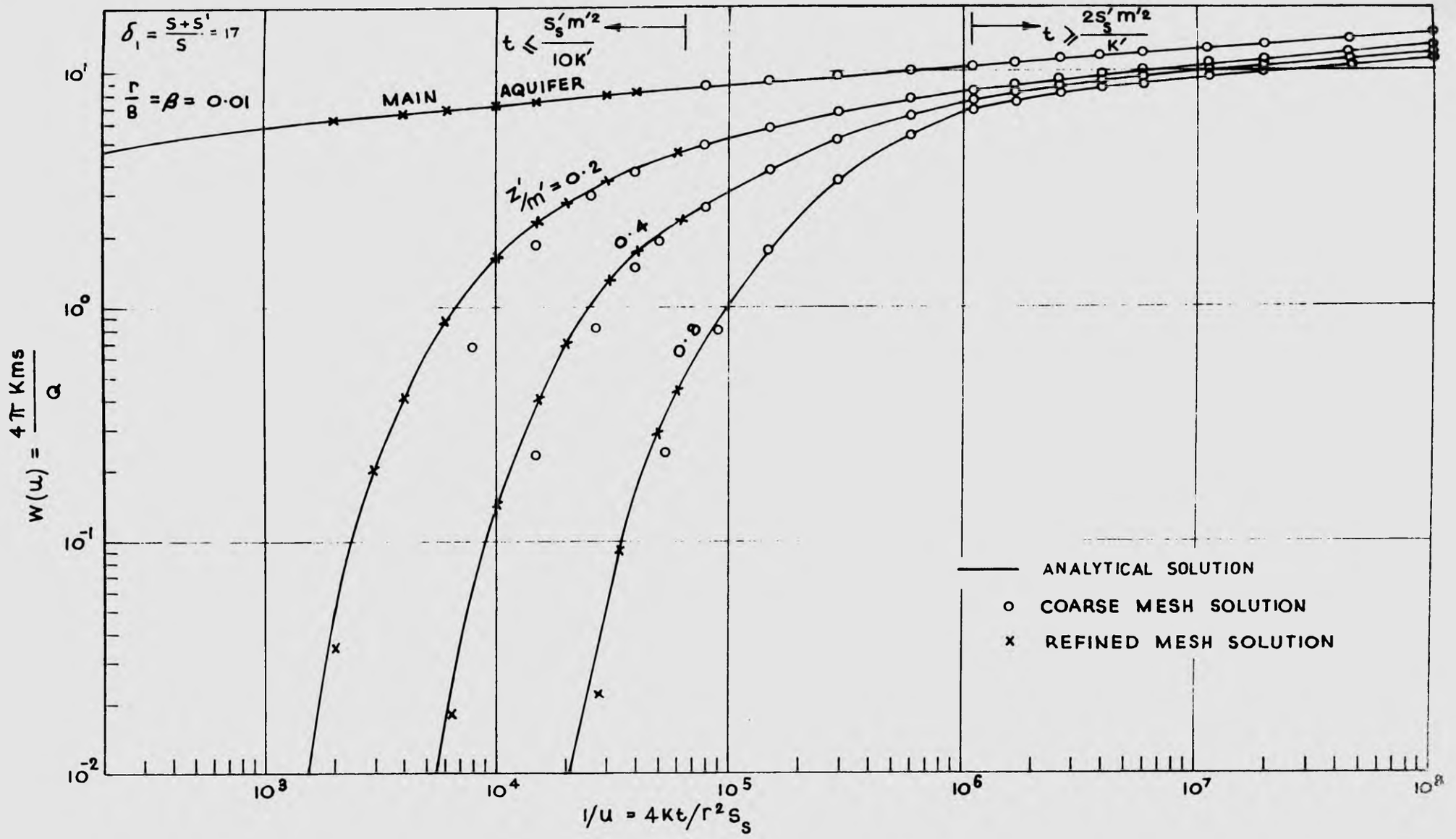

Fig. 5.23: Comparison of finite element and analytical solutions.

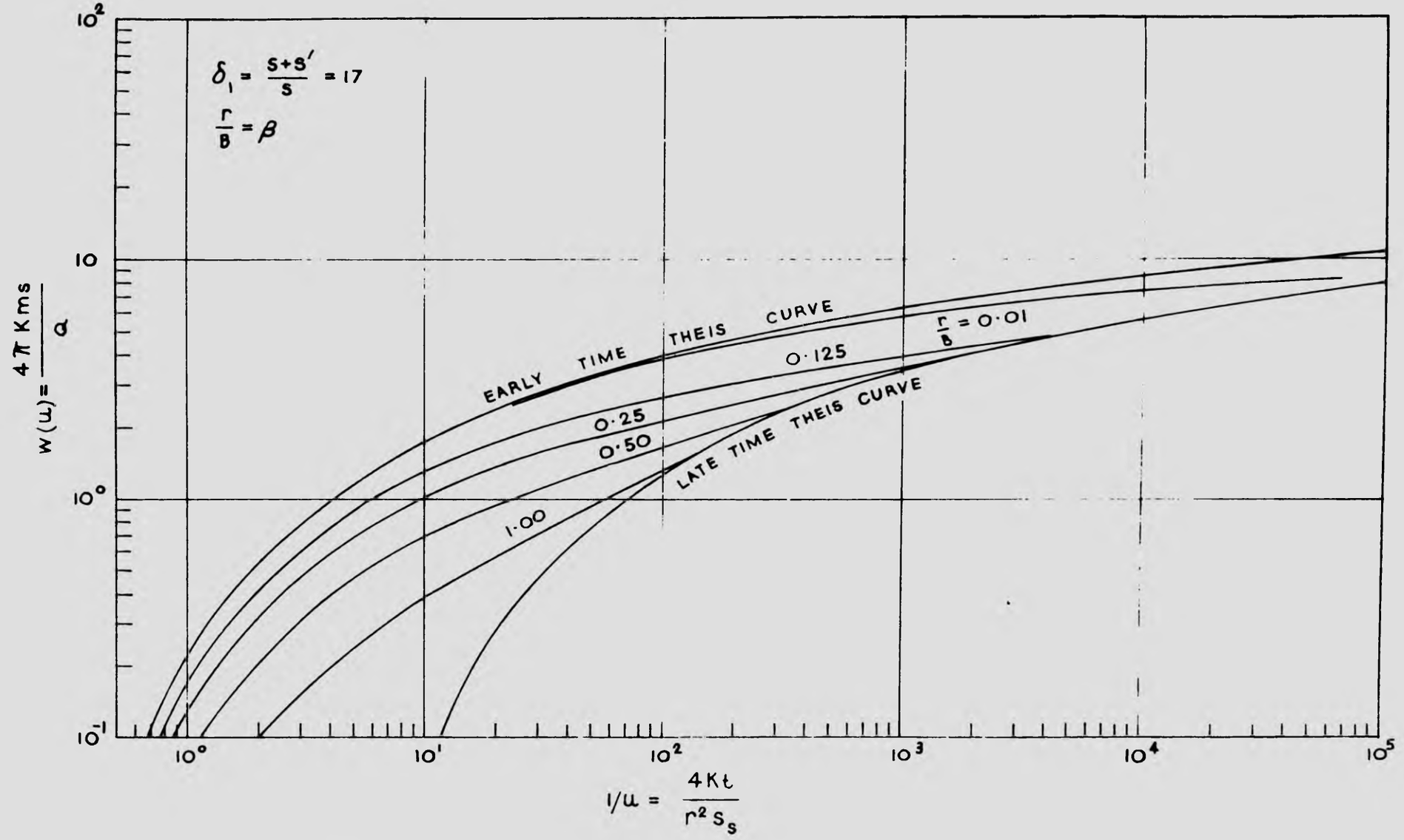

Fig. 5.24: Dimensionless drawdown type relationships for points in the main aquifer of a confined aquifer-aquitard system. (Darcy flow solution).

in the outer portion of the aquitard. A combination of rectangular and triangular elements was used. The network consists of 229 nodes and 204 elements. The initial time step was reduced to 0.28 minutes and a smaller time factor of 1.25 was used. Solution for 30 time steps was completed. The result obtained was compared once again with the analytical solutions for small values of time. It is seen in Figure 5.23 that the use of the refined network and smaller time step sizes resulted in better agreement with the analytical solutions.

A separate check was also made on the finite element solution by examining the drawdown-time relationships obtained from various nodal points in the main aquifer. These relationships are illustrated in Fig. 5.24. As expected, the numerical solution approaches Hantush's long time solution which corresponds to the late time Theis curve at time $t \geqslant 2\, S_s'\, m'^2 / K'$. This late time curve is spaced at a horizontal distance of $(\delta_1 - 1)/u$ from the conventional Theis curve, referred to as the early time Theis curve.

5.4.2 Two-regime Flow Solutions

To use the finite element method to investigate transient two-regime flow and study the effect of non-Darcy flow on late time drawdowns in the main aquifer, the problem defined in Fig. 5.20 was solved for six flow cases of different discharge. As before, the numerical solutions were obtained by employing the computer program used to solve the Darcy flow case. The coarse network shown in Fig. 5.21 was adopted as it can be seen in Fig. 5.23 that this network gave quite satisfactory drawdown values at late times. The external radius of the

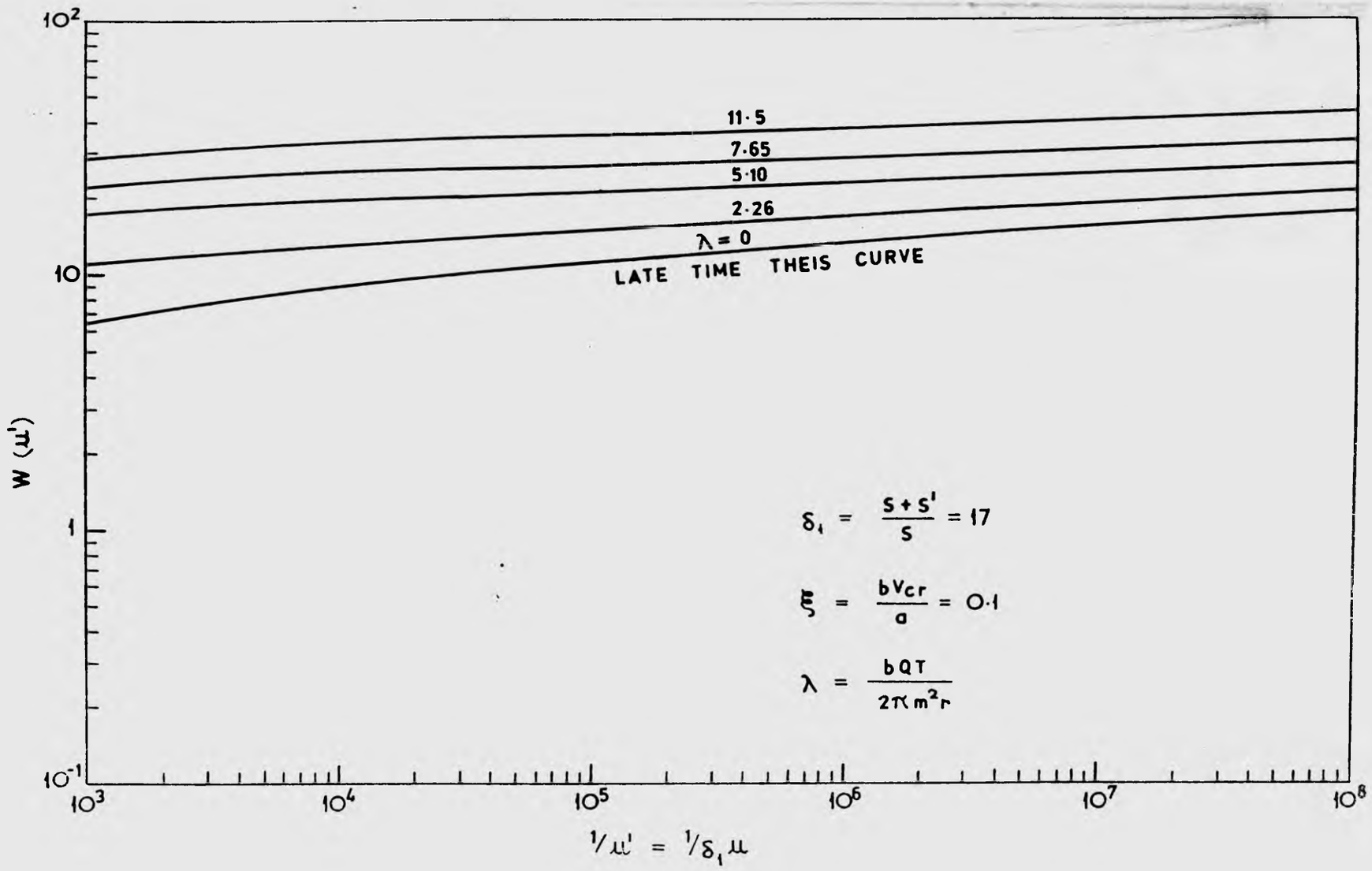

Fig. 5.25: Dimensionless drawdown-time relationships for points in the non-Darcy flow zone of the main aquifer. λ and ξ characterise non-Darcy flow.

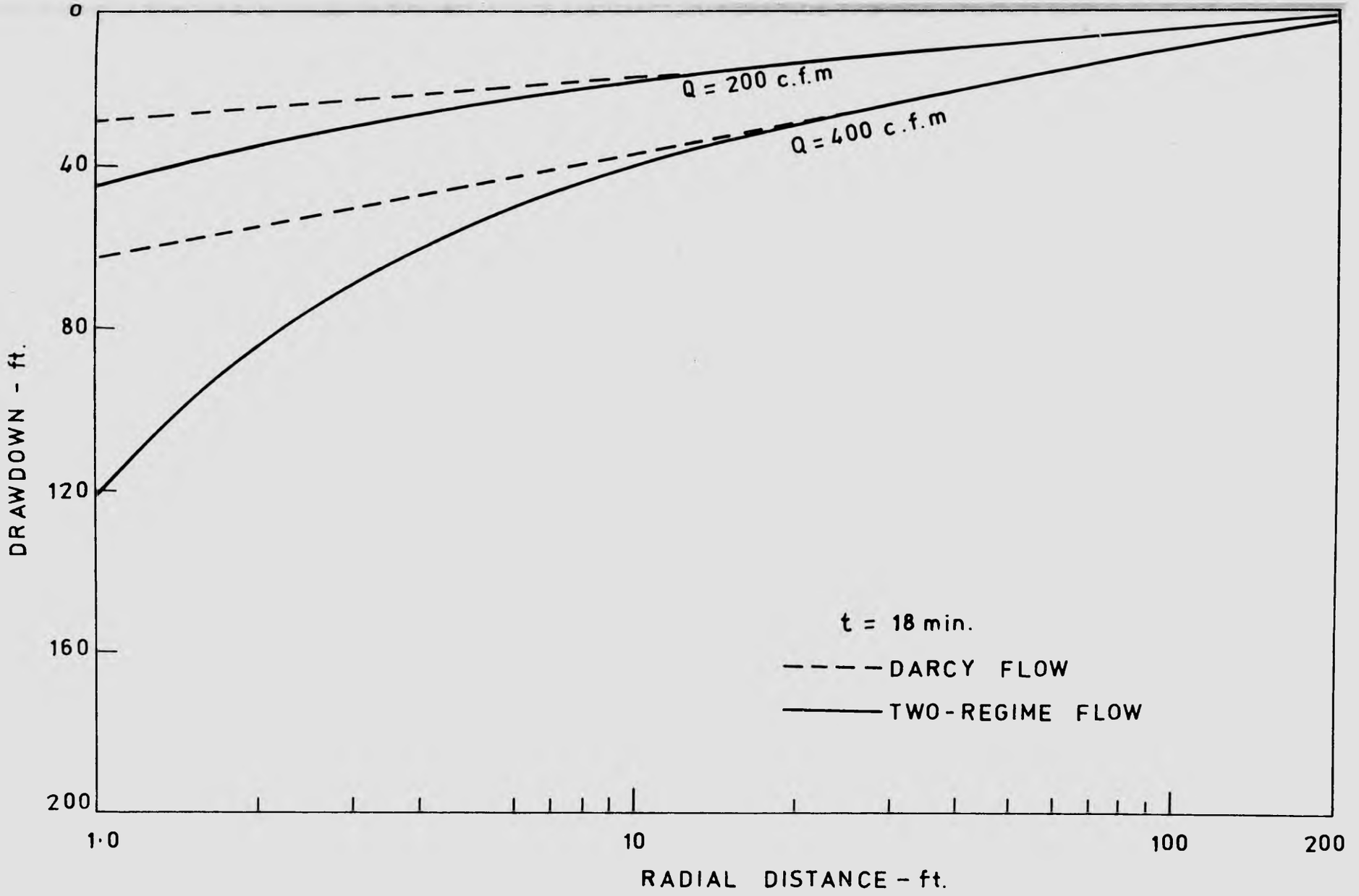

Fig. 5.26: Drawdown-distance curves at time t = 18 minutes.

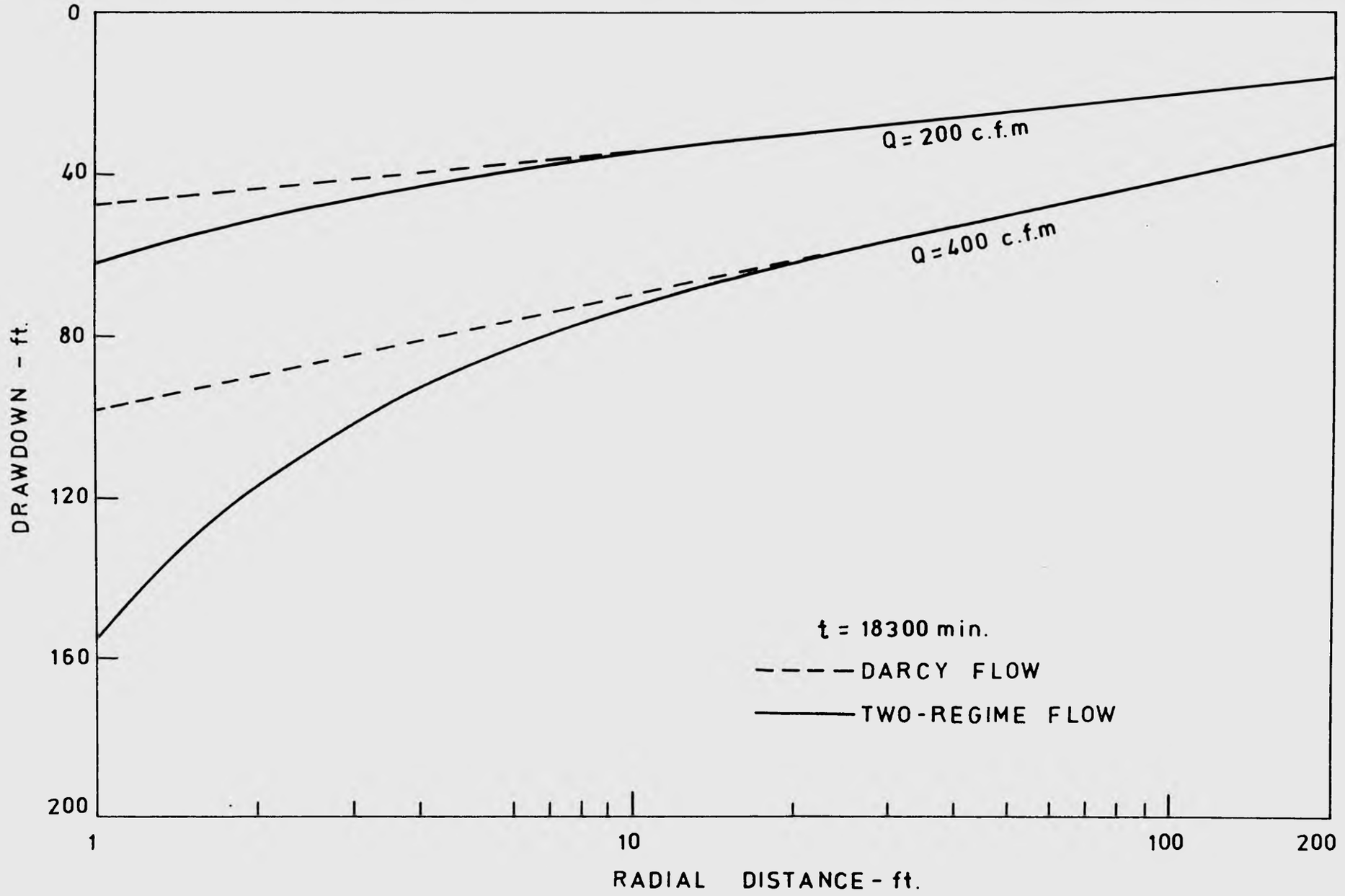

Fig. 5.27: Drawdown-distance curves at time t = 18,300 minutes.

network was extended to 10,000 ft. to ensure that the drawdown would not reach it at the end of the pumping period. The initial time step size was chosen to be 2.24 minutes. As in the Darcy flow case, the time multiplier of 1.4 was used to generate the remaining time steps. Thirty time steps were taken to reach the end of the pumping period at t = 36,000 minutes.

For flow case No. 6, Q = 1,000 cfm, a plot of the dimensionless drawdown-time relationships for selected points in the main aquifer at radial distances of 1, 1.50, 2.25 and 5.05 ft. from the pumped well is shown in Fig. 5.25. The late time Theis curve for the wholly Darcy flow case is also included. Once again the effect of the dimensionless parameter λ on the well function, $W = 4\pi Kms/Q$, may be observed.

For flow cases Nos. 2 and 4, semi-logarithmic plots of drawdown in the aquifer versus radial distance from the well are illustrated in Figs. 5.26 and 5.27 for times t = 18 and 18,300 minutes respectively. The Darcy flow solutions are also shown in dotted lines. It can be seen that, for each well discharge, the two-regime flow curve deviates from the linear Darcy flow solution at distances less than a certain critical radius. This radius, indicated by the junction of the solid and dotted lines, is observed to increase with increase in the well discharge. Comparison of Figs. 5.26 and 5.27 again leads to the conclusion that for transient flow at constant discharge the additional drawdown due to non-Darcy flow which has been fully developed near the well remains constant with time.

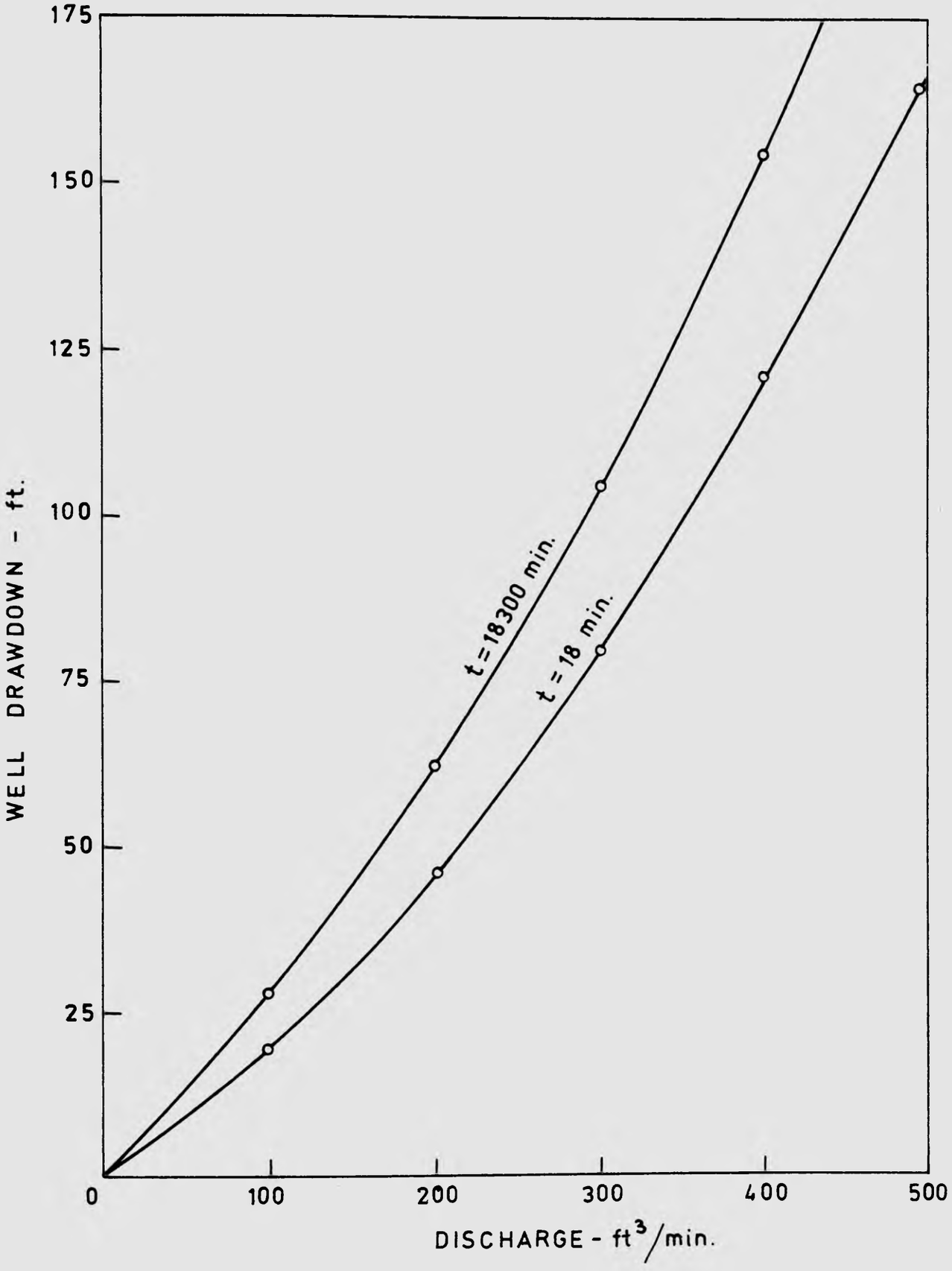

Fig. 5.28: Well discharge-drawdown relationships at times t = 18 and 18,300 minutes.

Finally, the effect of non-Darcy flow on the well discharge-drawdown relationships is illustrated in Fig. 5.28 for times t = 18 and 18,300 minutes. The relationships are non-linear and may be fitted by equation (5.6).

5.5 Flow towards a Well in an Unconfined Aquifer - Aquitard System

5.5.1 Darcy Flow Solutions

A diagrammatic sketch of a well in a flow system consisting of an aquifer and an overlying unconfined aquitard is shown in Fig. 5.29. The well is screened through the entire thickness of the aquifer and pumped at a constant discharge. An analytical approach to the transient Darcy flow problem was presented by Cooley and Case (1963, unpubl.) They considered the boundary value problem identical to the one solved by Hantush (1960) with the exception that the boundary condition at the top of the aquitard is replaced by Boulton's exponential integral to simulate variable yield from the unsaturated zone. Their complete analytical solution for drawdowns in the main aquifer is divided into short and long time segments. The short time solution, valid for $t \leqslant S_s' m'^2/10K'$, is identical to that given by Hantush (1964, p.312). The long time solution, valid for $t \geqslant 10 S_s' m'^2/K'$, is similar to Boulton's solution of the unconfined flow problem (Boulton, 1963, p.479).

To verify the finite element analysis, a hypothetical problem was formulated. The problem data are given in Fig. 5.29, flow case No.0. Two combinations of network and time discretisation were adopted. For the first combination, the coarse network shown in Fig. 5.21 was

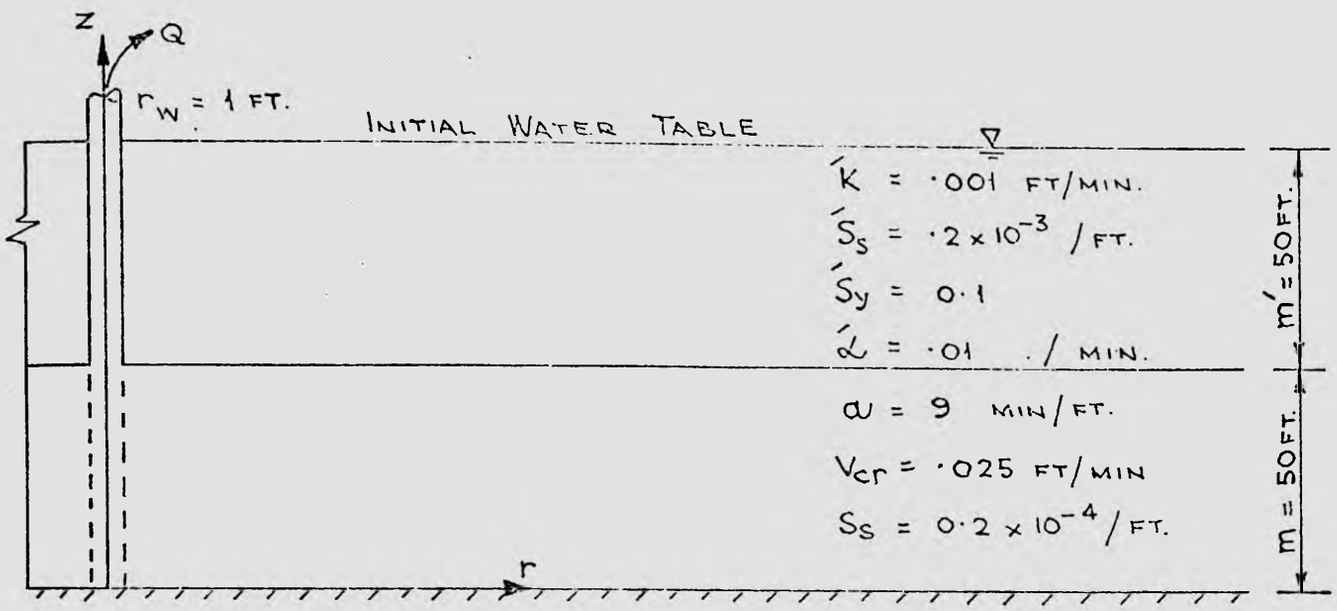

Flow Case No.	b(min.^{2}/ft.^{2})	Q(ft^3./min.)
0	0	100
1	40	100
2	40	200
3	40	300
4	40	400
5	40	500
6	40	1000

Fig. 5.29: Data for the problem of transient flow towards a well in an unconfined aquifer-aquitard system.

used. This network has been described previously in Section 5.4.1. The initial time step size of 1.12 minutes and the time multiplier of 1.4 were again chosen. The problem was solved for 30 time steps and the numerical solution obtained was checked against the long time solution for drawdowns in the aquifer. A plot of the dimensionless drawdown-time relationships for points in the aquifer which are located at distances of 57, 292 and 657 ft. from the pumped well is shown in Fig. 5.30. The dimensionless parameters, $\frac{r}{D}$ and δ_2, listed are given by

$$\frac{r}{D} = r\left/\left[\frac{Km}{\alpha S'_y} + \frac{Kmm'}{K}\right]^{1/2}\right. \qquad (5.11)$$

$$\delta_2 = 1 + \frac{S_s 'm' + S'_y}{S_s m} \qquad (5.12)$$

The remaining parameters, $\frac{r}{B}$ and β, are given by equations (5.7) and (5.8). It can be seen that good agreement between the finite element and the analytical solutions was achieved.

The second combination of network and time step sizes was used to study convergence of the finite element solution. The refined network shown in Fig. 5.22 was adopted. This network has been previously described in Section 5.4.1. The smaller initial time step size of 0.28 minutes and the time multiplier of 1.25 were chosen. The numerical solution obtained was compared with the result obtained previously by using the coarse network and larger time step sizes. Fig. 5.31 shows a plot of the dimensionless drawdown-time relationships for selected points in the flow system. All of these points are located at

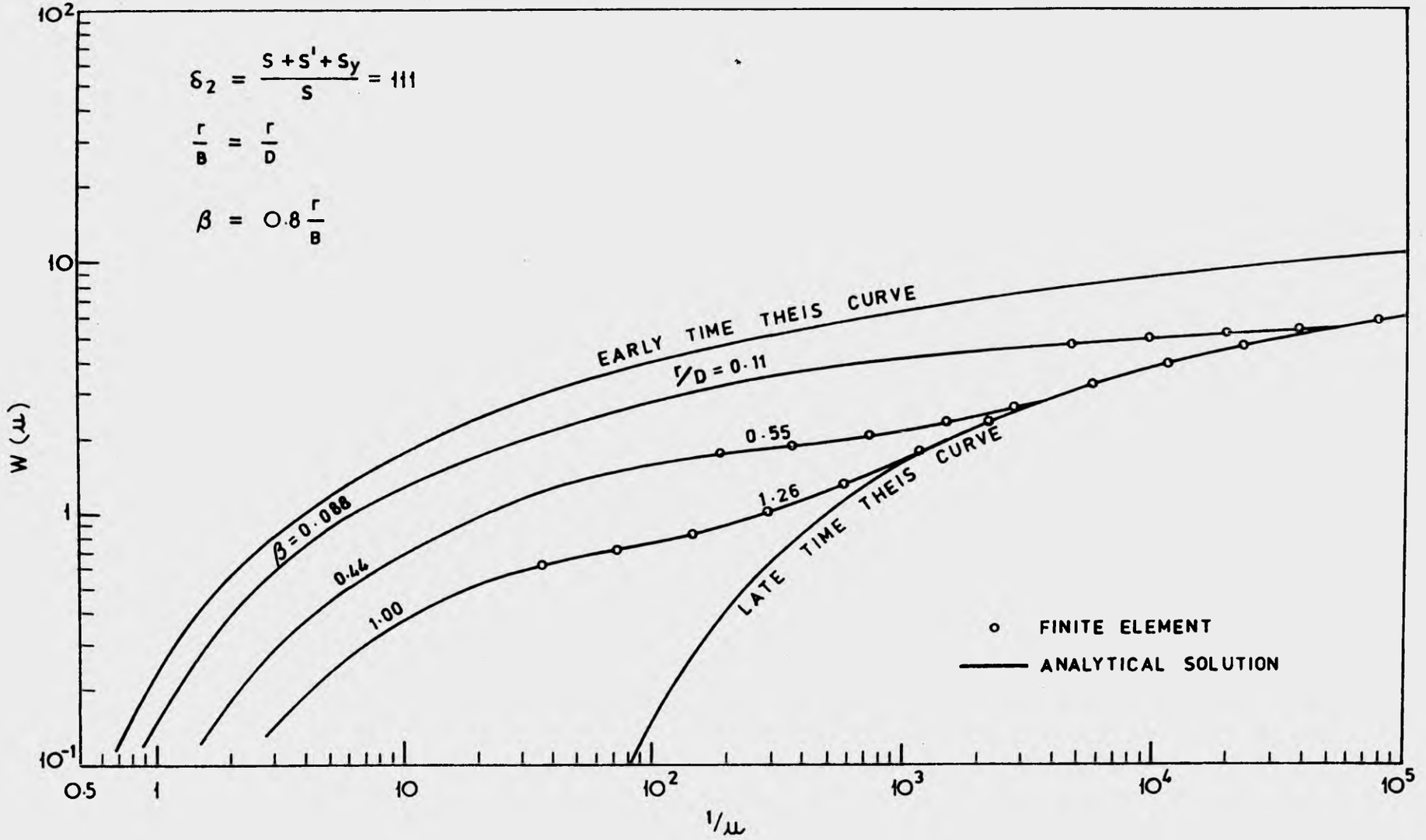

Fig. 5.30: Comparison of finite element and analytical solutions.

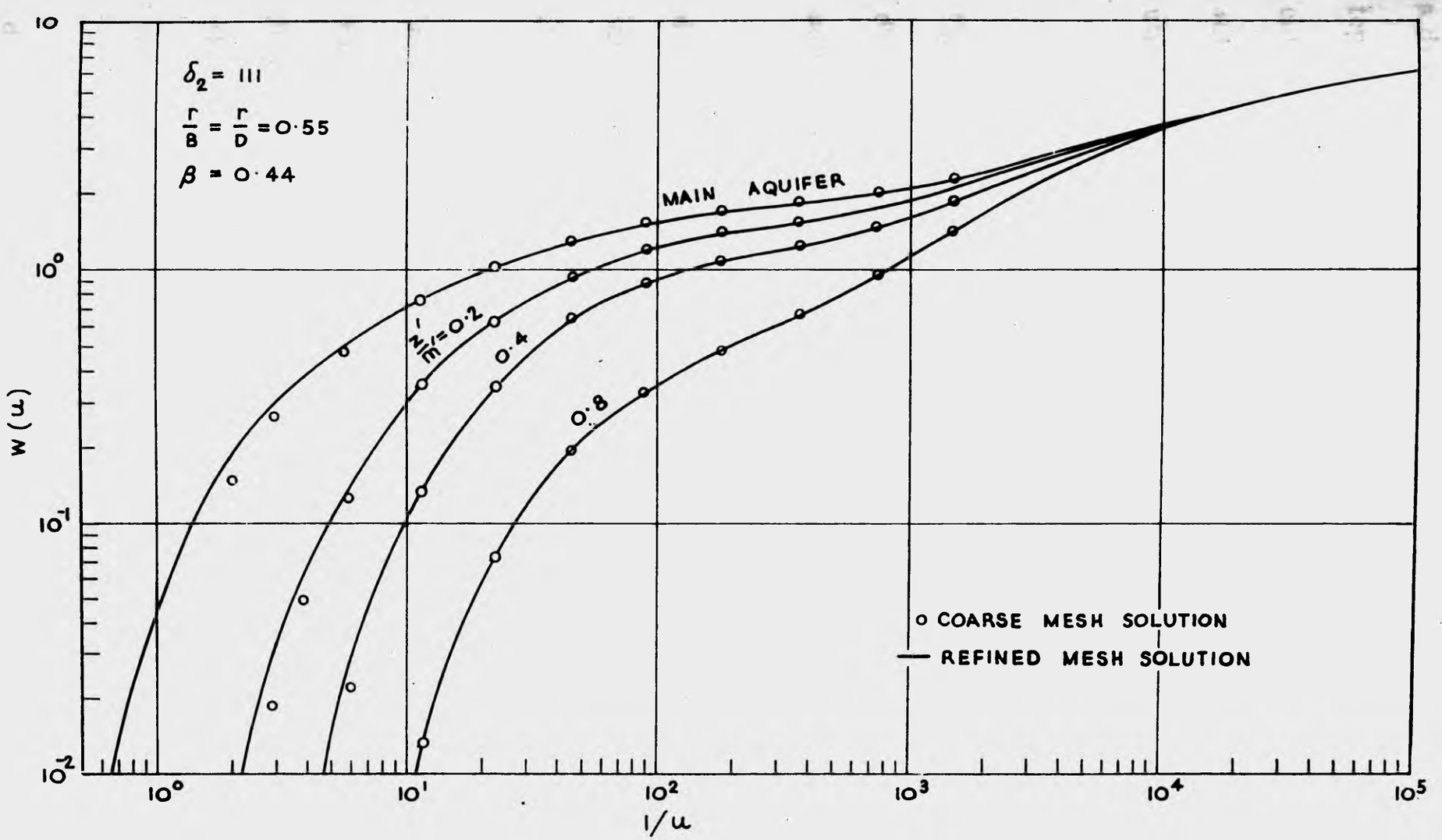

Fig. 5.31: Convergence of the finite element solutions. Dimensionless drawdown-time curves shown are for points in the flow system which are all located at the same radial distance from the well.

a distance of 292 ft. from the well but at different elevations from the top of the aquifer. It is noted that along the steep portions of the type curves the coarse mesh solution lies slightly below the refined mesh solution and that along the flatter portions of the curves the two solutions agree quite closely.

5.5.2 Two-regime Flow Solutions

A hypothetical transient two-regime flow problem was formulated. The problem data are listed in Fig. 5.29. Six flow cases of different discharge were solved by the finite element method. The numerical solutions were obtained in the manner described in Section 5.4.2.

For flow case No. 6, Q = 1,000 cfm, a plot of the dimensionless drawdown-time relationships for selected points in the aquifer at distances of 1, 1.5, 2.25, 5.07 ft. from the well is shown in Fig. 5.32. It can be seen that the type curves are similar to those shown in Fig. 5.2

For flow cases Nos. 2 and 5, semi-logarithmic plots of drawdown in the aquifer versus radial distance from the well are illustrated in Figs. 5.33 and 5.34 for times t = 18 and 4,580 minutes respectively. It is noted that flow case No. 5 cannot be realised in practice as the discharge of 500 cfm results in a well drawdown in excess of the maximum possible value of 100 ft. which is the drawdown to the base of the aquifer.

Finally, the effect of non-Darcy flow on the well discharge-drawdown relationships is illustrated in Fig. 5.35 for times t = 18 and 4,580 minutes. Once again it is noted that the relationships are non-

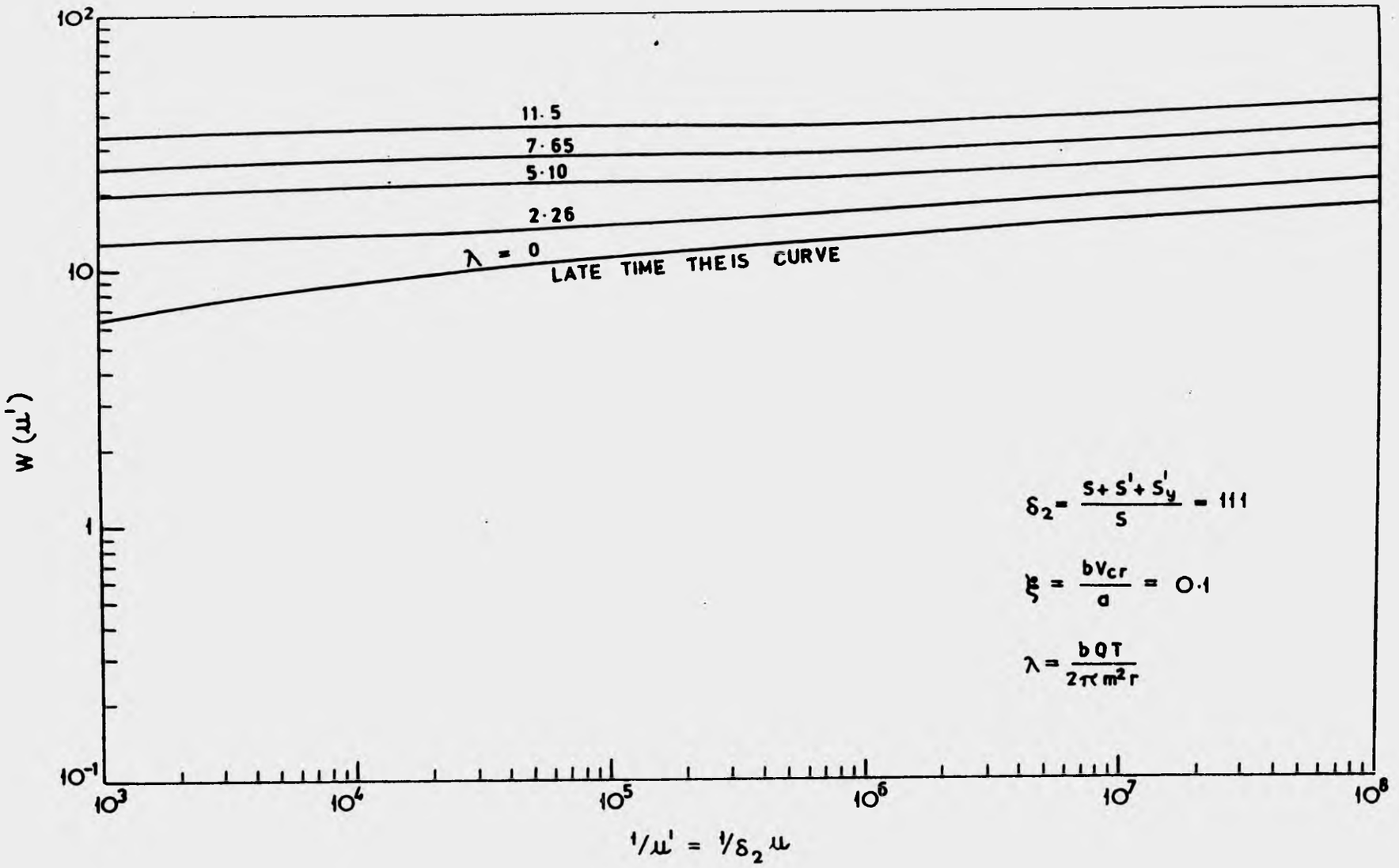

Fig. 5.32: Dimensionless drawdown-time relationships for points in the non-Darcy flow zone of the main aquifer. λ and ξ characterise non-Darcy flow.

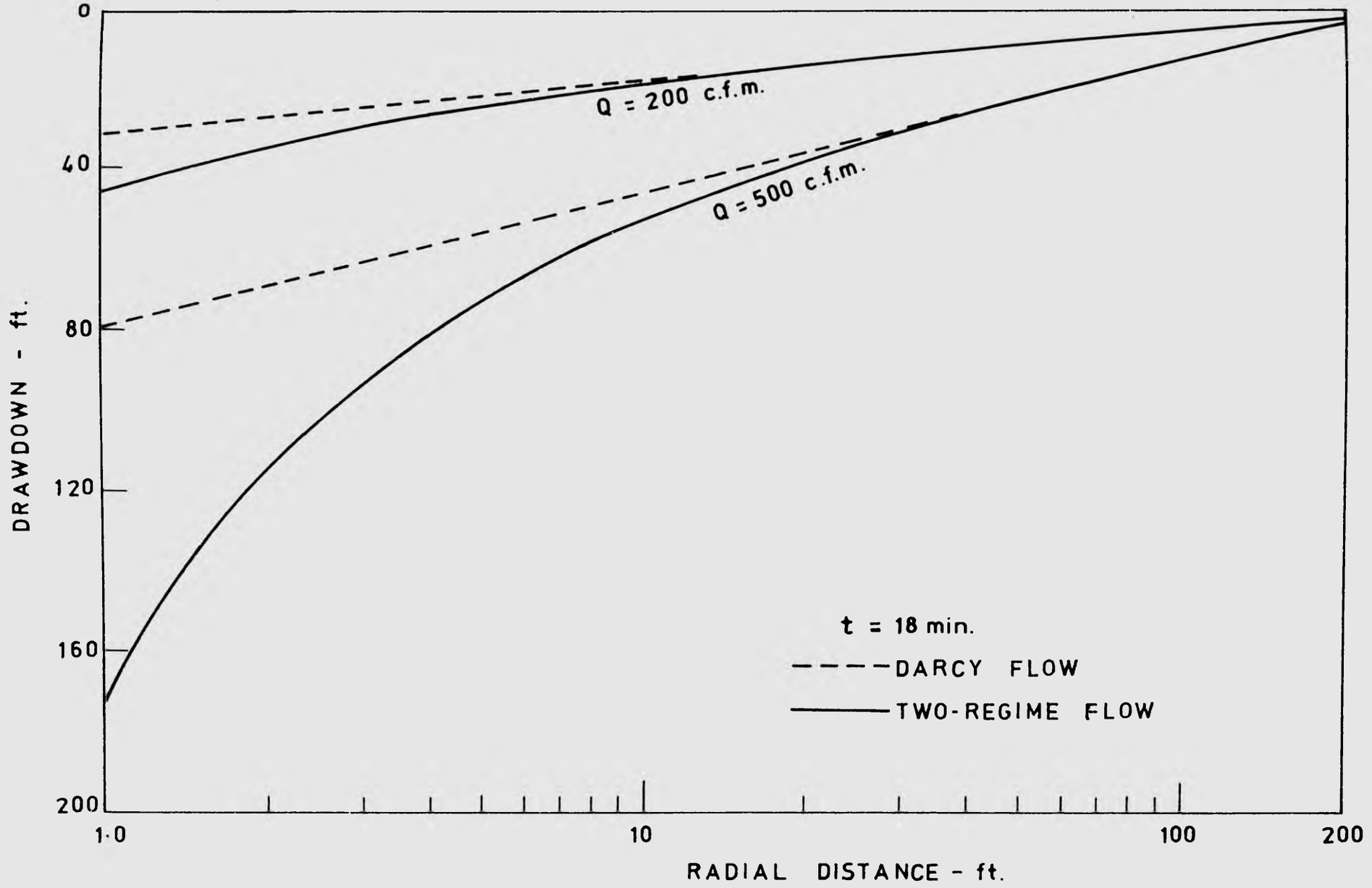

Fig. 5.33: Drawdown-distance curves at time t = 18 minutes.

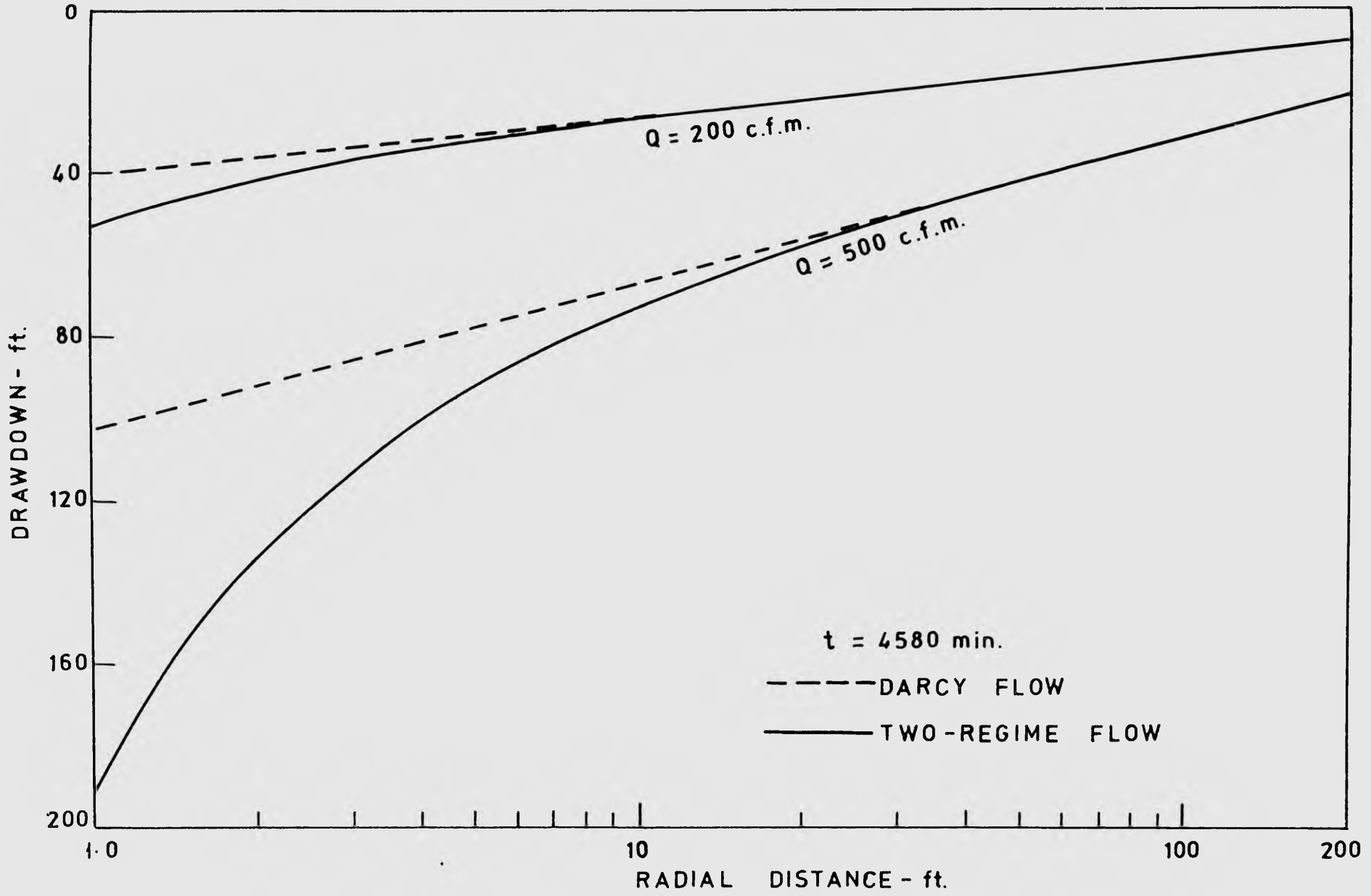

Fig. 5.34: Drawdown-distance curves at time t = 4580 minutes.

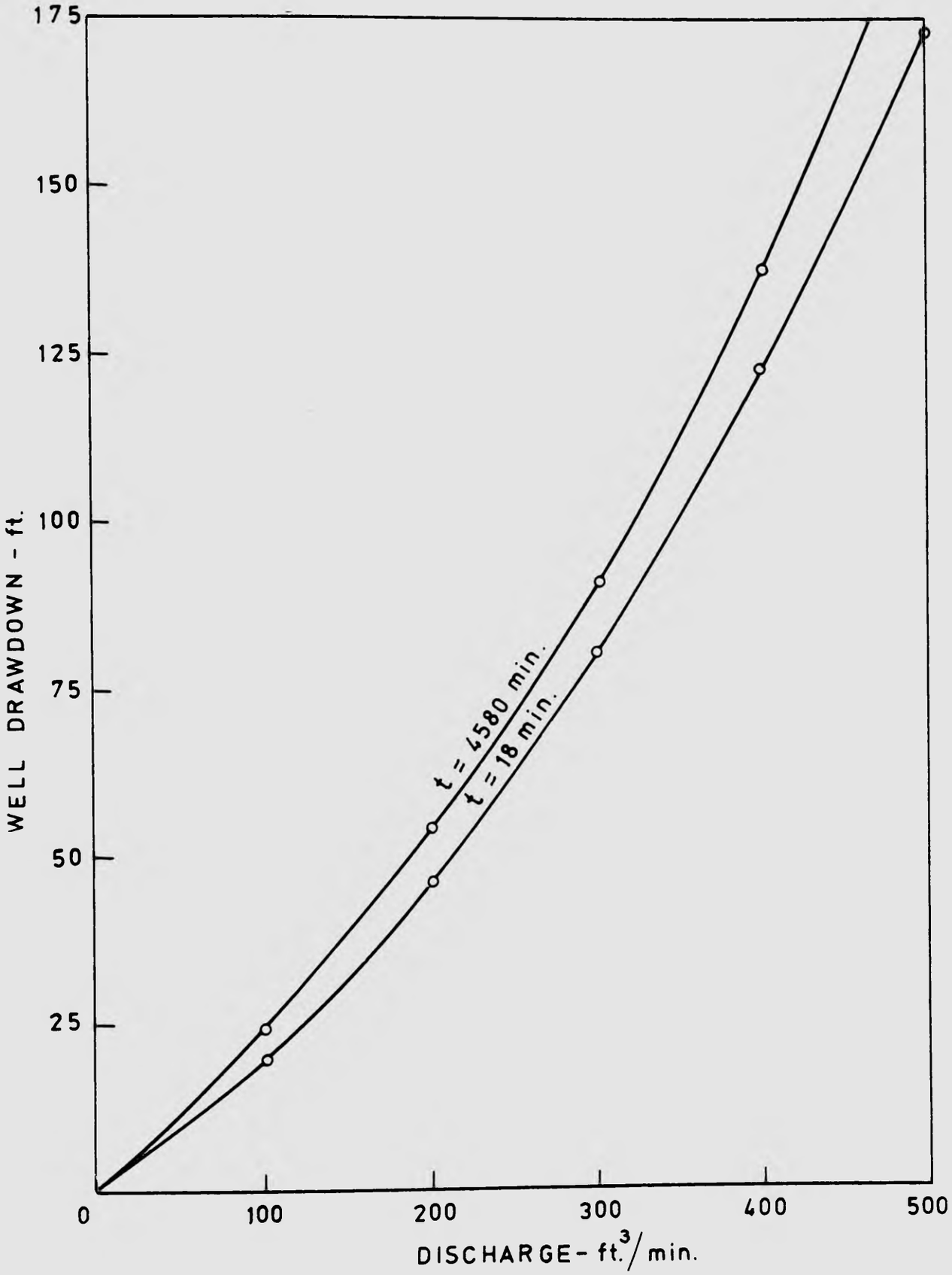

Fig. 5.35: Well discharge-drawdown relationships at times t = 18 and 4580 minutes.

linear and may be fitted by equation (5.6).

5.6 Flow towards a Well in an Unconfined Aquifer

5.6.1 Darcy Flow Solutions

A diagrammatic sketch of a well in an unconfined aquifer is shown in Fig. 5.36. The well is fully screened through the initial saturated thickness of the aquifer and pumped at a constant discharge. A simplified analytical approach to the problem of transient unconfined Darcy flow was presented by Boulton (1954), (1963). He used the exponential integral to approximate the delayed yield from the unsaturated zone and solved the one-dimensional field equation which was developed by considering only radial flow components. His complete analytical solution to the problem is based on the assumption that thickness of the aquifer is constant and equal to the initial saturated thickness.

The validity of Boulton's work was investigated by Cooley (1971) who applied the finite difference method to two-dimensional flow in both saturated and unsaturated zones of the aquifer. He discovered that Boulton's analytical solution corresponded closely to his numerical solution of the unconfined flow problem provided that the drawdown of the water table is small compared to the initial saturated thickness.

A hypothetical problem was formulated to verify the finite element analysis by using Boulton's analytical solution. The problem data are given in Fig. 5.36, flow case No.0. It was assumed a priori that Boulton's solution provided a close approximation to the complex

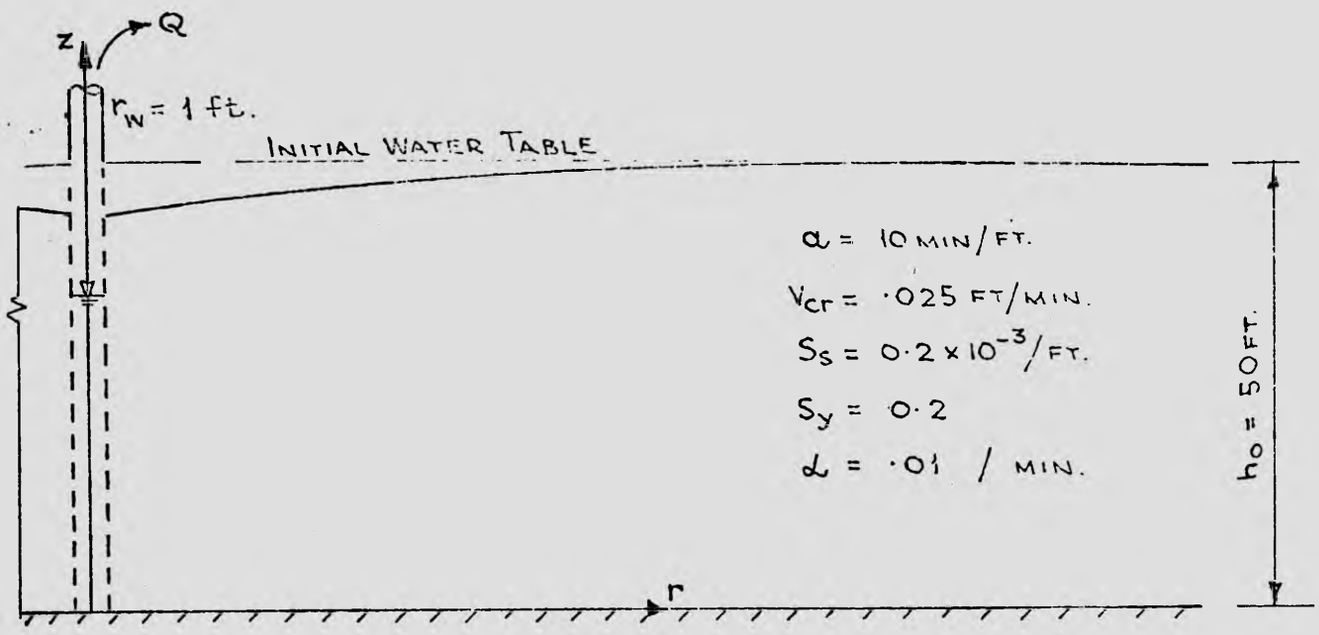

Flow Case No.	b(min.^{2}/ft.^{2})	Q(ft.^{3}/min.)
0	0	50
1	20	50

Fig. 5.36: Data for the problem of transient flow towards a fully screened well in an unconfined aquifer.

boundary value problem analysed by the finite element method, as an exact solution to this problem could not be obtained. The network similar to that shown in Fig. 5.37 was adopted. The external radius of this network is 2,000 ft. As seen in the figure, the saturated flow region is divided into two subregions, one where the mesh is held fixed and the remaining subregion where the mesh is allowed to contract or expand to accommodate free surface adjustments. The subdivision of each subregion into triangular elements has been described in Section 5.3.1. A total of 133 elements and 102 nodes was used. The initial time step size of 0.20 minutes and the time multiplier of 1.4 were chosen. The problem was solved for 30 time steps.

The numerical solution obtained was a hydraulic head distribution that varied with depth throughout the entire pumping period. Drawdowns at radial distances of 40 and 150 ft. from the well were averaged over the height of the water table and used for comparison with Boulton's solution. The justification for using the average drawdowns has been given by Cooley (1971). Values of the dimensionless drawdown W and the parameters r/D and η were calculated from

$$W = \frac{4\pi K h_o \bar{s}}{Q} \tag{5.13}$$

$$\frac{r}{D} = \frac{r}{\sqrt{\frac{K h_o}{\alpha S_y}}} \tag{5.14}$$

$$\eta = \frac{h_o S_s + S_y}{S_s h_o} \tag{5.15}$$

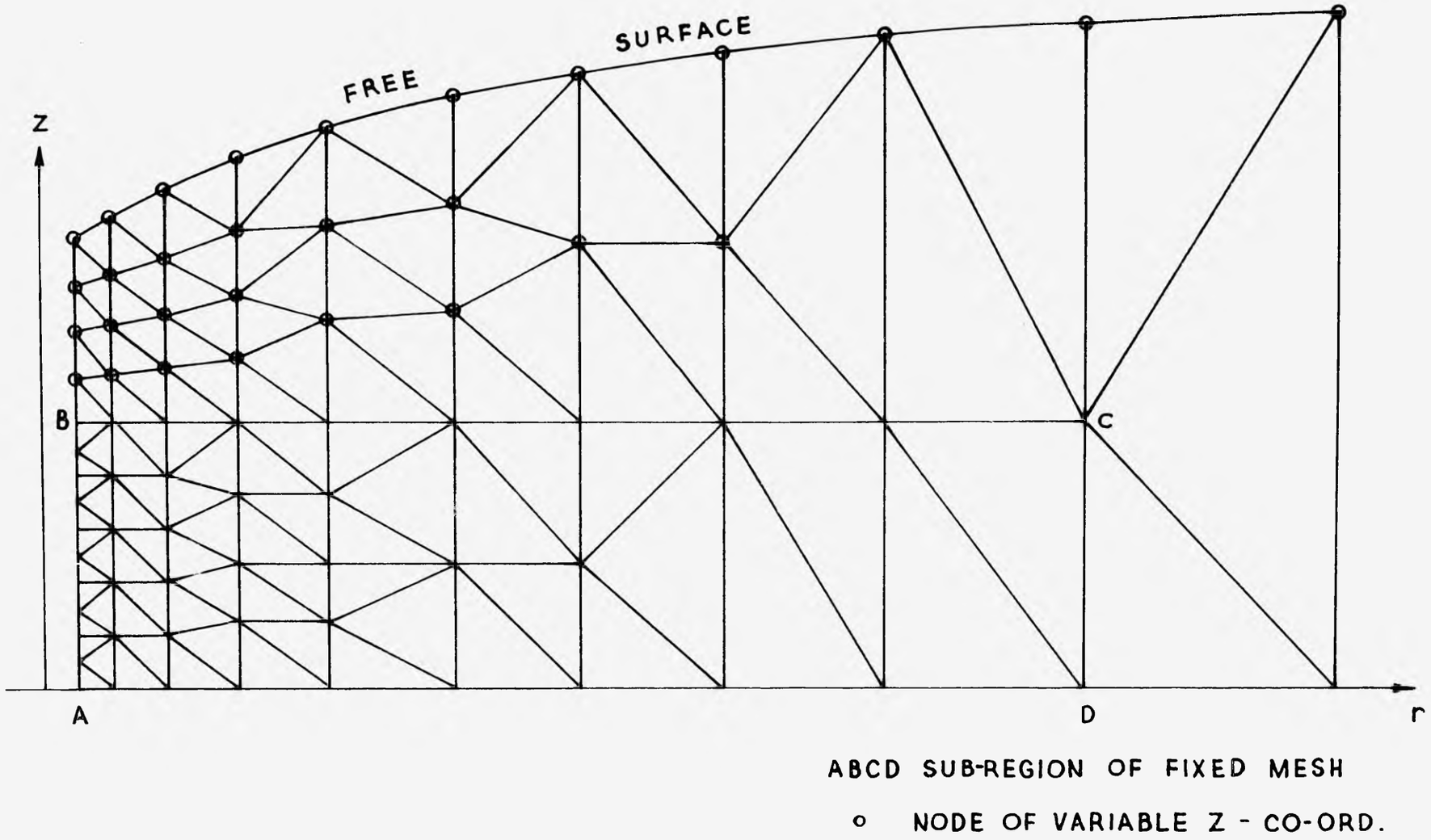

Fig. 5.37: Finite element network for an unconfined aquifer with a fully screened well.

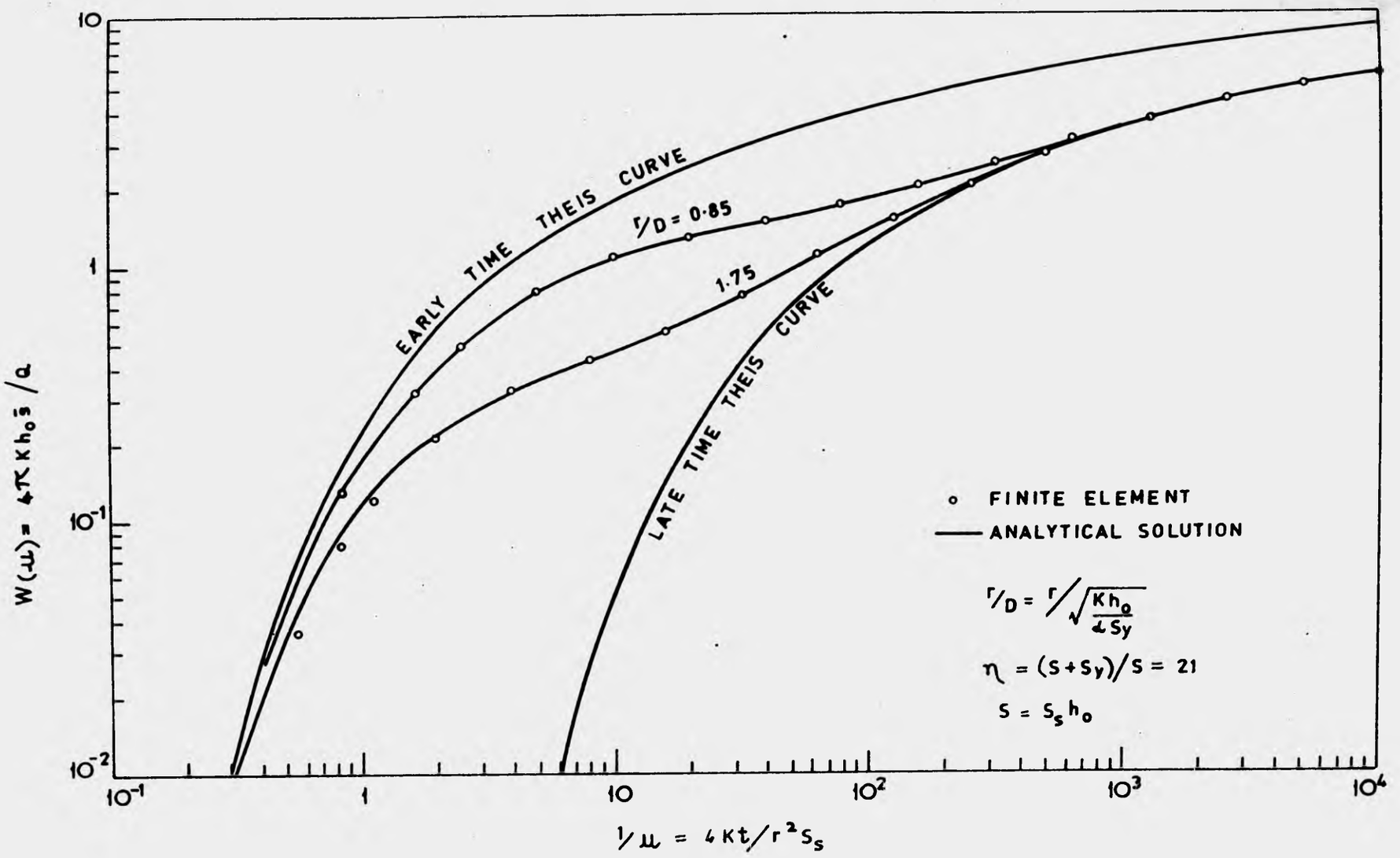

Fig. 5.38: Comparison of finite element and Boulton's analytical solutions. Values of r/D shown are calculated from original problem data. Values of r/D for the best fit Boulton type curves are 0.90 and 1.80, for upper and lower curves respectively.

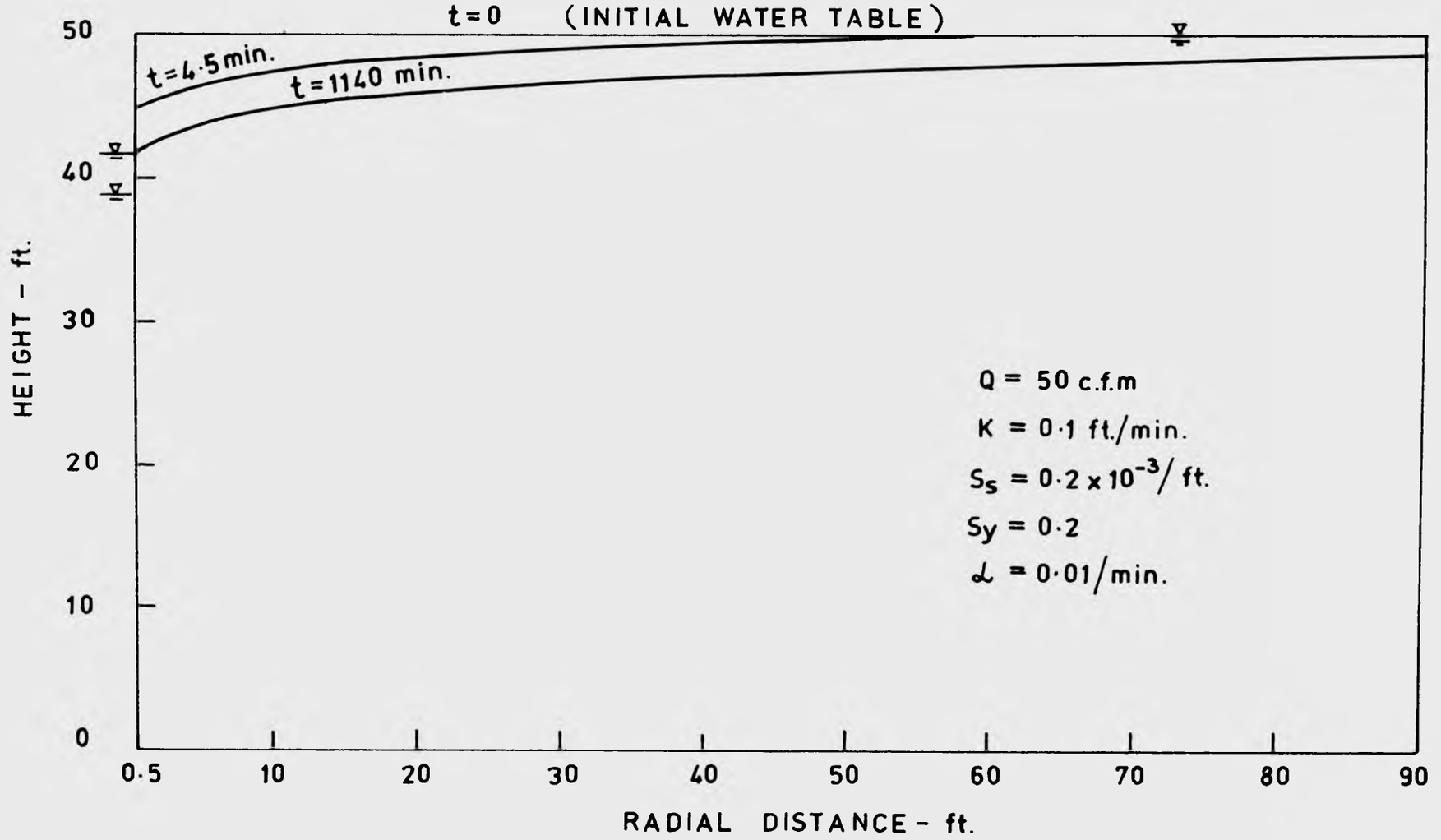

Fig. 5.39: Positions of the free surface and the water level in the well at times t = 4.5 and 1140 minutes. (Darcy flow solution).

where h_o is the initial saturated thickness of the aquifer, and $\bar{s}$ is the average drawdown, which is given by

$$\bar{s} = \frac{1}{z} \int_0^z (h_o - h)\, dz \qquad (5.16)$$

Comparison of the numerical and Boulton's analytical solutions was made by matching the numerical results against a family of Boulton's type curves. The numerical results and the matching type curves are shown in Fig. 5.38. The values of r/D for the best fit type curves are slightly different from those calculated from equation (5.14) by using the original problem data. The difference can be explained in terms of the fact that Boulton's solution is based on the simplifying assumption that the thickness of the aquifer is constant and equal to the initial saturated thickness. It can be seen that in general the numerical solution agrees closely with the analytical solution except along the steep portions of the type curves where slight deviation occurs. The deviation is probably due to the coarse network and time step sizes used.

Finally, the positions of the water table and water level in the well at times t = 4.5 and 1,140 minutes are illustrated in Fig. 5.39. These positions are compared in the next section with the corresponding positions obtained from the two-regime flow solution for the same well discharge.

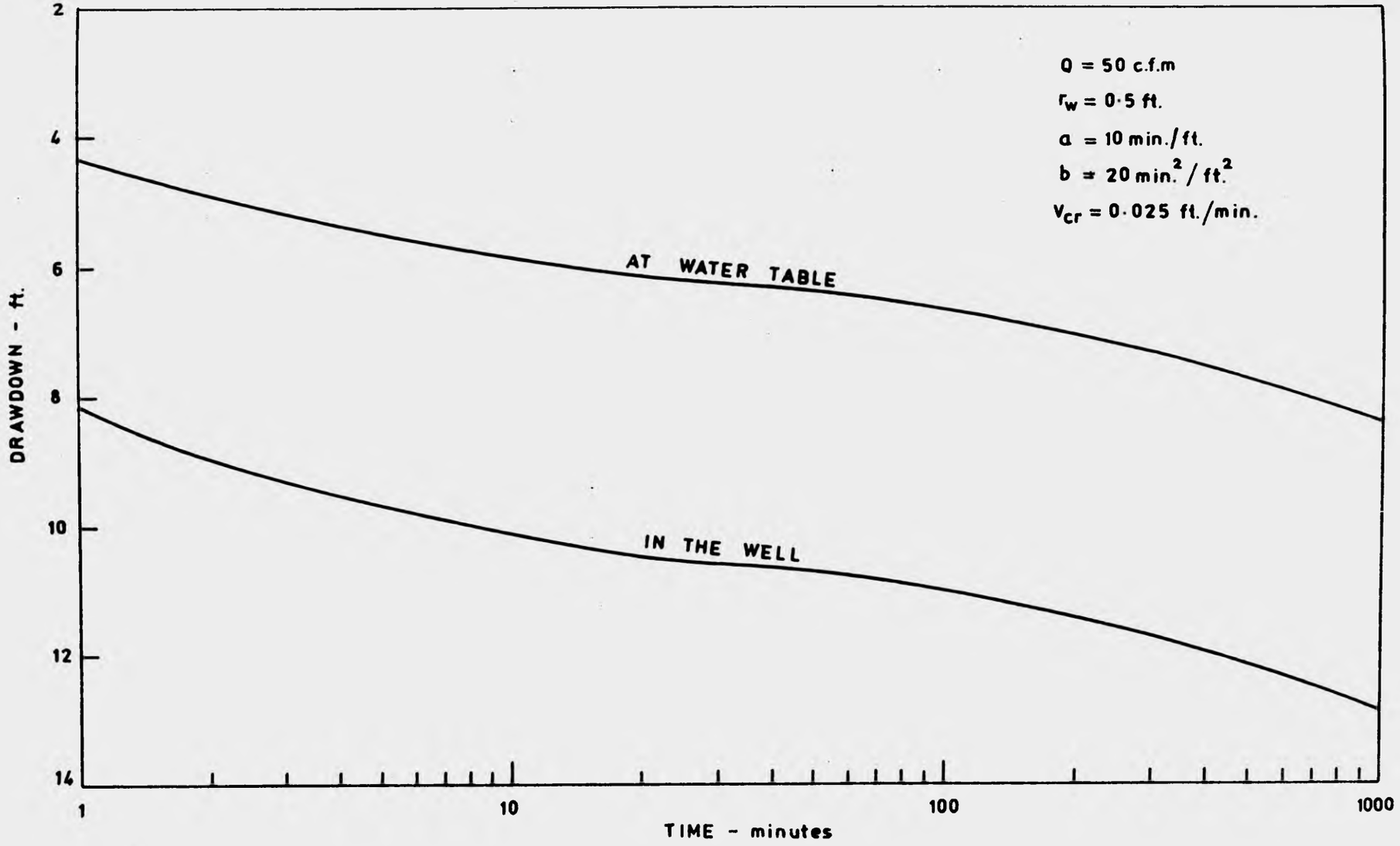

Fig. 5.40: Drawdown-time relationships for two points on the well boundary which are located at the top of the seepage face and located below the water level in the well (Two-regime flow solution).

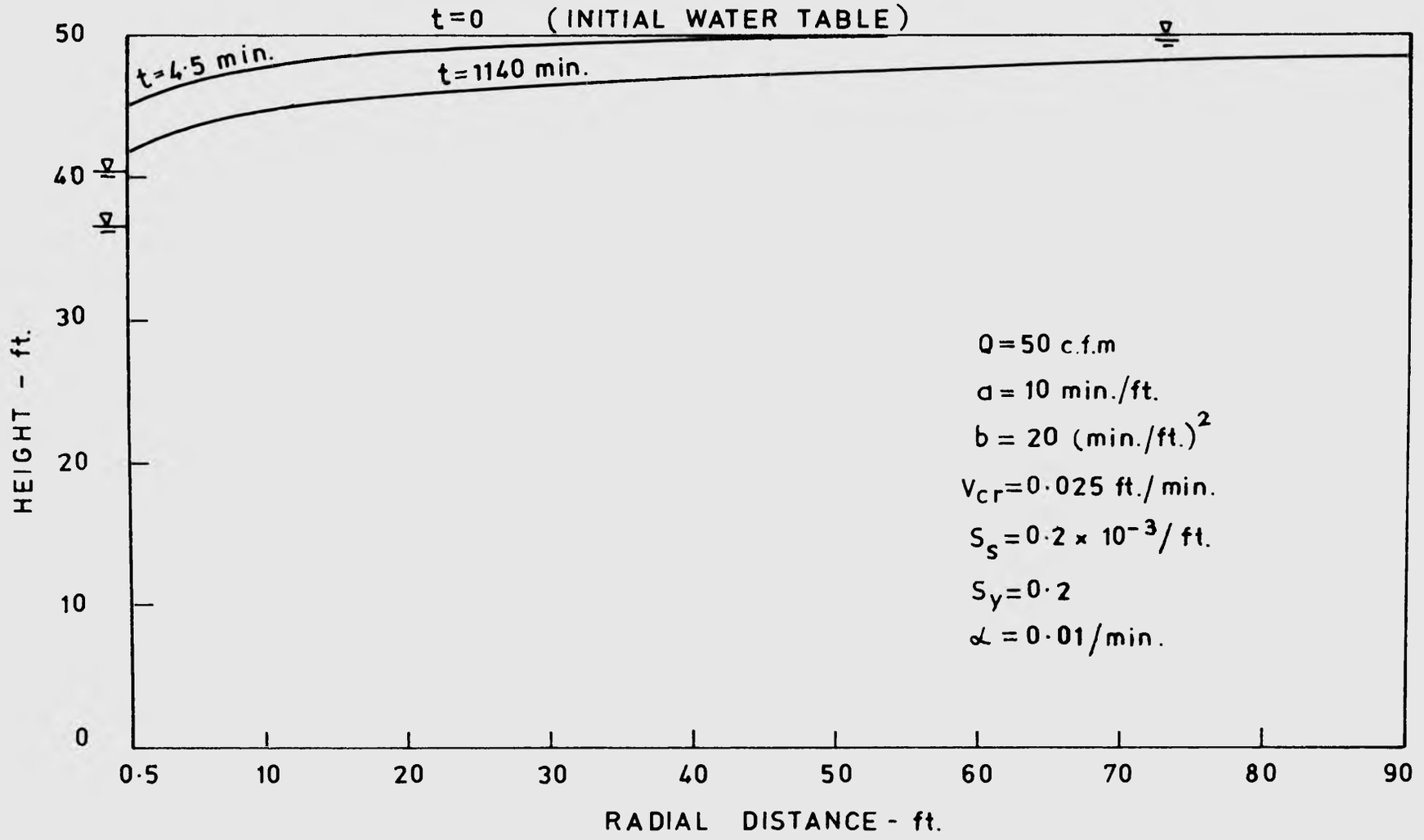

Fig. 5.41: Positions of the free surface and the water level in the well at times t = 4.5 and 1140 minutes (Two-regime flow solution).

5.6.2 Two-regime Flow Solutions

(i) Transient Flow Case

The transient two-regime flow case shown in Fig. 5.36 (flow case No.1) was solved by employing the computer program used previously to solve the Darcy flow problem. The network described in Section 5.6.1 was again adopted. The initial time step size of 0.20 minutes and the time multiplier of 1.40 were chosen.

Fig. 5.40 shows a semi-logarithmic plot of the drawdown-time relationships for two nodal points on the well boundary which are located at the top of the seepage face and below the water level in the well respectively. Due to the delayed yield effect which is incorporated in Boulton's exponential integral, the plot in the figure takes the familiar S-shape.

The effect of non-Darcy flow on the positions of the water table and water level in the well is illustrated in Fig. 5.41 for times t=4.5 and 1,140 minutes. On comparing this figure with Fig. 5.39 it is noted that for the same well discharge and pumping time the length of the seepage face from the two-regime flow solution is appreciably greater than that obtained from the Darcy flow solution.

(ii) Steady Flow Cases

To investigate steady state, two regime flow in an unconfined aquifer, the problem shown in Fig. 5.42 was solved for four selected flow cases. A network similar to the one shown in Fig. 5.37 was adopted. Its external radius was 1000 ft. For flow cases Nos. 1, 2 and

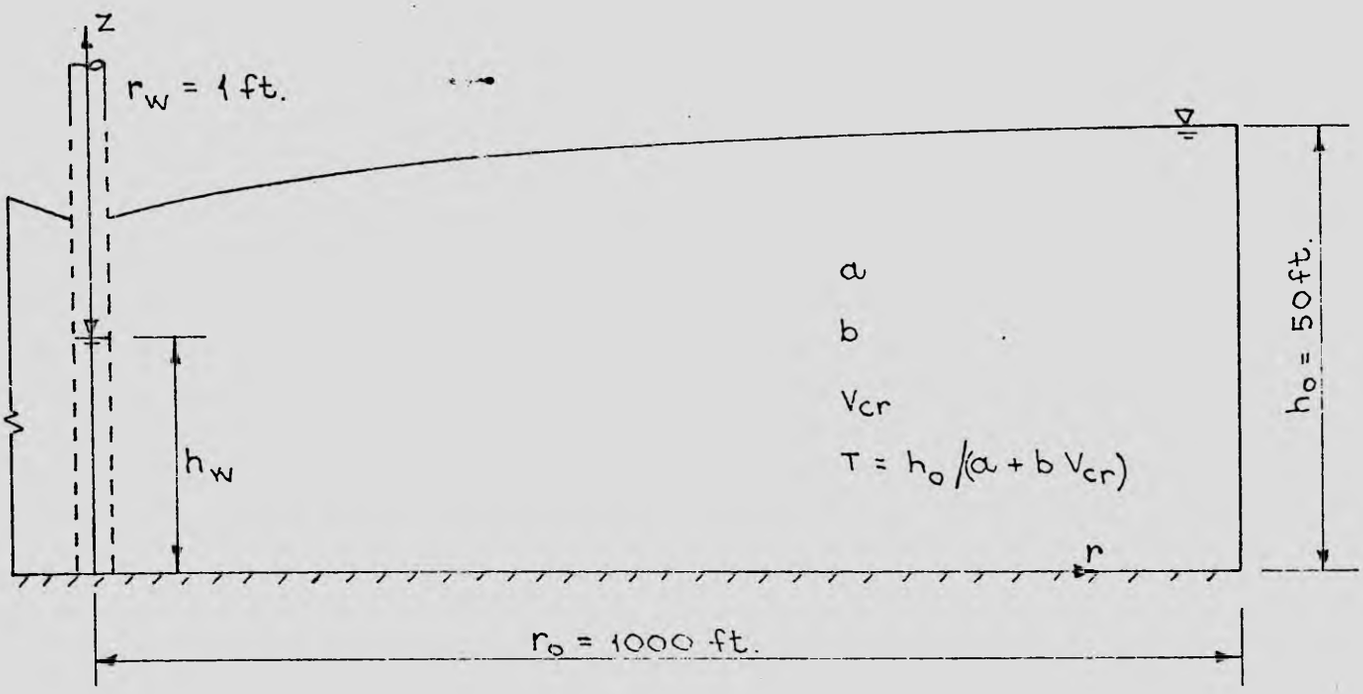

Flow Case No.	a min./ft.	b_2 $min.^2/ft.^2$	V_{cr} ft./min.	h_w ft.
1	1	0	0	10
2	1	0.8	0.125	10
3	1	4.0	0.025	10
4	1	2.0	0.050	10

Fig. 5.42: Data for the problem of steady flow towards a fully screened well in an unconfined aquifer.

where the height of the water level in the well is prescribed as 10 ft., the free surface and the base pressure head curves are plotted in Fig. 5.43 and 5.44 respectively. The effect of increasing the value of the non-linear coefficient b on the shape and position of these curves may be observed. Fig. 5.45 shows a semi-logarithmic plot of the dimensionless type curves of the base pressure head distribution for all flow cases. The dimensionless variables and parameters listed in the figure were calculated from

$$W = \frac{\pi K (h_o^2 - h_b^2)}{Q} \qquad (5.17)$$

$$u_o = \frac{r}{r_o} \qquad (5.18)$$

$$\lambda = \frac{bQK}{2\pi h_o r_o} \qquad (5.19)$$

$$\xi = \frac{bV_{cr}}{a} \qquad (5.20)$$

where h_b = base pressure head

h_o = height of the water table at the external radius

The remaining symbols have been defined previously.

The effect of the parameter λ on the shape of the type curves may be observed. For flow case No.1, which is the wholly Darcy flow case ($\lambda = 0$), the curve becomes a straight line. Flow cases Nos. 2, 3 and 4 correspond to $\lambda = .0017$, $.0035$ and $.0056$ respectively.

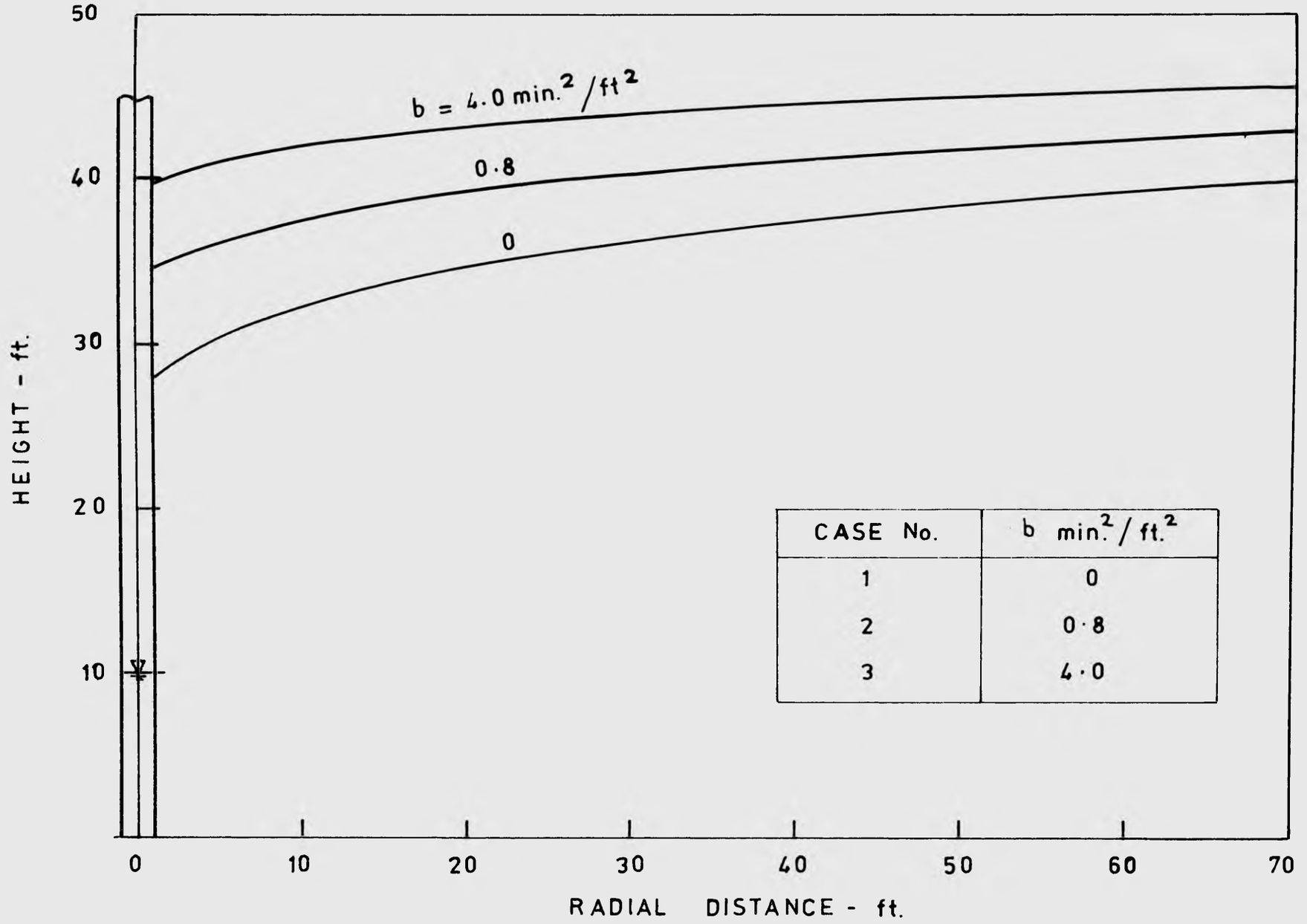

Fig. 5.43: Free surface curves for steady flow cases. Note the effect of the non-linear hydraulic coefficient, b.

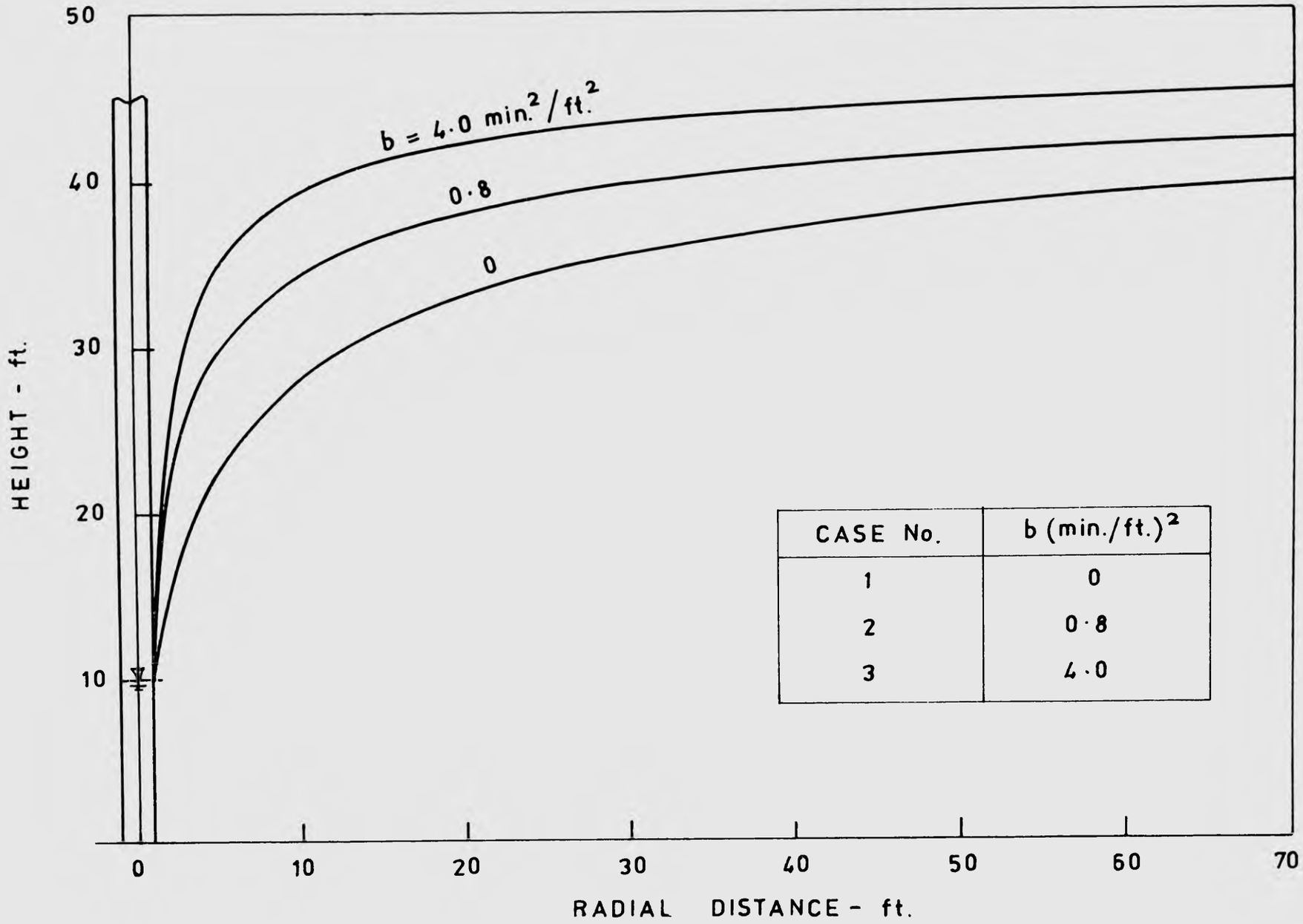

Fig. 5.44: Base pressure head curves for steady flow cases. Note the effect of the non-linear hydraulic coefficient, b.

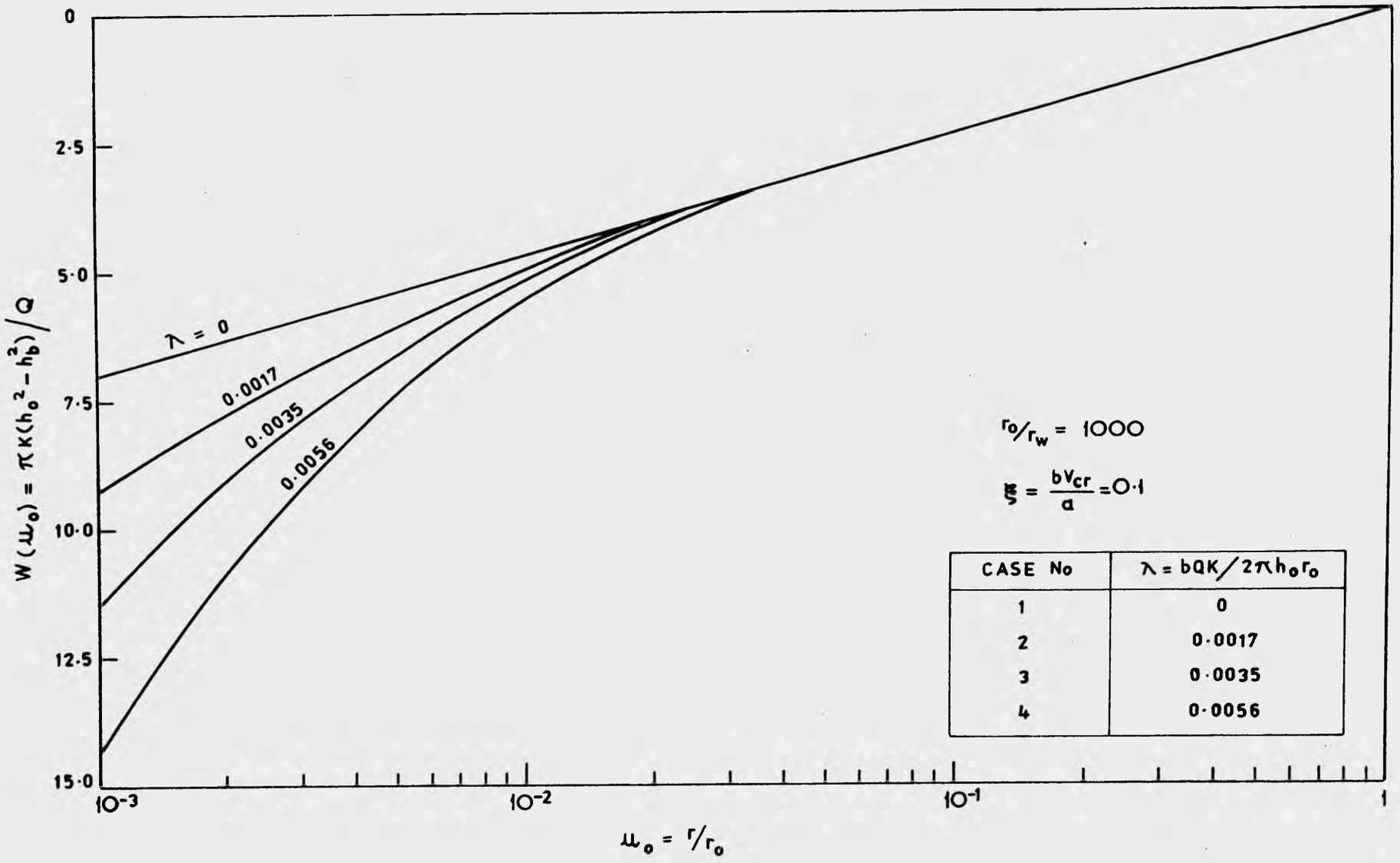

Fig. 5.45: Dimensionless base pressure head curves for steady unconfined flow. λ and ξ characterise non-Darcy flow.

6. Experimental Verification of Steady State, Two-regime Flow Solutions

6.1 General

The finite element analysis was experimentally verified using data obtained during a joint investigation of flow towards wells.[1]

The following flow conditions were investigated using a large scale hydraulic model:-

(i) Flow towards a fully screened well in a confined aquifer.

(ii) Flow towards a fully screened well in an unconfined aquifer.

(iii) Flow towards a partially screened well in a confined aquifer.

(iv) Flow towards a partially screened well in an unconfined aquifer.

Type curve methods were developed by the author to determine the in-situ hydraulic characteristics, namely a, b and K of the aquifer material used in the experiments. The determined values of the hydraulic coefficients were fed into the finite element model to obtain numerical solutions of the flow problems. Comparison of the experimental results and the numerical solutions is presented in this chapter. A general description of the hydraulic model and testing procedures is also included.

---

(1) The design and construction of the experimental equipment and some of the results have been previously reported by Dudgeon, Huyakorn and Swan (1973, Vol. 1). Additional data used in this thesis will be published in detail at a later date.

6.2 Description of Hydraulic Model

6.2.1 Essential Features

A plan view and a photograph of the model are shown in Figs. 6.1 and 6.2 respectively. The detailed design and construction of this model has been described by Dudgeon et al (1972, pp. D2-D13). The model, placed in a square reinforced concrete tank with internal dimensions of 16'x16'x11', was constructed to represent a quadrant portion of the well-aquifer system. The aquifer material was retained by a 16 ft. radius barrier which was made up of 16 gauge perforated steel sheets joined together to form a quadrant of the circle. The thickness of the aquifer was 5 ft. An inner barrier with a radius of 4 ft. was also provided to allow aquifer material close to the 5 inch quadrant well to be removed without disturbing the bulk of the entire aquifer. This provision was desirable as it served the purpose of speeding up the task of changing well screens. The inner barrier was made from a 16 gauge perforated steel sheet, curved and corrugated to allow it to resist compressive loads without buckling. The open area of the perforated sheet was 52%, which was considered sufficient to prevent additional flow resistance being introduced at this location.

Water was supplied to the tank from a 6 inch diameter inlet pipe located at the corner opposite to the quadrant well. The inflow water was passed through the aquifer medium towards the well from which it

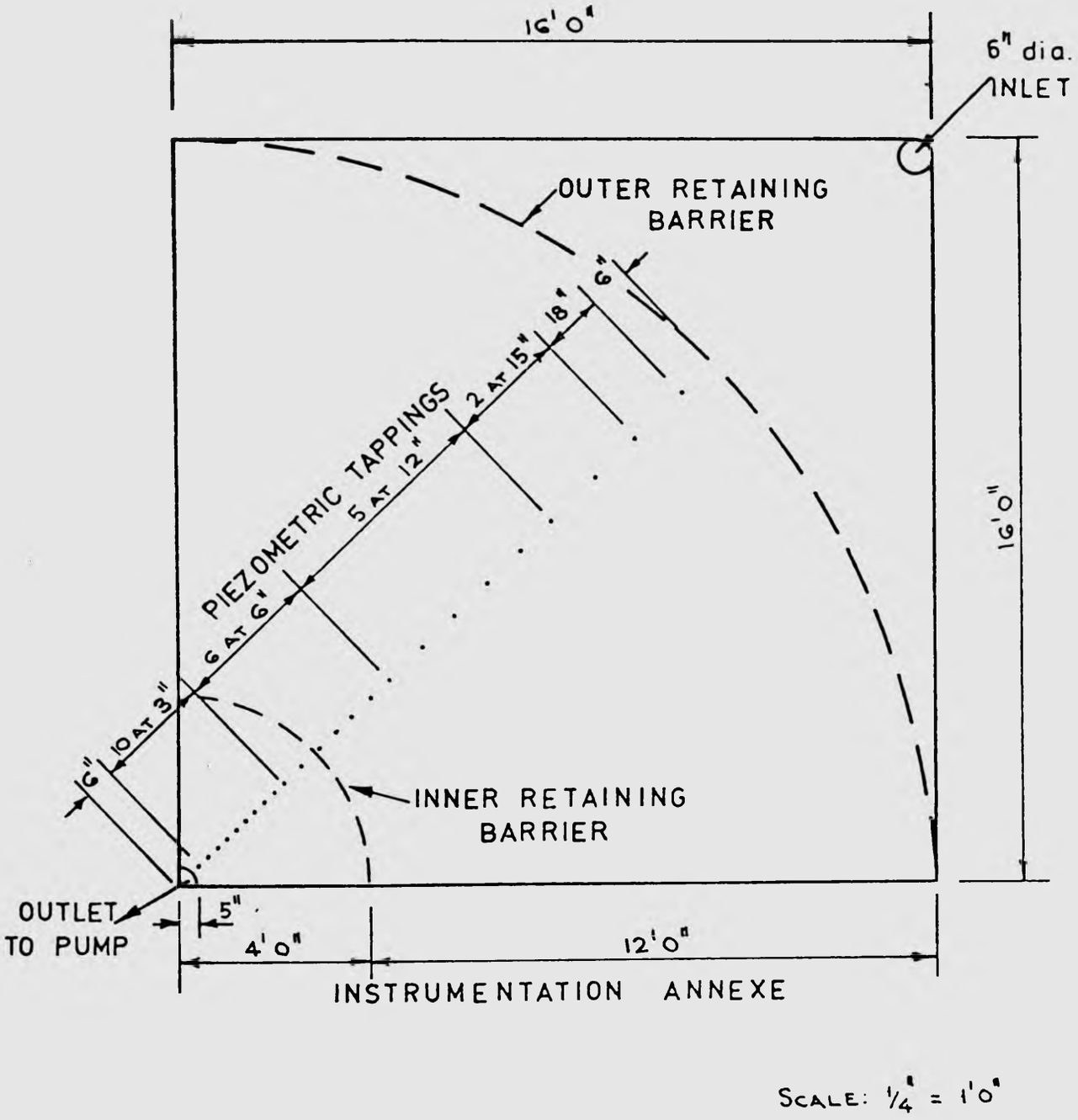

Fig. 6.1: Plan view of well-aquifer model showing essential features.

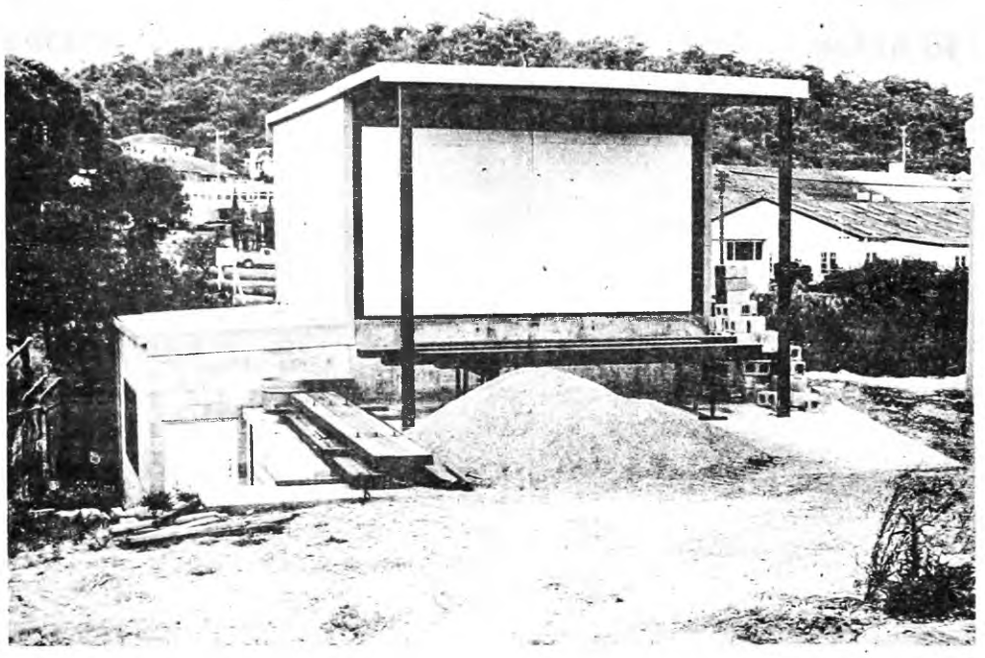

Fig. 6.2: General view of well-aquifer model showing reinforced concrete tank, instrumentation annexe and aquifer material.

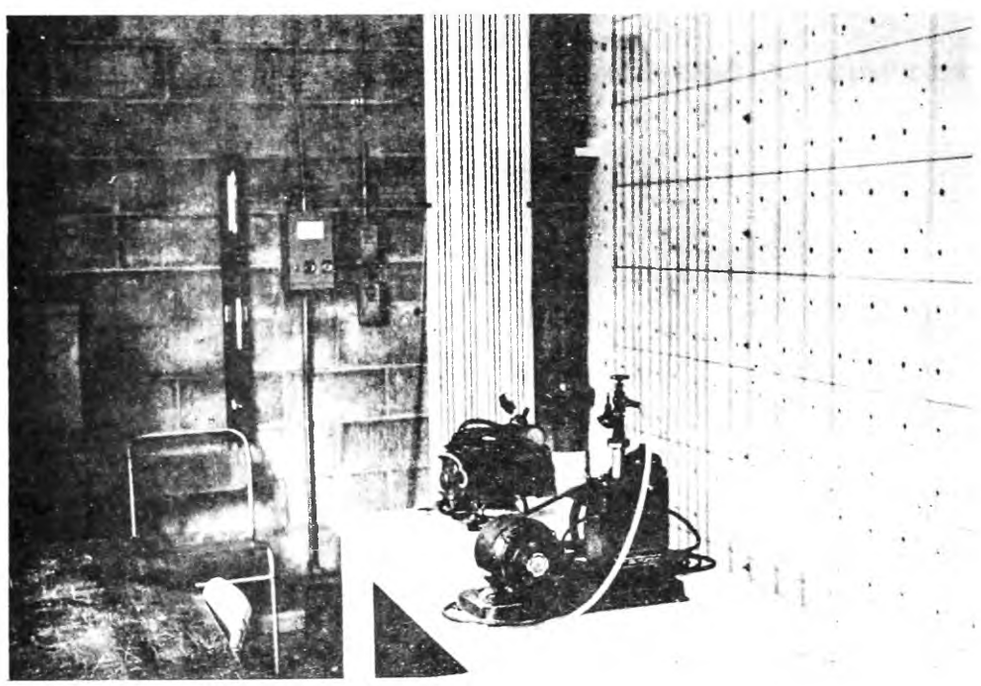

Fig. 6.3: Internal view of instrumentation annexe showing orifice manometer panel (centre) and piezometric tubes (right).

was pumped through a discharge measuring device back into the tank. A 6-inch centrifugal pump with a 20 H.P. motor capable of delivering 2 cfs against a head of 60 ft. was used to recirculate the water through the tank. Discharges were accurately measured by D and D/2 orifice plate meters manufactured and calibrated according to the British standard specification. To observe the hydraulic heads at various radial distances from the pumped well, a number of piezometric tappings, made from copper tubes, were installed in the base of the tank along a radial line extending from the well outlet to the diagonally opposite inlet pipe. The spacing of these tappings is indicated in Fig. 6.1. Closer spacing near the well allowed for steeper hydraulic gradients in that vicinity. The tappings were connected to manometer panels on two opposite walls of the tank. A photograph showing one of these panels on the wall inside the instrumentation annexe is given in Fig. 6.3.

6.2.2 Aquifer Material

A Nepean river gravel consisting of rounded particles was selected as an aquifer material which would allow non-Darcy flow to develop in the zone extending from the well to the inner barrier. Sieve analysis was performed on a sample of this gravel. The grain size distribution curve is given in Fig. 6.4. The characteristic grain diameter $\bar{d}$, chosen as the diameter such that 10 percent by weight of the sample is of smaller size, was obtained as 0.056 inches. It is

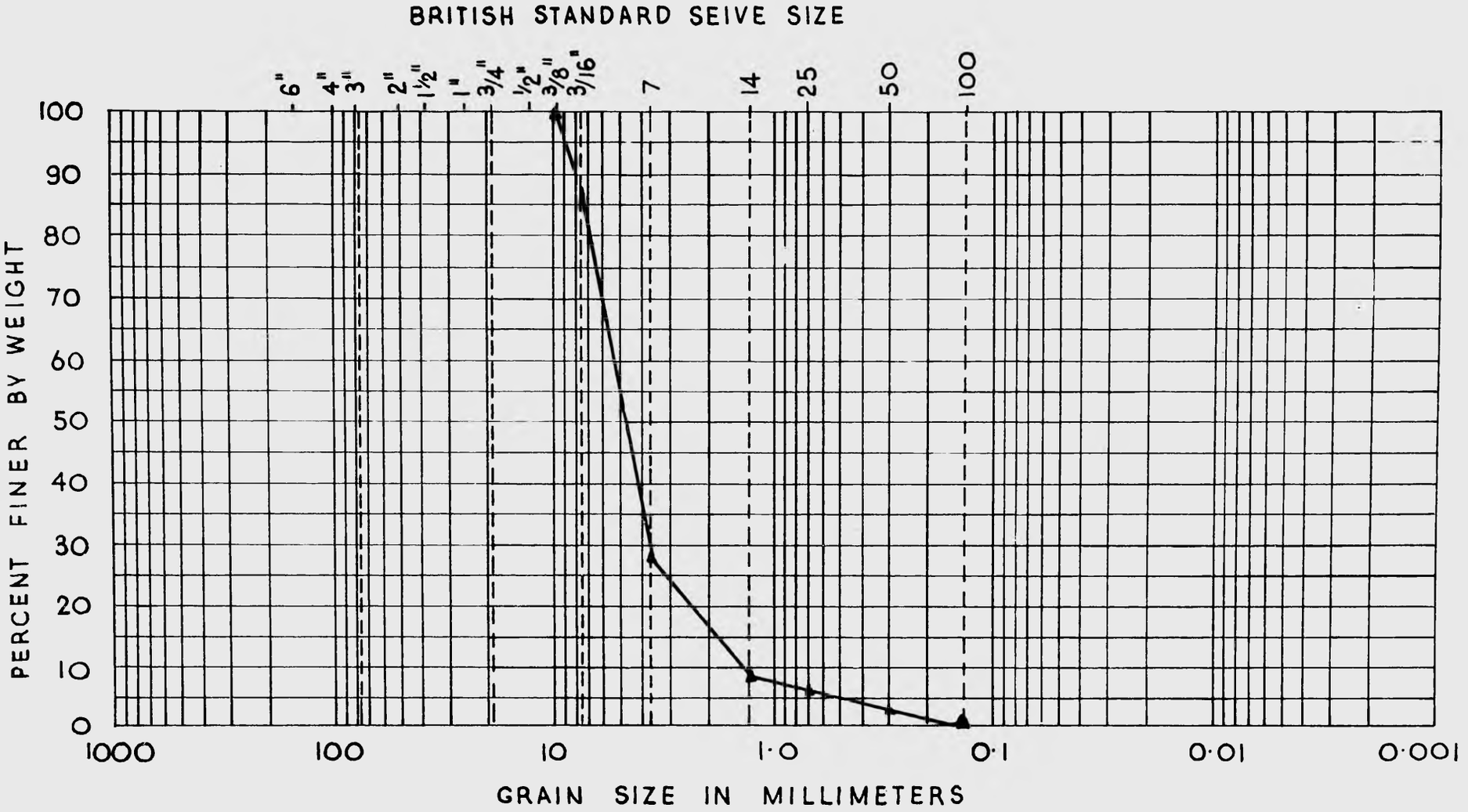

Fig. 6.4: Grain size distribution of aquifer material.

noted that the gravel was sufficiently coarse for unconfined flow to take place with negligible capillary effects.

Permeability tests were also carried out on the sample to determine the hydraulic coefficients for comparison with the values obtained by applying the newly developed type curve methods. The permeameter used in carrying out the tests was a downward vertical flow type similar to the one described by Dudgeon (1964, 1966). Its diameter was 8 inches and the diameter of the inner core section was 6 inches. As pointed out by Dudgeon, the purpose of the inner core was to eliminate wall effects.

The gravel was loaded into the permeameter in the same manner as was used to load the experimental tank in an attempt to obtain a similar porosity. Porosities determined from measurements of the volume of water required to fill the voids were 34.6% in the permeameter and 33.1% in the model tank.

Piezometric head measurements were taken over a 2 ft. long inner core section of the sample. The results obtained are presented in Fig. 6.5. The fitted Forchheimer velocity-hydraulic gradient curve was obtained by applying the curve fitting method suggested by Sunada (1965). The accuracy of the fit was assessed from the value of the standard error of estimate which was calculated as 5.6 percent Values of the hydraulic coefficients, a, b and K, and the critical velocity V_{cr} are also included in the figure. Using the determined value of $\bar{d}$ and the listed value of V_{cr}, the critical Reynolds number R_{cr} was found to be approximately 4.2

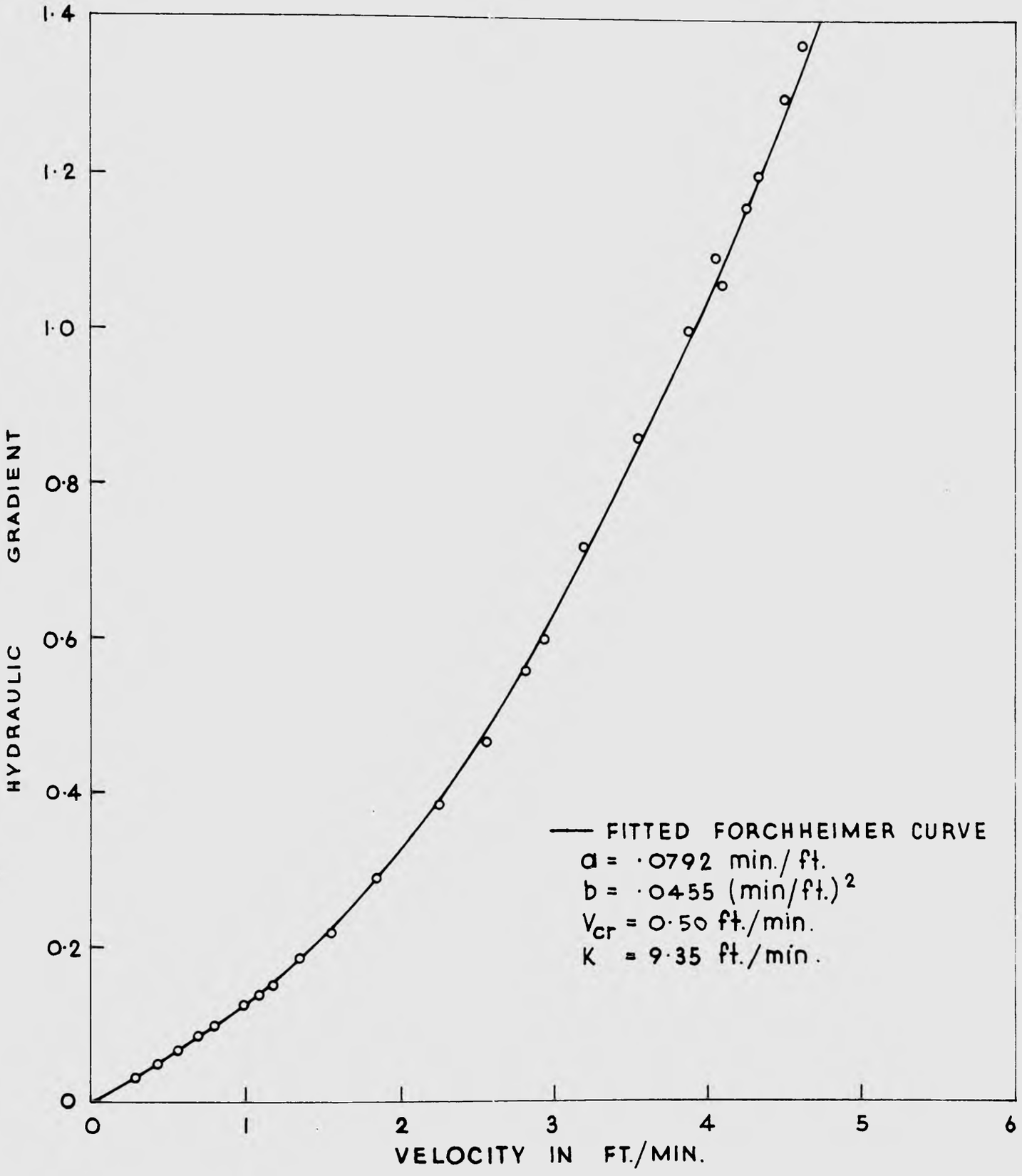

Fig. 6.5: Permeability test results for aquifer material.

6.3 Test Program and Procedures

To study two-regime flow under different aquifer and well conditions, four series of tests were performed.

(i) Fully Screened Well in a Confined Aquifer

The purpose of the first series was to investigate flow towards a fully screened well in a confined aquifer. A 5 ft. length well screen, made from a perforated steel sheet, curved to form a quadrant of a 5 inch diameter circle, was used. The top of the aquifer was covered with a polythene sheet to simulate an impermeable overlying layer as shown in Fig. 6.6. The sheet was held in position by several inches of aquifer material and sealed to the edges of the tank. Care was taken to avoid vertical leakage into the aquifer as much as possible. After the tank had been filled with water and the air entrained in the aquifer removed, several tests were carried out to establish the discharge-drawdown relationship for the fully screened well. For each test, measurements of the piezometric heads at the floor tappings and the water level in the well were made.

(ii) Fully Screened Well in an Unconfined Aquifer

The purpose of the second series of tests was to investigate flow towards a fully screened well in an unconfined aquifer. Following the first series, the model was filled slowly with water up to a depth of 4.3 ft. which was slightly less than the thickness of the aquifer. The model then represented an unconfined aquifer with a fully screened well. Several tests were performed to obtain the discharge-drawdown

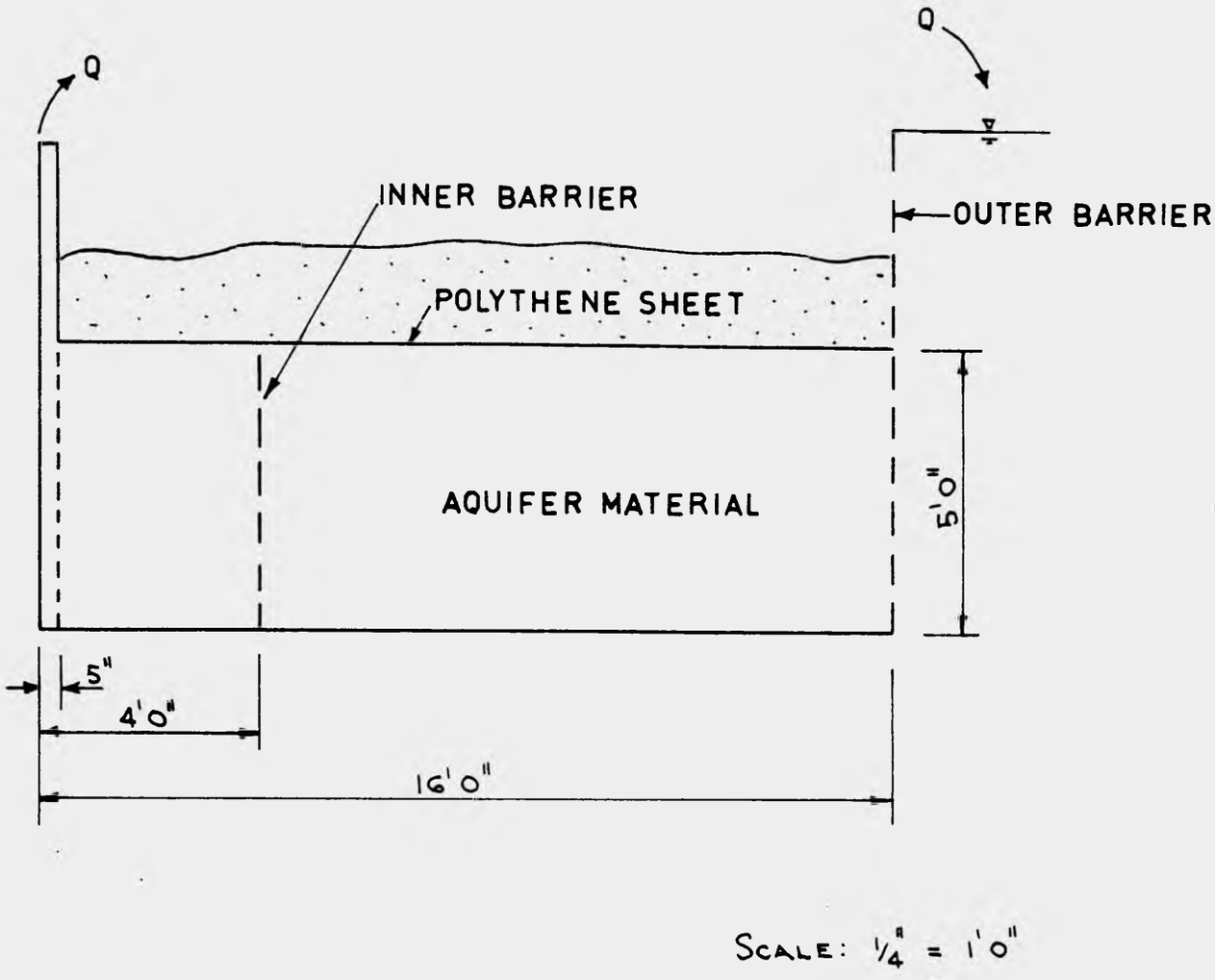

Fig. 6.6: Radial cross-section of well-aquifer model showing arrangement for confined flow testing.

relationship for the same well which became a water table well. For each test, the piezometric heads along the base of the aquifer and the water level in the well were measured. Attempts were also made but without success to locate the position of the free surface by observation through a series of 1 inch diameter holes spaced at 6 inch centres in a wall of the reinforced concrete tank.

(iii) Partially Screened Well in a Confined Aquifer

The third series of tests was intended to investigate flow towards a partially screened well in a confined aquifer. Following the second series, the 5 ft. screen shown in Fig. 6.6 was removed and a shorter screen of 1 ft. length was placed at the base of the aquifer. The remaining thickness of the aquifer was cased. In carrying out this task, it was necessary to remove and backfill the aquifer material in the zone inside the inner barrier. As in the first series, a number of tests were carried out to obtain the discharge-drawdown relationship.

(iv) Partially Screened Well in an Unconfined Aquifer

The last series of tests was carried out to study flow towards a partially screened well in an unconfined aquifer. As in the second series, the model was refilled slowly up to the depth of 4.3 ft. and several tests were performed to obtain the well discharge-drawdown relationship.

6.4 Comparison of Experimental Results and Finite Element Solutions

6.4.1 General

In comparing experimental results from a well-aquifer model with numerical solutions, it is essential that appropriate values of the hydraulic coefficients for the aquifer material be obtained and fed into the numerical model. Earlier workers (Volker, 1969), (Trollope et al 1971), resorted to permeability tests carried out over a range of velocities comparable with those in the model. While this approach may be justified in the absence of a more satisfactory approach, doubt usually exists as to whether the physical properties of the sample are similar to those of the model aquifer. Slight change in such properties as effective porosity and packing of grains can affect the hydraulic coefficients K, a and b quite considerably (Franzini, 1951), (Engelund, 1953, pp. 17-29), (Dudgeon, 1968). Unless the values of these coefficients used in obtaining the numerical solutions are comparable to the actual in-situ values, satisfactory agreement between the numerical and experimental results cannot be achieved.

In the present work, the in-situ hydraulic coefficients were determined by applying two newly developed type curve methods to the results obtained from the first and third series of pumping tests. These type curve methods are described in the following sections.

6.4.2 Flow towards a Fully Screened Well in a Confined Aquifer

The arrangement for the first series of tests is illustrated diagrammatically in Fig. 6.6. Results were obtained for a sufficient number of flows to establish the well discharge-drawdown relationship. For each test, the total discharge from the full well circle, Q, was calculated as 4 times the measured discharge from the quadrant well. To determine the in-situ hydraulic coefficients, the following type curve method was applied to the results from the test which gave Q = 68.77 cfm:-

(i) The piezometric readings were converted to drawdowns and plotted on a semi-logarithmic scale against the dimensionless radius r/r_o, where r_o corresponds to the 16 ft. radius of the outer barrier. A free hand curve was drawn to fit most of the experimental points. The plot was then superposed on the type curve for steady Darcy flow towards a fully screened well as shown in Fig. 6.7. It is noted that the experimental curve becomes non-linear as the well is approached. A certain radius r where the experimental plot is linear was selected and the corresponding values of the drawdown s and the dimensionless drawdown $2\pi s\ T/Q$ were read from the graph. Using these values, the transmissivity coefficient T was calculated as

$$T = \frac{1.25 \times 68.77}{2\pi \times 0.24} = 57 \quad ft^2/min.$$

(ii) Using the determined value of T, the experimental plot was converted to the dimensionless plot of $2\pi\ sT/Q$ versus r/r_o and

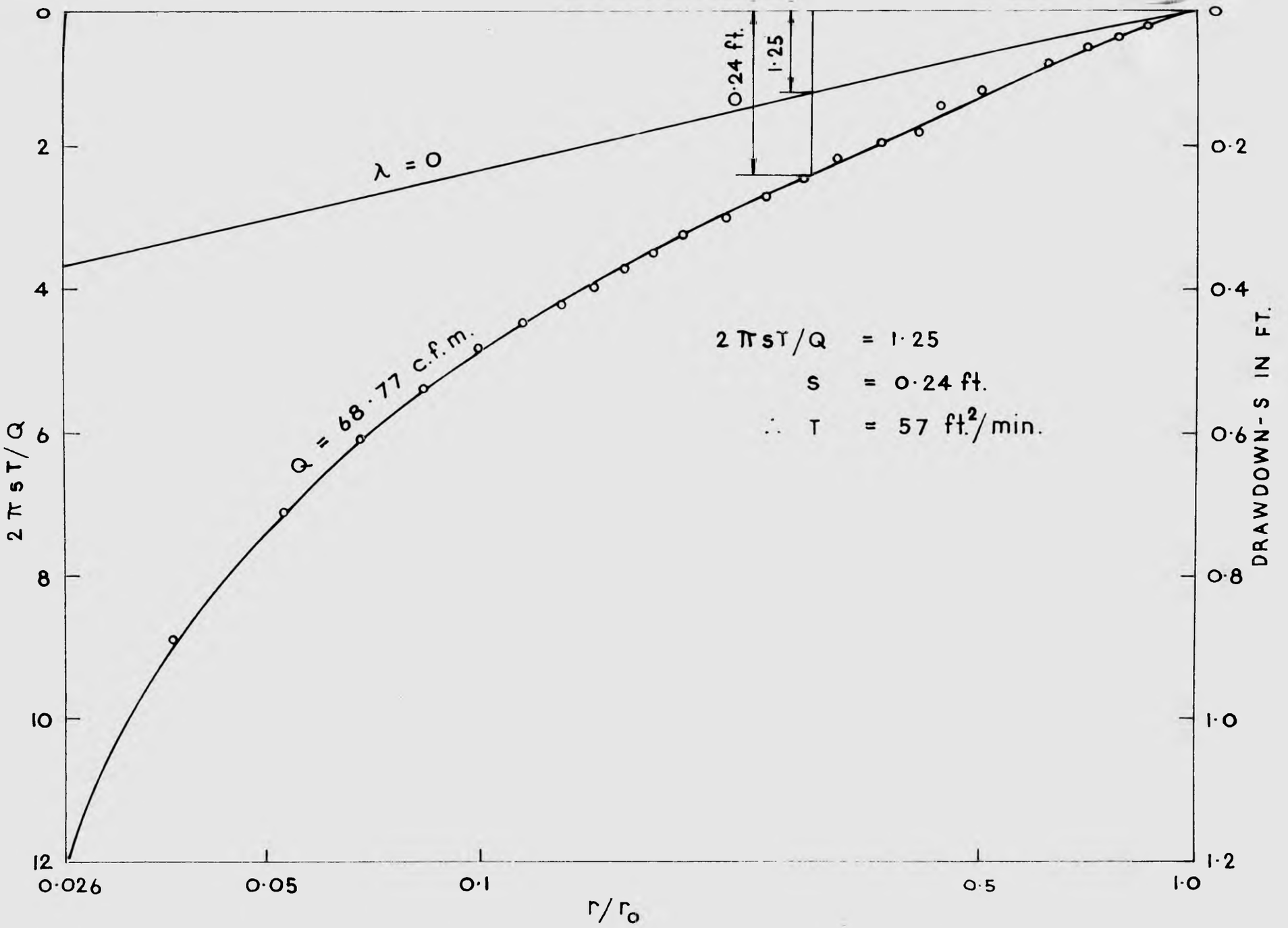

Fig. 6.7: Superposition of experimental results on dimensionless type curve $\lambda = 0$ to obtain transmissivity coefficient T (fully screened well).

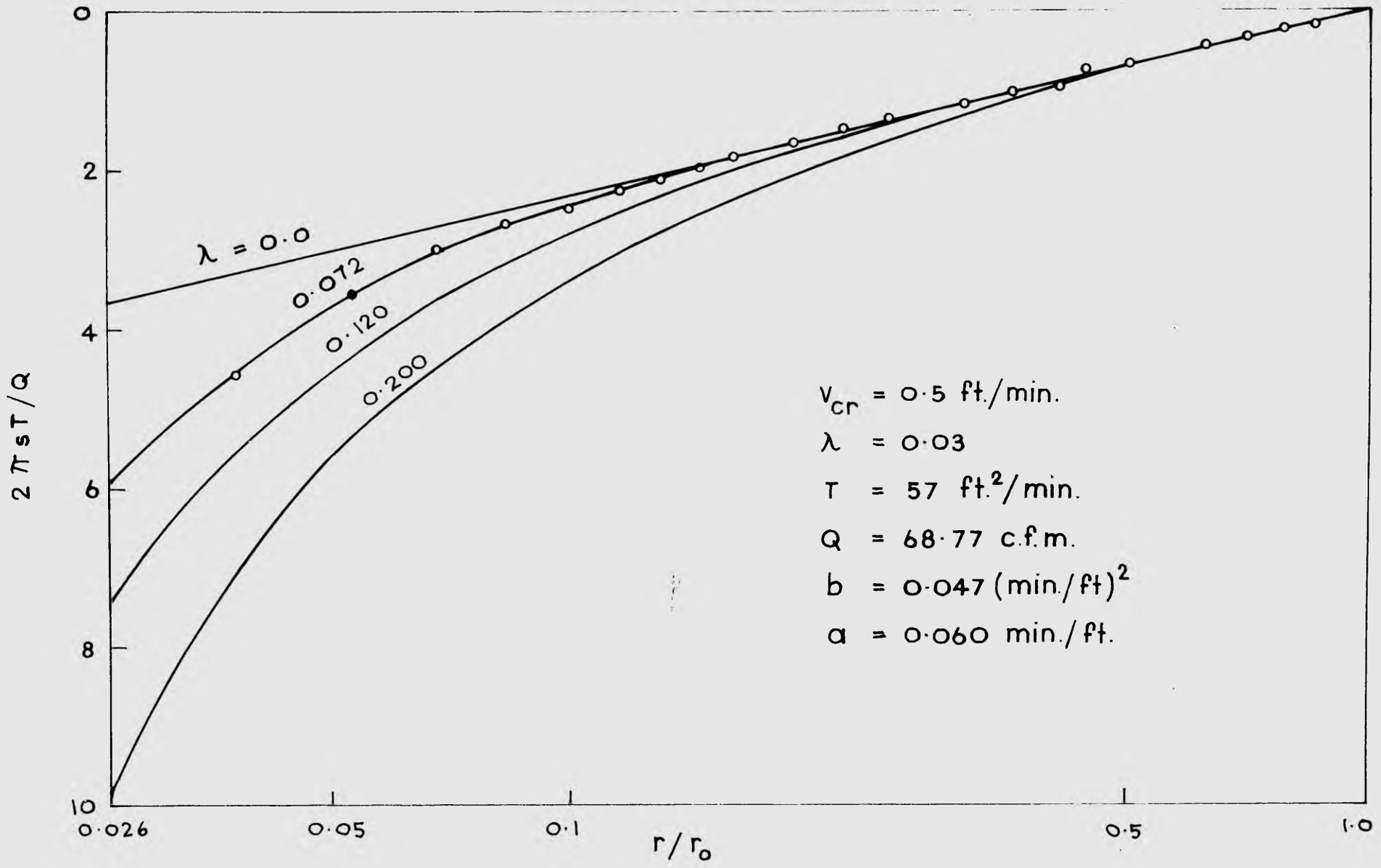

Fig. 6.8: Superposition of experimental results on a family of type curves to obtain Forchheimer coefficients a and b (fully screened well).

superposed on a family of type curves for steady state, two-regime flow as shown in Fig. 6.8. The value of the non-Darcy flow parameter λ for the best fit type curve was obtained and used together with the value of T in calculating the required in-situ values of the hydraulic coefficients a, b and K as follows:-

$$b = \frac{2\pi m^2 r_o \lambda}{QT}$$

$$= \frac{2\pi \times 5^2 \times 16 \times .072}{68.77 \times 57} = .047 \qquad \text{min}^2/\text{ft}^2.$$

$$a = \frac{m}{T} - bV_{cr}$$

$$= \frac{5}{57} - .047 \times 0.5 = .060 \qquad \text{min/ft.}$$

$$K = \frac{57}{5} = 11.4 \qquad \text{ft/min.}$$

The determined in-situ values were fed into the finite element model to obtain theoretical predictions of the experimental flow conditions. In the finite element analysis, the hydraulic heads on the well screen were prescribed as the measured heights of the water level in the well. In so doing, it was assumed that screen losses were negligible.

Figs. 6.9 and 6.10 show a comparison of the numerical solutions and the results from four tests chosen to cover a good range of the well drawdown. The plot in Fig. 6.9 represents the dimensionless drawdown-radial distance relationships. The discharges listed are the experimental discharges. It can be seen that the determined in-situ

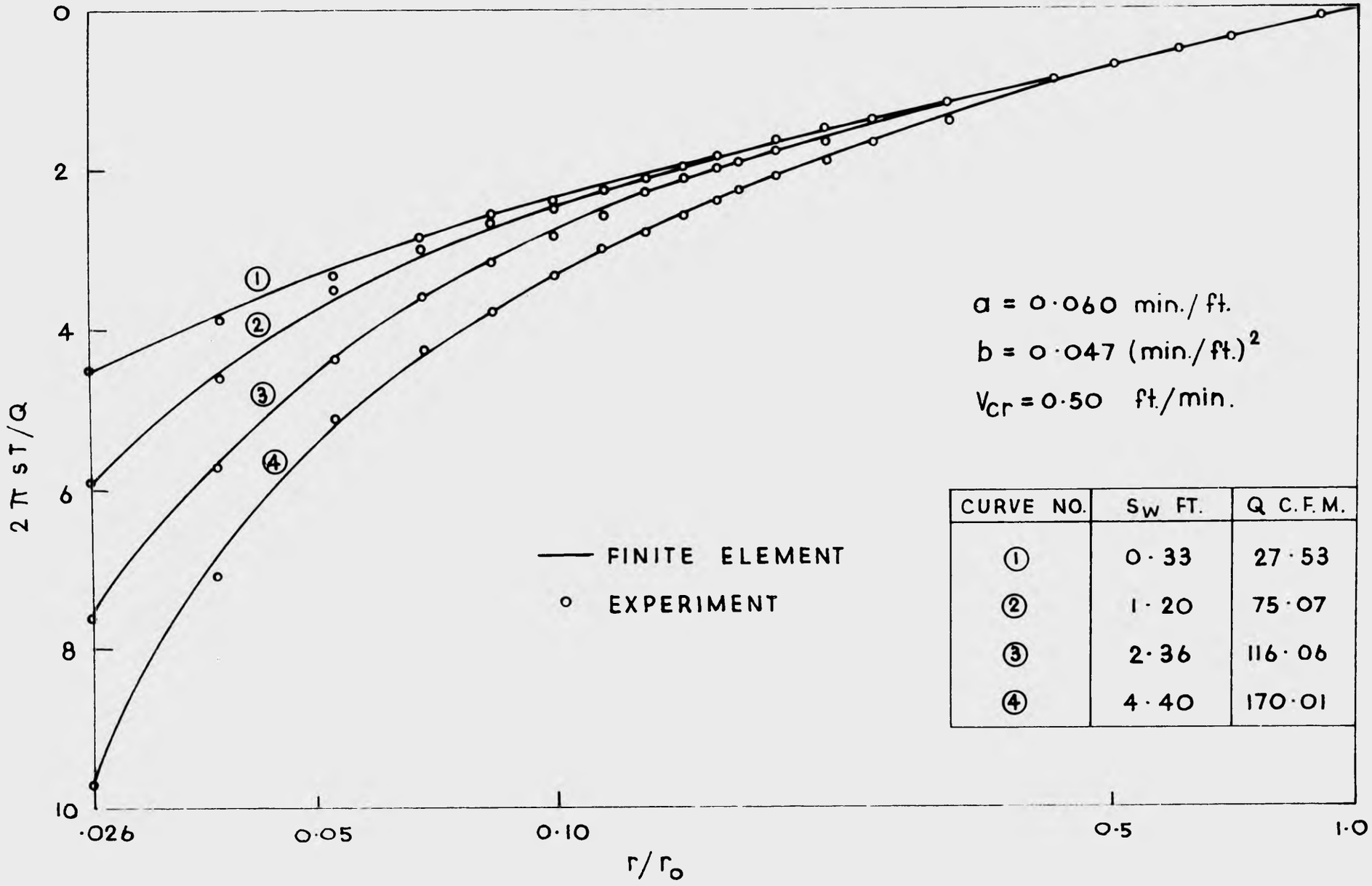

CURVE NO.	S_w FT.	Q C.F.M.
①	0·33	27·53
②	1·20	75·07
③	2·36	116·06
④	4·40	170·01

Fig. 6.9: Dimensionless drawdown - radial distance relationships showing comparison of experimental results and finite element solutions.

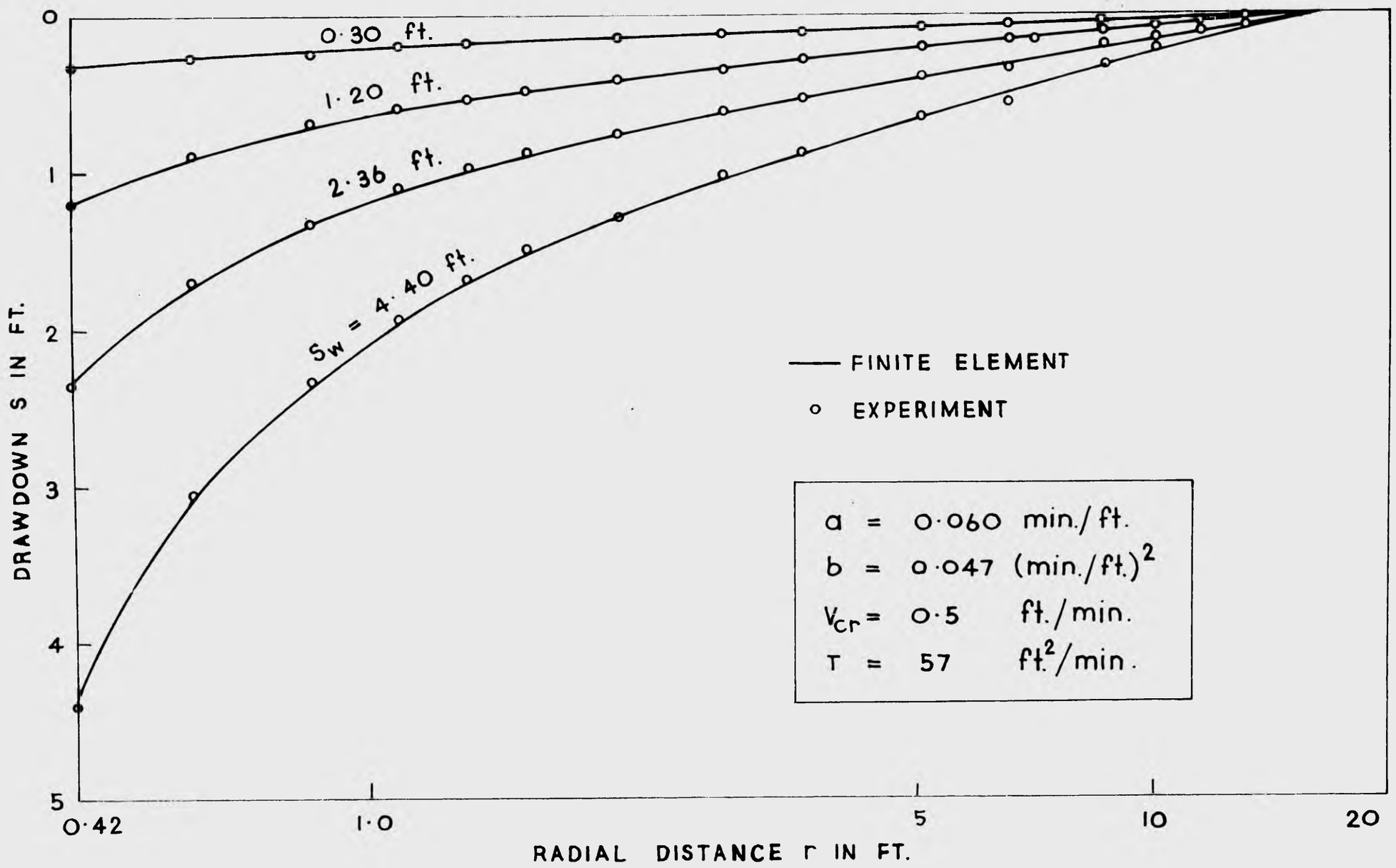

Fig. 6.10: Drawdown-radial distance relationships showing comparison of experimental results and finite element solutions.

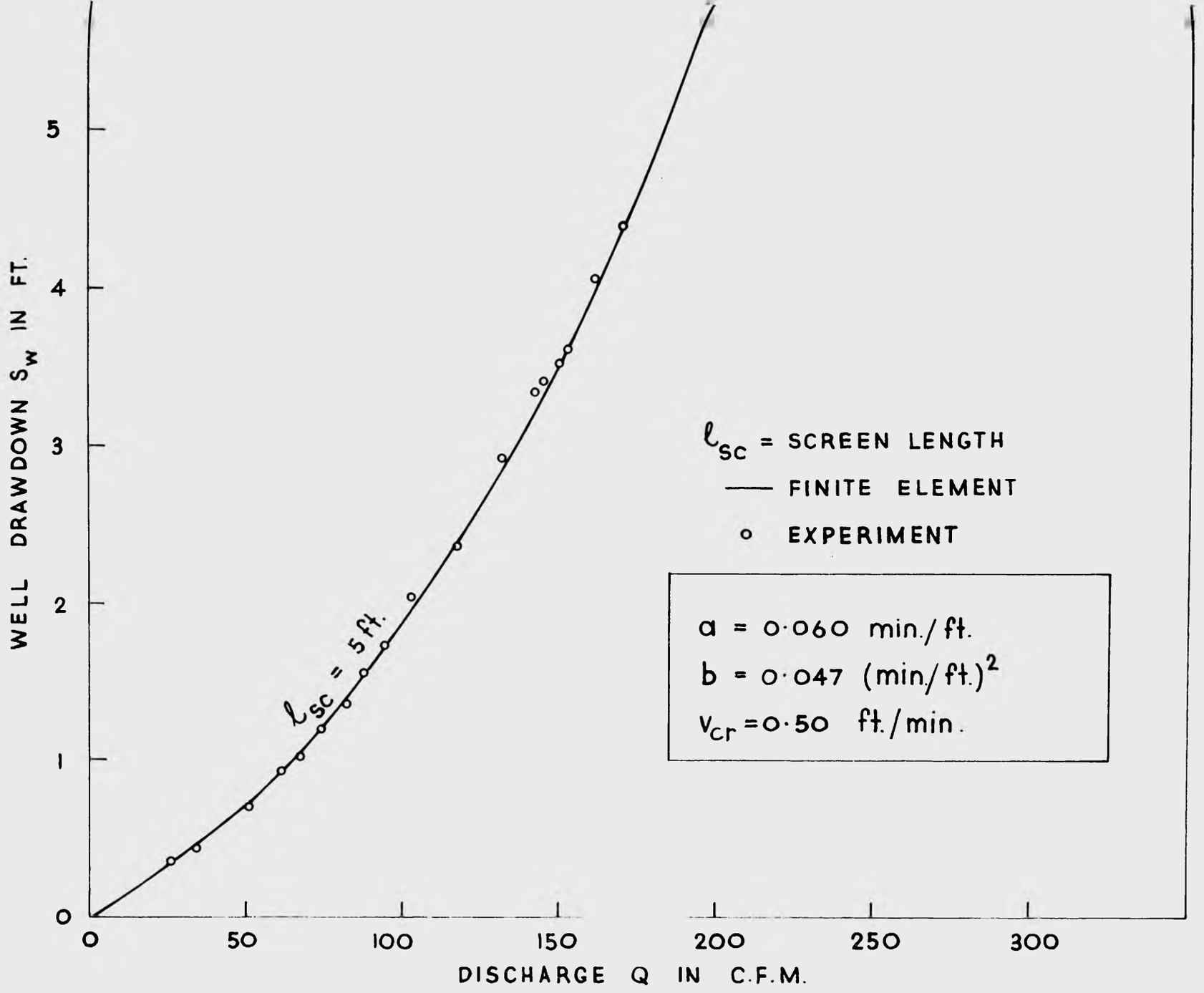

Fig. 6.11: Well drawdown-discharge relationship showing comparison of experimental results and finite element solutions.

values of the hydraulic coefficients led to good agreement between the theory and experiment. As a further check on the accuracy of these values, the well discharge-drawdown relationship is also plotted in Fig. 6.11. Good agreement between the theoretical prediction and experimental results may again be observed.

6.4.3 Flow towards a Fully Screened Well in an Unconfined Aquifer

The arrangement for the second series of tests was identical to that shown in Fig. 6.6 for the first series except that the height of the water table at the outer barrier was lowered to 4.30 ft. As the aquifer, which then became an unconfined aquifer, was not physically disturbed, its hydraulic properties would have remained unchanged. Consequently, the in-situ values of a, b and K were taken as those listed in section 6.4.2 and used in obtaining the finite element solutions. In the finite element analysis, the hydraulic heads on the portion of the screen below the seepage face were prescribed as the measured heights of the water level in the well.

Figs. 6.12 and 6.13 show the plots of the base pressure head against radial distance as obtained from the theory and experiment. As the positions of the free surface were not located satisfactorily in the experiments, only the theoretical free surface curves are included in the figures. The water levels in the well are also shown. It can be seen that in general the agreement between the numerical solutions and experimental results is quite acceptable. The experimental points tend to lie slightly below the theoretical curves. Possible explanations

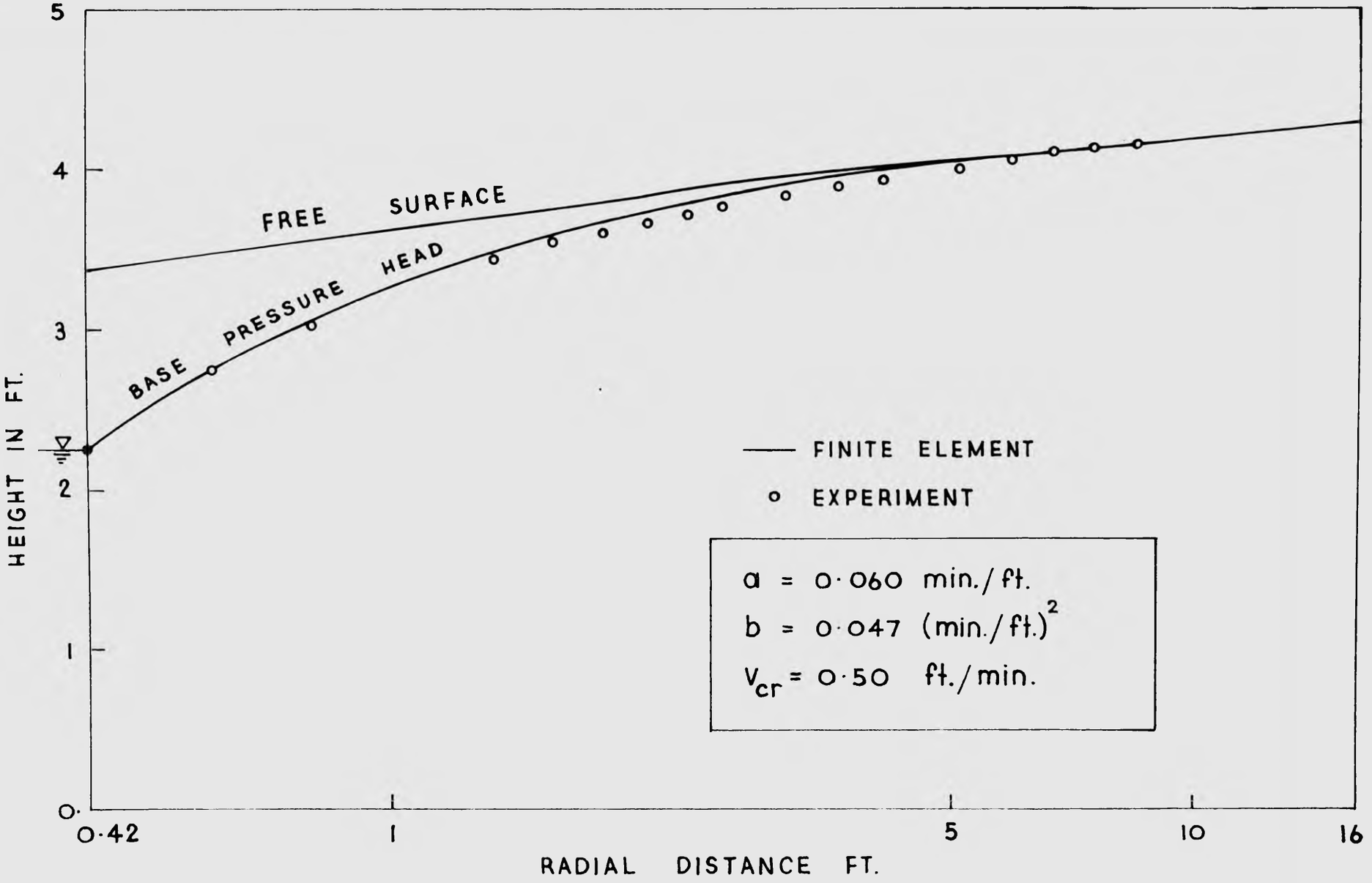

Fig. 6.12: Free surface and base pressure head curves showing comparison of experimental results and finite element solution (h_W = 2.2).

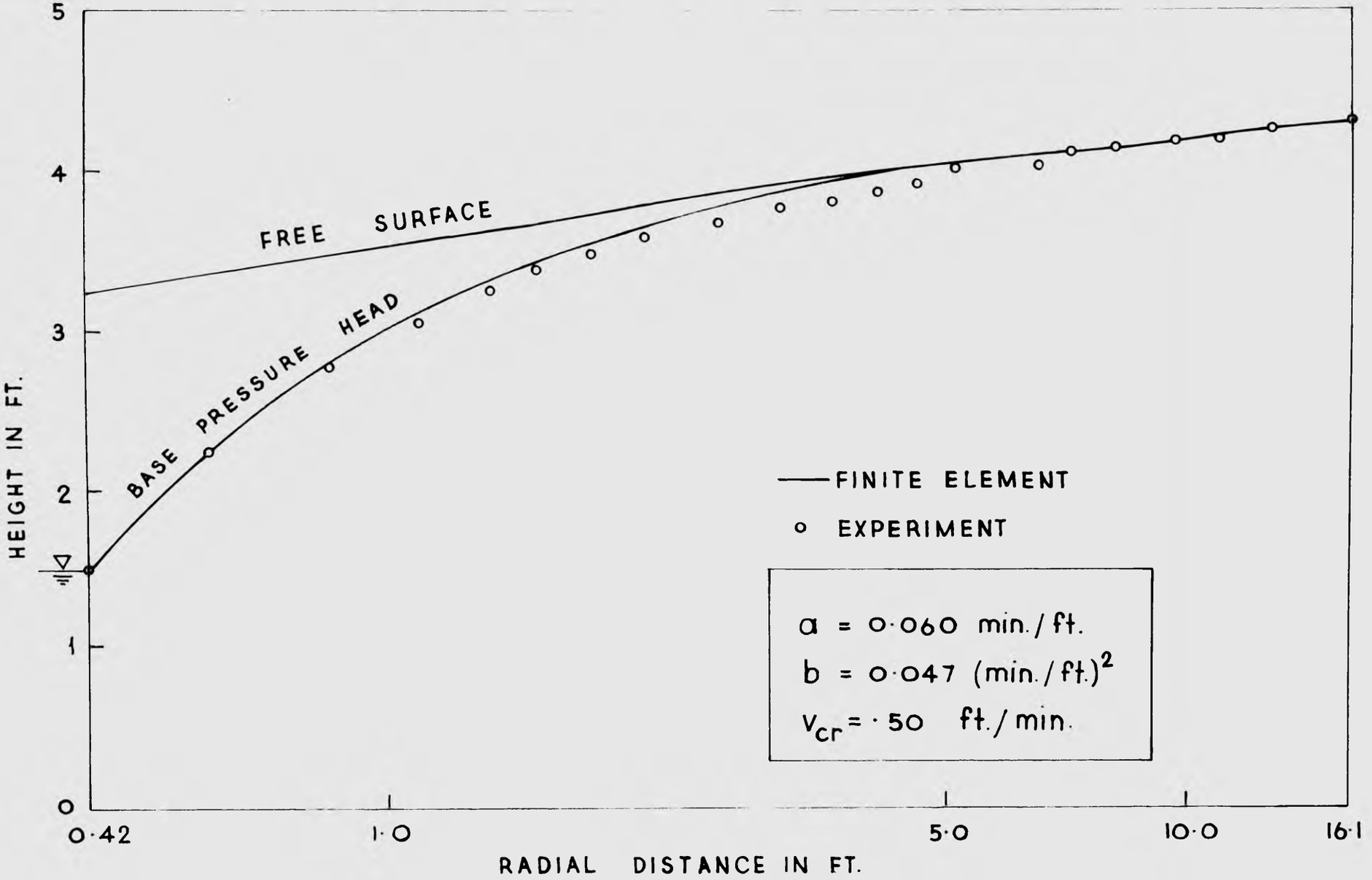

Fig. 6.13: Free surface and base pressure head curves showing comparison of experimental results and finite element solutions.

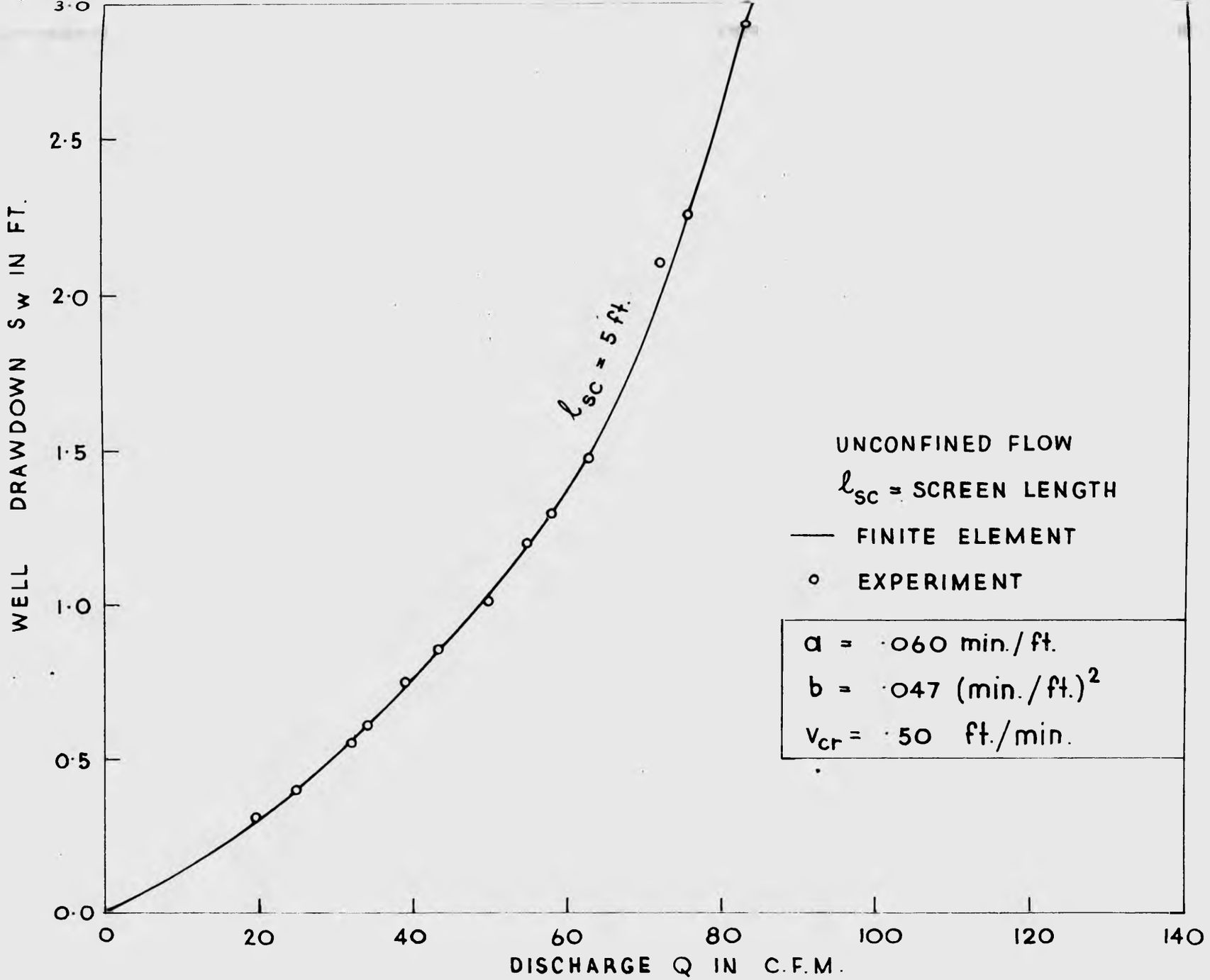

Fig. 6.14: Well discharge-drawdown relationship showing comparison of experimental results and finite element solutions.

for this are:-

(i) well screen losses which were neglected in the theoretical analysis,

(ii) the effects of convergent flow on the hydraulic coefficients a and b (Wright, 1968).

As a further check on the values of the hydraulic coefficients used, the well discharge-drawdown relationship is plotted in Fig. 6.14. Good agreement between the theory and experiment may be observed but it should be noted that the discharge-drawdown relationship is less sensitive to change in the values of a and b than is the base pressure head curve.

6.4.4 Flow towards a Partially Screened Well in a Confined Aquifer

In carrying out the third series of tests to investigate flow towards a partially screened well in a confined aquifer, it was necessary to remove and backfill the aquifer material inside the inner barrier. This process could lead to considerable change in its hydraulic properties. Thus the in-situ values of a, b and K were redetermined. The following type curve method was applied to the results obtained from the test which gave the total well discharge of 56.25 cfm:-

(i) The piezometric readings were converted to drawdowns and plotted on a semi-logarithmic scale against the dimensionless radius r/r_o. A free hand curve was drawn to fit most of the experimental points and the plot was then superposed on the type curve for steady Darcy flow towards a partially screened well as shown in Fig. 6.15. It is noted that the experimental curve is approximately linear beyond

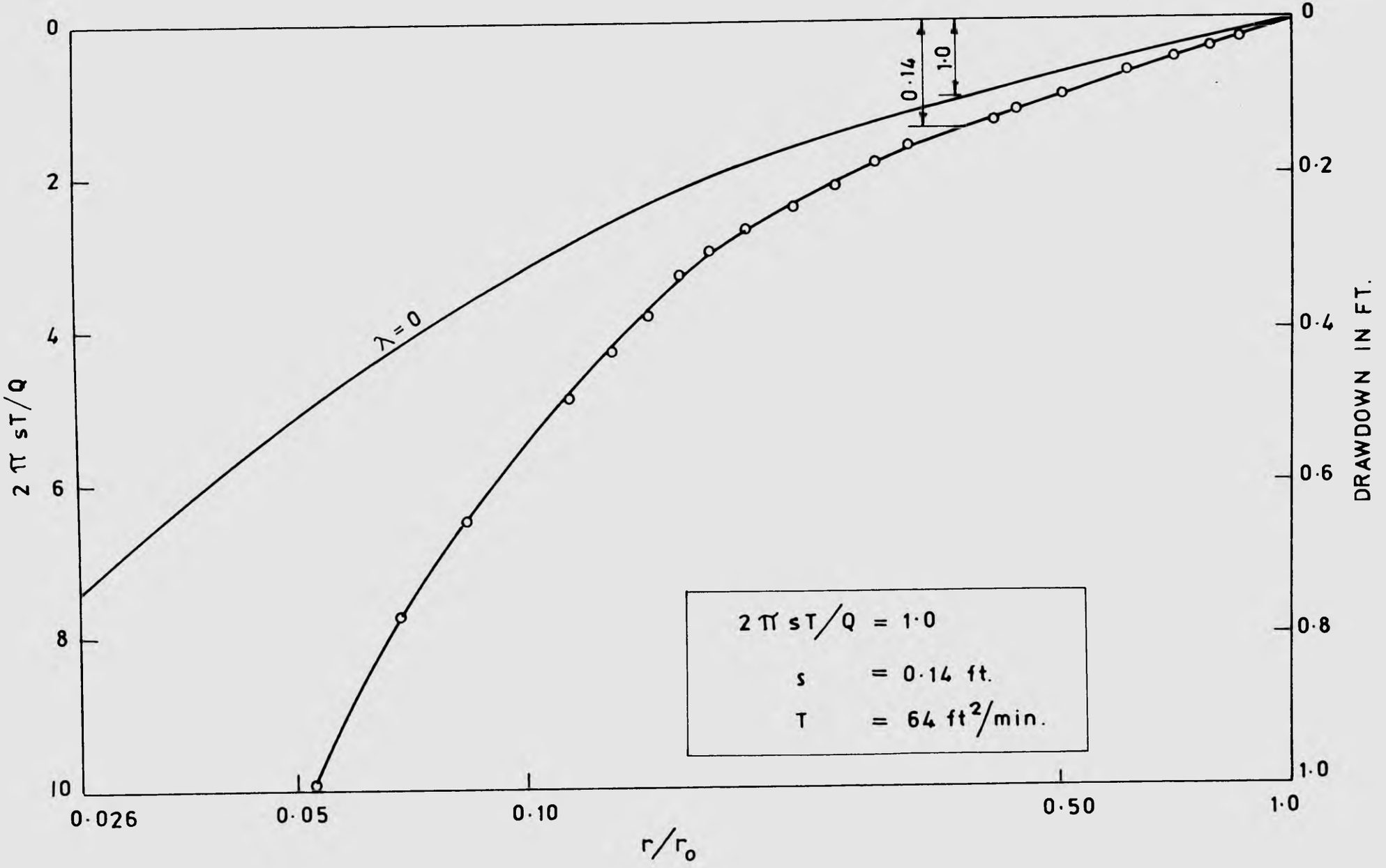

Fig. 6.15: Superposition of experimental results on dimensionless type curve $\lambda = 0$ to obtain transmissivity coefficient T (partially screened well).

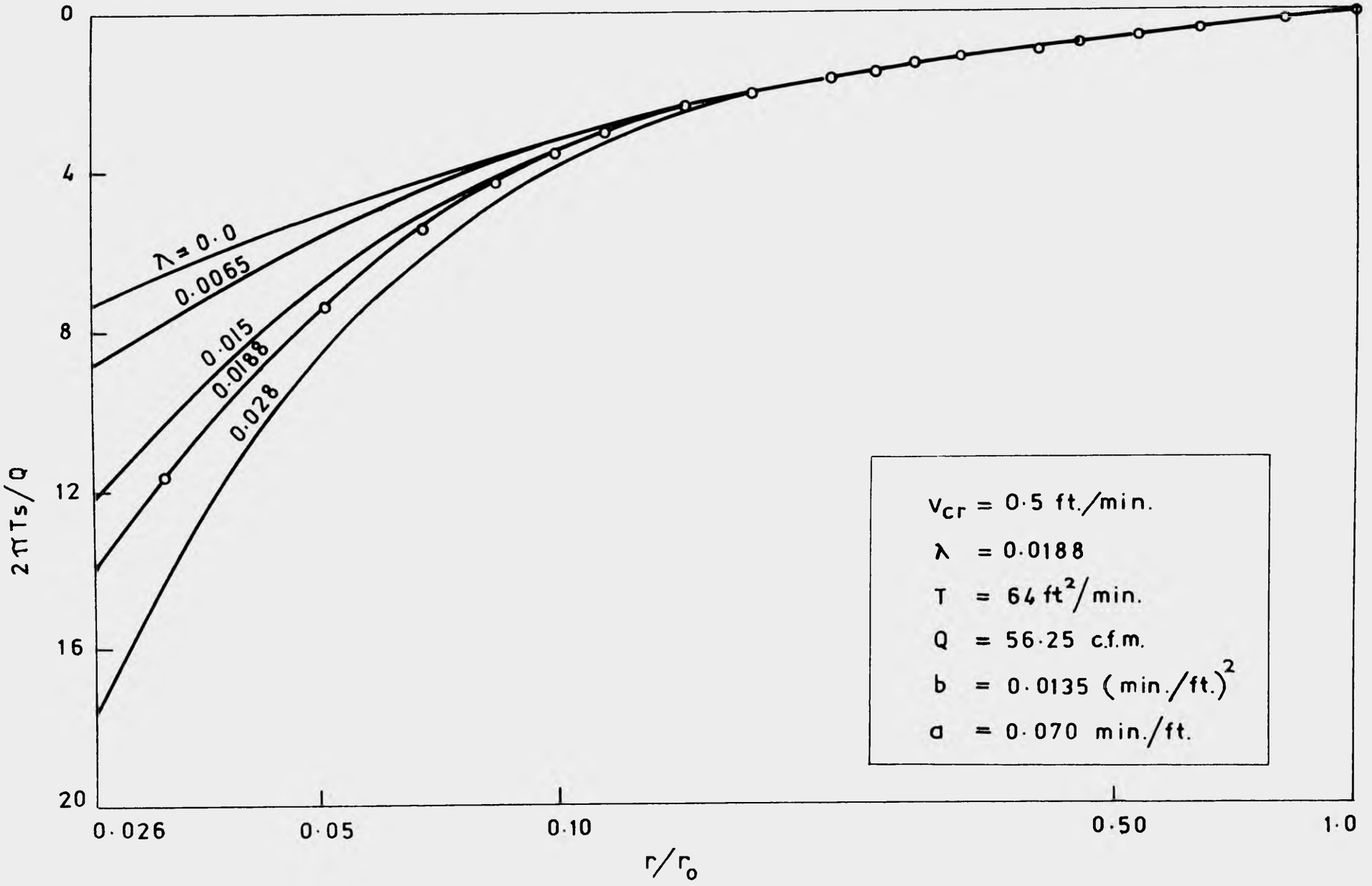

Fig. 6.16: Superposition of experimental results on a family of type curves to obtain Forchheimer coefficients a and b.

a certain radius where the effects of non-Darcy flow and partially screening become negligible. At this radius, the values of the drawdown s and the dimensionless drawdown $2\pi sT/Q$ were read from the graph. Using these values, the transmissivity of the aquifer T was calculated as

$$T = \frac{1.0 \times 56.25}{2\pi \times 0.14} = 64 \quad ft^2/min$$

(ii) Using the determined value of T, the experimental plot was converted to the dimensionless plot of $2\pi sT/Q$ versus r/r_o and superposed on a family of type curves for steady state, two-regime flow towards a partially screened well as shown in Fig. 6.16. The value of the non-Darcy flow parameter λ for the best fit type curve was obtained and used together with the value of T in calculating the required in-situ values of a, b and K as follows:-

$$b = \frac{2\pi m^2 r_o \lambda}{QT}$$

$$= \frac{6.28 \times 5^2 \times 16 \times .0188}{56.25 \times 64} = .0135 \ min^2/ft^2$$

$$a = \frac{m}{T} - bV_{cr}$$

$$= \frac{5}{64} - .0135 \times .5 = .071 \quad min/ft.$$

$$K = \frac{64}{5} = 12.8 \quad ft/min.$$

These values were fed into the finite element model to obtain theoretical predictions of the experimental results. In the finite element analysis, the hydraulic heads on the well screen were prescribed as the measured heights of the water level in the well. It

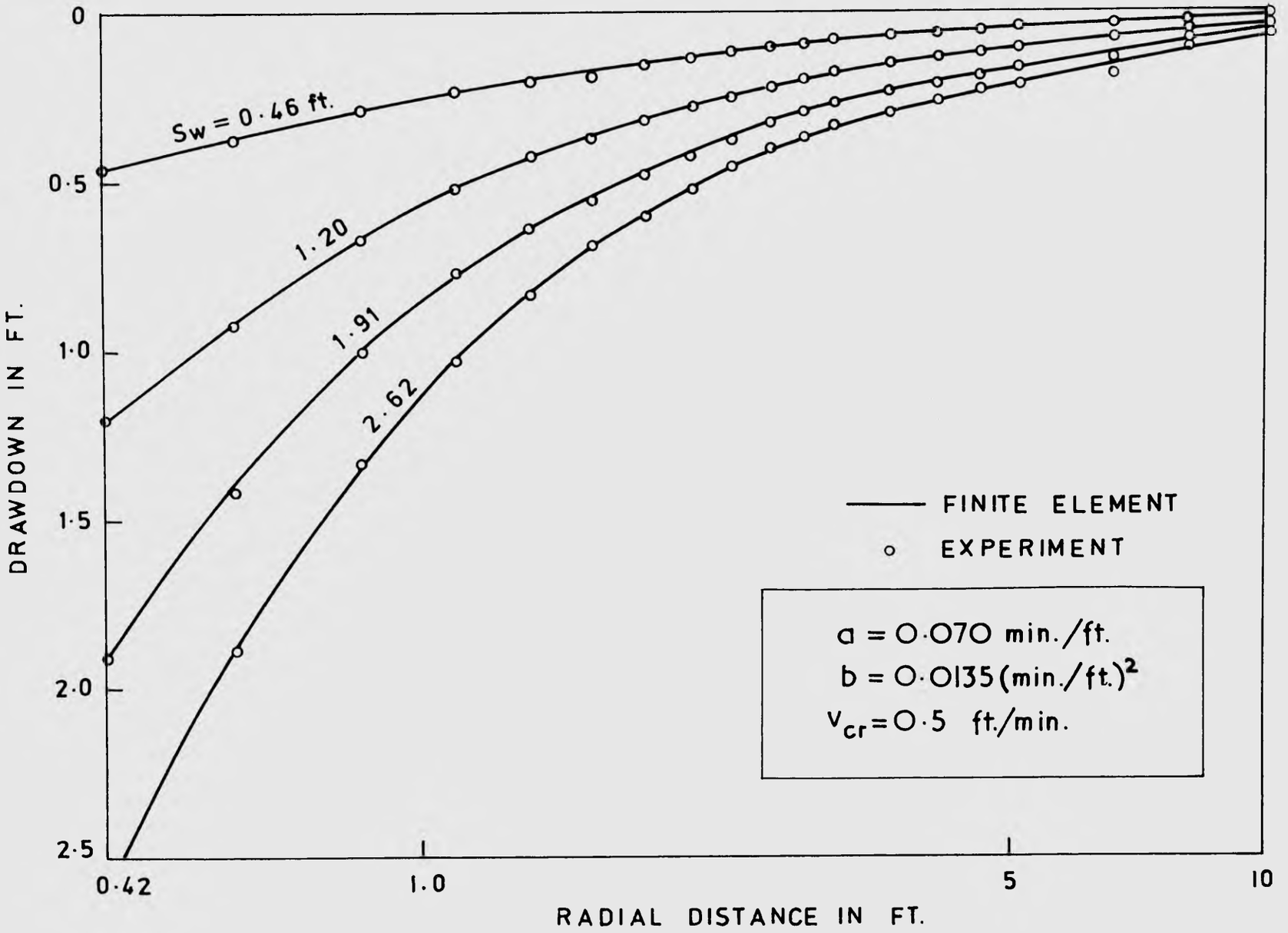

Fig. 6.17: Drawdown-radial distance relationships showing comparison of experimental results and finite element solutions.

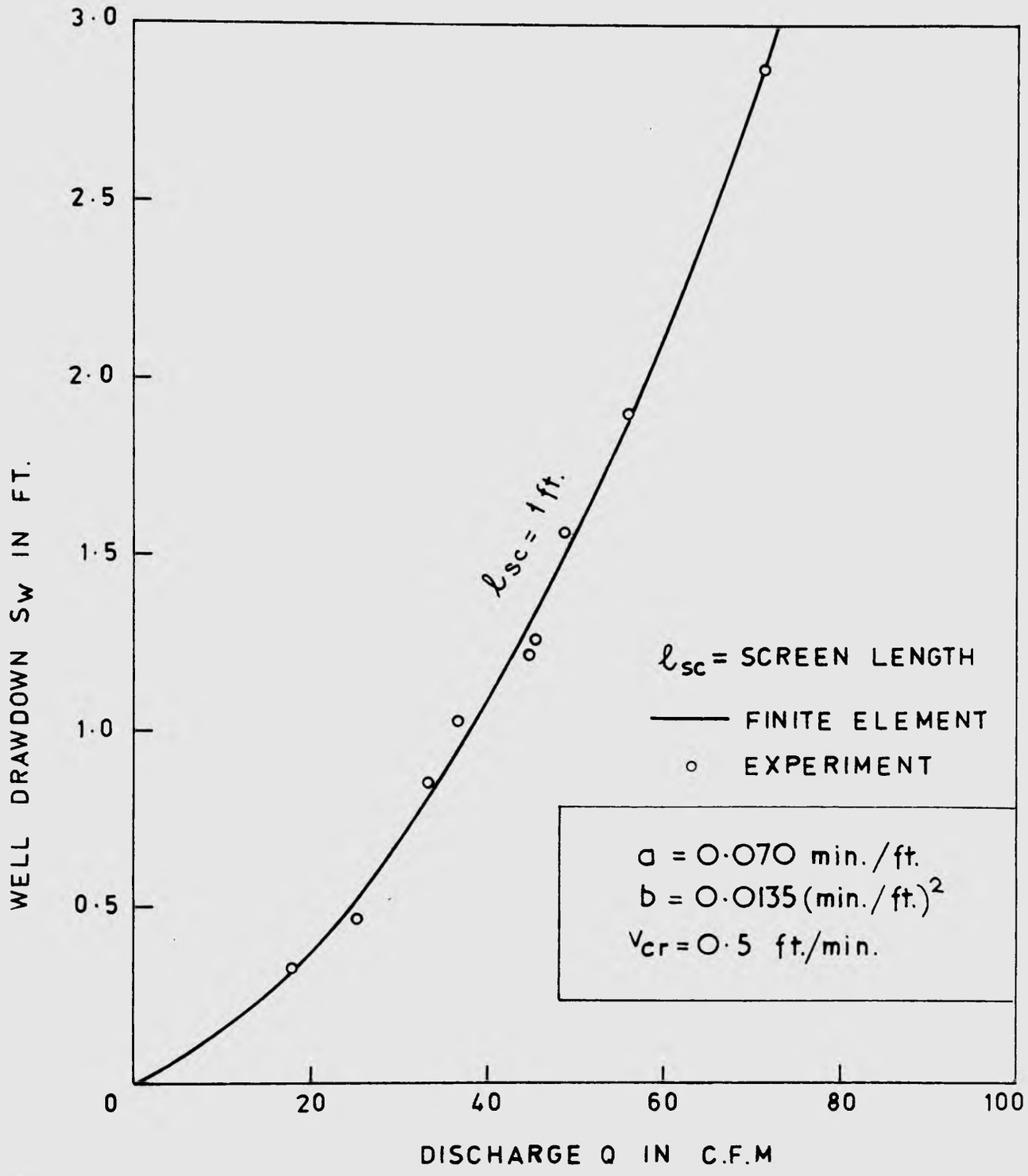

Fig. 6.18: Well discharge-drawdown relationship showing comparison of experimental results and finite element solutions.

was assumed that the newly determined coefficients were applicable throughout the entire aquifer. The additional refinement of a two zone treatment was considered unwarranted as the properties of the material within the inner barrier are decisive in determining the discharge. Fig. 6.17 shows a plot of the drawdown-radial distance relationships for four values of the prescribed well drawdown. It can be seen that the numerical solutions agree quite closely with the experimental results.

As a further check on the theoretical analysis, a plot of the well discharge-drawdown relationship is shown in Fig. 6.18. Good agreement between the theory and experiment may again be observed.

6.4.5 Flow towards a Partially Screened Well in an Unconfined Aquifer

As in the second series, the results from the final series of tests to investigate flow towards a partially screened well in an unconfined aquifer were obtained without disturbing the physical condition of the aquifer material. Consequently, the same in-situ values of the hydraulic coefficients obtained in section 6.4.4 were used to obtain the finite element solutions.

Figs. 6.19 and 6.20 show the plots of the base pressure head against radial distance as obtained from the theory and experiment. The theoretical free surface curves and prescribed water level in the well are also illustrated. It is noted that due to the effect of partial

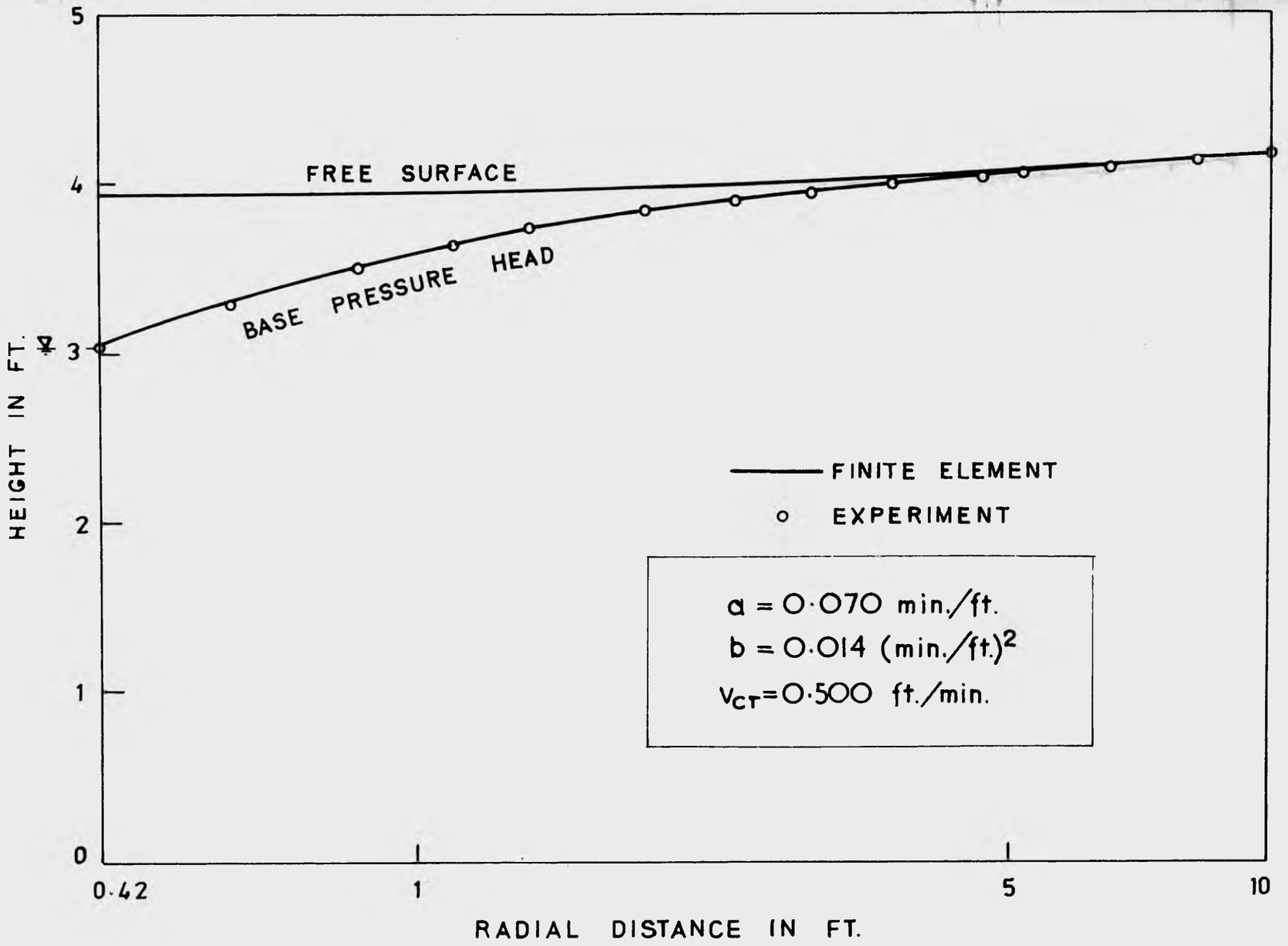

Fig. 6.19: Free surface and base pressure head curves showing comparison of experimental results and finite element solutions (h_W = 3 ft.).

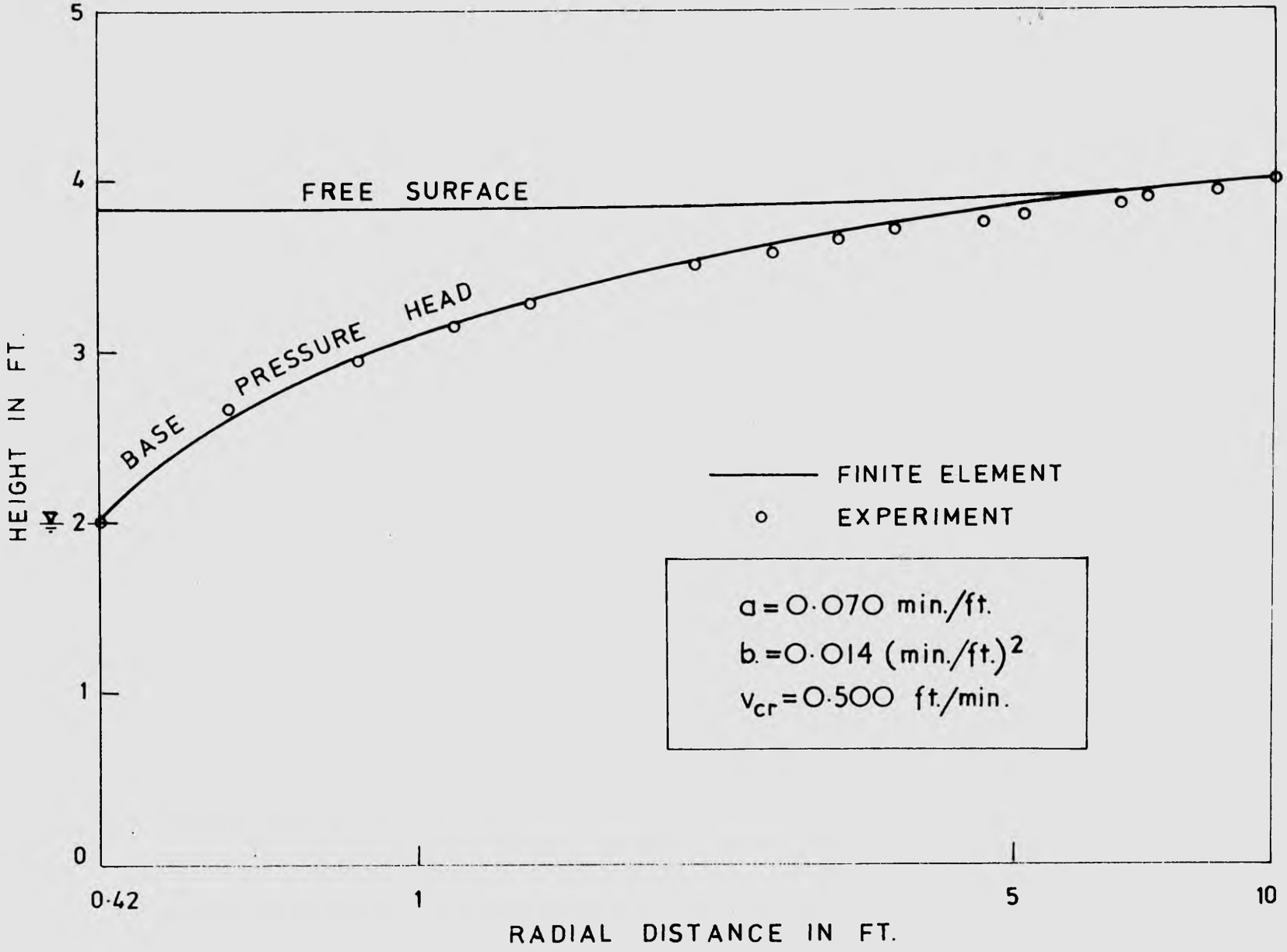

Fig. 6.20: Free surface and base pressure head curves showing comparison of experimental results and finite element solutions (h_w - 2 ft.).

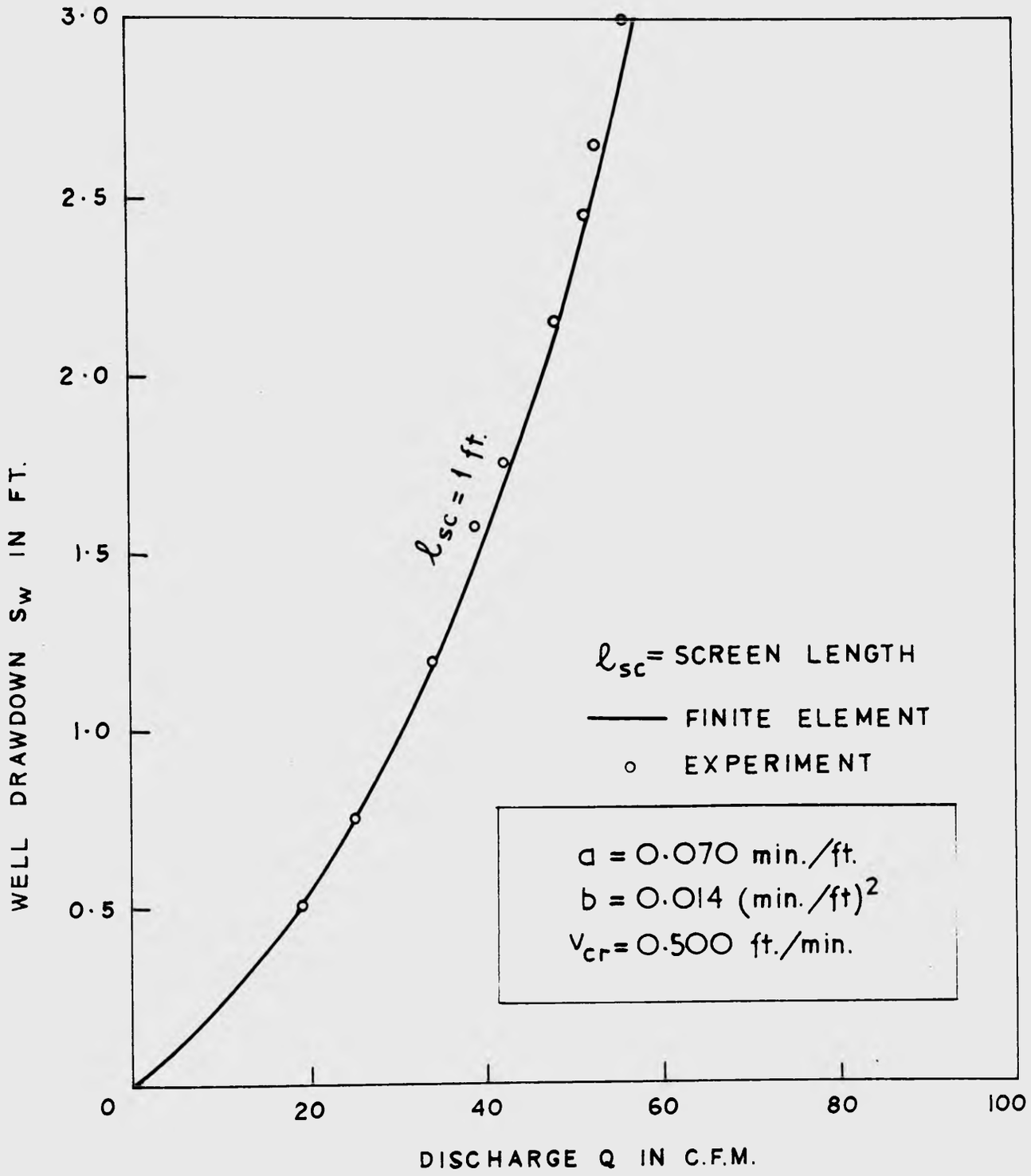

Fig. 6.21: Well discharge-drawdown relationship showing comparison of experimental results and finite element solutions.

screening, the free surface curve is a horizontal line up to a radius approximately equal to the aquifer thickness and that beyond this radius it approaches the base pressure head curve. Good agreement between the theoretical predictions on the base pressure head curves and the experimental results may also be observed.

As a further check on the values of the hydraulic coefficients used in the finite element analysis, the well discharge-drawdown relationship is also plotted in Fig. 6.21. It can be seen that the experimental points lie quite close to the theoretical curve.

7. Field Verification of Transient Flow Solutions

7.1 General

In order to provide field verification of the finite element analysis of transient, two-regime flow problems, two sets of data were collected from pumping tests[1] carried out at the following sites (see Fig. 7.1):-

(i) Site A - Gumly Gumly Island, near Wagga Wagga, New South Wales, where there exists a deep aquifer overlain by a confined aquitard;

(ii) Site B - Rosevale, Southeast Queensland, where there exists a shallow aquifer overlain by a water table aquitard.

Type curve methods were developed and applied to the test data to determine the hydraulic coefficients of the main aquifer and the overlying aquitard in each case. The determined coefficients were fed into finite element models of the two field systems to obtain the theoretical predictions of the actual flow behaviours. Comparison of the numerical solutions and field data is presented in this chapter.

7.2 Site A - Gumly Gumly Island, New South Wales

7.2.1 General Data

A pumping test was performed in co-operation with the Water Conservation and Irrigation Commission of New South Wales, from September 26 to 29, 1972. A group of wells (Fig. 7.2) located on an alluvial area of the Murrumbidgee River, known as Gumly Gumly Island,

(1). A detailed description of the field investigations and results have been published by Dudgeon, Huyakorn and Swan (1973, Vol. 2)

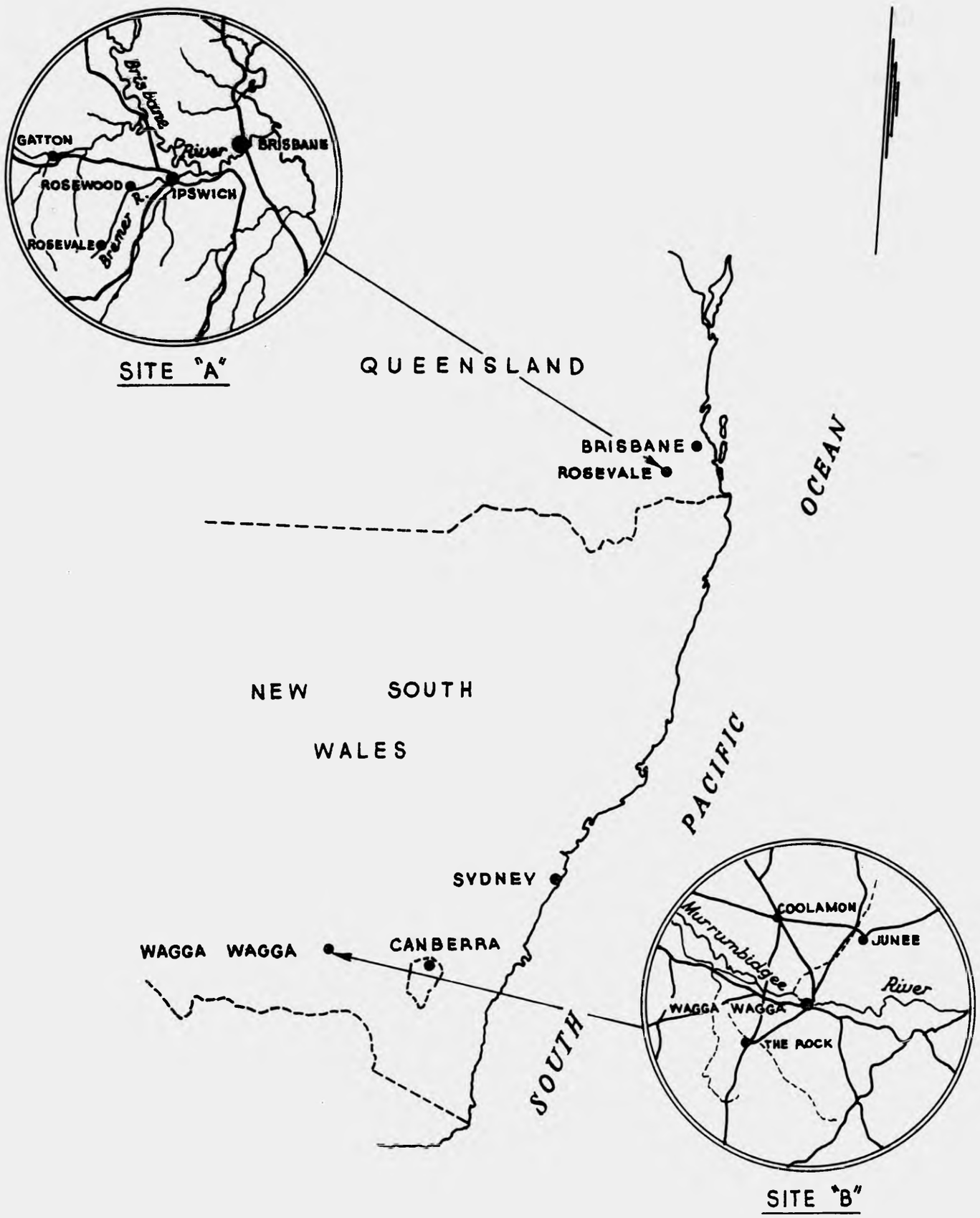

Fig. 7.1: Location of Sites A and B.

was used for the test. The construction features and available driller logs of these wells are given in Fig. 7.3. Well30638 was a 24 inch diameter, gravel packed production well whose detailed features are shown in Fig. 7.4. Wells 30577 and 30568 were two close observation wells located at distances of 7 and 22 ft. from the production well whilst the remaining wells were distant observation wells located at radial distances indicated in Table 7.1.

To observe drawdowns in the aquifer and the overlying aquitard, the production well and the closest observation well 30577 were each fitted with 4 slotted P.V.C. piezometers (see Fig. 7.4) placed at depths indicated in Table 7.1 and Fig. 7.3. The response of these piezometers to pumping was monitored by means of multiple contact electric probes developed for the measurement of the rapidly falling water level. The detailed description of these probes has been presented by Dudgeon et al (1973, Vol. 2, Appendix III).

Pumping was started at 3.00 p.m. on September 26 and was continued for a period of 4320 minutes at an approximately constant rate of 48,000 igph (128 cfm) until 3.00 pm on September 29. A continuous record of water levels in the production well, all observation wells and piezometers was maintained for a period of 3960 minutes. The piezometers in the shallow aquifer, illustrated in Fig. 7.3, were discovered to show no response, indicating that there was virtually no hydraulic connection between this aquifer and the confined flow system

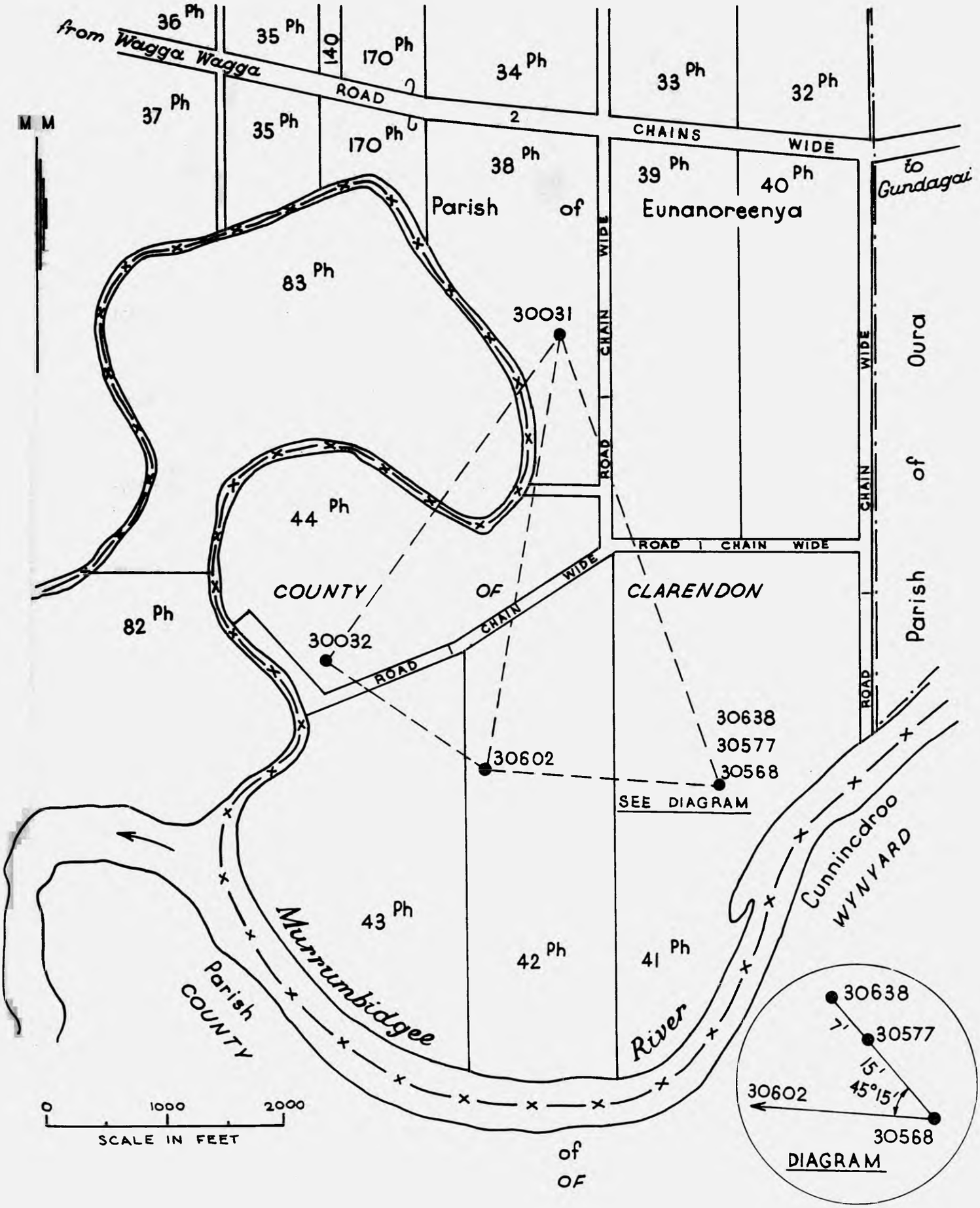

Fig. 7.2: General plan of Site A.

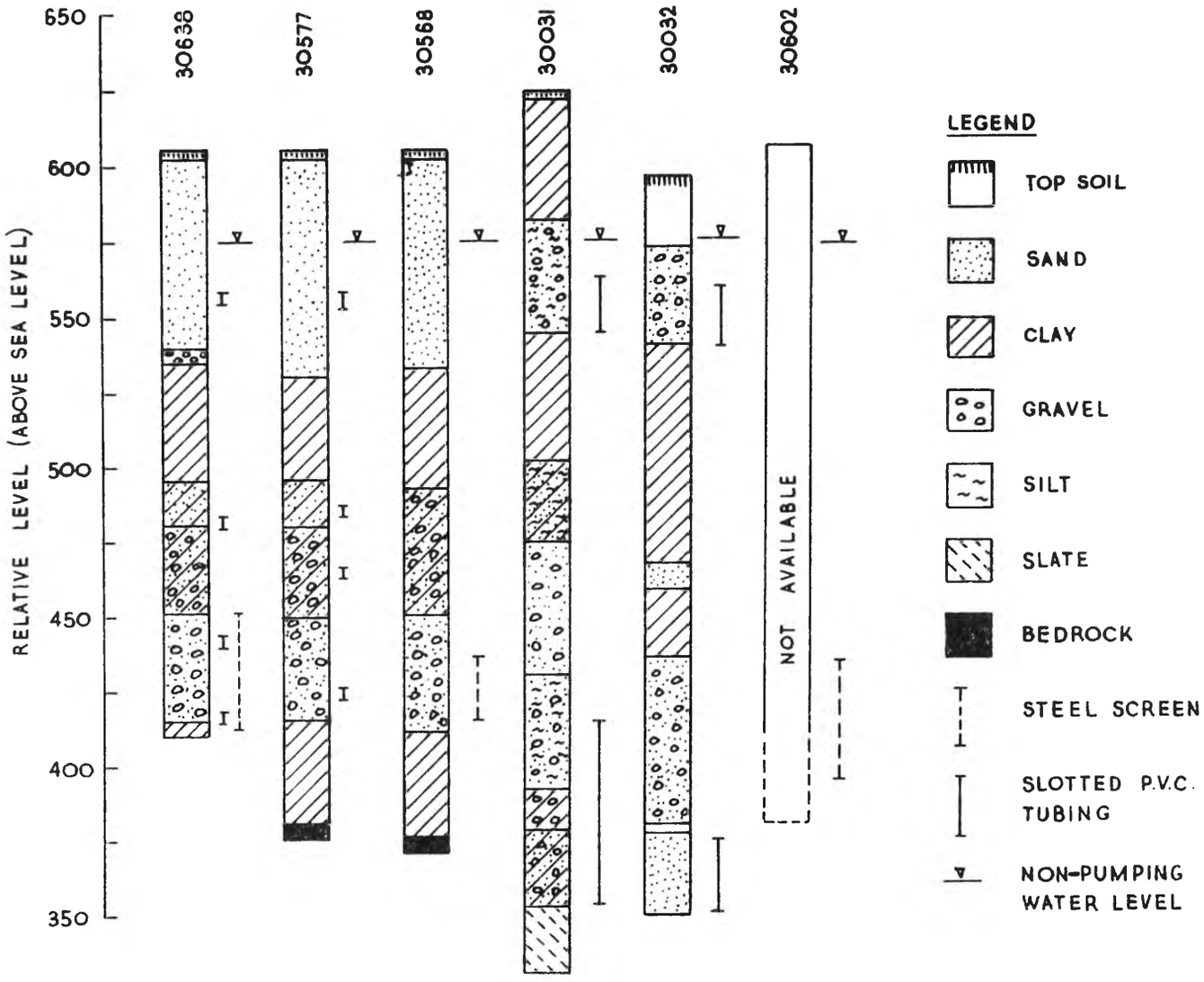

Fig. 7.3: Construction features and available driller-logs of wells at Site A.

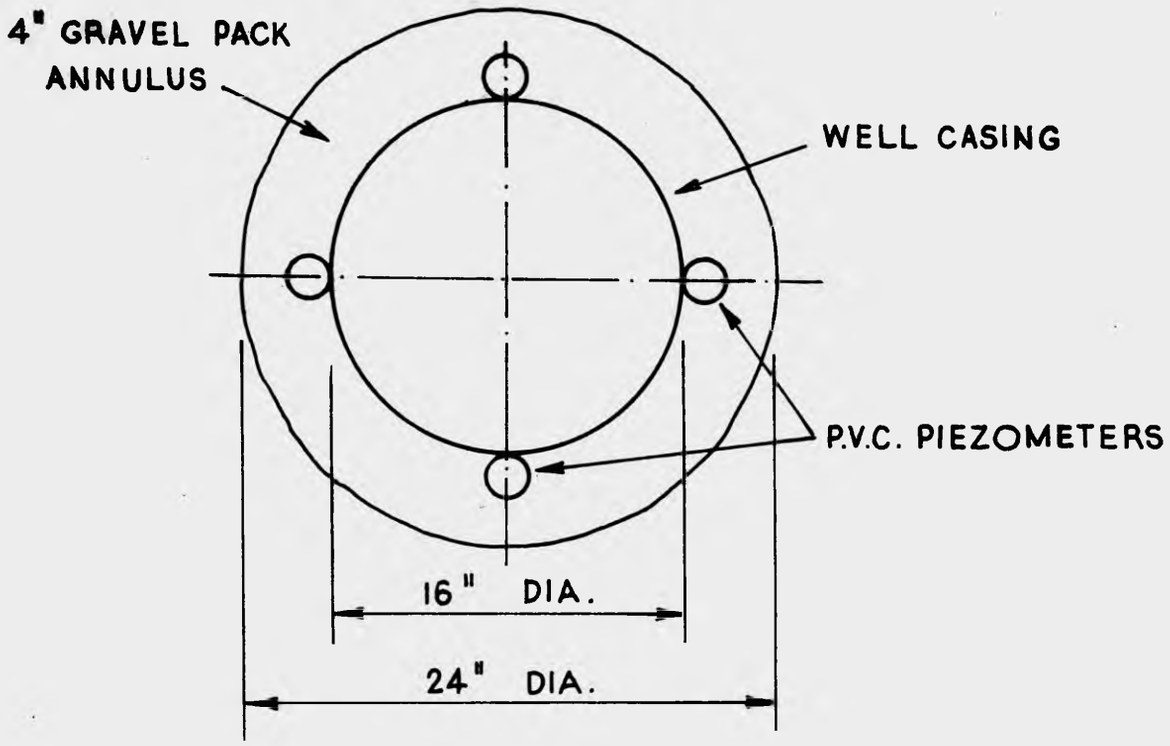

(a)

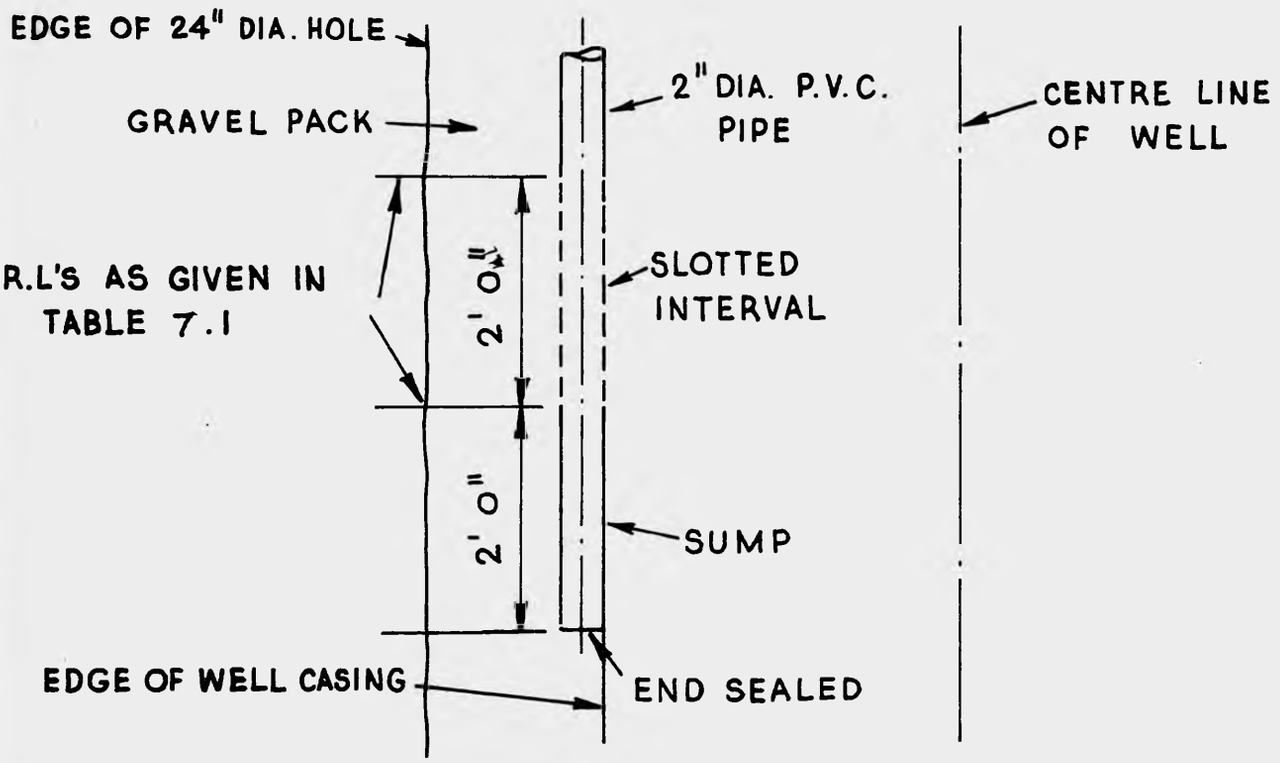

(b)

Fig. 7.4: Detailed features of production well 30638 showing location of slotted P.V.C. piezometers in the gravel pack.

Table 7.1: Radial distances from production well 30638 and screened intervals of observation wells and piezometers at Site A.

Well	Piezometer No.	Radial Distance from Well 30638 (ft.)	Screened Interval R.L. above sea level (ft.)	Remarks
30638			412-452	Inside production well
	1	1	555-557)	
	2*	1	480-482)	Gravel pack
	3*	1	440-442)	piezometers
	4	1	420-422)	
30577**	5	7	555-557	No response to pumping 30638
	6	7	485-487	
	7	7	465-467	
	8	7	420-422	
30568		22	416-436	
30602		1385	398-437	
30032	1	2600	355-375	No response to pumping 30638
	3	2600	457-465	
	2	2600	540-560	
30031	1	3050	533-553	
	2	3050	353-413	No response to pumping 30638

* Blocked during construction

** Well 30577 hydraulically sealed from 52 ft. to 110 ft. below ground surface.

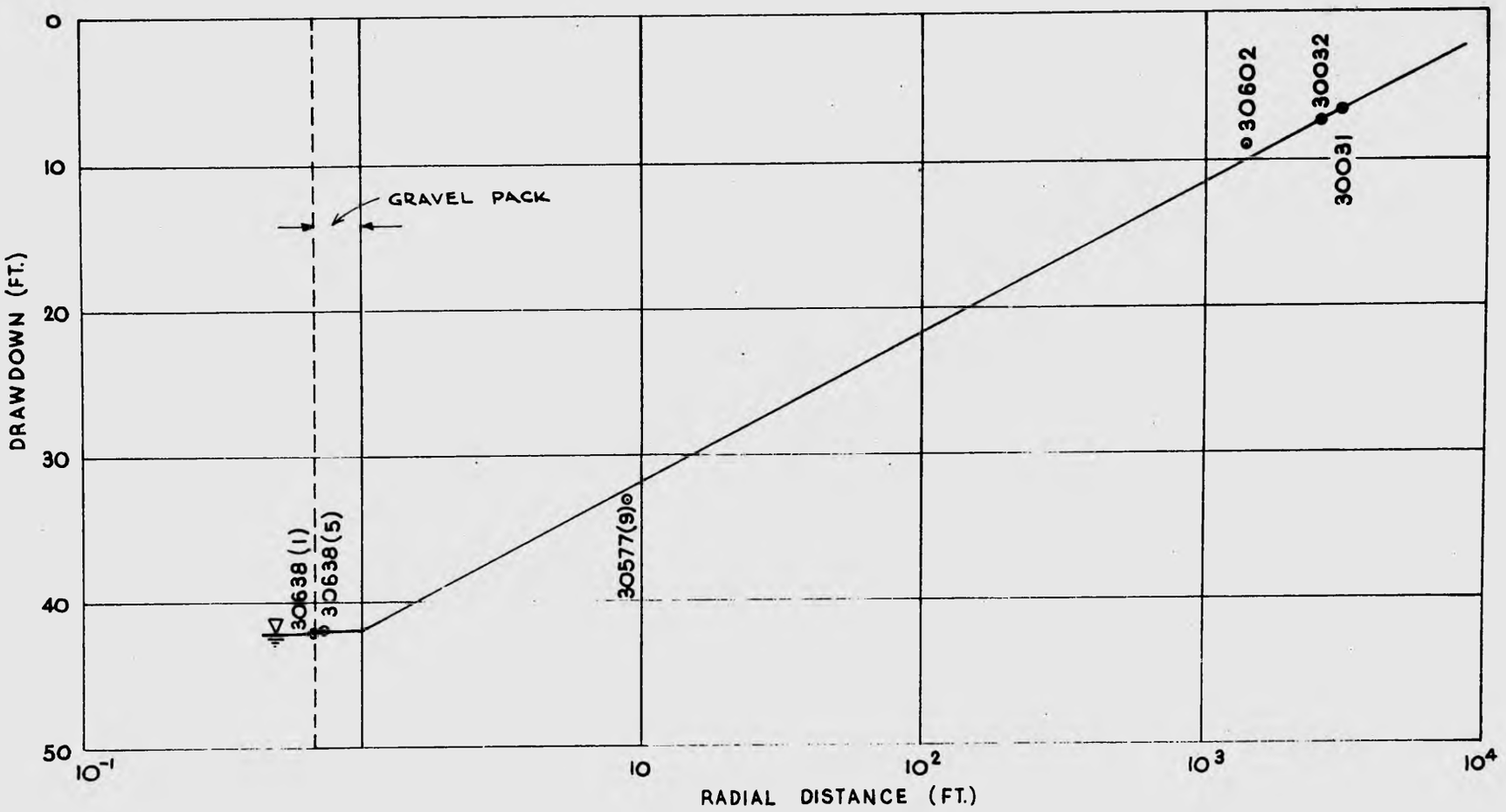

Fig. 7.5: Drawdown-radial distance plot at time t = 3800 minutes.

under consideration.

The drawdown-time field data obtained from the production well and nearby observation well 30577 were used to verify the finite element analysis as the aim was to examine flow conditions and aquifer characteristics near the pumped well. To check whether non-Darcy flow existed in the main aquifer at the pumping rate of 128 cfm, a semi-logarithmic plot of drawdown at time t = 3800 minutes versus radial distance was made using the drawdowns in observation wells 30577, 30602, 30032 and 30031 and the drawdowns inside the gravel pack and the production well. The plot is presented in Fig. 7.5. It can be seen that non-Darcy flow did not exist and that head losses in the gravel pack and inside the pumped well were negligible.

7.2.2 Finite Element Model and Type Curves for the Field System

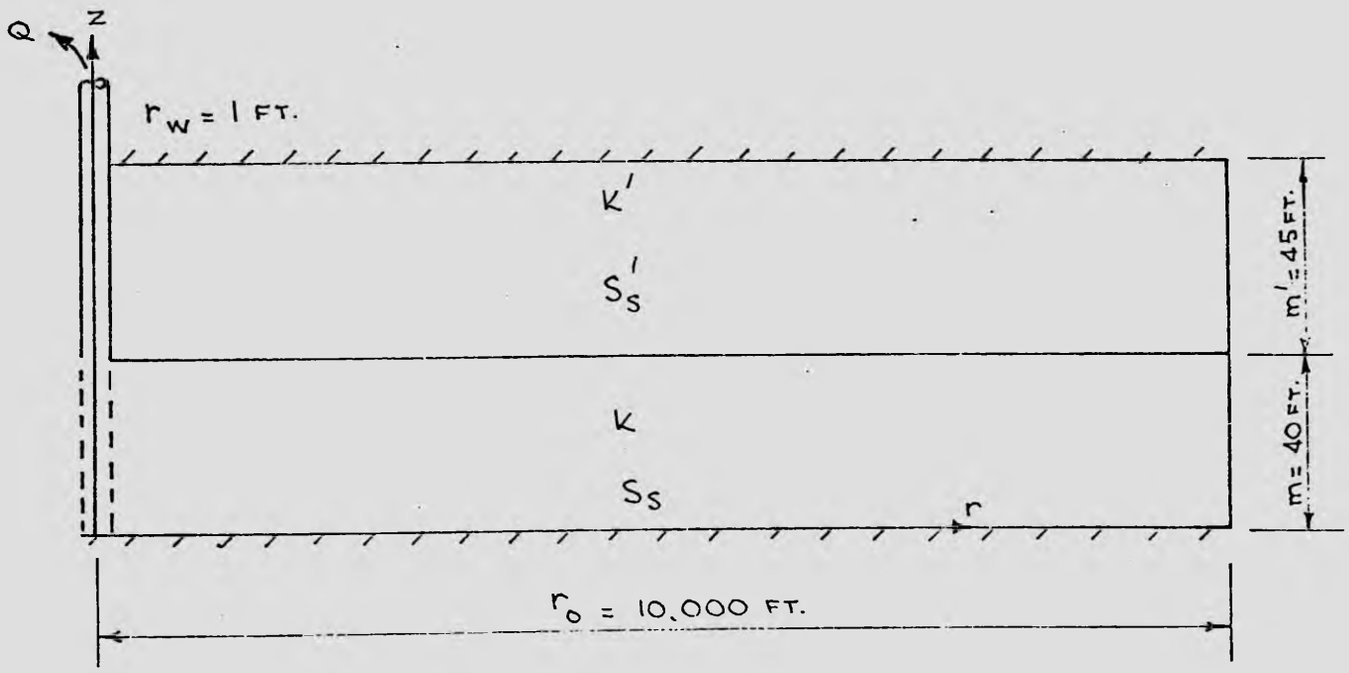

Fig. 7.6: Model of the Gumly Gumly Island Field System

From the general data presented in the preceding section, a model of the field system was constructed. As shown in Fig. 7.6, the model represents a confined aquifer-aquitard system with an external radius of 10,000 ft. The average thicknesses of the aquifer and aquitard were taken as 40 and 45 ft. respectively. Both layers were assumed to be homogeneous and isotropic. The top of the aquitard was also assumed to be impermeable.

The finite element method was used to solve several flow cases which were simulated to obtain families of type curves characterising the behaviour of the field system. As non-Darcy flow did not exist in the field, only the Darcy flow type curves were obtained for the main aquifer.

Typical families of type curves are shown in Figs. 7.7 and 7.8 for the main aquifer and in Figs. 7.9a to 7.11 for the aquitard. The dimensionless parameters of the type curves, $\frac{r}{B}$, β and δ_1 which is proportional to $\beta/\frac{r}{B}$, have been defined in Section 5.4.1. Only a limited practical range of values of these parameters was considered as a vast amount of computer time would have been required to cover a wide range. On comparing Fig. 7.7 with Fig. 7.8, it may be observed that the horizontal spread between the two envelope Theis curves for the aquifer decreases as δ_1 decreases and that for a given value of W(u), the difference between the values of (1/u) read from the two envelope curves is equal to $(\delta_1 - 1)\frac{1}{u}$.

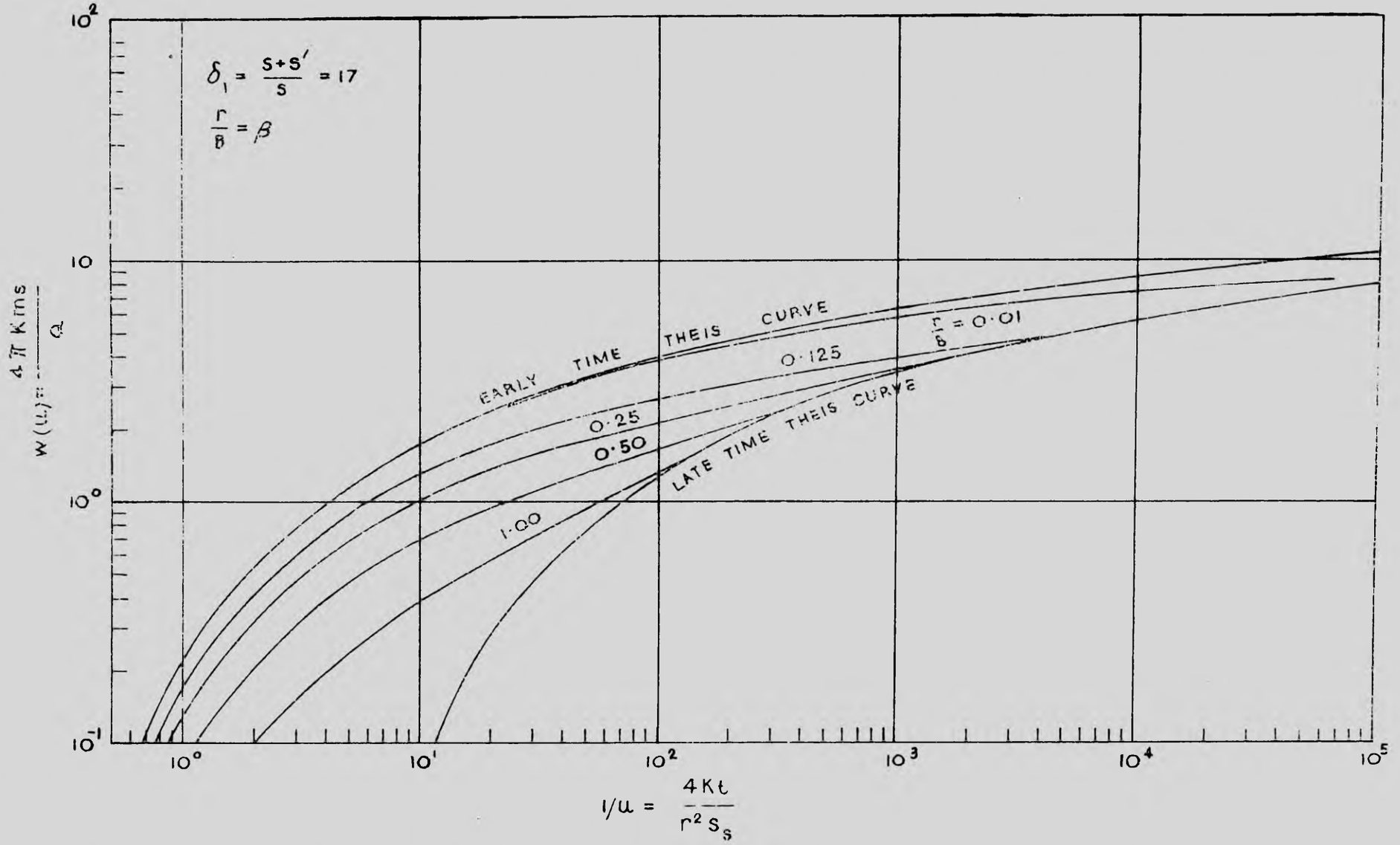

Fig. 7.7 Type curves for the main aquifer of the Gumly Gumly Island system ($r/B = \beta$; $\delta_1 = 17$).

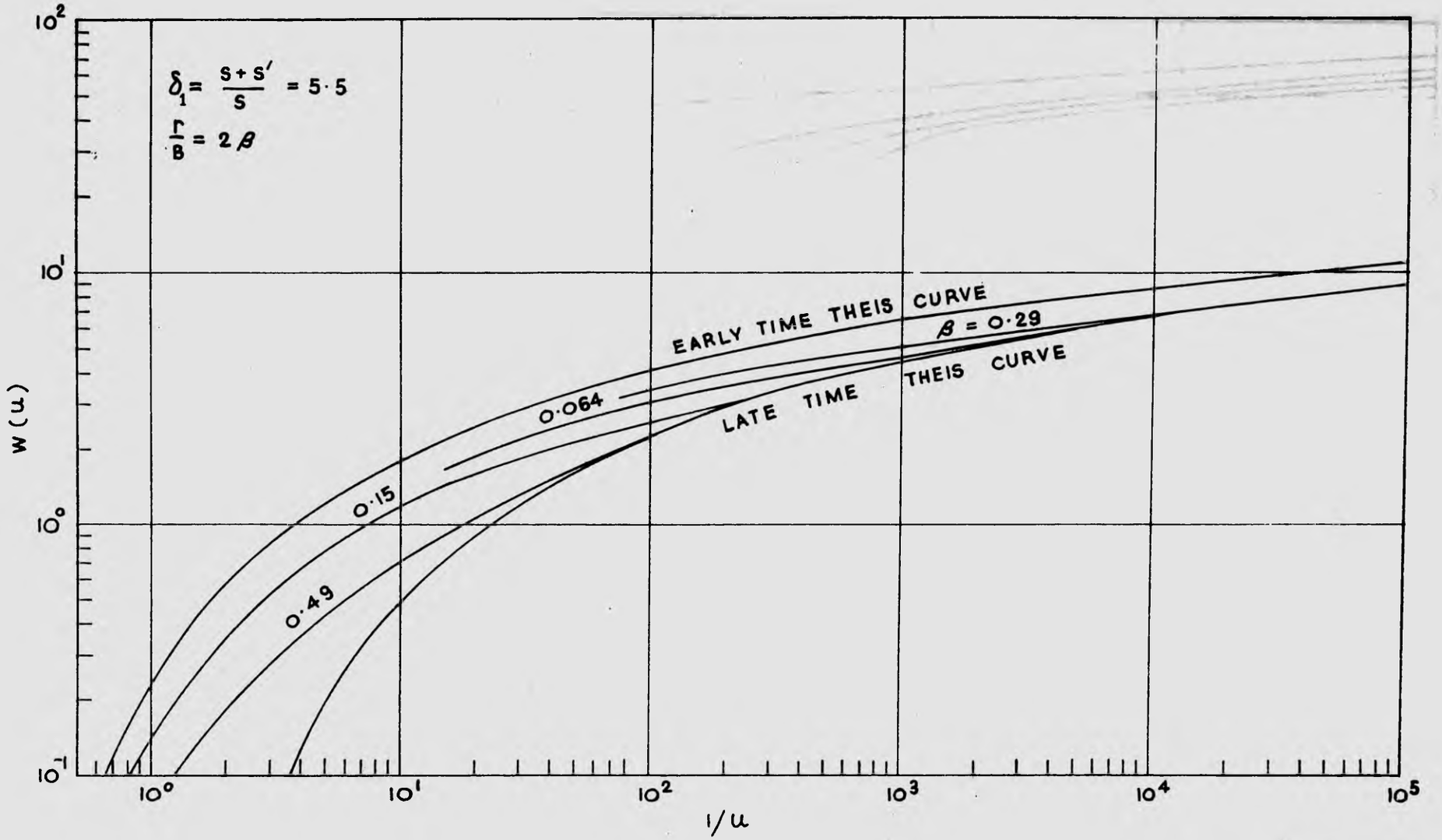

Fig. 7.8: Type curves for the main aquifer of the Gumly Gumly Island system ($r/B = 2\beta$; $\delta_1 = 5.5$).

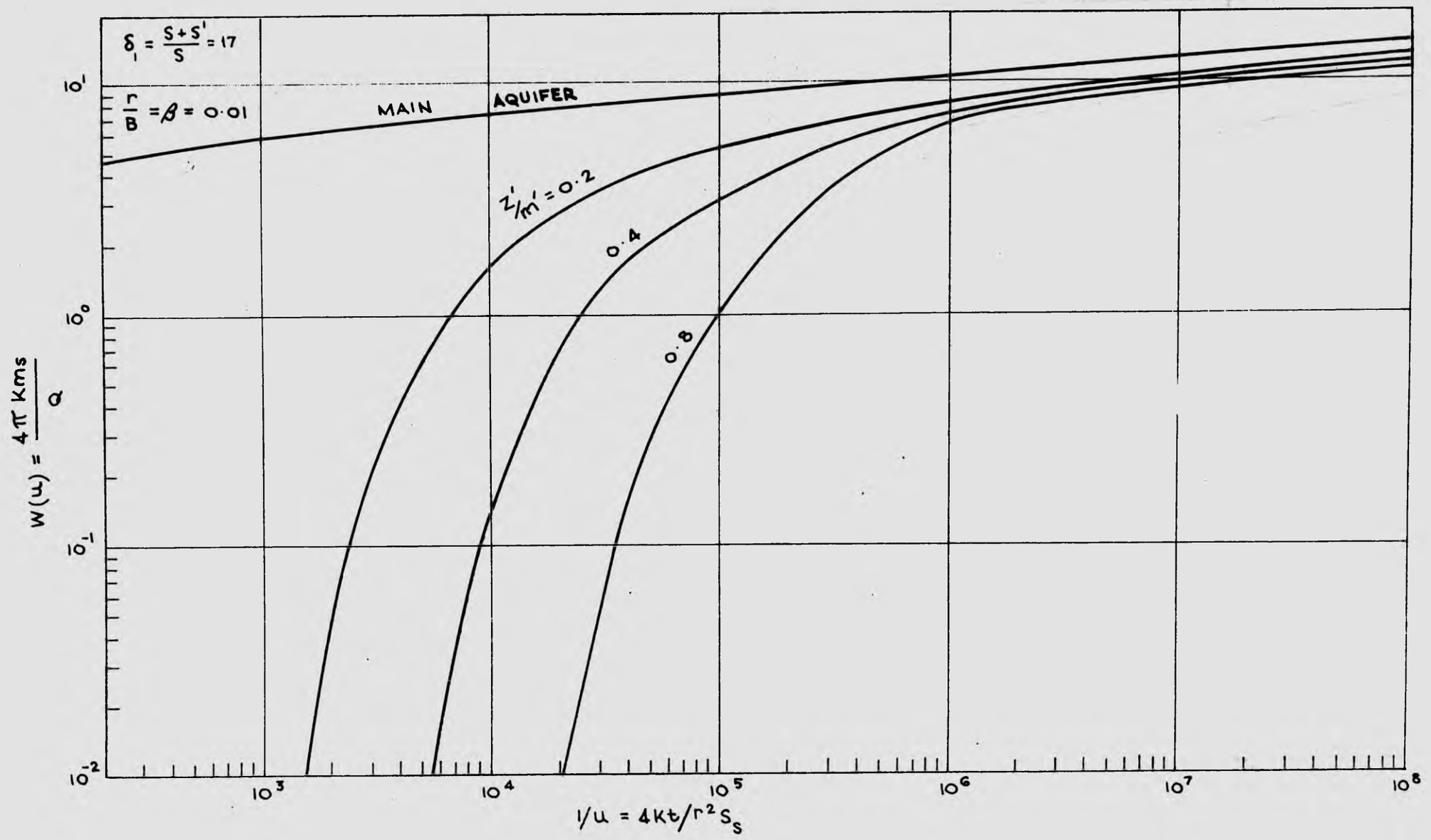

Fig. 7.9a: Type curves for the main aquifer of the Gumly Gumly Island field system ($\frac{r}{B} = \beta = .01$; $\delta_1 = 17$)

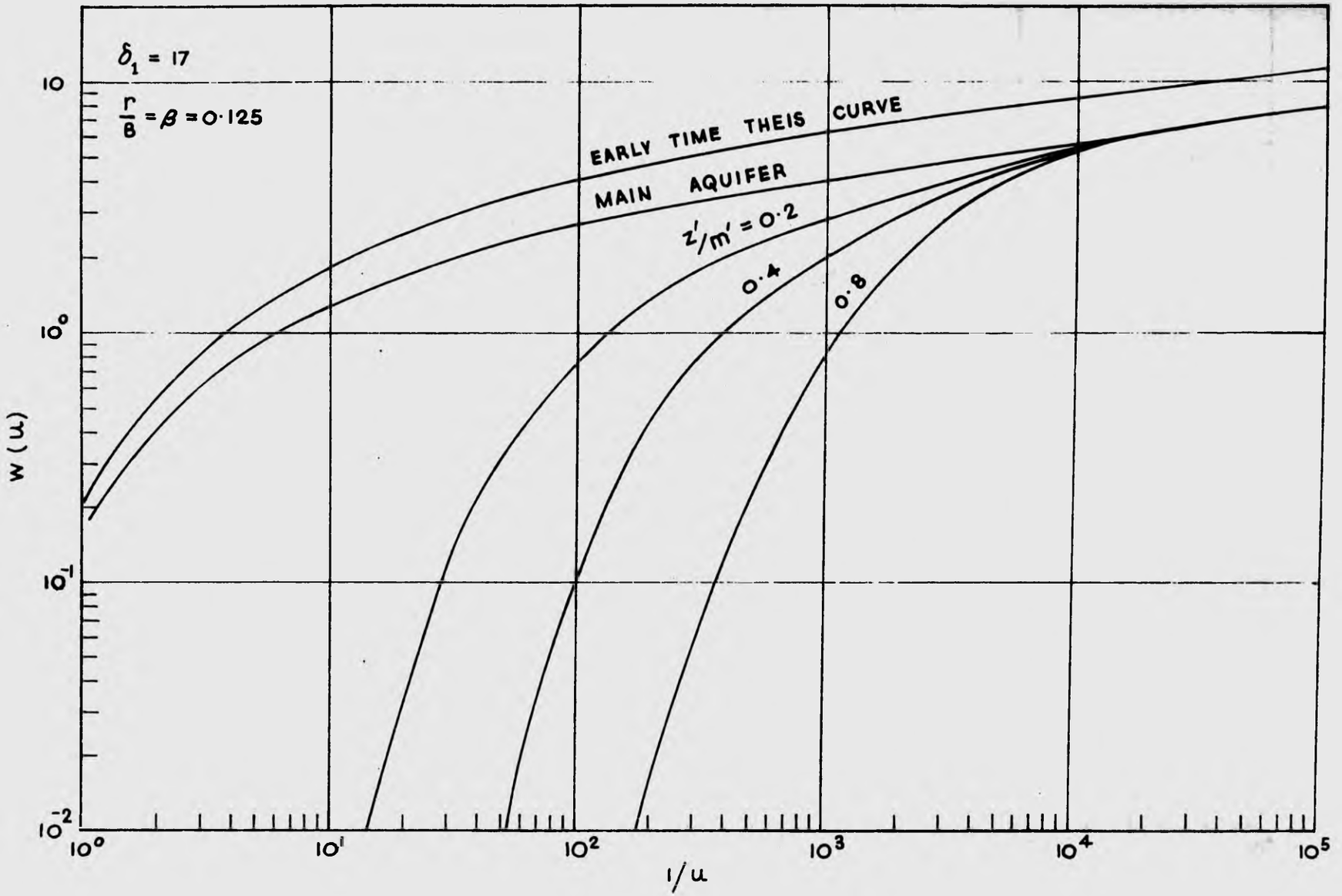

Fig. 7.9b: Type curves for the overlying aquitard of the Gumly Gumly Island system ($r/B = \beta = 0.125$, $\delta_1 = 17$)

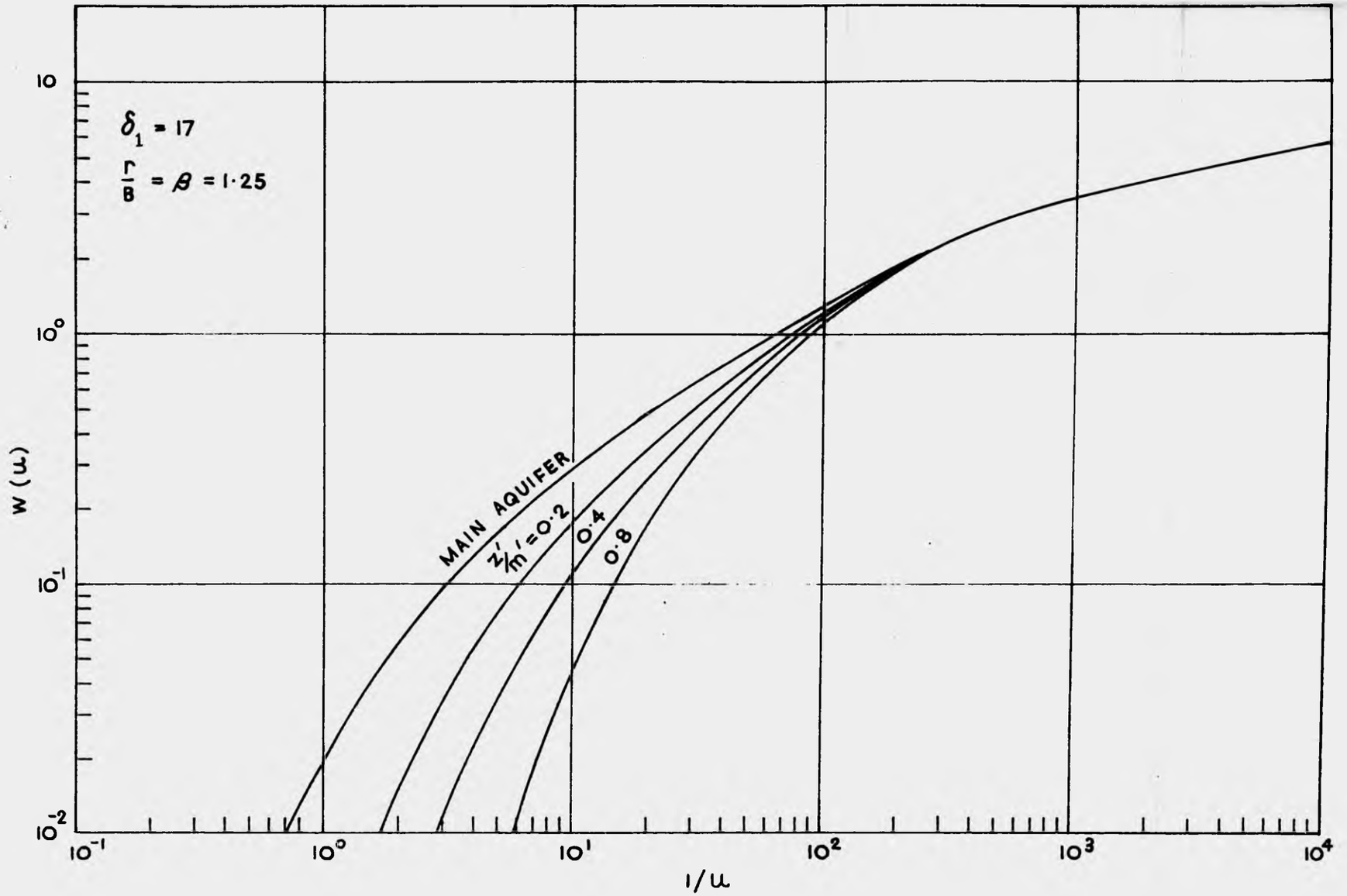

Fig. 7.10: Type curves for the overlying aquitard of the Gumly Gumly Island system ($r/B = \beta = 1.25$; $\delta_1 = 17$).

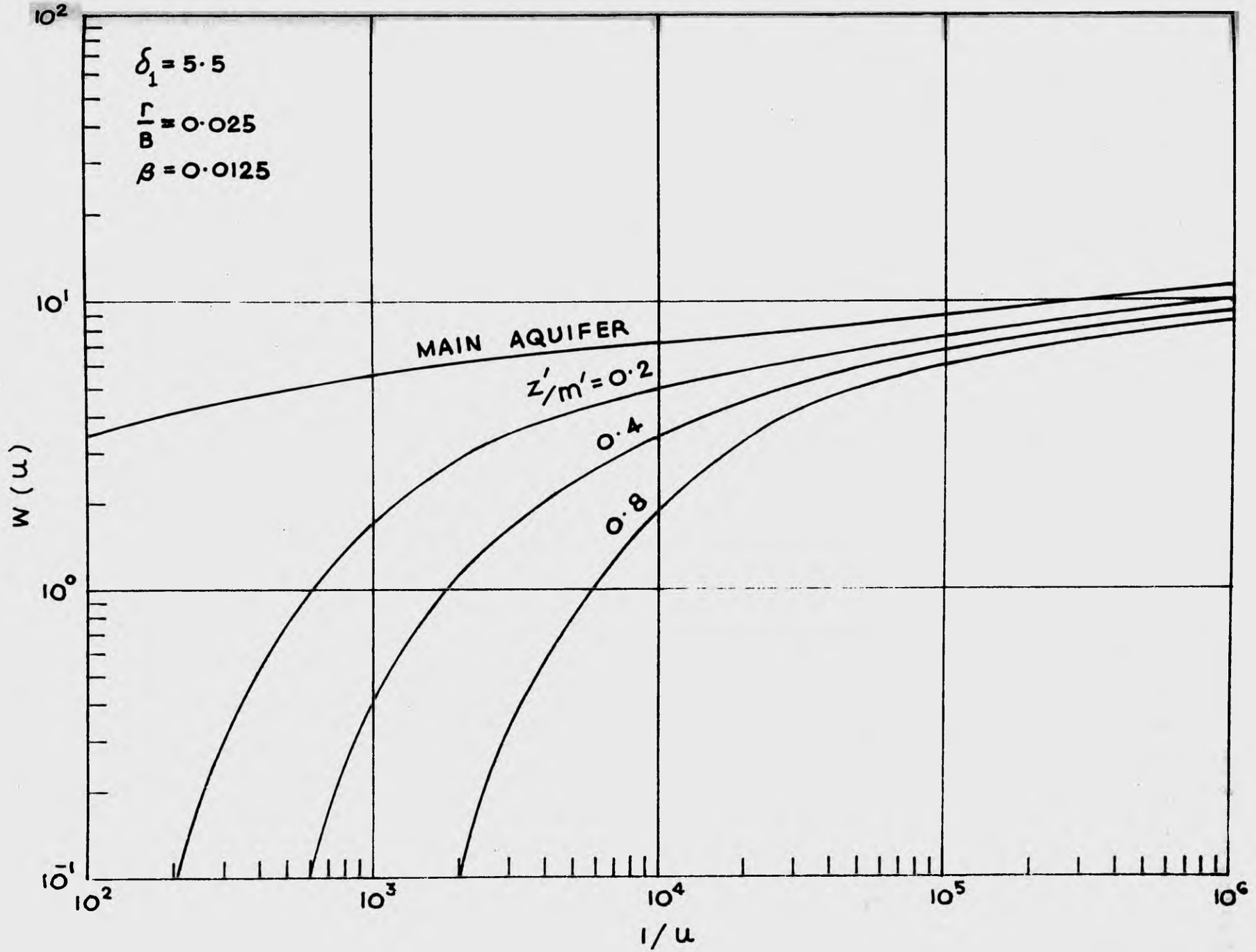

Fig. 7.11: Type curves for the overlying aquitard of the Gumly Gumly Island system (r/B = .025; β = .0125; δ_1 = 5.5).

The effect of the parameters $\frac{r}{B}$ and β on the horizontal and vertical spread of type curves for the aquitard may also be noted from Figs. 7.9a to 7.11. It can be seen that for constant $\frac{r}{B}/\beta$ the spread between the type curves decreases as the values of β and $\frac{r}{B}$ increase from .01 to 1.25 and that when $\frac{r}{B}/\beta$ increases from 1 to 2 (Figs. 7.9a and 7.11) the spread also decreases. This fact was used to great advantage in matching the field data plot against the theoretical type curves.

7.2.3 Comparison of Field Data and Finite Element Solutions

The following type curve method was used to determine the hydraulic coefficients of the aquifer and aquitard:-

(i) The drawdown-time data for the observation point located in the main aquifer, observation well 30577 (r = 7 ft.), was converted to a log-log plot of s versus t on a sheet of transparent paper. The plot was then matched on a selected family of type curves for the aquifer as shown in Fig. 7.12. Matching was performed by shifting the field data plot over the type curve plot while maintaining their axes parallel and ensuring that the late time portion of the field data fell on the late time Theis curve. Satisfactory matching was found when the remaining portion of the field data coincided with the corresponding type curve branching from the late time Theis curve. The final matching and values of $\frac{r}{B}$ and β for the matching type curve are shown in Fig. 7.12.

As a check to ensure that the appropriate family of type curves had been selected, matching of the field data collected from pumped well

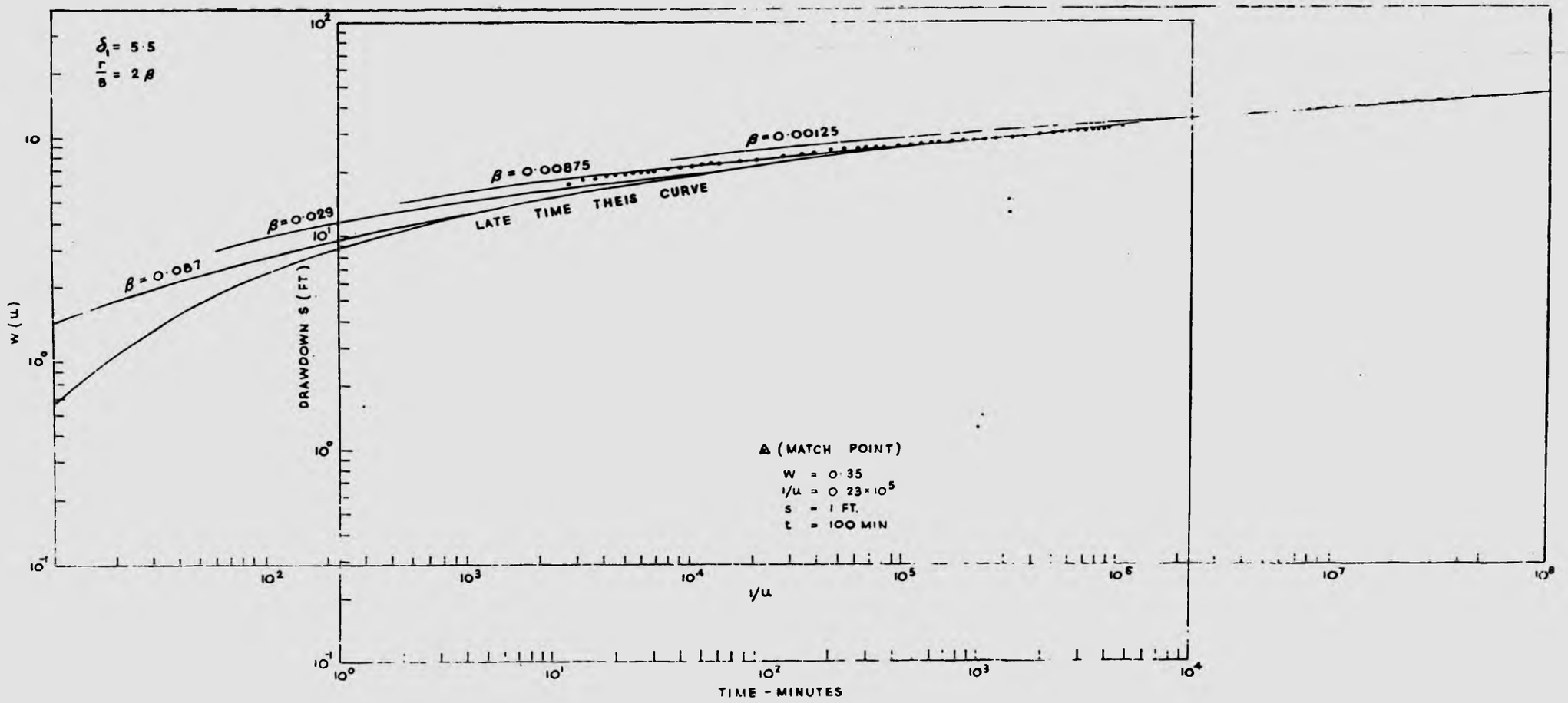

Fig. 7.12: Matching of field data plot on type curves for the main aquifer (observation well 30577).

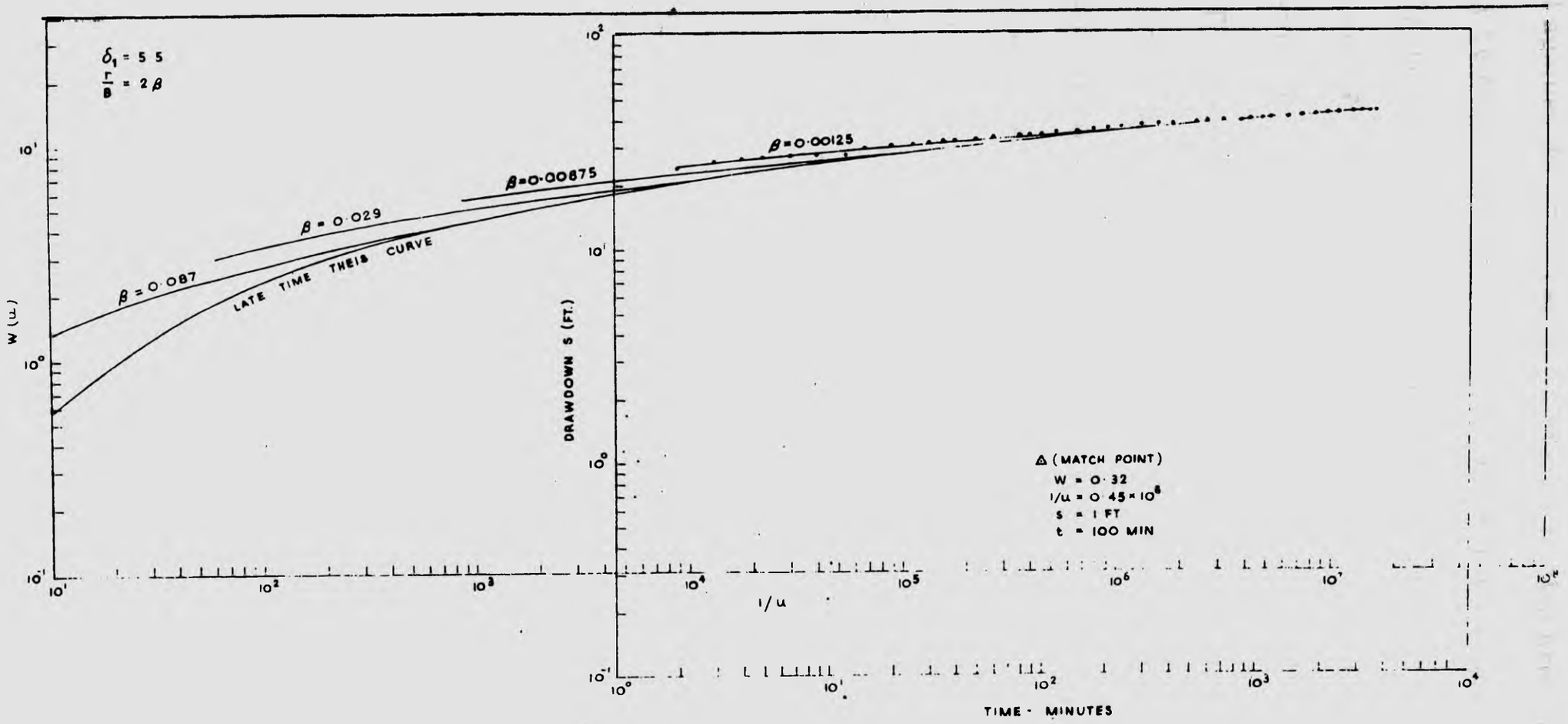

Fig. 7.13: Matching of field data plot on type curves for the main aquifer (observation well 30568).

30568 against the same family of curves is also presented in Fig. 7.13. It may be noted that the listed value of β for the matching type curve in this figure is approximately 1/7 times the value in Fig. 7.12. The two values of β are thus proportional to the radial distances from the pumped well.

(ii) The drawdown-time data for all observation points in well 30577 (at z'/m' = 0, 0.25 and 0.75) were plotted together on another sheet of transparent paper. Using the values of β and $\frac{r}{B}$ given in Fig. 7.12, the type curves for z'/m' = 0, 0.25 and 0.75 were constructed and matched on the field data plot. Minor adjustments of the values of β and $\frac{r}{B}$ were found necessary to obtain a satisfactory match. The final matching and values of β and $\frac{r}{B}$ are shown in Fig. 7.14. A match point was selected to determine the hydraulic coefficients K, S_s and K', S'_s for the main aquifer and the aquitard respectively. The calculation is presented as follows:-

Let (W, 1/u) and (s, t) denote the coordinates of the match point. The coefficients K and S_s for the aquifer are given by

$$K = \frac{QW}{4\pi sm}$$

and

$$S_s = \frac{4Ktu}{r^2}$$

where W = 0.40, $\frac{1}{u} = 0.115 \times 10^6$

s = 1 ft., t = 100 min.

r = 7 ft., Q = 128 cfm

m = 40 ft., m' = 45 ft.

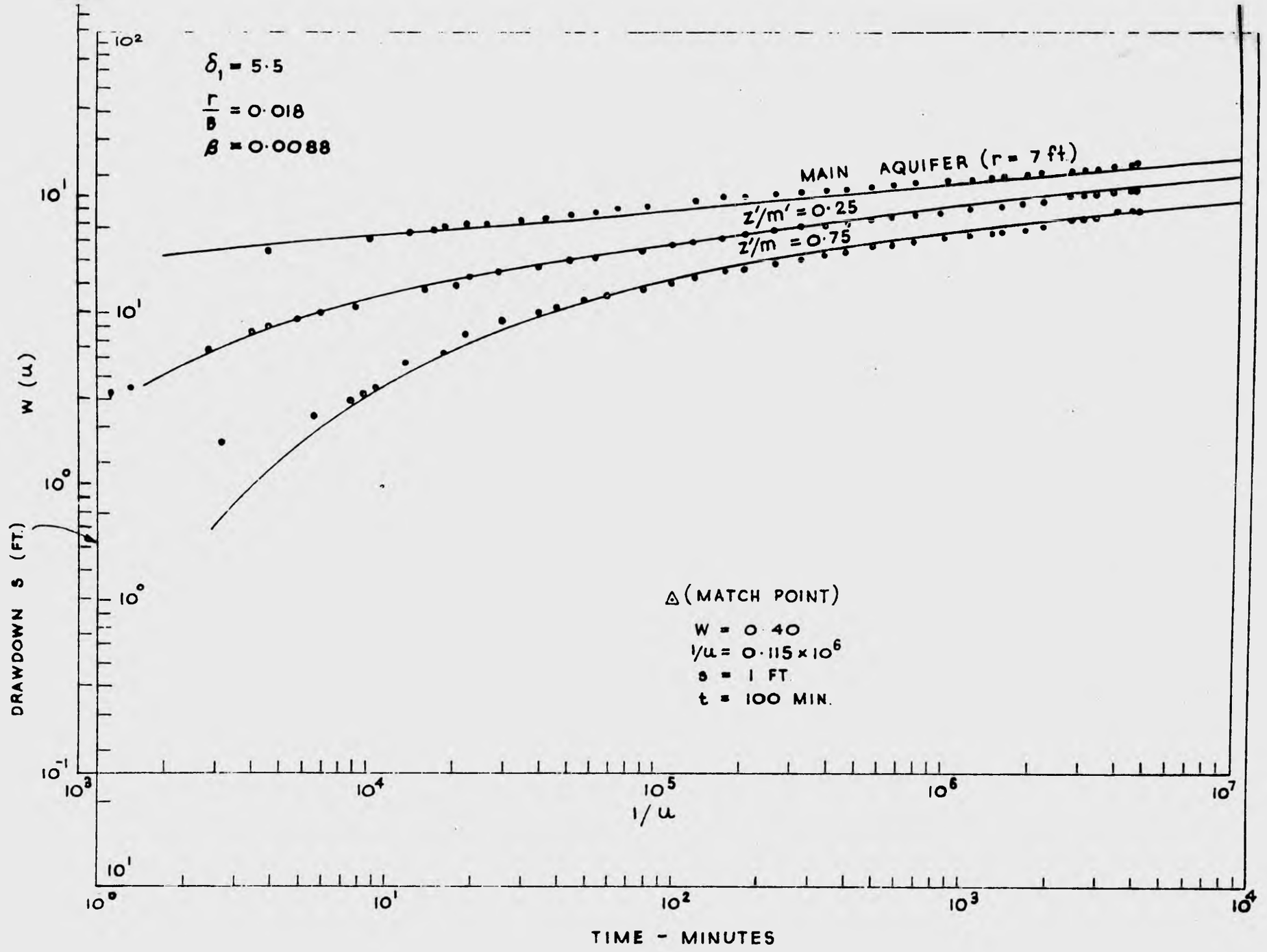

Fig. 7.14: Maching of field data on type curves for the overlying aquitard (observation well 30577).

Thus

$$K = \frac{128 \times 0.40}{4\pi \times 1 \times 40} = 0.103 \quad \text{ft./min.}$$

$$S_s = \frac{4 \times .103 \times 100}{7^2 \times .115 \times 10^6} = 0.73 \times 10^{-5} \quad \text{ft.}^{-1}$$

The coefficients of K' and S_s' for the aquitard are given by

$$K' = \frac{\left(\frac{r}{B}\right)^2 K\, mm'}{r^2}$$

and $$S_s' = \frac{16 \beta^2 m^2 K S_s}{K' r^2}$$

where $\frac{r}{B} = .018$, $\beta = .0088$

$$K = 0.103 \text{ ft/min}, \quad S_s = 0.73 \times 10^{-5} \quad \text{ft.}^{-1}$$

Thus

$$K' = \frac{(.018)^2 \times .103 \times 40 \times 45}{7^2} = .0012 \quad \text{ft/min.}$$

$$S_s' = \frac{16 \times (.0088)^2 \times 40^2 \times .103 \times .73 \times 10^{-5}}{.0012 \times 7^2}$$

$$= 0.29 \times 10^{-4} \quad \text{ft.}^{-1}$$

The determined values of K, S_s, K' and S_s' were fed into the finite element model and the flow problem was solved for Q = 128 cfm and pumping period t = 4320 minutes. The calculated drawdown versus time relationships at selected nodes (r = 1 and 7 ft.) in the aquifer were then compared with the field data plot for the corresponding points in the field system. Slight adjustment of the values of S_s and S_s' was made and the adjusted values were fed back into the model. Fig. 7.15 shows the final comparison of theoretical solution and field data. It can be seen

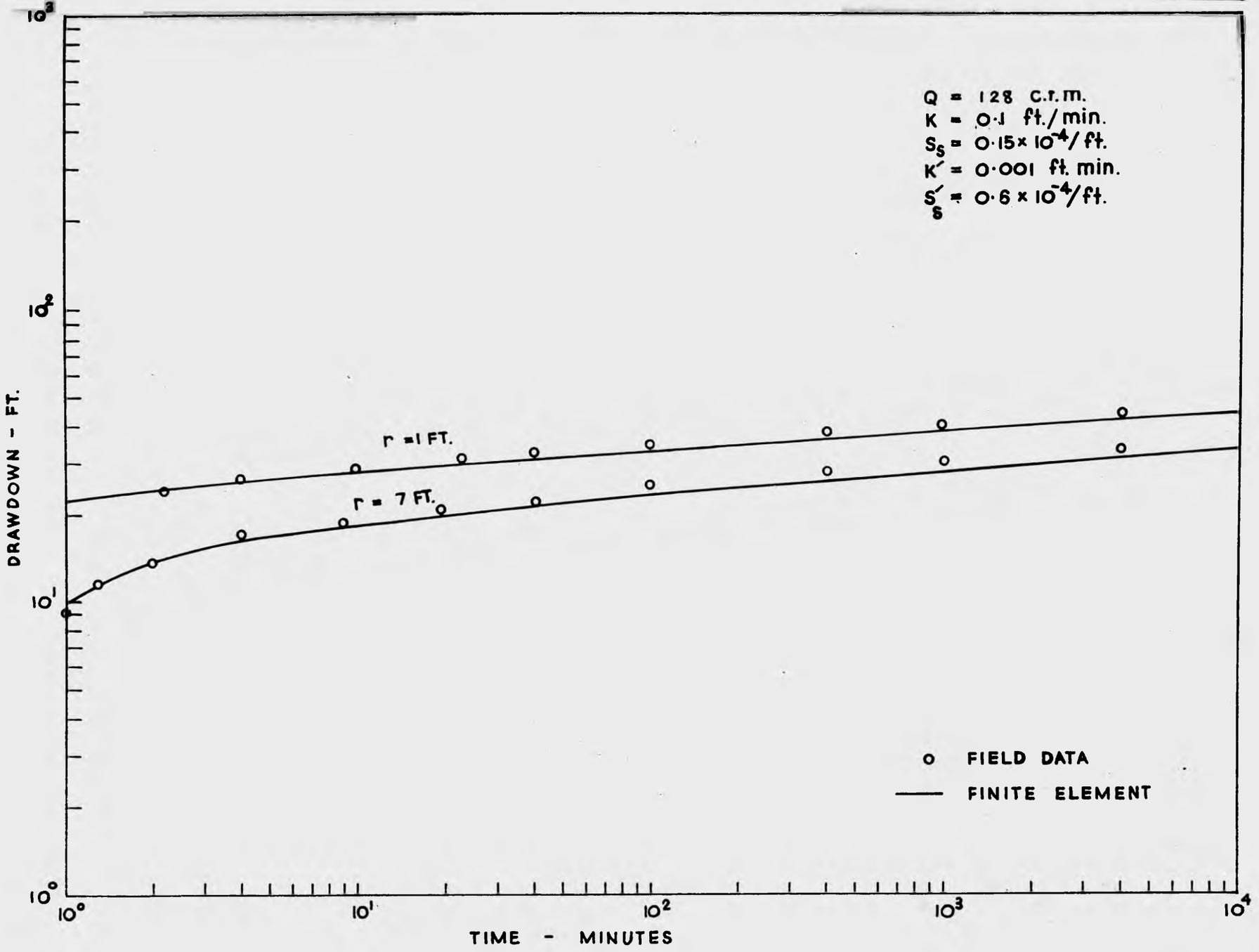

Fig. 7.15: Comparison of field data from main aquifer with finite element solutions.

that good agreement between the theoretical prediction and the actual behaviour of the field system was achieved.

As a further check, the final values of K and S_s for the aquifer, listed in Fig. 7.15, were compared with those determined by applying conventional type curve methods to the field data collected from the distant observation wells, 30602, 30031 and 30032. Detailed description of the conventional methods used has been presented by Swan and Huyakorn (see Dudgeon et al (1973), Vol. II).

Table 7.2 lists the values obtained by fitting the Theis curve to the late time portion of the field data.

Table 7.2: Summary of values of the hydraulic coefficients obtained by fitting Theis curve to the field data.

Observation Well	Radial Distance (ft.)	T $ft^2/min.$	S	K ft/min.	S_s ft.
30602	1385	3.42	8.2×10^{-4}	0.085	2.1×10^{-5}
30031	3050	3.42	3.53×10^{-4}	0.085	0.88×10^{-5}
30032	2600	3.42	4.05×10^{-4}	0.085	1.0×10^{-5}
Mean values		3.42	5.26×10^{-4}	0.085	1.33×10^{-5}

It may be observed that the average values of K and S_s in the table are reasonably close to those used in obtaining the finite element solutions. This evidence suggests that the aquifer of the actual field system was quite uniform in physical and hydraulic properties. The evidence is further supported by the well log data shown in Fig. 7.3.

7.3 Site B - Rosevale, Southeast Queensland

7.3.1 General Data

Several pumping tests were conducted at this site in co-operation with the Irrigation and Water Supply Commission of Queensland. The

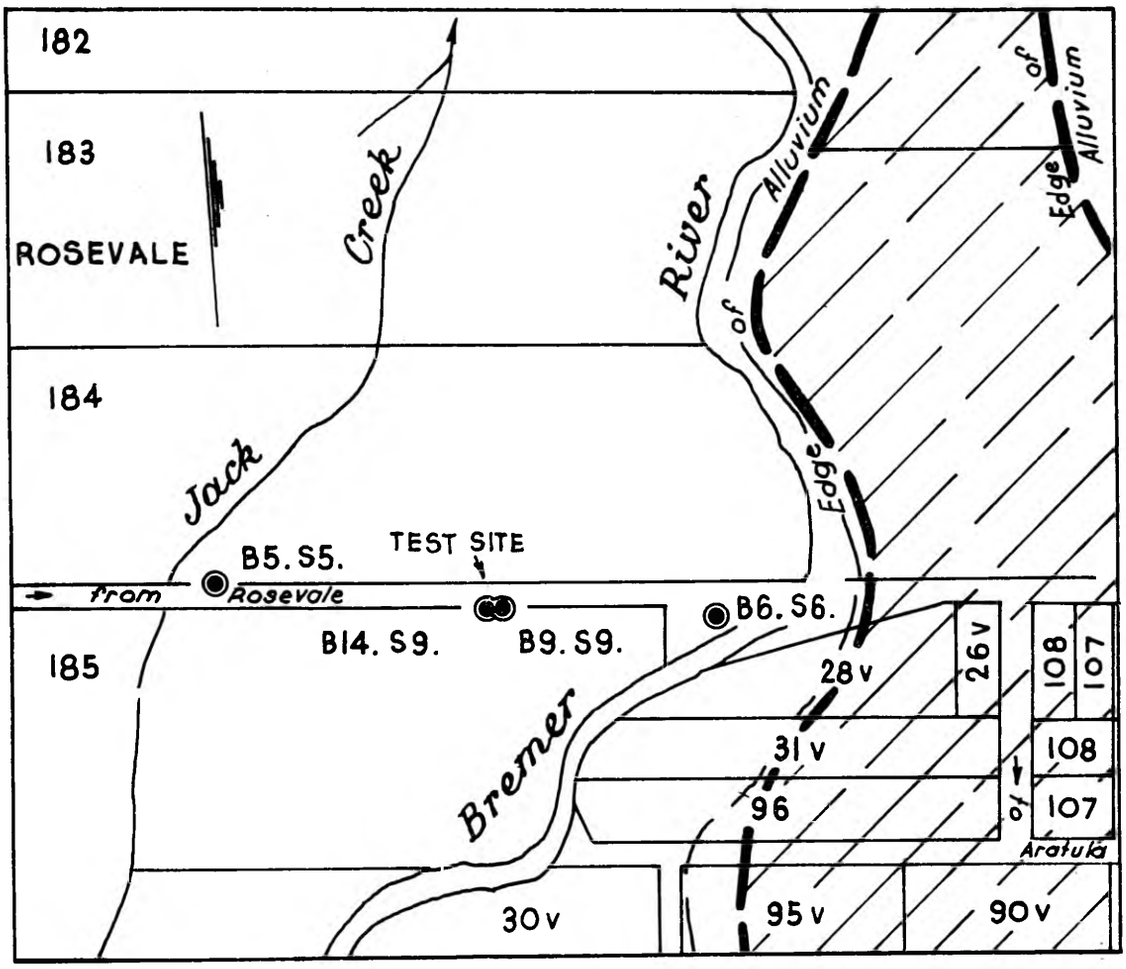

Fig. 7.16: General plan of Site B.

test selected for use in this thesis was a 24 hour test carried out during June 8 to June 9 using a group of wells located on an alluvial area near the Bremer River (Figs. 7.16 and 7.17). The construction features and driller's logs are shown in Fig. 7.18. It may be observed from the log data that the thin aquifer and the overlying aquitard were quite variable in thickness. Wells 2 and 3 were two 4 inch diameter trial production wells with the screened intervals indicated in Table 7.3.

Table 7.3: Radial distances from pumped well 3 and screened intervals of wells at Site B.

Well	Radial distance from well 3 (ft.)	Screened interval assumed R.L. (ft.)
3	r_w = 0.167	51-59
5	8.0	51-55
2	10.0	51-61
1	38.0	52-56
1A	39.3	81-83
4	57.4	51-55
14S9A	80.6	53-58

All of the wells were drilled by using a percussion rig. Samples of the aquifer material were taken continuously from wells 2 and 3. The grain size distribution curve obtained from sieve analysis of one of the samples is presented in Fig. 7.19. A wide range of grain diameter, from .04 to 3 inches, may be observed.

Pumping was started at 11.00 p.m. on June 8 and was continued at an approximately constant rate of 7050 igph (18.8 cfm) until 11.00 a.m. on June 9. The water levels were measured continuously in pumped well 3 and all observation wells. Well 1A, which penetrated the water

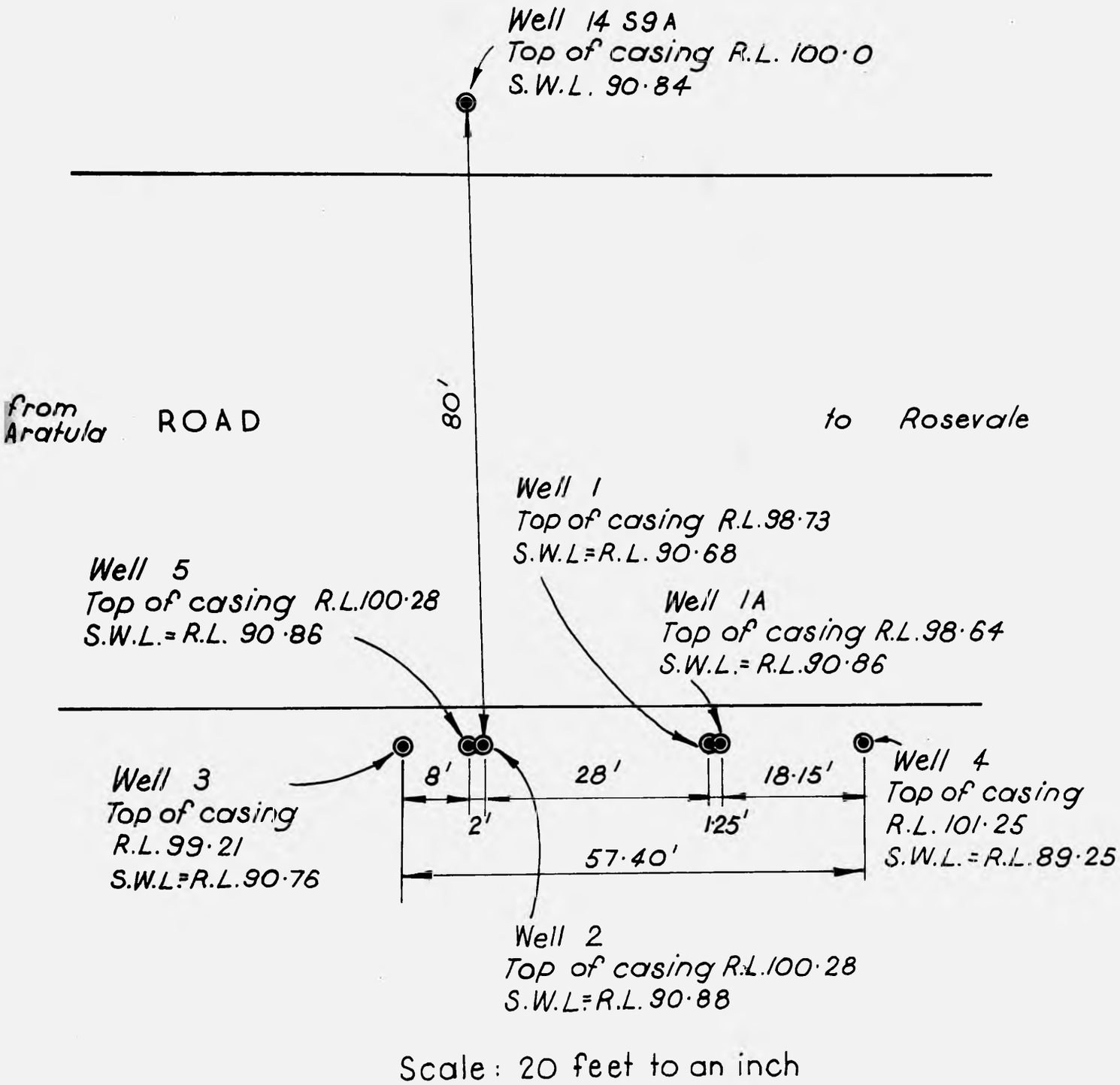

Fig. 7.17: Location of wells at Site B.

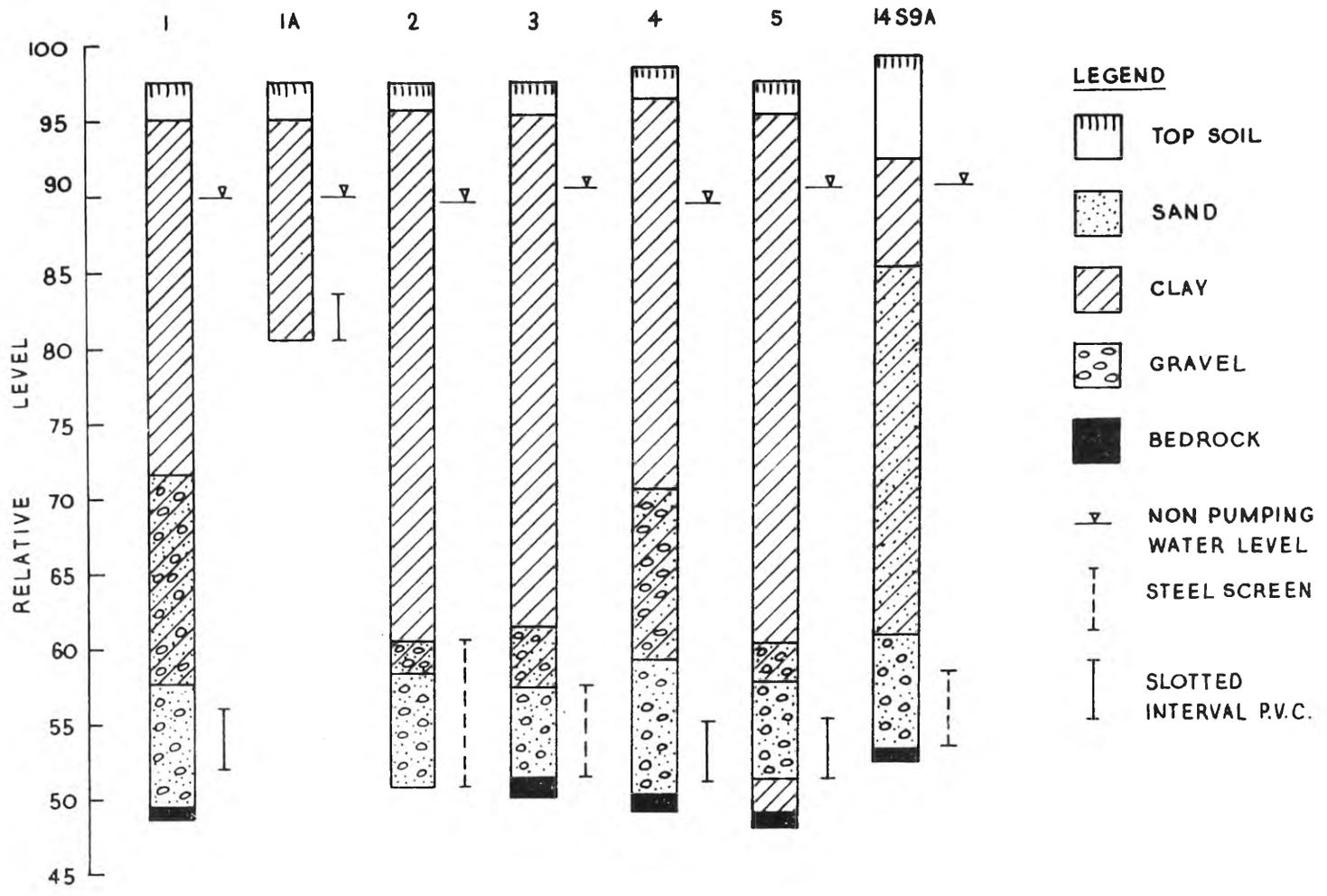

Fig. 7.18: Construction features and available driller logs of wells at Site B.

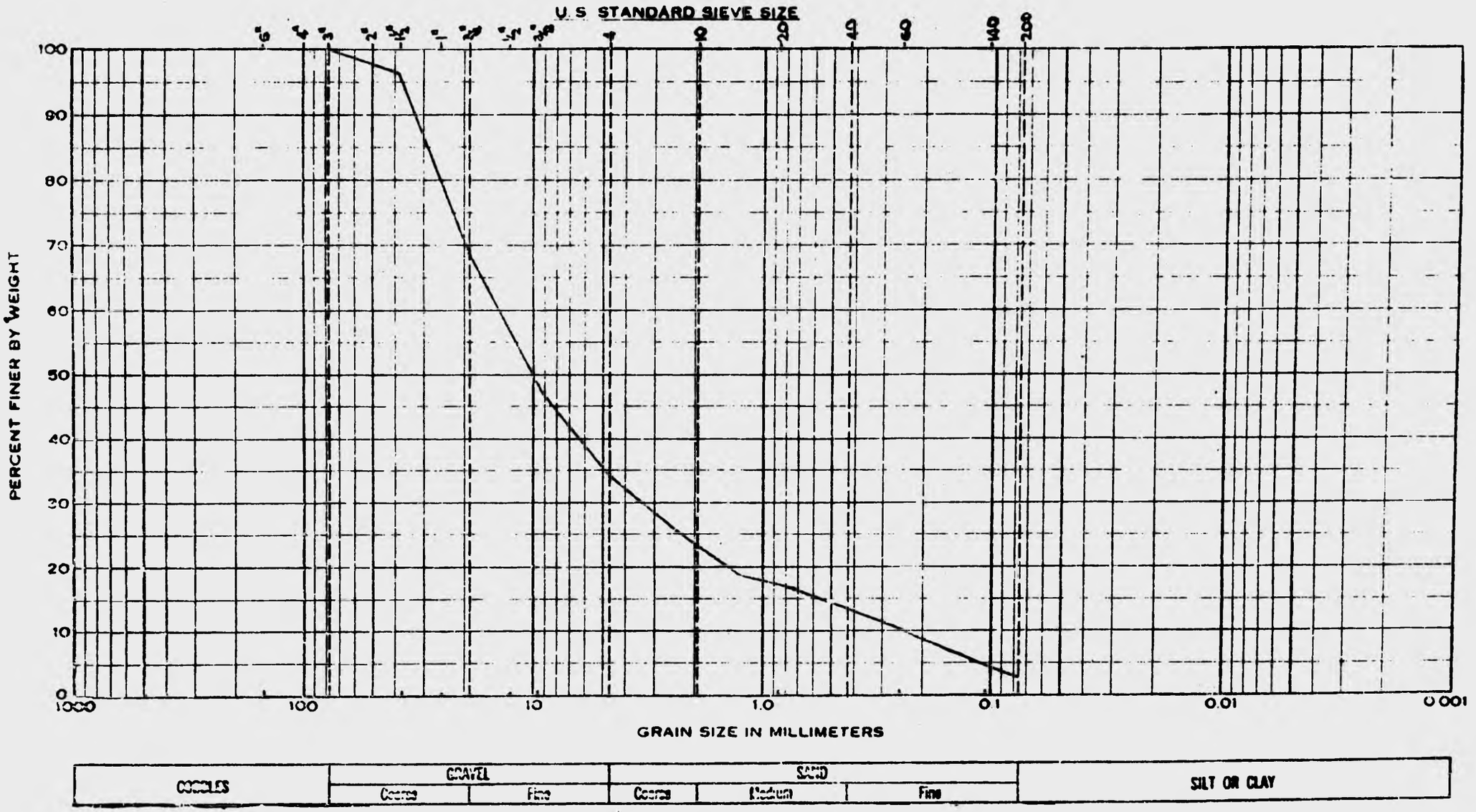

Fig. 7.19: Sieve analysis of sample of aquifer material.

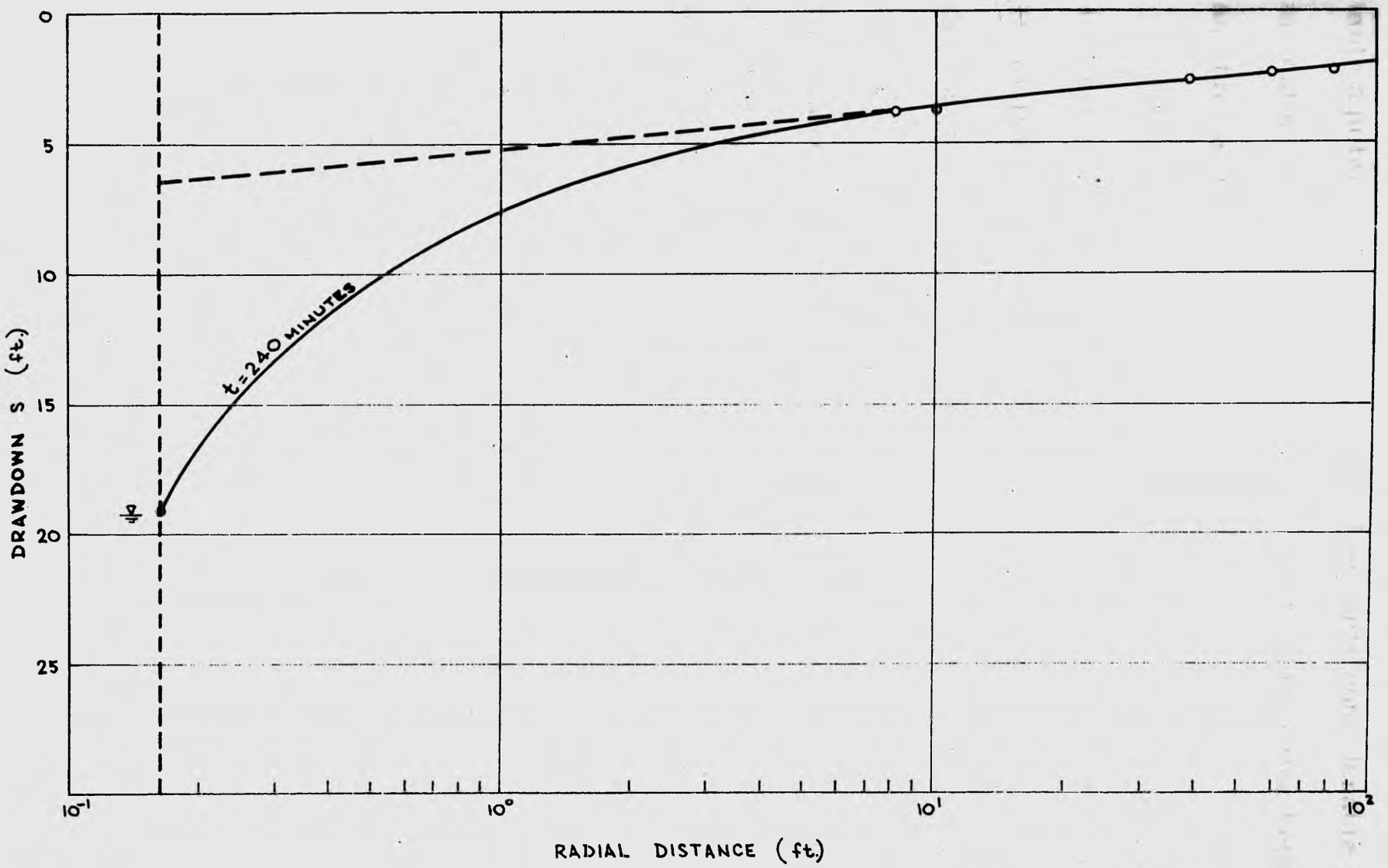

Fig. 7.20: Drawdown-radial distance plot at time t = 240 minutes.

table aquitard, was discovered to show quite considerable response, indicating that there was a direct hydraulic connection between this aquitard and the aquifer.

The drawdown-time field data collected from wells 2, 3, 1 and 1A were used to verify the finite element analysis. To check if non-Darcy flow existed in the main aquitard the discharge of 18.8 cfm, the drawdowns obtained from all observation wells and the pumped well at time t = 240 minutes were plotted against radial distances. The plot is illustrated in Fig. 7.20. It can be seen that non-Darcy flow evidently existed within a radius of approximately 8 ft. from the pumped well where the plot is non-linear.

7.3.2 Finite Element Model and Type Curves for the Field System

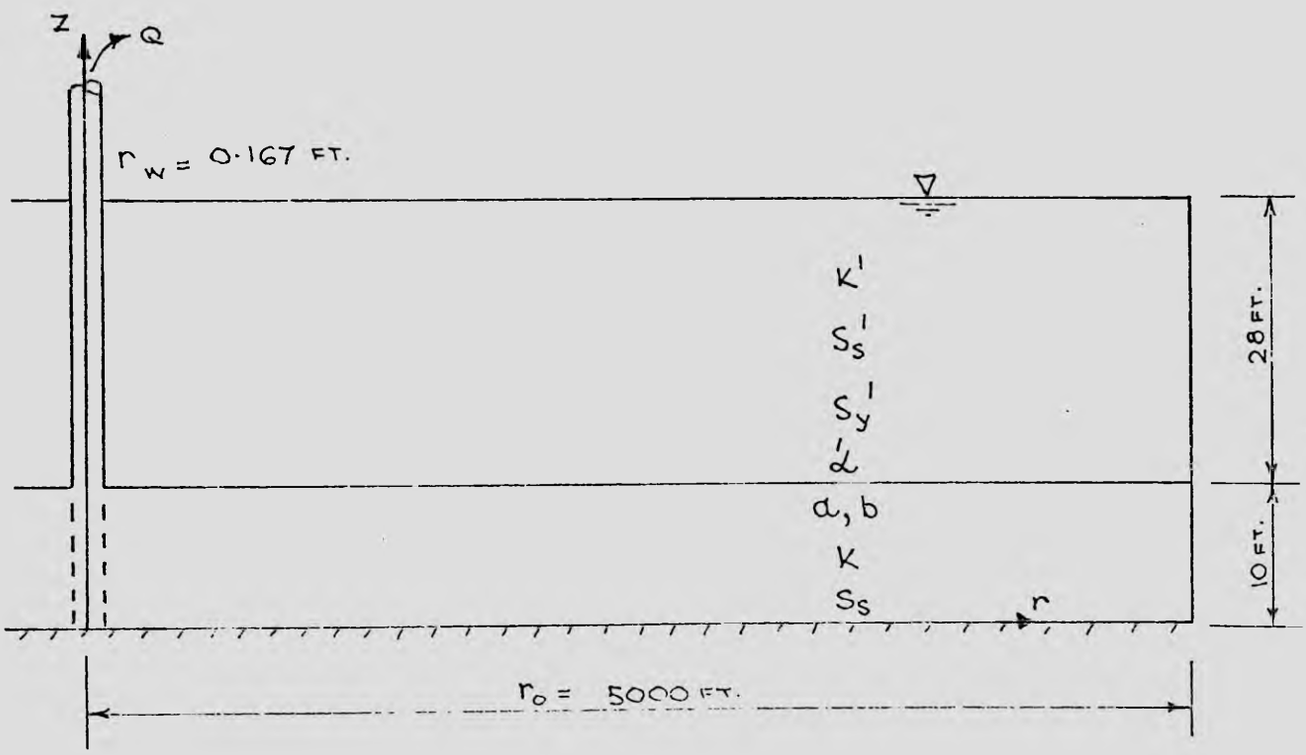

Fig. 7.21: Model of the Rosevale Field System.

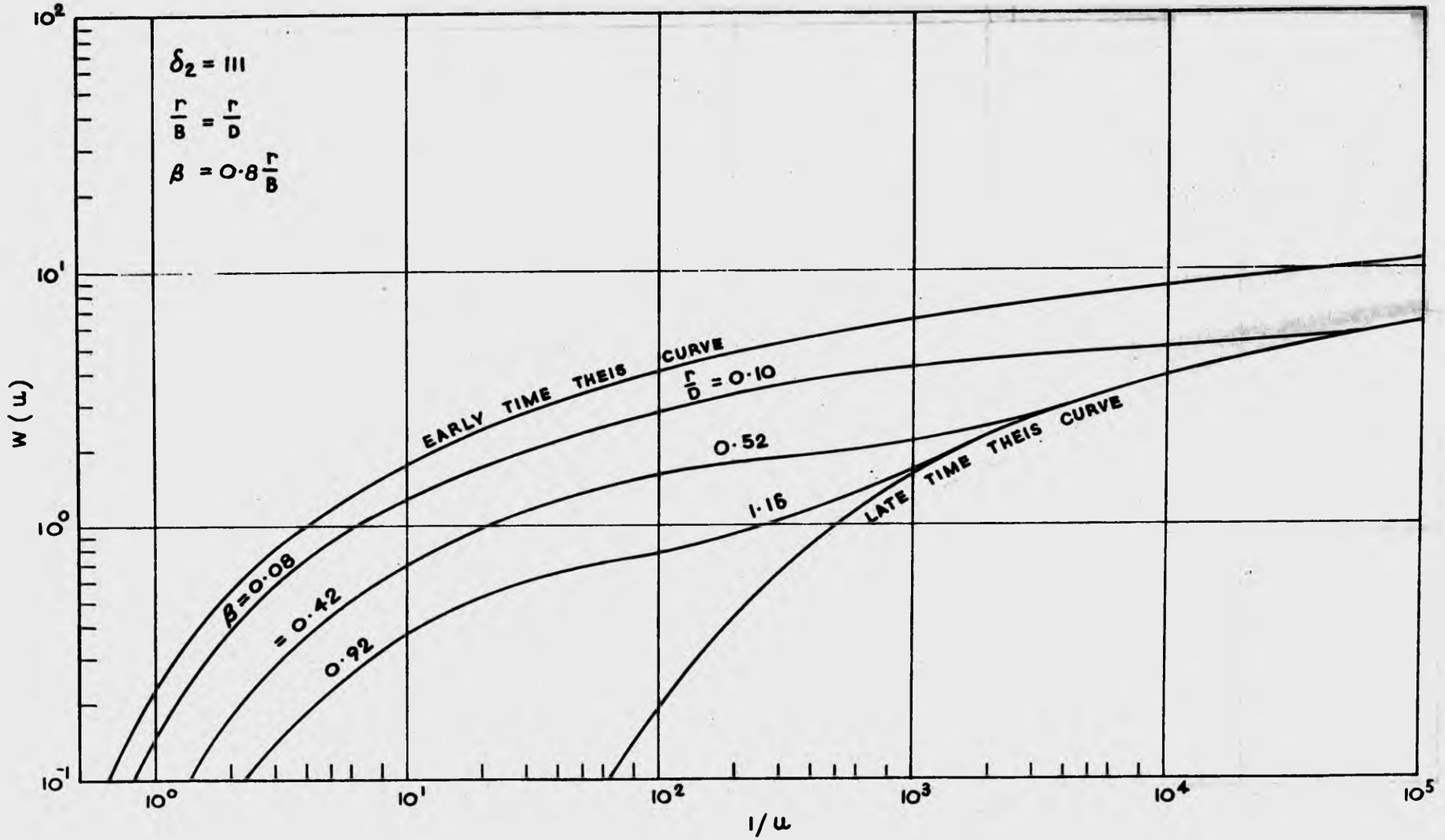

Fig. 7.22: Type curves for the main aquifer of the Rosevale field system ($\frac{r}{B} = \frac{r}{D}$; $\beta = 0.8\ \frac{r}{B}$; $\delta_2 = 111$)

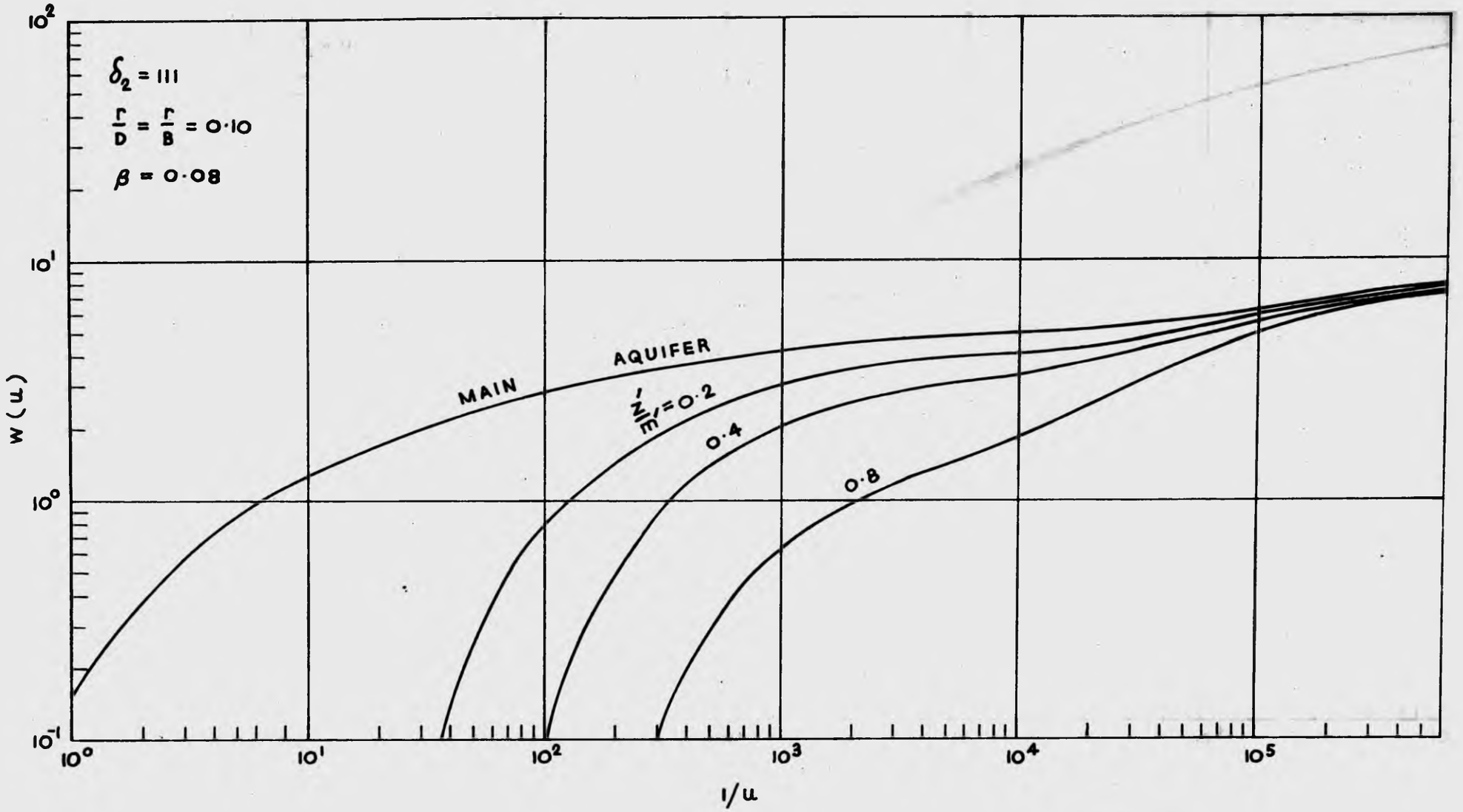

Fig. 7.23: Type curves for the overlying aquitard of the Rosevale field system ($\frac{r}{B} = \frac{r}{D} = 0.20$; $\beta = .08$; $\delta_2 = 111$)

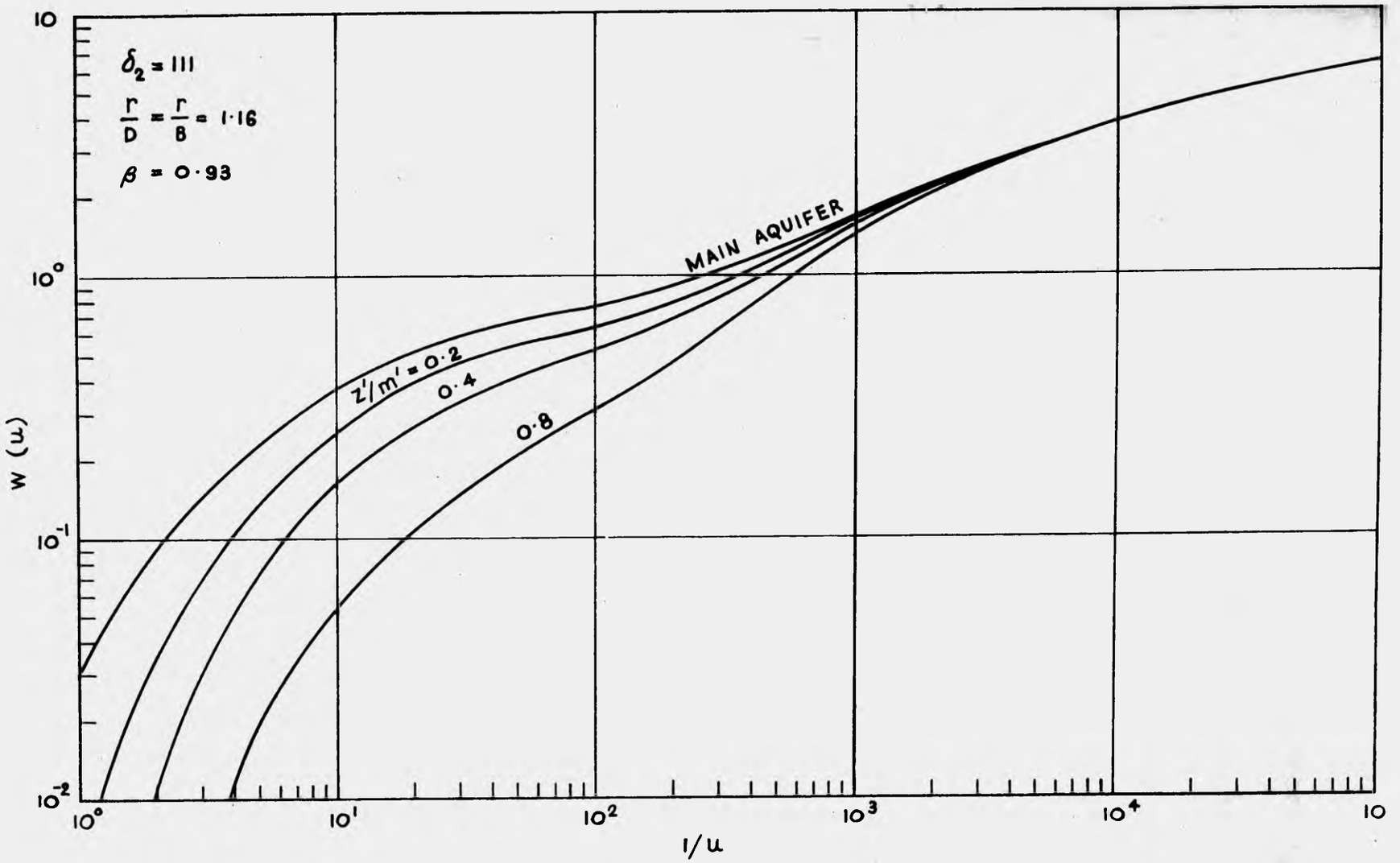

Fig. 7.24: Type curves for the overlying aquitard of the Rosevale field system. ($\frac{r}{B} = \frac{r}{D} = 1.16$; $\beta = .93$; $\delta_2 = 111$)

From the general data presented in the preceding section, a model of the field system was constructed and is shown in Fig. 7.21. The model represents an unconfined aquifer-aquitard system with an external radius of 5000 ft.

Although the well log data showed that the aquifer and aquitard were quite variable in physical properties, both layers were assumed to be homogeneous and isotropic as there were insufficient data available to define a more complex model.

Average thicknesses of 10 and 28 ft. were assigned to the aquifer and the aquitard respectively.

The finite element method was used to solve several flow cases which were simulated to obtain type curves characterising Darcy and non-Darcy flow behaviour of the field system. Typical families of type curves are shown in Figs. 7.22 and 7.27 for the main aquifer and in Figs. 7.23 and 7.24 for the aquitard. The dimensionless parameters of the Darcy flow type curves, $\frac{r}{D}$, $\frac{r}{B}$, β and δ_2, and the non-Darcy flow parameters, λ and ξ, have been defined in Section 5.5.

7.3.3 Comparison of Field Data and Finite Element Solutions

The following type curve method was used to determine the hydraulic coefficients of the aquifer and aquitard:-

(i) The drawdown-time data collected from observation wells Nos. 2 and 1 (r = 10, 38 ft.), outside the non-Darcy flow zone, were converted to log-log plots of s versus t on two separate sheets of transparent

paper. Each plot was then matched on a selected family of type curves for the main aquifer as shown in Figs. 7.25 and 7.26 respectively. Matching was performed in the manner described previously in Section 7.2.3. For each observation well, a match point was selected and the hydraulic coefficients were calculated as follows:-

Well No.2 (r = 10 ft.)

From Fig. 7.25, it follows that

$W = 2.30$; $1/u = 0.5 \times 10^5$

$s = 1$ ft.; $t = 10$ min.

$r/D = 0.22$

The coefficients K and T are given by

$$K = \frac{QW}{4\pi sm} = \frac{18.8 \times 2.3}{4 \times 3.14 \times 10}$$

$$= 0.345 \quad \text{ft/min.}$$

$$T = Km = 3.45 \quad \text{ft}^2/\text{min.}$$

Assuming $S_y' \doteq S_y' + S_s' m' + S_s m$

Thus $$S_y' = \frac{4\,Tt\delta_2\,u}{r^2} = \frac{4 \times 3.45 \times 10 \times 251}{10 \times 10 \times 0.5 \times 10^5}$$

$$= .0070$$

$$D = \frac{10}{0.22} = 46 \quad \text{ft.}$$

Well No.1 (r = 38 ft.)

From Fig. 7.26, it follows that

$W = 1.7$; $1/u = 2.75 \times 10^4$

$s = 1$ ft., $t = 100$ min.

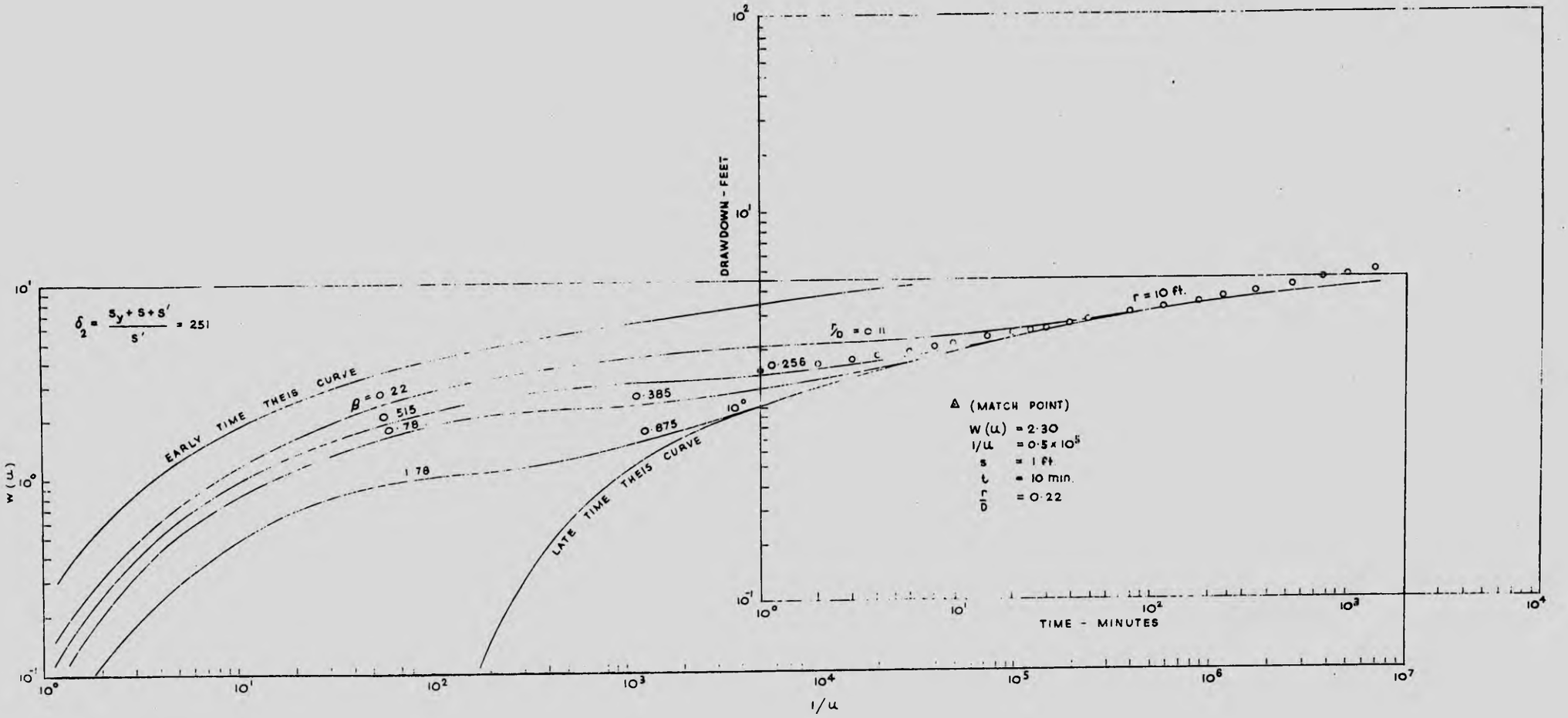

Fig. 7.25: Matching of field data plot on type curves for the main aquifer (observation well 2).

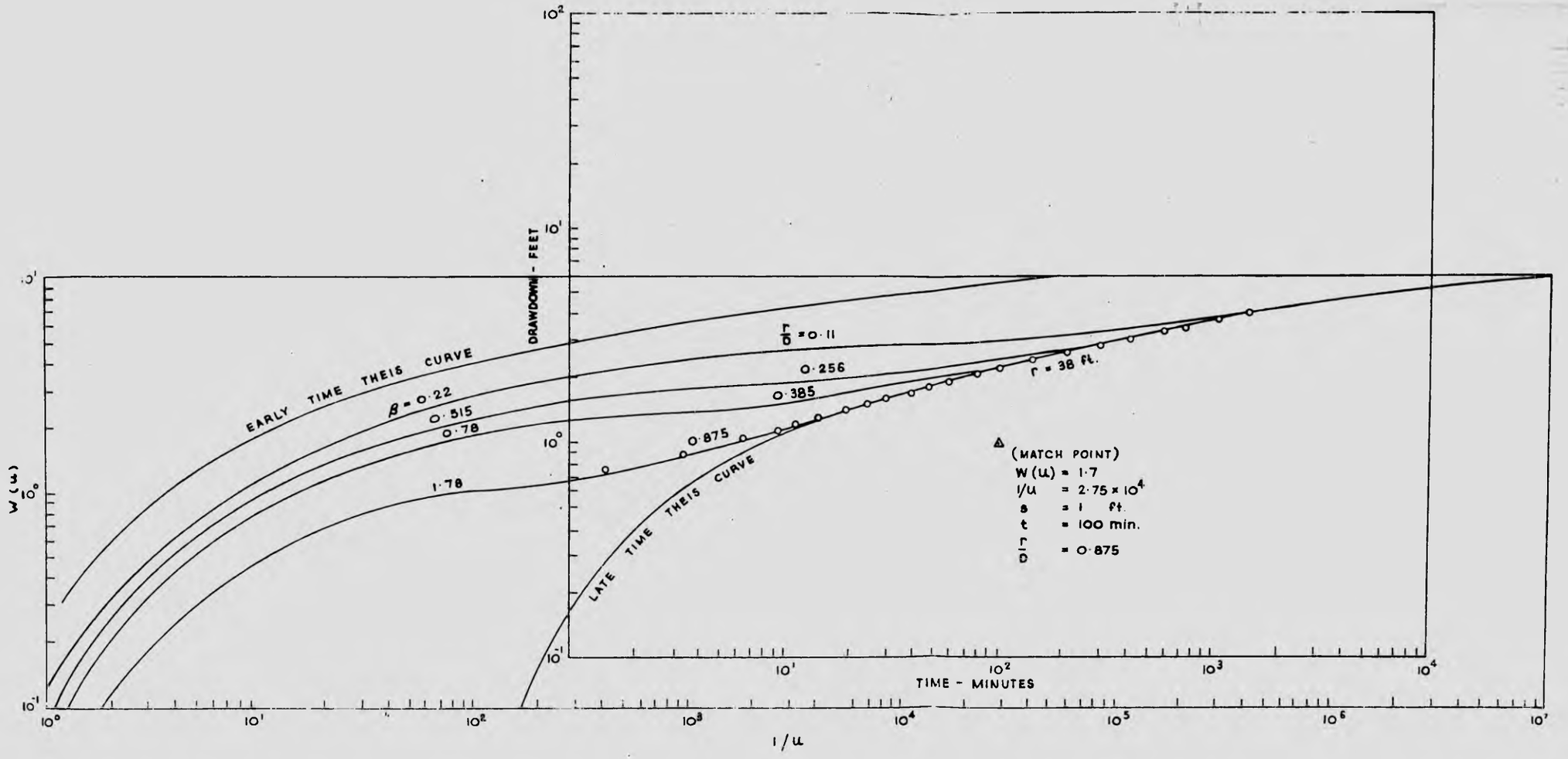

Fig. 7.26: Matching of field data plot on type curves for the main aquifer (observation well 1).

Thus $K = \frac{QW}{4\pi sm}$

$= \frac{18.8 \times 1.7}{4 \times 3.14 \times 10} = 0.254$ ft/min.

$T = Km = 2.54$ $ft^2/min.$

$S_y' = \frac{4\,Tt\,\delta_2\,u}{r^2}$

$= \frac{4 \times 2.54 \times 100 \times 251}{38 \times 38 \times 2.75 \times 10^4} = .0064$

$D = \frac{38}{0.875} = 43.5$ ft.

(ii) The drawdown-time data collected from observation wells 1 and 1A ($r \doteq 38$ ft.; $z'/m' = 0, 0.8$) were plotted together on another sheet of transparent paper and matched on a selected family of type curves for the aquitard. Using the average values of T and D obtained from (i), appropriate values of r/D, β and $\frac{r}{B}$ which gave the best fit were determined. The coefficients K', S_s', α' were calculated using the following expressions:-

$$K' = \left(\frac{r}{B}\right)^2 \left[\frac{Kmm'}{r^2}\right]$$

$$S_s' = \frac{16\,\beta^2\,m^2\,K\,S_s}{K'r^2}$$

$$\alpha' = \frac{T}{S_y'\left[D^2 - \frac{Tm'}{K'}\right]}$$

In obtaining S_s', an estimate was made as to the value of S_s of the aquifer as the early time portion of the field data was missing for observation well 1. The estimate was based on the value of S_s obtained by applying the conventional Hantush type curve fitting method to the

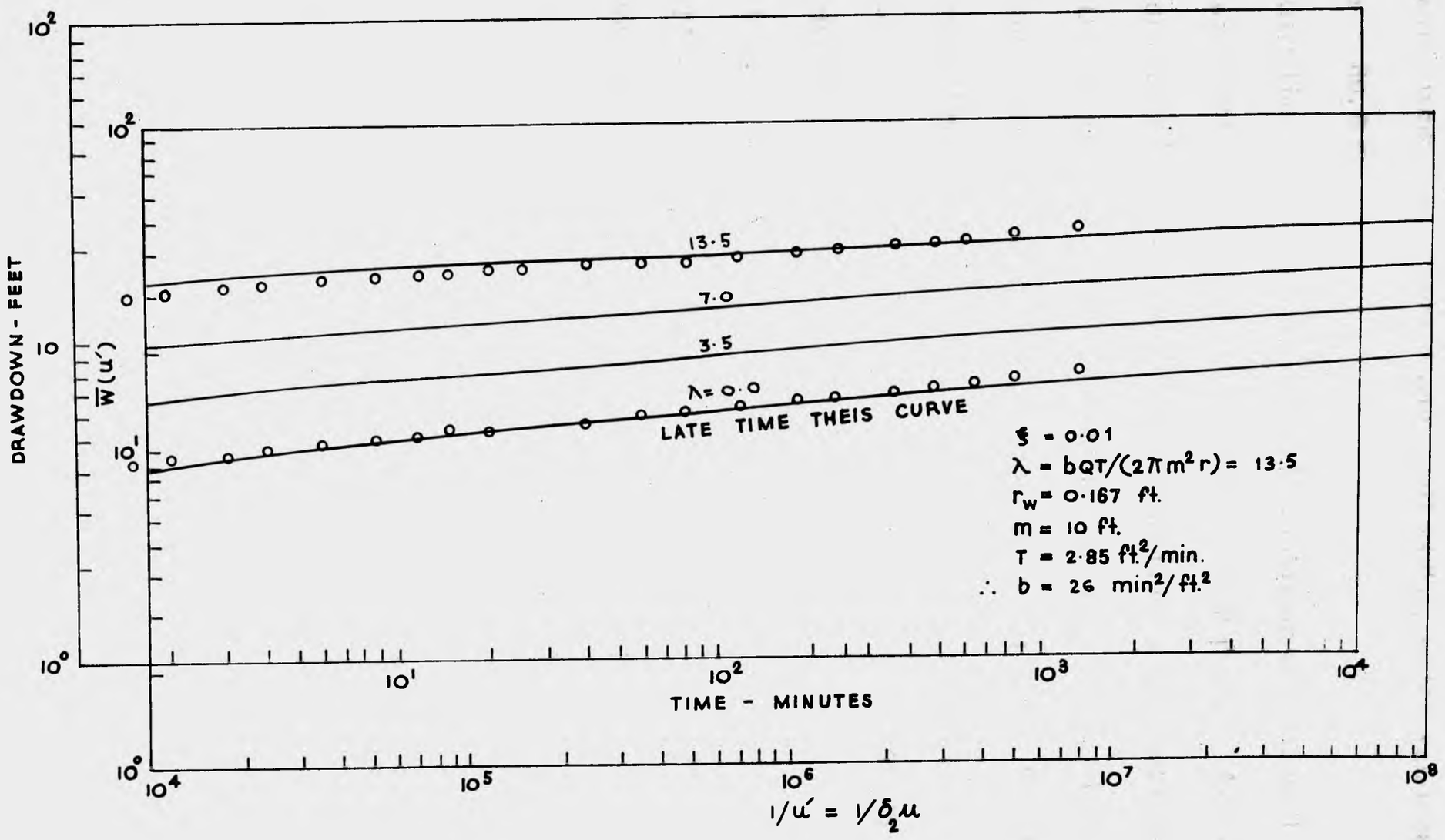

Fig. 7.27: Matching of field data plot from pumped well on non-Darcy flow type curves for the main aquifer.

early time data collected from well 14S9A, which was located at r = 80.6 ft.

(iii) The drawdown-time data collected from pumped well 3 (r_w=0.167 ft.) was plotted on another sheet of transparent paper. As the observed drawdowns in this well would have included additional loss due to non-Darcy flow, the corresponding drawdowns for wholly Darcy flow at the same pumping times were obtained by extrapolating the straight line semi-log plot of s versus r to the well radius. The Darcy flow drawdowns so determined were also plotted on the same sheet of paper. The field data plot was then superposed on a family of non-Darcy flow type curves for the aquifer as shown in Fig. 7.28. The value of the non-Darcy flow parameter for the best fitting type curve was determined and used to obtain the Forchheimer coefficient b as follows:-

$$b = \frac{2\pi m^2 r}{QT}$$

$$= \frac{6.28 \times 10^2 \times 0.167 \times 13.5}{18.8 \times 2.85} = 26 \text{ min}^2/\text{ft}^2.$$

In obtaining b, it was assumed that additional well loss due to flow into and inside the well was negligible as this loss was not measured in the field.

(iv) The values of the hydraulic coefficients computed from (i) to (iii) were fed into the finite element model and the flow problem was solved for Q = 18.8 cfm and the pumping period of 1440 minutes. The theoretical drawdown versus time relationships at selected nodes in the aquifer and aquitard were then compared with the field data for the

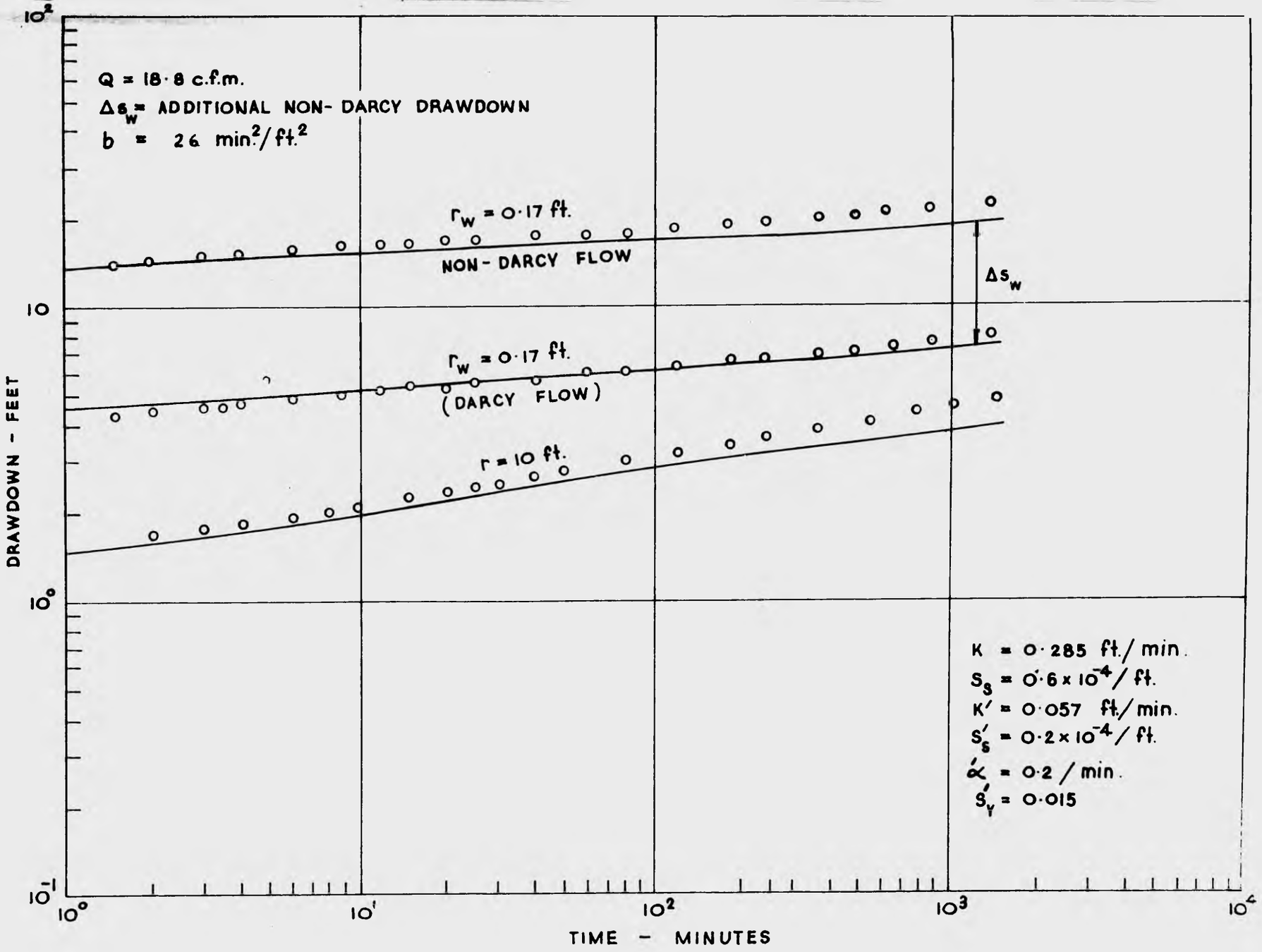

Fig. 7.28: Comparison of finite element model results and field data (pumped well 3 and observation well 2).

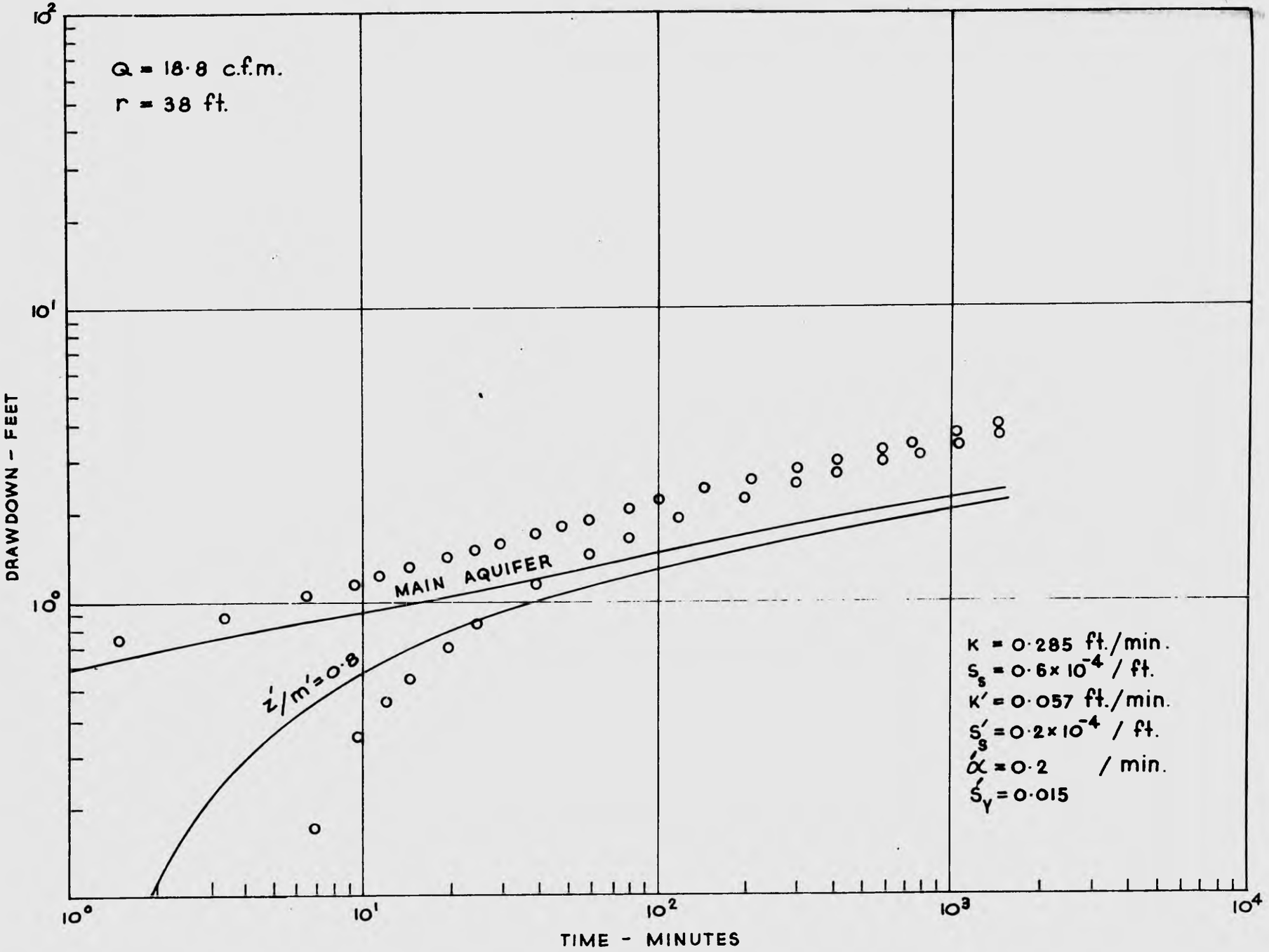

Fig. 7.29: Comparison of finite element model results with field data (observation wells 1 and 1A).

corresponding points in the field system. Several adjustments of the values of the hydraulic coefficients were made and the adjusted values were fed back into the finite element model. The final comparison is presented in Figs. 7.28 and 7.29. It can be seen that reasonable agreement was obtained for the prediction of drawdowns in the pumped well and observation well 2 whilst much poorer agreement was achieved for observation wells 1 and 1A. This could be due to the fact that the aquifer and the aquitard of the field system were quite variable in physical and hydraulic properties and the assumptions made in the theoretical analysis of the field data were seriously violated.

8. Conclusions

1. The theory, variational principle and finite element method for transient, three-dimensional, two-regime flow towards a pumped well have been developed. It was assumed that the two flow regimes, linear and non-linear, are distinct and that the Forchheimer non-linear velocity-hydraulic gradient relationship may be used to describe non-Darcy flow. Anisotropy of the aquifer material has been taken into account only in the Darcy flow zone.

2. The analysis of non-Darcy flow behaviour in anisotropic material involves complex non-linear velocity-hydraulic gradient relationships, the theoretical and experimental basis of which have not been established. Further research is required in order to develop a better understanding of the anisotropic character of the two coefficients of hydraulic resistance in the Forchheimer constitutive relation, namely a and b.

3. The finite element method has been used to solve a variety of axi-symmetric flow problems, ranging from the simplest problem of one-dimensional radial flow through a confined aquifer to the most complex problem of transient free surface flow. Solutions for both wholly Darcy flow and two-regime flow situations have been obtained and presented in graphical form for each problem. Type curves characterising two-regime flow have been included. The non-Darcy flow parameters of the type curves are $\lambda = \frac{bQT}{2\pi m^2 r}$ and $\xi = \frac{bV_{cr}}{a}$.

4. The effect of non-Darcy flow on drawdown distribution near the well and on the well discharge-drawdown relationship has been investigated. It was found that type curves of the dimensionless drawdown versus time for points in the non-Darcy flow zone lie above the conventional Theis curve for wholly Darcy flows through confined aquifers and confined and unconfined aquifer-aquitard systems. For all of the transient flow problems solved, except the problem of transient free surface flow in an unconfined aquifer, the well discharge-drawdown relationships for the two-regime flow situations are non-linear and may be fitted by Jacob's empirical equation. The term CQ^2 of this equation was interpreted as the additional head loss due to non-Darcy flow and was found to remain constant with time once the non-linear regime had been fully established near the well.

5. A rigourous check has been made on the numerical solutions for the transient Darcy flow cases by comparing them with known analytical solutions. It was found that in general the agreement between the finite element results and the analytical solutions was excellent. Where deviation occurred considerable improvement of the finite element results was observed when a more refined network and smaller time steps were used.

6. The numerical solutions for steady state two-regime flow through confined and unconfined aquifers have been verified by comparison with pumping test results obtained from laboratory experiments. Type

curve methods have been developed for determining the hydraulic coefficients a, b and K of the aquifer material. It was found that these methods led to good agreement between the theory and experiment and that the determined values of the hydraulic coefficients changed quite considerably when the aquifer was disturbed.

7. The numerical solutions for transient flow in aquifer-aquitard systems have also been verified by comparison with pumping test data obtained from field investigations carried out at two sites. Type curve methods have been developed for determining the hydraulic properties of the aquifer and the overlying aquitard at each site. For the first site, where the aquifer and aquitard are relatively uniform in thickness and hydraulic properties, the type curve method led to good agreement between the finite element results and the field data. However, it was not possible to determine from the field data the Forchheimer non-linear coefficient, b, for the aquifer as non-Darcy flow did not exist near the 24 inch diameter well at the discharge of 48,000 igph. To induce non-Darcy flow having significant effects on well drawdowns would have required either a reduction in well diameter for the same discharge or a significant increase in discharge for the same diameter.

For Site B, where the main aquifer and the aquitard are variable in physical and hydraulic properties and non-Darcy flow evidently existed, less satisfactory agreement between the theoretical predictions and field data was achieved. This can be explained in terms of the limiting assumptions made in constructing the finite element model,

particularly that of a homogeneous, isotropic aquifer of uniform thickness. To construct a more complex model would have required additional data regarding the variability of the aquifer and aquitard of this site. The aquisition of this data would have greatly increased the cost of the field investigation.

It is finally pointed out that the value of coefficient b determined from the type curve method is based on the assumption that head losses due to flow through the well screen and inside the well can be separated from the total well drawdown or neglected. This value so determined would represent an over-estimate of the true value if these losses were significant.

8. The theory, numerical techniques and type curve methods developed in this work may be applied to specific cases of well flow encountered in practice. Alternatively, they may be used to produce solutions to a wider range of problems than that covered in this thesis.

Appendix 1.

Formation of Matrices $[C^e]$ and $[D^e]$ for rectangular ring elements.

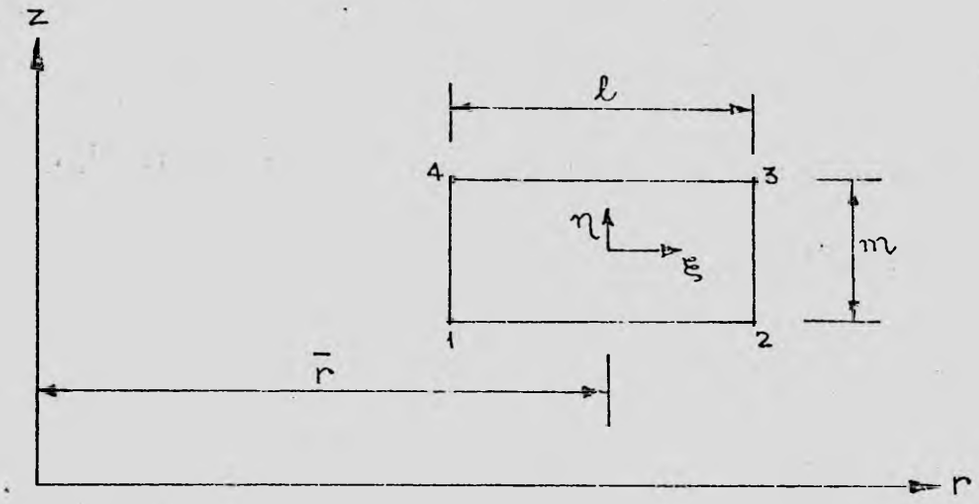

Fig. A1.1: Cross-section of a rectangular ring element.

Consider a typical rectangular element shown in Fig. A1.1. As indicated, the four corner nodes are numbered in an anti-clockwise sense, and $\bar{r}$ denotes the radial coordinate of the centroid.

From equation (4.67a) in chapter 4, the expression for the element matrix $[C^e]$ may be rewritten as

$$[C^e] = 2\pi \int_{-1}^{1} \int_{-1}^{1} E\, [S]^T [S]\, N_I\, r_I\, |J|\, d\xi\, d\eta \qquad \text{(A1.1)}$$

Equation (A1.1) may be approximated by

$$[C^e] = 2\pi \bar{E} \bar{r} \int_{-1}^{1} \int_{-1}^{1} [S]^T [S]\, |J|\, d\xi\, d\eta \qquad \text{(A1.2)}$$

where $\bar{E}$ is the coefficient of effective hydraulic conductivity at the centroid.

For rectangular elements, it can be shown that $|J|$ and $[S]$ are given by

$$|J| = \frac{lm}{4} \qquad \text{(A1.3a)}$$

$$[S] = \begin{bmatrix} 2/l & 0 \\ 0 & 2/m \end{bmatrix} \begin{bmatrix} \frac{\partial N_1}{\partial \xi} & \frac{\partial N_2}{\partial \xi} & \frac{\partial N_3}{\partial \xi} & \frac{\partial N_4}{\partial \xi} \\ \frac{\partial N_1}{\partial \eta} & \frac{\partial N_2}{\partial \eta} & \frac{\partial N_3}{\partial \eta} & \frac{\partial N_4}{\partial \eta} \end{bmatrix} \qquad \text{(A1.3b)}$$

where l and m are the width and height of the rectangle respectively.

Now $[S]^T$ may be obtained as

$$[S]^T = \begin{bmatrix} \frac{\partial N_1}{\partial \xi} & \frac{\partial N_1}{\partial \eta} \\ \frac{\partial N_2}{\partial \xi} & \frac{\partial N_2}{\partial \eta} \\ \frac{\partial N_3}{\partial \xi} & \frac{\partial N_3}{\partial \eta} \\ \frac{\partial N_4}{\partial \xi} & \frac{\partial N_4}{\partial \eta} \end{bmatrix} \begin{bmatrix} 2/l & 0 \\ 0 & 2/m \end{bmatrix} \qquad \text{(A1.3c)}$$

Substitution of equations (A1.3a) to (A1.3c) into (A1.2) leads to

$$[C^e] = 2\pi \bar{E} \bar{r} \left(\frac{m}{l} [G^e] + \frac{l}{m} [H^e] \right) \qquad \text{(A1.4)}$$

where $[G^e]$ and $[H^e]$ are the influence coefficient matrices whose elements are given by

$$G^e_{IJ} = \int_{-1}^{1} \int_{-1}^{1} \frac{\partial N_I}{\partial \xi} \frac{\partial N_J}{\partial \xi} \, d\xi \, d\eta \qquad \text{(A1.5a)}$$

and

$$H^e_{IJ} = \int_{-1}^{1} \int_{-1}^{1} \frac{\partial N_I}{\partial \eta} \frac{\partial N_J}{\partial \eta} \, d\xi \, d\eta \qquad \text{(A1.5b)}$$

On applying the 9-point Gaussian quadrature formula given by Zienkiewicz((1971), pp.147-149), the integrals in equations (A1.5a) and (A1.5b) may be evaluated. The matrices $[G^e]$ and $[H^e]$ are obtained as

$$[G^e] = \begin{bmatrix} \frac{1}{3} & -\frac{1}{3} & -\frac{1}{6} & \frac{1}{6} \\ -\frac{1}{3} & \frac{1}{3} & \frac{1}{6} & -\frac{1}{6} \\ -\frac{1}{6} & \frac{1}{6} & \frac{1}{3} & -\frac{1}{3} \\ \frac{1}{6} & -\frac{1}{6} & -\frac{1}{3} & \frac{1}{3} \end{bmatrix} \qquad \text{(A1.6a)}$$

$$[H^e] = \begin{bmatrix} \frac{1}{3} & \frac{1}{6} & -\frac{1}{6} & -\frac{1}{3} \\ \frac{1}{6} & \frac{1}{3} & -\frac{1}{3} & -\frac{1}{6} \\ -\frac{1}{6} & -\frac{1}{3} & \frac{1}{3} & \frac{1}{6} \\ -\frac{1}{3} & -\frac{1}{6} & \frac{1}{6} & \frac{1}{3} \end{bmatrix} \qquad \text{(A1.6b)}$$

Substitution of equations (A1.6a) and (A1.6b) leads to the required expression for matrix $[C^e]$.

Similarly, from equation (4.67c), the expression for matrix $[D^e]$ may be rewritten as

$$[D^e] = 2\pi \int_{-1}^{1} \int_{-1}^{1} S_s [N]^T [N] N_I r_I |J| \, d\xi \, d\eta \qquad \text{(A1.7)}$$

Equation (A1.7) may be approximated by

$$[D^e] = 2\pi (S_s \bar{r} \frac{lm}{4} \int_{-1}^{1} \int_{-1}^{1} [N]^T [N] \, d\xi \, d\eta \qquad \text{(A1.8)}$$

On applying the 9-point Gaussian quadrature formula, the integral in equation (A1.8) can be evaluated. The expression for matrix $[D^e]$ is obtained as

$$[D^e] = \frac{\pi \bar{r}}{2} \, lm \, S_s \begin{bmatrix} \frac{4}{9} & \frac{2}{9} & \frac{1}{9} & \frac{2}{9} \\ \frac{2}{9} & \frac{4}{9} & \frac{2}{9} & \frac{1}{9} \\ \frac{1}{9} & \frac{2}{9} & \frac{4}{9} & \frac{2}{9} \\ \frac{2}{9} & \frac{1}{9} & \frac{2}{9} & \frac{4}{9} \end{bmatrix} \qquad (A1.9)$$

Appendix 2.

Analytical Solution to Steady, One-dimensional, Two-regime Well Flow.

A2.1 General

An analytical approach to the problem of steady state, one-dimensional, two-regime well flow was first presented by Engelund ((1953), pp. 49-53)). In his work an expression describing the well discharge-drawdown relationship was derived but a more general expression describing the drawdown-radial relationship was not presented. It is shown in this appendix that the latter expression can be obtained and written in dimensionless form using the parameters which have been developed to characterise two-regime well flow.

A2.2 General Solution

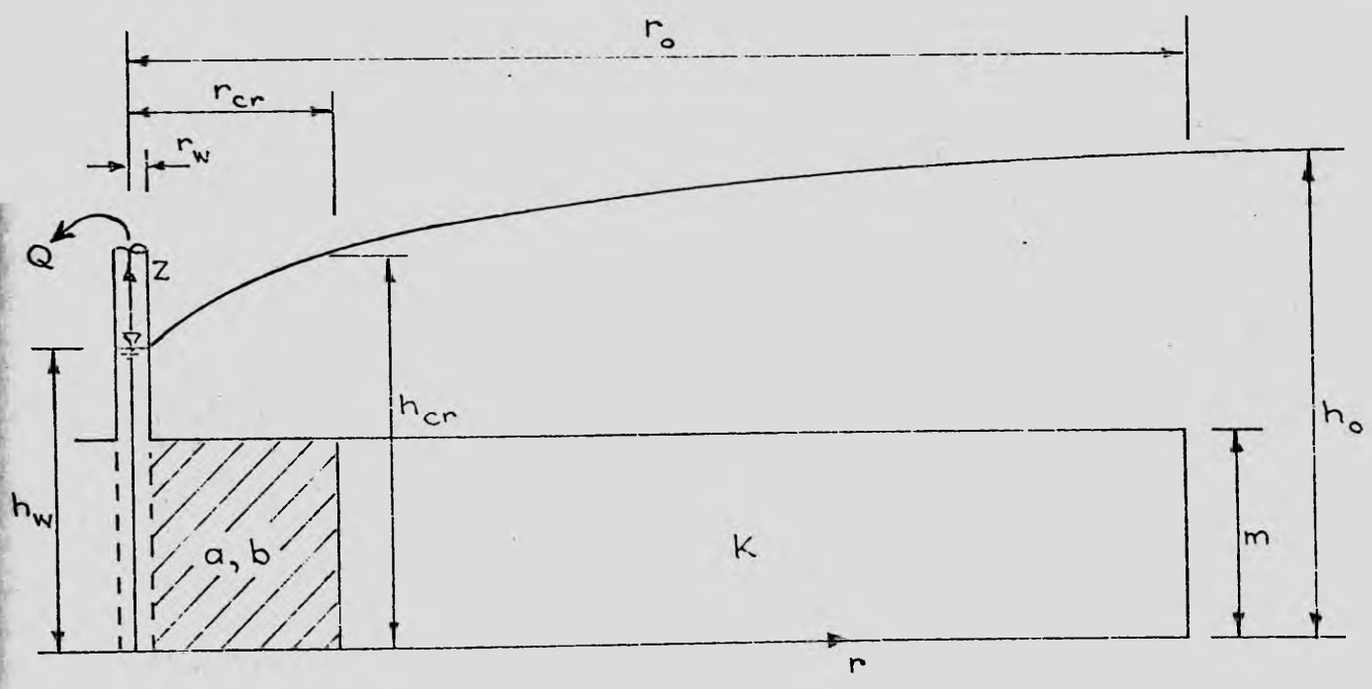

Fig. (A2.1): Diagrammatic sketch of a confined well-aquifer system.

A diagrammatic sketch of a confined well-aquifer system is shown in Fig. (A2.1). The well is fully screened through the entire thickness of the aquifer and pumped at a known discharge. Non-Darcy flow is assumed to occur in the shaded zone extending from the well radius to the critical radius r_{cr}. The equation relating hydraulic gradient and flow velocity in this zone is given by

$$-\frac{dh}{dr} = aV + bV^2 \qquad \text{(A2.1)}$$

The flow velocity and the well discharge are related by

$$V = -\frac{Q}{2\pi r m} \qquad \text{(A2.2)}$$

Substituting equation (A2.2) into equation (A2.1) gives

$$\frac{dh}{dr} = \frac{aQ}{2\pi m r} - \frac{bQ^2}{4\pi^2 m^2 r^2}$$

On integrating, the following expression is obtained

$$\int_r^{r_{cr}} \frac{dh}{dr}\, dr = \int_r^{r_{cr}} \frac{aQ}{2\pi m}\,\frac{dr}{r} - \int_r^{r_{cr}} \frac{bQ^2}{4\pi^2 m^2}\,\frac{dr}{r^2}$$

$$h_{cr} - h = \frac{aQ}{2\pi m} \ln\left(\frac{r_{cr}}{r}\right) + \frac{bQ^2}{4\pi^2 m^2}\left(\frac{1}{r} - \frac{1}{r_{cr}}\right)$$

$$\text{for } r_w \leq r \leq r_{cr} \qquad \text{(A2.3)}$$

Now the equation describing Darcy flow in the remaining portion of the aquifer may be written as

$$K\frac{dh}{dr} = \frac{Q}{2\pi m r} \qquad \text{(A2.4)}$$

Equation (A2.4) may be integrated to result in

$$\int_{r}^{r_o} K\frac{dh}{dr}\,dr = \int_{r}^{r_o} \frac{Q}{2\pi m}\,\frac{dr}{r}$$

$$h_o - h = \frac{Q}{2\pi Km}\ln\left(\frac{r_o}{r}\right)$$

$$\text{for } r_{cr} \leq r \leq r_o \qquad \text{(A2.5)}$$

Substituting $r = r_{cr}$ in equation (A2.5) leads to

$$h_o - h_{cr} = \frac{Q}{2\pi Km}\ln\frac{r_o}{r_{cr}} \qquad \text{(A2.6)}$$

Adding equations (A2.3) and (A2.6) gives

$$h_o - h = \frac{Q}{2\pi Km}\ln\frac{r_o}{r_{cr}} + \frac{aQ}{2\pi m}\ln\frac{r_{cr}}{r} + \frac{bQ^2}{4\pi^2 m^2}\left(\frac{1}{r} - \frac{1}{r_{cr}}\right)$$

$$\text{for } r_w \leq r \leq r_{cr} \qquad \text{(A2.7)}$$

Equations (A2.7) and (A2.5) are the expressions for the head distributions in the non-Darcy and Darcy flow subregions respectively.

A2.3 Dimensionless drawdown-radial distance relationships

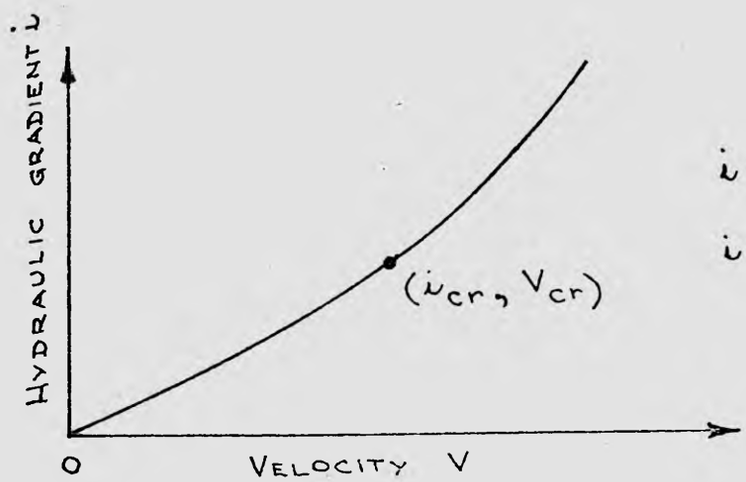

Fig. (A2.2): Velocity-gradient relationship showing the critical point where non-Darcy flow commences.

Equations (A2.5) and (A2.7) may be written in dimensionless form as follows:-

Let the drawdown s and the coefficient of transmissivity for the aquifer T be defined in accordance with

$$s = h_o - h \qquad \text{(A2.8)}$$

and $$T = Km \qquad \text{(A2.9)}$$

From Fig. (A2.2) the coefficient of permeability K is given by

$$K = \frac{1}{a+bV_{cr}} \qquad \text{(A2.10)}$$

Substitution of equations (A2.8) and(A2.9) into equation (A2.5) leads to

$$\frac{2\pi s\, T}{Q} = \ln\left(\frac{r_o}{r}\right) \qquad \text{(A2.11)}$$

Similarly, subsitution of equation (A2.8) and (A2.9) into equation (A2.7) leads to

$$\frac{2\pi s\, T}{Q} = \ln\left(\frac{r_o}{r_{cr}}\right) + K\alpha \ln\left(\frac{r_{cr}}{r_o}.\frac{r_o}{r}\right) + \frac{bQT}{2\pi m^2 r_o}\left(\frac{r_o}{r} - \frac{r_o}{r_{cr}}\right) \qquad \text{(A2.12)}$$

Replacement of K in equation (A2.12) by $\frac{1}{a+bV_{cr}}$ gives

$$\frac{2\pi sT}{Q} = \ln\left(\frac{r_o}{r_{cr}}\right) + \frac{1}{1+\frac{bV_{cr}}{a}} \ln\left(\frac{r_{cr}}{r_o}.\frac{r_o}{r}\right) + \frac{bQT}{2\pi m^2 r_o}\left(\frac{r_o}{r} - \frac{r_o}{r_{cr}}\right) \qquad \text{(A2.13)}$$

The following dimensionless parameters are now defined.

$$u_o = \frac{r}{r_o} \qquad \text{(A2.14a)}$$

$$\lambda = \frac{bQ'T}{2\pi m^2 r_o} \qquad \text{(A2.14b)}$$

$$\xi = \frac{bV_{cr}}{a} \qquad \text{(A2.14c)}$$

Substituting these expressions into equations (A2.11) and (A2.13) results in the required dimensionless equations for two-regime well flow

$$\frac{2\pi sT}{Q} = \ln\left(\frac{1}{u_o}\right) \quad \text{for } \frac{r_{cr}}{r_o} \leqslant u_o \leqslant 1 \qquad \text{(A2.15)}$$

and

$$\frac{2\pi sT}{Q} = \ln\left(\frac{r_o}{r_{cr}}\right) + \frac{1}{1+\xi}\left[\ln\left(\frac{r_{cr}}{r_o} \cdot \frac{1}{u_o}\right)\right] + \lambda\left(\frac{1}{u_o} - \frac{r_o}{r_{cr}}\right) \quad \text{for } \frac{r_w}{r_o} \leqslant u_o \leqslant \frac{r_{cr}}{r_o} \qquad \text{(A2.16)}$$

Introduction of the well function W allows equations (A2.15) and (A2.16) to be written in compact functional form.

Thus from equation (A2.15), it follows that

$$\frac{2\pi sT}{Q} = W\left(\frac{1}{u_o}\right) \quad \text{for } \frac{r_{cr}}{r_o} \leqslant u_o \leqslant 1 \qquad \text{(A2.17)}$$

Equation (A2.16) may also be written as

$$\frac{2\pi s T}{Q} = W\left(\frac{1}{u_o}, \lambda, \xi, \frac{r_{cr}}{r_o}\right) \qquad \text{(A2.18)}$$

$$\text{for } \frac{r_w}{r_o} \leqslant u_o \leqslant \frac{r_{cr}}{r_o}$$

A2.4 Dimensionless Parameters for Steady Non-Darcy Flow

From equation (A2.18), it can be seen that the dimensionless parameters characterising drawdown distributions in the non-Darcy flow zone near the well are λ, ξ and $\frac{r_{cr}}{r_o}$. The expressions for λ and ξ are given by equations (A2.14b) and (A2.14c) respectively.

The parameter ξ was recognised by Engelund ((1953), pp. 14-15)) as a type of Reynolds number. He interpreted ξ as the ratio of the inertial and viscous terms in the basic Forchheimer non-linear velocity-hydraulic gradient relation (i.e. $\xi = \frac{bV^2}{aV}$). He also listed some values for ξ as obtained from published experimental results available to him. Based on these and some additional published experimental results, a practical range of values $0.01 \leqslant \xi \leqslant 0.1$ was adopted in the present work for the analysis of various steady and transient flow problems by the finite element method.

Amongst the three parameters λ, ξ and $\frac{r_{cr}}{r_o}$, the parameter λ is recognised in this work as the most significant parameter characterising non-Darcy flow. This conclusion is derived from the results of numerical experiments designed to investigate the effects of λ, ξ and $\frac{r_{cr}}{r_o}$ on values of the well function. In the experiments, a computer subroutine coded in FORTRAN IV was employed to perform numerical evaluation of the analytical solutions

given by equations (A2.15) and (A2.16) for the range of values λ , ξ and $\frac{r_o}{r_{cr}}$ considered to be of practical significance. The results showed that ξ had only a slight effect on $W(1/u_o)$ for fixed values of λ and that the effect of r_o/r_{cr} was negligible.

A2.5 Dimensionless Relationships and Parameters for Transient Non-Darcy Flow

The two significant dimensionless parameters characterising steady non-Darcy flow were discovered to be λ and ξ, which are defined in equations (A2.14b) and (A2.14c). Although the analytical solutions to transient, one-dimensional, two-regime flow at constant discharge have not been obtained, the following dimensionless relationships are proposed to characterise it.

$$\frac{4\pi Ts}{Q} = W\left(\frac{1}{u}, \lambda, \xi\right) \qquad \text{(A2.21)}$$

where

$$\frac{1}{u} = \frac{4\,Tt}{r^2 S} \qquad \text{(A2.22a)}$$

$$\lambda = \frac{bQT}{2\pi m^2 r} \qquad \text{(A2.23b)}$$

$$\xi = \frac{bV_{cr}}{a} \qquad \text{(A2.23c)}$$

Equation (A2.21) may be derived by applying dimensional analysis to the transient flow problem and neglecting the dimensionless terms which are insignificant.

For wholly Darcy flow, equation (A2.21) reduces to

$$\frac{4\pi Ts}{Q} = W\left(\frac{1}{u}\right) \qquad \text{(A2.24)}$$

where $W\left(\frac{1}{u}\right)$ is the well-known Theis exponential integral.

A family of type curves for the general transient well function in equation (A2.21) was obtained by employing the one-dimensional finite element computer program. These type curves are presented in Chapter 5.

Appendix 3.

Analytical Solutions used to verify the Finite Element Analysis.

The analytical solutions listed herein have been evaluated numerically by a number of computer subroutines which were coded in FORTRAN IV language.

A3.1 Flow towards a Fully Screened Well in a Confined Aquifer

(i) Darcy Flow Solution

The analytical solution to the transient flow problem shown in Fig. (5.1), Chapter 5, was derived by Hantush ((1959), (1964, p. 318)).

$$s = \frac{Q}{4\pi T} W(\tau, \rho) \qquad \text{(A3.1)}$$

where s = drawdown in the aquifer

$$W(\tau,\rho) = \frac{4}{\pi} \int_0^\infty [1 - \exp(-\tau u^2)] R\,du \qquad \text{(A3.2a)}$$

$$R = \frac{1}{u^2}[J_1(u) y_o(\rho u) - y_1(u) J_o(\rho u)]$$

$$/\,[J_1^2(u) + y_1^2(u)] \qquad \text{(A3.2b)}$$

$$\rho = r/r_w \qquad \text{(A3.2c)}$$

$$\tau = \frac{Tt}{S r_w^2} \qquad \text{(A3.2d)}$$

J_o and J_1 = zero- and first- order Bessel functions of the first kind

y_o and y_1 = zero- and first- order Bessel functions of the second kind

For $\rho > 30$ and $\tau > 20$, equation (A3.1) becomes the well-known Theis solution, which is given by

$$s = \frac{Q}{4\pi T} \int_{u}^{\infty} \frac{e^{-u}}{u} du \qquad \text{(A3.3)}$$

where

$$u = \frac{r^2 S}{4Tt} \qquad \text{(A3.4)}$$

(ii) Two-regime Flow Solution

The problem of steady state, one-dimensional, two-regime flow was solved analytically by Engelund ((1953), pp. 49-53)). His work has been reviewed and extended in Appendix 2. The general solutions are given by equations (A2.15) and (A2.16)

A3.2 Flow towards a Partially Screened Well in a Confined Aquifer

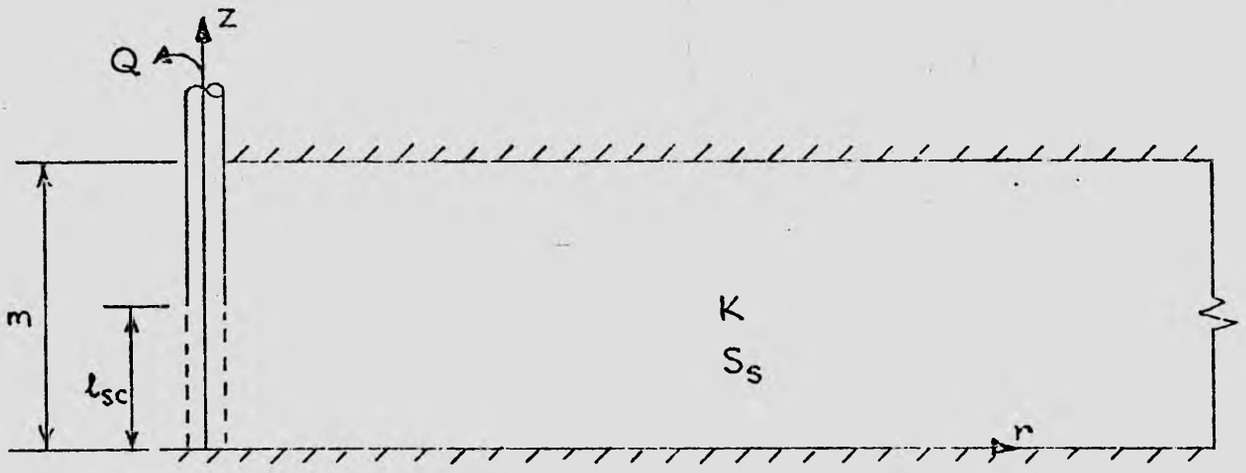

Fig. (A3.1): Model of a confined aquifer with a partially screened well.

The problem of transient Darcy flow towards a partially screened well as shown in Fig. (A3.1) was solved analytically by Hantush (1961). The simplified solution for the drawdown distribution along the base of the aquifer is given by

$$s = \frac{Q}{4\pi Km} W(u, \frac{r}{m}, \gamma) \qquad (A3.5)$$

where s = drawdown along the base of the aquifer

$$W(u, \frac{r}{m}, \gamma) = \int_u^\infty \frac{e^{-u}}{u} du + \frac{2m}{\pi l_{sc}} \sum_{n=1}^{\infty} \frac{1}{n} \sin(n\pi\gamma)$$

$$\times \int_u^\infty \exp\left[-y - \frac{(n\pi\, r/m)^2}{4y}\right] \frac{dy}{y} \qquad (A3.6a)$$

$$u = \frac{r^2 S_s}{4Kt} \qquad (A3.6b)$$

$$\gamma = \frac{l_{sc}}{m} \qquad A3.6c)$$

l_{sc} = length of well screen

For $\frac{r}{m} \geqslant 1.5$, equation (A3.5) may be approximated by the Theis solution as given by equation (A3.3).

A3.3 Flow towards a Well in a Confined Aquifer-Aquitard System

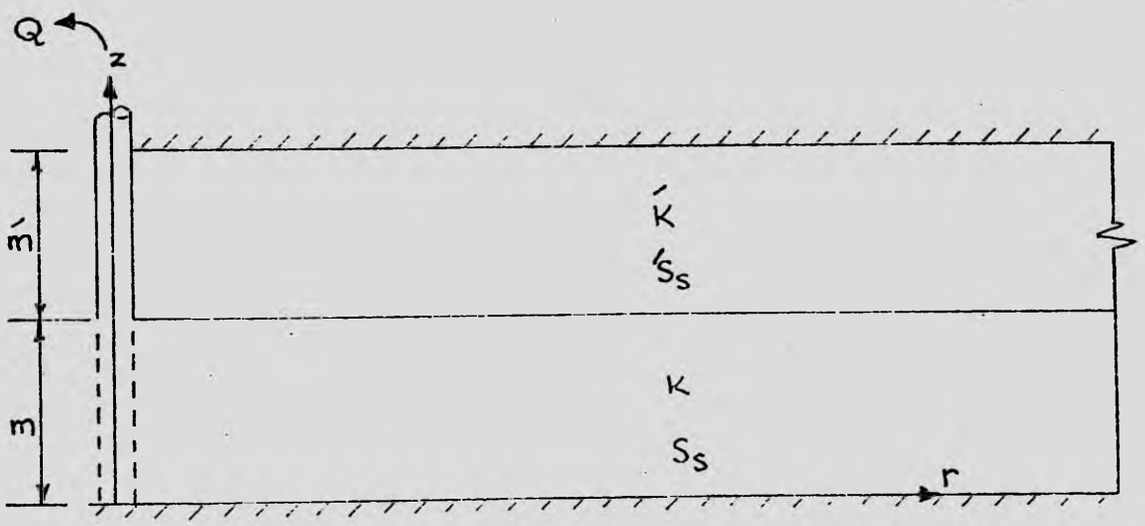

Fig. (A3.2): Model of a confined aquifer-aquitard system with a well which is screened through the thickness of the aquifer.

A diagrammatic sketch of a confined aquifer-aquitard system with a well which is fully screened through the entire thickness of the main aquifer is shown in Fig. (A3.2). In the figure K, S_s, m and K', S_s', m' denote the coefficients of hydraulic conductivity, specific storage and thickness of the aquifer and the overlying aquitard respectively.

Asymptotic solutions of short and long time drawdowns in the aquifer were first obtained by Hantush (1959), (1964). They may be written in the following forms:-

(i) Short time solution, for $t \leqslant \dfrac{S_s' m'^2}{10K'}$

$$s = \frac{Q}{4\pi Km} W(u, \beta) \qquad \text{(A3.7)}$$

where

$$W(u, \beta) = \int_u^\infty \frac{e^{-y}}{y} \operatorname{erfc}\left[\frac{\beta\sqrt{u}}{\sqrt{y\,(y-u)}}\right] dy \qquad \text{(A3.8a)}$$

$$u = \frac{r^2 S_s}{4Kt} \qquad \text{(A3.8b)}$$

$$\beta = \frac{r}{4m}\sqrt{\frac{K'S_s'}{KS_s}} \qquad \text{(A3.8c)}$$

(ii) Long time solution, for $t \geqslant$ both $\dfrac{2'm^2 S_s'}{K'}$ and $30\delta_1 r_w^2 \dfrac{S_s}{K}$

$$s = \frac{Q}{4\pi Km} W(\delta_1 u) \qquad \text{(A3.9)}$$

where

$$W(\delta_1 u) = \int_{\delta_1 u}^\infty \frac{e^{-u}}{u} du \qquad \text{(A3.10a)}$$

$$\delta_1 = 1 + \frac{S_s' m'}{S_s m} \qquad \text{(A3.10b)}$$

The short time solution for drawdowns in the aquitard was first obtained by Neuman and Witherspoon (1969, p. 122). It may be written as follows:-

For $t \leqslant {}'S_s{}'m^2/10K'$

$$s' = \frac{Q}{4\pi Km} W(u, \beta, \bar{t}_{D1}, z'/m') \qquad \text{(A3.11)}$$

where

s' = drawdown in the aquitard

$$W(u, \beta, \bar{t}_{D1}, z'/m') = \int_u^{\infty} \frac{e^{-y}}{y} \left\{ \operatorname{erfc}\left[\frac{\beta\sqrt{u} + y(z'/m')/\sqrt{4\bar{t}_{D1}}}{\sqrt{y(y-u)}} \right] dy \right.$$

$$\left. - \operatorname{erfc}\left[\frac{\beta\sqrt{u} + y(2 - z'/m')/\sqrt{4\bar{t}_{D1}}}{\sqrt{y(y-u)}} \right] \right\} dy \qquad \text{(A3.12a)}$$

$$z'/m' = \frac{z - m}{m'} \qquad \text{(A3.12b)}$$

$$\bar{t}_{D1} = \frac{K' t}{S_s' m'^2} \qquad \text{(A3.12c)}$$

A3.4 Flow towards Wells in an Unconfined Aquifer-Aquitard System

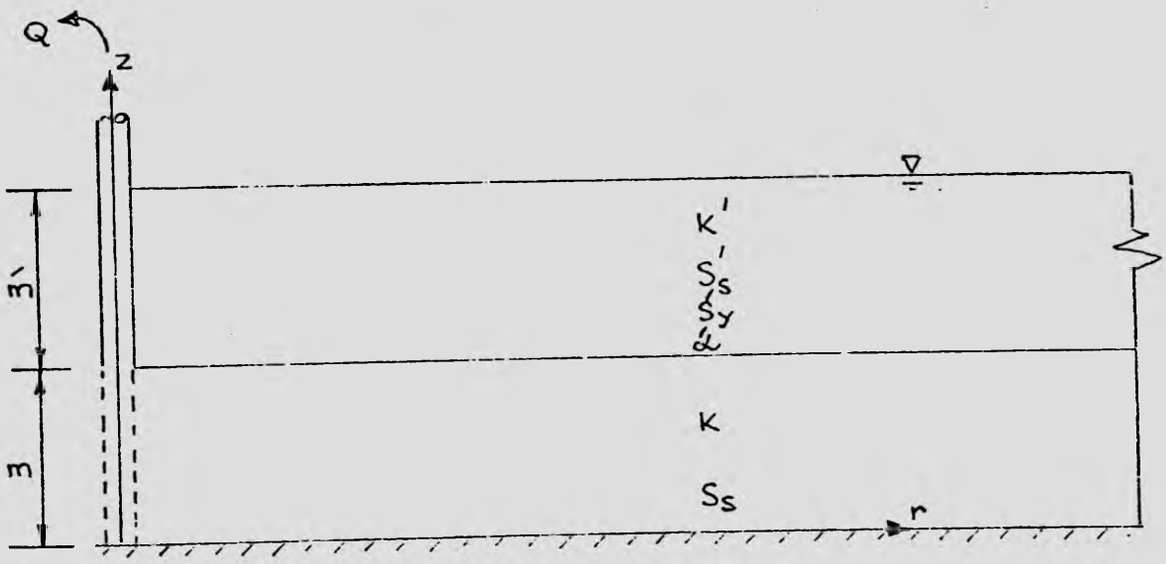

Fig. (A3.3): Model of an unconfined aquifer-aquitard system with a well which is screened through the thickness of the aquifer.

A diagrammatic sketch of an unconfined aquifer-aquitard system with a well which is fully screened through the thickness of the main aquifer is shown in Fig. (A3.3). In the figure, S_y' and α' denote the coefficient of specific yield and the reciprocal of delayed yield index for the unconfined aquitard. The flow problem was solved analytically by Cooley and Case (1963, unpublished paper). The asymptotic solutions for short and long time drawdowns in the main aquifer were later published by Cooley (1971). They are presented in the following manner:-

(i) Short time solution, for $t \leqslant \frac{S_s' m^2}{10K'}$

$$s = \frac{Q}{4\pi Km} W(u, \beta) \qquad \text{(A3.13)}$$

where the expression for $W(u, \beta)$ is given by equation (A3.8a).

(ii) Long time solution, for $t \geqslant \frac{10 S_s' m^2}{K'}$

$$s = \frac{Q}{4\pi Km} W(\delta_2 u, r/D) \qquad \text{(A3.14)}$$

where

$$W(\delta_2 u, r/D) = \int_0^\infty 2 J_0(2y) \left\{1 - \frac{(r/D)^2}{(r/D)^2 + 4y^2} \times \exp\left[\frac{-(r/D)^2 y^2}{\delta_2 u((r/D)^2 + 4y^2)}\right]\right\} \frac{dy}{y} \qquad \text{(A3.15a)}$$

$$\delta_2 = 1 + \frac{S_y' + S_s' m'}{S_s m} \qquad \text{(A3.15b)}$$

$$u = r^2 S_s / 4 Kt \qquad \text{(A3.15c)}$$

$$D = \left[\frac{Km}{\alpha' S_y'} + \frac{Kmm'}{K'} \right]^{\frac{1}{2}} \qquad \text{(A3.15d)}$$

The short time solution for drawdowns in the overlying aquitard is given by

$$s' = \frac{Q}{4\pi Km} W(u, \beta, \bar{t}_{D1}, z'/m') \qquad \text{(A3.16)}$$

where the expression for $W(u, \beta, \bar{t}_{D1}, z'/m')$ is given by equation (A3.12a).

A3.5 Flow towards a Well in an Unconfined Aquifer

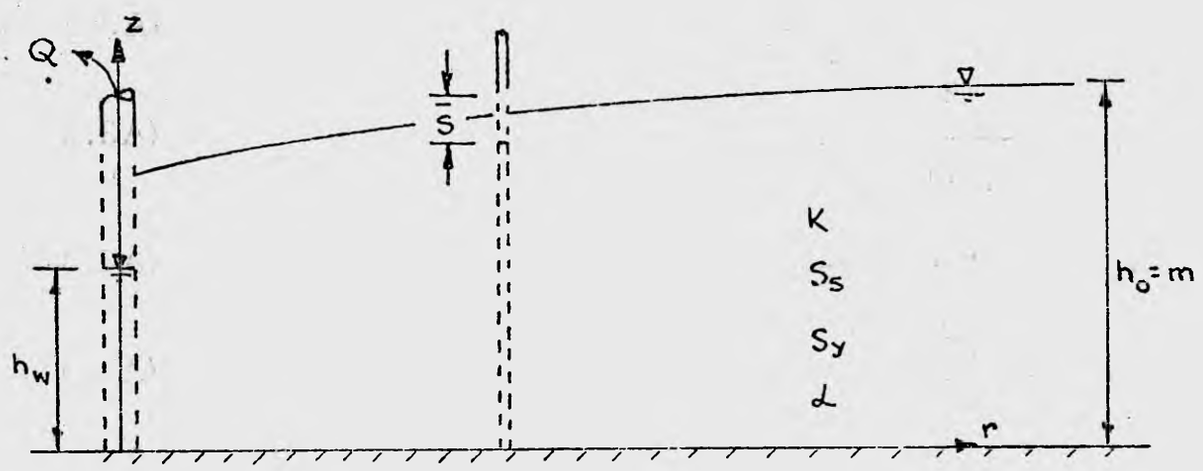

Fig. (A3.4): Model of an unconfined aquifer with a fully screened well.

A diagrammatic sketch of a model of an unconfined aquifer with a well which is fully screened through its saturated thickness is shown in Fig. (A3.4). In the figure, K, S_s, S_y and α denote the coefficients of hydraulic conductivity, specific storage, specific yield, and the reciprocal of the delayed yield index for the aquifer respectively. The flow problem was solved analytically by Boulton (1954, 1963).

The general solution for the average drawdown (Boulton 1963, p. 479) was derived under the assumptions of constant saturated aquifer thickness and constant head distribution along the vertical direction. For large values of $\frac{S + S_y}{S}$, it may be approximated by the following equation:-

$$\bar{s} = \frac{Q}{4\pi Km} W(u, u_y, r/D) \qquad (A3.17)$$

where

$\bar{s}$ = drawdown in the observation well screened through the entire thickness of the aquifer

$$W = \int_0^\infty 2 J_o \left(\frac{r}{D} x\right)\left[1 - \frac{1}{x^2+1} \exp\left(-\frac{\alpha t x^2}{x^2+1}\right) - \epsilon\right] \frac{dx}{x} \qquad (A3.18a)$$

$$\epsilon = \frac{x^2}{x^2+1} \exp\left[-\alpha\eta t (x^2+1)\right] \qquad (A3.18b)$$

$$\eta = 1 + \frac{S_y}{S_s m} \qquad (A3.18c)$$

$$u = \frac{r^2 S_s}{4kt} \qquad (A3.18d)$$

$$u_y = (\eta - 1) u \qquad (A3.18e)$$

$$D = \left[\frac{Km}{\alpha S_y}\right]^{\frac{1}{2}}$$

J_o = Bessel function of the first kind of zero order

For sufficiently small values of t, equation (A3.18a) reduces to

$$W = \int_0^\infty 2 J_o \left(\frac{r}{D} x\right) \frac{x^2}{x^2+1} \left\{1 - \exp\left[-\alpha\eta t(x^2+1)\right]\right\} \frac{dx}{x} \qquad (A3.19)$$

List of References

1. Ahmed, N. and Sunada, D.K. - "Non linear flow in porous media", A.S.C.E. Jour., Vol. 95, HY6, pp.1847-1857, (1969).

2. Aitken, R.R. and Alexander, E.L. - "Optimum hole diameter for water wells", Water Well Jour., Jan. (1967).

3. Ames, W.F. - "Numerical methods for partial differential equations", Thomas Nelson and Sons Ltd., London, (1969).

4. Anandakrishnan, M. and Varadarajulu, G.H. - "Laminar and turbulent flow of water through sand", ASCE Jour., Vol. 89, SM5, pp. 1-15, (1963).

5. Aris, R. - "Vectors, tensors and the basic equations of fluid mechanics", Prentice-Hall Inc., Englewood Cliff, New Jersey, (1962).

6. Baturic-Rubcic, J. - "An electrical analog for some cases of non-linear flow through porous media", Jour. of Hydraulic Research, Vol. 4, No. 2, pp.1-20, (1966).

7. Baturic-Rubcic, J. - "An electrical analog for non-linear fields", Jour. of Scientific Instruments, Series 2, Vol. 1, pp.1090-1095, (1968).

8. Bear, J. - "Dynamics of fluids in porous media", American Elsevier Publishing Co., New York, (1972).

9. Boulton, N.S. - "Flow pattern near gravity well in uniform water bearing medium", Jour. Inst. Civ. Engrs. (U.K.), Vol. 36, No. 10, pp.534-550, (1951).

10. Boulton, N.S. - "Unsteady radial flow to a pumped well allowing for delayed yield and storage", IASH General Assembly of Rome, Vol. 2, Publ. No. 37, pp.472-477, (1954).

11. Boulton, N.S. - "Analysis of data from non-equilibrium pumping test allowing for delayed yield from storage", Proc. Inst. Civ. Engrs. (U.K.), Vol. 26, No. 6693, pp.469-482, (1963).

12. Bruin, J. and Hudson, H.E. (jr.) - "Selected methods for pumping test analysis", Illinois State Water Survey, Report of Investigation 25, Urbana, 3rd printing, (1961).

List of References (cont'd.)

13. Calcote, L.R. - "Introduction to continu um mechanics", D. Van Nostrand Co., Inc., New York, (1968).

14. Cooley, R.L. - "A finite difference method for unsteady flow in variably saturated porous media: Application to a single pumping well", Water Resources Research, Vol. 7, No. 6, pp.1607-1625, (1971).

15. Crandal, S.H. - "Engineering analysis", McGraw-Hill Book Co., New York, (1965).

16. Desai, C.S. and Abel, J.F. - "Introduction to the finite element method, a numerical method for engineering analysis", Van Nostrand Reinhold Co., New York, (1972).

17. Desai, C.S. - "Approximate solution for unconfined seepage" ASCE Jour., Vol. 99, pp. 71-86, (1973).

18. De Wiest, R.J.M. - "Flow through porous media", Academic Press, New York, (1969).

19. Dudgeon, C.R. - "An experimental study of flow of water through coarse granular media", La Houille Blanche, Vol. 21, No. 7, pp. 785-801, (1966).

20. Dudgeon, C.R. - "Wall effects in permeameters", ASCE Jour., Vol. 93, HY4, pp. 137-148, (1967).

21. Dudgeon, C.R. - "Relationship between porosity and permeability of coarse granular materials", Inst. of Engrs., Australia, Proc. of 3rd Australasian Conf. on Hydraulics and Fluid Mech., Sydney, pp. 76-80, (1968).

22. Dudgeon, C.R. et al - "Hydraulics of flow near wells in unconsolidated sediments", Univ. of New South Wales, Australia, Water Research Lab., Report No. 126, Vols. 1 and 2, (1972), (1973).

23. Engelund, F. - "On the laminar and turbulent flows of groundwater through homogeneous sand", Hydraulic Lab., Tech. Univ. of Denmark, Bull. No. 4, (1953).

24. Ergatoudis, O.C. et al - "Curve isoparametric quadrilateral elements for finite element analysis", Int. Jour. Solids Struct., Vol. 4, pp. 31-42, (1968).

List of References (cont'd.)

25. Finn, A.D.L. - "Finite-element analysis of seepage through dams", ASCE Jour., Vol. 93, SM6, pp.41-48, (1967).

26. Forchheimer, P.H. - "Wasserbewegung durch Boden" Zeitschrift, Verein Deut. Ing. 49, (1901).

27. France, P.W. et al - "Numerical analysis of free surface problems", ASCE Jour., Vol. 97, IR1, pp. 165-179, (1971).

28. Frederick, C.O. et al - "Two-dimensional automatic mesh generation for structural analysis", Int. Jour. for Numr.Meth. in Eng., Vol. 4, pp. 133-144, (1972).

29. Franzini, J.B. "Porosity factor for case of laminar flow through granular media", Trans. A.G.U., Vol. 32, No. 3, pp. 443-446, (1951).

30. Grcic, J.A. - "Model test of steady flow toward a well", IAHR, 9th Convention Proc., pp. 591-600, (1961).

31. Gurtin, M.E. - "Variational principles for linear initial-value problems", Quart. of Appl. Math., Vol. 22, No. 3, p. 252,(1964).

32. Hall, H.P. - "An investigation of steady flow towards a gravity well", La Houille Blanche, Vol. 10, pp. 8-35, (1955).

33. Hansen, V.E. - "Unconfined groundwater flow to multiple wells", ASCE Trans., Vol. 118, pp. 1098-1130, (1953).

34. Hantush, M.S. - "Drawdown around a partially penetrating well", ASCE Jour., Vol. 87, HY4, pp.83-98, (1961).

35. Hantush, M.S. - "Modification of the theory of leaky aquifers", Jour. Geophys. Res., Vol. 65, p. 3713, (1960).

36. Hantush, M.S. - "Hydraulics of Wells", Advances in Hydroscience, edited by Chow, V.T., Academic Press, New York, Vol. 1, (1964).

37. Harrison, W. et al - "Groundwater flow in a sandy tidal beach, (1) One-dimensional finite element analysis", Water Resources Research, Vol. 7, No. 5, pp. 1313-1322, (1971).

38. Hazen, A. - "Some physical properties of sands and gravels with special reference to their use in filtration", 24th Annual Report, Mass. State Bd. Health, Boston, (1893).

39. Holand, I. and Bell, K. - "Finite element methods in stress analysis", published by TAPIR., The Technical Univ. of Norway, Trodheim-Norway, (1969).

List of References (cont'd.)

40. Hubbert, M. - "Darcy's law and the field equations of the flow of underground fluids", Jour. Petrol. Tech., Vol. 8, (1956).

41. Huisman, L. o.-"Groundwater recovery", Macmillan Press Ltd., London, (1972).

42. Huyakorn, P.S. and Dudgeon, C.R. - "Groundwater and well hydraulics: an annotated bibliography", Univ. of New South Wales, Australia, Water Research Lab., Report No. 121, (1972).

43. Huyakorn, P.S. - "Theoretical and numerical analysis of two-regime flow toward wells", Univ. of New South Wales, Australia, Water Research Lab., Report No. 126, Vol. 1, Section B, pp. B1-B67, (1972).

44. Irmay, S. - "On theoretical derivation of Darcy and Forchheimer formulas", A.G.U. Trans., Vol. 39, pp. 702-707, (1958).

45. Jacob, C.E. - "Drawdown test to determine effective radius of artesian well", ASCE Proc., Vol. 79, No. 5, pp. 1047-1070 (1946).

46. Javandel, I. and Witherspoon, P.A. - "Analysis of transient fluid flow in multi-layered systems", Univ. of California, Berkeley, Water Resources Center Contribution No. 124, (1968).

47. Karanjac, J. - "Well losses due to reduced formation permeability", Groundwater, Vol. 10, No. 4, pp. 42-49, (1972).

48. Kirkham, C.E. - "Turbulent flow in porous media - an analytical and experimental model study", Univ. of Melbourne, Australia, Dept. of Civ.Eng. Bull. No. 11, (1967).

49. Kovacs, G. - "Relationship between velocity of seepage and hydraulic gradient in the zone of high velocity", IAHR, 13th Cong., Kyoto, Subj. D7, pp. 25-38, (1969).

50. Kristianovich, S.A. - "Movement of groundwaters violating Darcy's law", Jour. of Appl. Math. and Mech., Vol. 4, pp. 33-52, (1940).

51. Lane, K.S. - "Laminar and turbulent flow of water through sand" ASCE Jour., Vol. 90, SM3, pp. 171-176, (1964).

52. Lindquist, E. - "On the flow of water through porous media", Rep. First Cong. on Large Dams, Vol. 5, pp. 81-101, (1933).

List of References (cont'd.)

53. Luthin, J.N. and Scott, V.H. - "Numerical analysis of flow through aquifers toward wells", Agric. Eng., Vol. 33, pp. 279-282, (1952).

54. McCorquodale, J.A. and Ng, H.C. - "Non-Darcy flow solved by finite element analysis", IAHR, 13th Cong. Proc., Vol. 4, Subj. D, pp. 347-355 (1969).

55. McCorquodale, J.A. - "Variational approach to non-Darcy flow" ASCE Jour., Vol. 96, HY11, pp. 2265-2278 (1970).

56. Mauersberger, P. - "A variational principle for steady state groundwater flow with a free surface", Pure Appl. Geophys., Vol. 60, p. 101, (1965).

57. Mauersberger, P. - "The use of variational methods and of error distribution principles in groundwater hydraulics", Int. Assoc. of Sci. Hydrol. Bull., Vol. 13, No. 2, pp. 169-186, (1968).

58. Mogg, J.L. - "Effect of aquifer turbulence on well drawdown", ASCE Jour., Vol. 85, HY11, Nov., (1959).

59. Mogg, J.L. - "Step-drawdown test needs critical review", Groundwater, Vol. 7, No. 1, pp. 28-34, (1969).

60. Muskat, M. - "The flow of homogeneous fluids through porous media", McGraw-Hill, New York, (1937).

61. Neuman, S.P. and Witherspoon, P.A. - "Transient flow of groundwater to wells in multiple-aquifer systems", Univ. of California, Berkeley, Dept. of Civ. Eng., Geotech. Eng., Publ. No. 69-1, (1969).

62. Neuman, S.P. and Witherspoon, P.A. - "Finite element method of analysing seepage with a free surface", Water Resources Research, Vol. 6, No. 3, pp. 889-897, (1970).

63. Neuman, S.P. and Witherspoon, P.A. - "Variational principles for fluid flow in porous media", ASCE Jour., Vol. 97, EM2, pp. 359-374, (1971).

64. Neuman, S.P. and Witherspoon, P.A. - "Analysis of nonsteady flow with a free surface using the finite element method", Water Resources Research Vol. 7, No. 3, pp. 611-623 (1971).

List of References (cont'd.)

65. Oden, J.T. - "Finite elements of nonlinear continua", McGraw-Hill Book Co., New York, (1972).

66. Oka, T. - "A study on the seepage around sheet pile by applying Forchheimer's law", IAHR, 13th Cong., Kyoto, Vol. 4, Subj. D, pp. 135-142, (1969).

67. Parekh, C.J. - "A finite element solution of time dependent field problems", M.Sc. Thesis, Univ. of Wales, Swansea, (1967).

68. Parkin, A.K. - "Field solutions for turbulent seepage flow", ASCE Jour., Vol. 97, SM1, pp. 209-218, (1971).

69. Pinder, G.F. - "Application of Galerkin's procedure to aquifer analysis", Water Resources Research, Vol. 8, No. 1, pp. 108-120, (1972).

70. Peterson, D.G. (Jr.) - "Hydraulics of wells", ASCE Trans., Vol. 133, pp. 502-517, (1957).

71. Polubarinova-Kochina, P. Ya - "Theory of ground water movement", Princeton Univ. Press, Princeton, New Jersey, (1962).

72. Ponter, A.R.S. - "The application of dual minimum theorems to the finite element solution to potential problems with special reference to seepage", Int. Jour. for Numr. Meth. in Eng., Vol. 4, pp. 85-93, (1972).

73. Remson, I. et al - "Numerical methods in subsurface hydrology, with an introduction to the finite element method", Wiley-Interscience Book Co., New York, (1971).

74. Rorabaugh, M.I. - "Graphical and theoretical analysis of step drawdown test of artesian wells", ASCE Trans., Vol. 79, (1953).

75. Rose, H.E. - "An investigation into the laws of flow of fluids through beds of granular materials", Inst. Mech. Engrs. (U.K.), Proc., Vol. 153, pp. 141-148, (1945).

76. Rose, H.E. and Rizk, A.M. - "Further researches in fluid flow through beds of granular material", Inst. Mech. Engrs. (U.K.). Proc., Vol. 160, pp. 493-511, (1949).

List of References (cont'd.)

77. Rowan, R. and Clegg, M.W. - "An approximate method for non-Darcy radial gas flow", Trans. A.I.M.M.P.E., pp.96-114,(1964).

78. Sanhu, R.S. and Wilson, E.L. - "Finite-element analysis of seepage in elastic media", A.S.C.E., Jour. Vol. 95, EM3, pp.641-652, (1969).

79. Scheidegger, A.E. - "The physics of flow through porous media", Macmillan Co., New York, (1960).

80. Sheahan, N.T. - "Type-curve solution of step-drawdown test", Groundwater, Vol. 9, No.1, pp.25-29, (1971).

81. Slepicka, F. - "Hydraulic function of a cylindrical well in an artesian aquifer with regard to new research on flow through porous media", IAHR, 9th Convention, Proc., pp.395-407,(1961).

82. Stark, K.P. and Volker, R.E. - "Non-linear flow through porous materials", Univ. College of Townsville (now James Cook Univ. of North Queensland) Australia, Dept. of Eng., Res. Bull. No.1, (1967).

83. Sunada, D.K. - "Turbulent flow through porous media", Univ. of California, Berkeley, Hydraulic Lab., Contribution No. 103, (1965).

84. Swan, W.H.C. and Huyakorn, P.S. - "Field studies of the Gumly Gumly Island and Rosevale well-aquifer systems", Univ. of New South Wales, Australia, Water Research Lab., Report No. 126, Vol. 2, Section E, (1973).

85. Swift, G.W. and Kel, O.G. - "The prediction of gas-well performance including the effect of non-Darcy flow", Trans. A.I.M.M.P.E., Soc. of Petrol.Engrs., Vol. 225, (1962).

86. Taylor, R.L. and Brown, C.B. - "Darcy flow solutions with a free surface", ASCE Jour., Vol. 93, HY2, pp.25-33, (1967).

87. Taylor, R.L. - "On completeness of shape functions for finite element analysis", Int.Jour. for Numr. Meth. in Eng., Vol. 4, pp.17-22, (1972).

88. Tek, M.R. et al - "The effect of turbulence on flow of natural gas through porous reservoirs", Trans. A.I.M.M.P.E., Soc. of Petrol. Engrs., Vol. 225, pp. 799-806, (1962).

List of References (cont'd.)

89. Theis, C.V. - "The relationship between the lowering of the piezometric surface and the rate and duration of discharge of a well using groundwater storage", A.G.U. Trans., 16 Annual Meeting, Pt. 2, pp. 519-524 (1935).

90. Todd, D.K. - "Groundwater and Hydrology", John Wiley and Sons Inc., New York, (1959).

91. Trollope, D.H. et al - "Complex flow through porous media", James Cook Univ. of North Queensland, Australia, Dept. of Eng., Research Bull. No. C2, (1970).

92. Uchida, S. - "On the non-linear percolation at high Reynolds Number", 1st Japan National Congress for Appl. Math., pp. 437-442, (1951).

93. Varga, R.S. - "Matrix iterative analysis", Prentice-Hall, Englewood Cliffs, New Jersey, (1962).

94. Verma, R.D. and Brutsaert, W. - "Unconfined aquifer seepage by capillary flow theory", ASCE, Jour., Vol. 96, HY6, pp. 1331-1344, (1970).

95. Verruijt, A. - "Theory of groundwater flow", Macmillan and Co., London, (1970).

96. Volker, R.E. - "Non-linear flow in porous media by finite elements", A.S.C.E. Jour., Vol. 95, HY6, pp. 2093-2112, (1969).

97. Walton, W.C. - "Groundwater resource evaluation", McGraw-Hill Book Co., New York, (1970).

98. Wentworth, C.K. - "Laminar flow in Honolulu aquifer", A.G.U. Trans., Vol. 27, No. IV, (1946).

99. Wright, D.E. - "Non-linear flow through granular media", ASCE Jour., Vol. 94, HY4, pp. 851-872, (1968).

100. Zienkiewicz, O.C. and Cheung, Y.K. - "Finite elements in the solution of field problems", The Engineer (U.K.), pp. 220, Sept., (1965).

101. Zienkiewicz, O.C. and Cheung, K.K. - "The finite element method in structural and continuum mechanics" McGraw-Hill Book Co., London, (1967).

102. Zienkiewicz, O.C. - "The finite element method in engineering science", McGraw-Hill Book Co., London, (1971).

103. Zienkiewicz, O.C. and Phillips, D.V. - "An automatic generation scheme for plane and curved surfaces by isoparametric coordinates", Int. Jour. for Numr. Meth. in Eng., Vol. 3, pp. 519-528, (1971).

List of Figures

List of Figures (cont'd.)

List of Figures (cont'd.)

List of Figures (cont'd.)

List of Figures (cont'd.)

List of Figures (cont'd.)

List of Figures (cont'd.)

List of Figures (cont'd.)

List of Figures (cont'd.)

List of Figures (cont'd.)

List of Tables

Nomenclature

		Dimensions
a	linear coefficient of hydraulic resistance of aquifer	TL^{-1}
b	non-linear coefficient of hydraulic resistance of aquifer	T^2L^{-2}
$\bar{d}$	characteristic grain diameter	L
$\vec{e}_i$	unit vectors along Cartesian coordinate axes	
h	hydraulic head	L
h^o	initial hydraulic head	L
$\bar{h}$	prescribed hydraulic head	L
h_o	saturated thickness of unconfined aquifer	L
$\left\|\frac{\partial h}{\partial l}\right\|$, i	absolute hydraulic gradient	
l_{sc}	length of well screen	L
m, m'	thicknesses of aquifer and aquitard respectively	L
n_i	components of unit outward normal vector	
p/γ	pressure head	L
$\bar{q}$	prescribed flux per unit area	LT^{-1}
r	radial distance from pumped well	L
r/B	$r\Big/\left[\frac{Kmm'}{K'}\right]^{\frac{1}{2}}$	
r/D	$r\Big/\left[\frac{Km}{\alpha S_y}\right]^{\frac{1}{2}}$	
r/D	$r\Big/\left[\frac{Km}{\alpha' S_y'} + \frac{Kmm'}{K'}\right]^{\frac{1}{2}}$	
r_{cr}	critical radius	L

		Dimensions
r_o	external radius	L
r_w	radius of well	L
s	drawdown in aquifer	L
s'	drawdown in aquitard	L
s_w	well drawdown	L
t	time since pumping started	T
Δt	time increment	T
1/u	$\frac{4\ Tt}{r^2 S}$, dimensionless time	
u_o	r/r_o; dimensionless radius	
v_i	components of velocity vector	LT^{-1}
x_i	Cartesian coordinates	L
z	vertical coordinate	L
z'/m'	(z-m)/m'	
z	elevation of free surface above datum plane	L
B	empirical coefficient of well discharge-drawdown equation	TL^{-2}
C	empirical coefficient of well discharge-drawdown equation	T^2L^{-5}
E	coefficient of effective hydraulic conductivity of aquifer	LT^{-1}
H	prescribed elevation of water level in the well	L
I	net specific rate of infiltration at free surface	LT^{-1}
K, K'	coefficients of hydraulic conductivity of aquifer and aquitard respectively	LT^{-1}

		Dimension
Q	calculated well discharge	L^3T^{-1}
$\bar{Q}$	prescribed well discharge	L^3T^{-1}
$\mathbb{R}$	$V\bar{d}\rho/\mu$; Reynolds number	
$\mathbb{R}_{cr}$	$\frac{\rho\bar{d}V_{cr}}{\mu}$; critical Reynolds number	
S_s, S_s'	coefficients of specific storage of aquifer and aquitard respectively	L^{-1}
S, S'	coefficients of storage of aquifer and aquitard respectively	
Sy, Sy'	coefficients of specific yield of aquifer and aquitard respectively	
T	coefficient of transmissivity of aquifer	L^2T^{-1}
V, $\|V\|$	absolute flow velocity	LT^{-1}
V_{cr}	critical flow velocity	LT^{-1}
$W(u_o)$	$2\pi Ts/Q$; dimensionless drawdown for steady state flow	
$W(u)$	$4\pi Ts/Q$; dimensionless drawdown for transient flow	
α, α'	reciprocal of delayed yield index of aquifer and aquitard respectively	T^{-1}
β	$\frac{r}{4m}\left[\frac{K'S_s'}{KS_s}\right]^{\frac{1}{2}}$	
γ	specific weight of water	$ML^{-2}T^{-2}$
γ	lsc/m; screen length ratio	
ρ	density of water	ML^{-3}
μ	coefficient of dynamic viscosity of water	$ML^{-1}T^{-1}$
ν	$\frac{K}{S_s}$; diffusivity of aquifer	L^2T^{-1}

		Dimensions
δ_1	$1 + \frac{S_s' m'}{S_s m}$	
δ_2	$1 + \frac{S_s' m' + S_y}{S_s m}$	
η	$1 + \frac{S_y}{S_s m}$	
ξ	$\frac{b\, Vcr}{a}$; non-Darcy flow parameter	
(ξ, η)	isoparametric coordinates	
ω	over-relaxation factor	
λ	$\frac{bQT}{2\pi m^2 r}$; transient non-Darcy flow parameter	
$\dot{\phi}$	dissipation function	LT^{-1}
$\dot{\Omega}$	rate of dissipation of hydraulic energy	L^4T^{-1}
$[\Omega(h)]_R$	functional over region R	
Ω^e	functional over a finite element region	
$\int_B (\quad) dB$	integral over boundary B	
B	boundary of entire flow region	
B_1	portion of B where flux is prescribed	
B_2	portion of B where hydraulic head is prescribed	
B^c	impervious boundary	
B^F	free surface boundary	
B^s	seepage face boundary	
$\int_R (\quad) dR$	integral over region R	
$\bar{R}$	closed flow region	
R	interior of R	

Dimensions

R^D, R^N	Darcy and non-Darcy flow subregions
R^e	finite element subregion
δ	variational operator
$\vec{\nabla}$	gradient operator
$[C^e], [C^e]$	element matrices
$[D^e], [F^e]$	element matrices
[C] , [D]	gross matrices
[F]	gross matrix
[J]	Jacobian matrix
[K]	hydraulic conductivity matrix
[N]	shape function matrix
[S]	element slope matrix
i, j	subscripts referring to components along coordinate axis
i, j	subscripts referring to nodes of the flow region which are not on the well screen
k	superscript referring to iteration number
n	superscript or subscript referring to time step number
I, J	subscripts referring to either nodes on the boundary or nodes in the entire flow region
α, β	subscripts referring to nodes on the well screen